การเปรียบเทียบสมบัติจีโอพอลิเมอร์ฐานเถ้าลอยและฐานดินขาวเผาสำหรับการดูดซับโลหะหนัก

นางสาวสุจิตรา อ่อนอุทัย

วิทยานิพนธ์นี้เป็นส่วนหนึ่งของการศึกษาตามหลักสูตรปริญญาวิทยาศาสตรดุษฎีบัณฑิต
สาขาวิชาวัสดุศาสตร์ ภาควิชาวัสดุศาสตร์
คณะวิทยาศาสตร์ จุฬาลงกรณ์มหาวิทยาลัย
ปีการศึกษา 2560

COMPARISION OF FLY ASH AND METAKAOLIN BASED GEOPOLYMER PROPERTIES FOR HEAVY METAL ADSORPTION

Miss Sujitra Onutai

A Dissertation Submitted in Partial Fulfillment of the Requirements
for the Degree of Doctor of Philosophy Program in Materials Science
Department of Materials Science
Faculty of Science
Chulalongkorn University
Academic Year 2017

Thesis Title	COMPARISION OF FLY ASH AND METAKAOLIN BASED GEOPOLYMER PROPERTIES FOR HEAVY METAL ADSORPTION
By	Miss Sujitra Onutai
Field of Study	Materials Science
Thesis Advisor	Assistant Professor Sirithan Jiemsirilers, Ph.D.
Thesis Co-Advisor	Professor TAKAOMI KOBAYASHI, D.Eng.
	Parjaree Thavorniti, D.Eng.

Accepted by the Faculty of Science, Chulalongkorn University in Partial Fulfillment of the Requirements for the Doctoral Degree

.....Dean of the Faculty of Science

(Professor Polkit Sangvanich, Ph.D.)

THESIS COMMITTEE

.....Chairman

(Assistant Professor Dujreutai Pongkao Kashima, D.Eng.)

.....Thesis Advisor

(Assistant Professor Sirithan Jiemsirilers, Ph.D.)

.....Thesis Co-Advisor

(Professor TAKAOMI KOBAYASHI, D.Eng.)

.....Thesis Co-Advisor

(Parjaree Thavorniti, D.Eng.)

.....Examiner

(Assistant Professor Thanakorn Wasanapiarnpong, D.Eng.)

.....Examiner

(Associate Professor Rojana Pornprasertsuk, Ph.D.)

.....External Examiner

(Assistant Professor Duangrudee Chaysuwan, Ph.D.)

สุจิตรา อ่อนอุทัย : การเปรียบเทียบสมบัติจีโอพอลิเมอร์ฐานเถ้าลอยและฐานดินขาวเผาสำหรับการดูดซับโลหะหนัก (COMPARISION OF FLY ASH AND METAKAOLIN BASED GEOPOLYMER PROPERTIES FOR HEAVY METAL ADSORPTION) อ.ที่ปรึกษาวิทยานิพนธ์หลัก: ผศ. ดร.ศิริธันว์ เจียมศิริเลิศ, อ.ที่ปรึกษาวิทยานิพนธ์ร่วม: ศ. ดร.ทาคาโอมิ โคบายาชิ, ดร.ปาจรีย์ ถาวรนิติ, 224 หน้า.

งานวิจัยนี้มีจุดมุ่งหมายเพื่อประเมินประสิทธิผลผงจีโอพอลิเมอร์ฐานเถ้าลอยและฐานดินขาวเผาและเส้นใยคอมโพสิตจีโอพอลิเมอร์ฐานเถ้าลอยและฐานดินขาวเผาที่ใช้เป็นสารดูดซับในการกำจัดไอออนโลหะหนักจากสารละลาย โดยใช้เถ้าลอยและดินขาวเผาจากประเทศไทยเป็นวัตถุดิบในการวิจัยครั้งนี้ จีโอพอลิเมอร์ฐานเถ้าลอยสังเคราะห์โดยผสมกับสารละลายอัลคาไล หลังจากนั้นได้เกิดกระบวนการจีโอโพลีเมอร์ไรเซชันและเก็บตัวอย่างจีโอโพลิเมอร์ไว้ที่อุณหภูมิ 60 องศาเซลเซียสเป็นเวลา 24 ชั่วโมงและทิ้งไว้ที่อุณหภูมิ 25 องศาเซลเซียสเป็นเวลา 6 วัน จากนั้นนำจีโอโพลิเมอร์จากเถ้าลอยไปบด ล้าง และ ผ่านตะแกรงร่อนเบอร์ 100 เพื่อให้ได้ผงจีโอโพลิเมอร์ ผงจีโอพอลิเมอร์ฐานดินขาวเผาใช้กระบวนการสังเคราะห์เช่นเดียวกับผงจีโอพอลิเมอร์ฐานเถ้าลอย นอกจากนี้เส้นใยคอมพอสิตผสมกับพอลิอีเทอร์ซัลโฟนพอลิเมอร์และสารละลายเอ็นเมทิลทูไพโรลิโดน และจะถูกอัดผ่านหัวฉีดไปยังอ่างตกตะกอน เส้นใยคอมพอสิตจีโอพอลิเมอร์ถูกสร้างเป็นเส้นใยโดยใช้วิธีการผกผันแบบเฟส หลังจากการสังเคราะห์จีโอพอลิเมอร์และการขึ้นรูปเส้นใยคอมพอสิตจีโอพอลิเมอร์ ได้ศึกษาผลของเวลาในการสัมผัส ปริมาณของตัวดูดซับ ค่าความเป็นกรดด่างของสารละลาย อุณหภูมิ และความเข้มข้นเริ่มต้นของสารละลายต่อประสิทธิภาพของการดูดซับ นอกจากนี้ยังได้ศึกษาประสิทธิภาพของการดูดซับในสารละลายที่มีองค์ประกอบรวมและองค์ประกอบเดี่ยวของไอออนตะกั่ว ทองแดง แคดเมียม และนิกเกิลในสารละลาย นอกจากนี้นังได้ศึกษาไอโซเทอมของการดูดซับและจลนพลศาสตร์ของการดูดซับ ผลการทดลองแสดงให้เห็นว่าผงจีโอพอลิเมอร์มีเฟสที่เป็นกึ่งผลึกและส่วนใหญ่ประกอบด้วยซิลิกาและอลูมินา สำหรับพื้นที่ผิวของผงจีโอพอลิเมอร์ฐานเถ้าลอย ผงจีโอพอลิเมอร์ฐานดินขาวเผา เส้นใยคอมโพสิตจีโอพอลิเมอร์ฐานเถ้าลอยและเส้นใยคอมโพสิตจีโอพอลิเมอร์ฐานดินขาวเผา เท่ากับ 85.31, 20.36, 71.67 และ 53.11 ตารางเมตรต่อกรัม ตามลำดับ ผลการทดลองยังแสดงให้เห็นว่าไอออนของโลหะในสารละลายในน้ำได้รับการกำจัดออกด้วยผงจีโอพอลิเมอร์และเส้นใยคอมโพสิตจีโอพอลิเมอร์

ภาควิชา	วัสดุศาสตร์	ลายมือชื่อนิสิต	.....
สาขาวิชา	วัสดุศาสตร์	ลายมือชื่อ อ.ที่ปรึกษาหลัก	.....
ปีการศึกษา	2560	ลายมือชื่อ อ.ที่ปรึกษาร่วม	.....
		ลายมือชื่อ อ.ที่ปรึกษาร่วม	.....

5672850923 : MAJOR MATERIALS SCIENCE
KEYWORDS: FLY ASH / METAKAOLIN / GEOPOLYMER / ADSORPTION / POLYMER COMPOSITE / WASTEWATER TREATMENT

SUJITRA ONUTAI: COMPARISION OF FLY ASH AND METAKAOLIN BASED GEOPOLYMER PROPERTIES FOR HEAVY METAL ADSORPTION. ADVISOR: ASST. PROF. SIRITHAN JIEMSIRILERS, Ph.D., CO-ADVISOR: PROF. TAKAOMI KOBAYASHI, D.Eng., PARJAREE THAVORNITI, D.Eng., 224 pp.

This work aims to evaluate the effectiveness of fly ash and metakaolin based geopolymer powder and fly ash and metakaolin based geopolymer composite fiber as an adsorbent for removal of heavy metal ions from aqueous solution. The fly ash and metakaolin used as raw materials in this research was from Thailand. Fly ash based geopolymer (FAG) was synthesized by mix with an alkali solution. After that, the geopolymerization process was occurred and then cured geopolymer samples at 60°C for 24 h and left at 25 °C for 6 days. The fly ash based geopolymer was ground, washed and sieved through 100 mesh to obtain geopolymer powder. The process of metakaolin based geopolymer (MKG) powder was synthesized as same as that of fly ash based geopolymer powder. In addition, the geopolymer composite fiber was fabricated by mixing geopolymer powder with Polyethersulfone (PES)/ N-Methyl-2-pyrrolidone (NMP) solution and then being extruded through a nozzle to coagulation bath. The geopolymer composite fiber was formed to be fiber by phase inversion method. After synthesis of geopolymer powder and fabrication of geopolymer composite fiber, the effect of contact time, adsorbent amount, pH of a solution, temperature and initial concentration of solution on the adsorption efficiency were studied. Furthermore, the multi- and mono- Pb^{2+}, Cd^{2+}, Cu^{2+} and Ni^{2+} solutions were demonstrated to compare the efficiency of each metal ions. The adsorption isotherm and kinetics study were also studied. The results showed that the geopolymer powder had the semi-crystalline phases and mainly composed of silica and alumina. The surface area of FAG powder, MKG powder, FAG composite fiber and MKG composite fiber were 85.31, 20.36, 71.67 and 53.11 m^2/g, respectively. The results showed that metal ions in aqueous solution are effectively removed by geopolymer powder and geopolymer composite fiber.

Department:	Materials Science	Student's Signature .....
Field of Study:	Materials Science	Advisor's Signature .....
Academic Year:	2017	Co-Advisor's Signature .....
		Co-Advisor's Signature .....

ACKNOWLEDGEMENTS

This thesis could not have been realized without a great deal of guidance, and both mental and practical support. I would like to thank deeply those people who, during my study of my double doctoral program, provided me with everything I needed.

First of all, I would like to thank my thesis advisor, Asst. Prof. Dr. Sirithan Jiemsirilers who supported all research necessities. Grateful acknowledgment is made to my co-advisors, Prof. Dr. Takaomi Kobayashi of Department of Materials Science at the Nagaoka University of Technology (NUT), Japan and Dr. Pajaree Thavornniti of National Metal and Materials Technology Center., Thailand for discussing, good advising supporting, and helping in my research. I would like to thank the rest of my thesis committees who support, and guidance made my thesis work possible.

The author is grateful to the 100th Anniversary Chulalongkorn University Fund, National Center of Excellence of Petroleum, Petrochemicals and Advanced Materials and the Cultivation of Global Engineering by Pacific Rim Green Innovation project of Nagaoka University of Technology for financial support in the form of grants and Doctoral scholarships.

I would like to thank present and past members also the secretary of Department of Materials Science, Chulalongkorn University, Thailand and Biosustainable Environmental Materials engineering Laboratory, Nagaoka University of Technology, Japan for sharing their discussions, experiences, and knowledge during the time of the study. Special thanks to Dr. Kohtaroh Nakamoto, Ms. Lisa Nakajima, and Mr. Yuta Watanabe for helping to finish up my various projects.

Finally, I would also like to thank my parents, family, as well as my friends, for their continuing support, give me the love and encouragement.

CONTENTS

Page

Page

Page

Page

Page

Page

Page

LIST OF TABLES

Page

LIST OF FIGURES

Page

CHAPTER 1
INTRODUCTION

1.1 BACKGROUND AND MOTIVATIONS

The rapid growths of an industrial society are producing progressively more industrial waste and wastewater. They have a detrimental effect on the environment. For example, elimination of improper waste treatment can probably lead to contaminated soil, specifically waste consist of heavy metal has a significantly negative impact on the environment. The heavy metals in waste are mostly derived from a battery, electroplating, printed circuit board and metal surface coating treatment. There is a variety of methods that can be able to eliminate heavy metal from industrial waste such as coagulation, ion exchange, adsorption, immobilization and solvent extraction. Recently, it seems that the adsorption technique is widely known and focused due to its efficiency, uncomplicated protocol, and low cost.

Adsorption technique for industrial wastewater treatment mostly used zeolite in this process because zeolite possesses adsorbent properties that can remove heavy metals from wastewater. Adsorption of wastewater by zeolite is feasible due to its unique three-dimensional network structure, with fixed-sized pores and paths that allow the only heavy metal to pass through. With this, geopolymer also consists of three-dimensional polymeric structure and pores formed by the condensation of alumino-silicate mineral powder in addition to an alkali solution at a temperature below 100 °C which is similar to zeolite. The geopolymer synthesis process is simpler than zeolite. Geopolymer could be composed of metakaolin or wastes, such as fly ash, slag, and tailing. Therefore, geopolymer is one of the candidate materials for adsorption application because it is easier to syntheses, low cost and can use industrial wastes as raw materials. Then, wastewater treatment using a geopolymer as an

adsorbent should be more feasible, and it can be applied for treatment of industrial wastewaters in the future.

The purpose of this study is to synthesize fly ash and metakaolin based geopolymer in powder and composite fiber forms and to use the produced materials as adsorbent for removal of heavy metal from aqueous solution. Moreover, adsorption of heavy metal are studied as a function of the geopolymer dosage, heavy metal initial concentration, contact time, pH and temperature. In addition, to study adsorption isotherm of on the synthesized geopolymer is carried out by using equilibrium technique. Based on the experimental results many indicators are determined and two isotherm models are examined using obtained data.

1.2 OBJECTIVES OF THIS RESEARCH

1.2.1 To prepare geopolymer powder and geopolymer composite fiber by using fly ash and metakaolin as raw materials

1.2.2 To study factors that affect the heavy metal adsorption of prepared fly ash and metakaolin based geopolymer powder and geopolymer composite fiber

1.2.3 To obtain adsorption model for explain adsorption mechanism of geopolymer

1.3 SCOPE OF STUDY

Firstly, this research focused on the success of synthesis geopolymer powder and geopolymer composite fiber from fly ash and metakaolin. Secondly, the good conditions for adsorption ability of heavy metal of these materials.

1.4 EXPECTED BENEFIT

Obtain geopolymer materials for heavy metal adsorption applications.

CHAPTER 2

LITERATURE REVIEW

Nowadays, the rapid development of an industrial society made a critical level of heavy metal pollution. This pollution affects human health, animals, and ecological environment. Geopolymer is one of the materials that can be used to treat wastewater containing heavy metal ions. Geopolymer can be synthesized by natural mineral or industrial waste as raw materials. Fly ash based and metakaolin based geopolymer were synthesized for heavy metals adsorption in wastewater. Also, geopolymer can apply new type of composite adsorbent with polymer. This chapter reviews each materials which is concerned with geopolymer adsorbents.

2.1 GEOPOLYMER

2.1.1 Background and definition

In the 1950s, soil silicate was described for alkaline alumino-silicate cementitious systems which were contained calcium silicate hydrated and alumino-silicate phases and used to build a tall building by Victor Glukhovsky et al [1]. In 1972, Joseph Davidovits [2-4] called "Geopolymer" which is the new material, has cementitious property using silicon and aluminum activated with a high alkali solution and has a three-dimensional structure alumino-silicates. Geopolymer has amorphous to a semi-crystalline structure. Moreover, geopolymer has the three-dimensional Si-O-Al polymeric structure which has SiO_4 and AlO_4 tetrahedral are linked together by sharing all oxygen atoms, with the Al in four-fold coordination. Geopolymer has three basic forms depending on Si/Al ratios, namely poly(sialate), poly(sialate-siloxo) and poly(sialate-disiloxo) [5] as shown in Fig. 2.1.

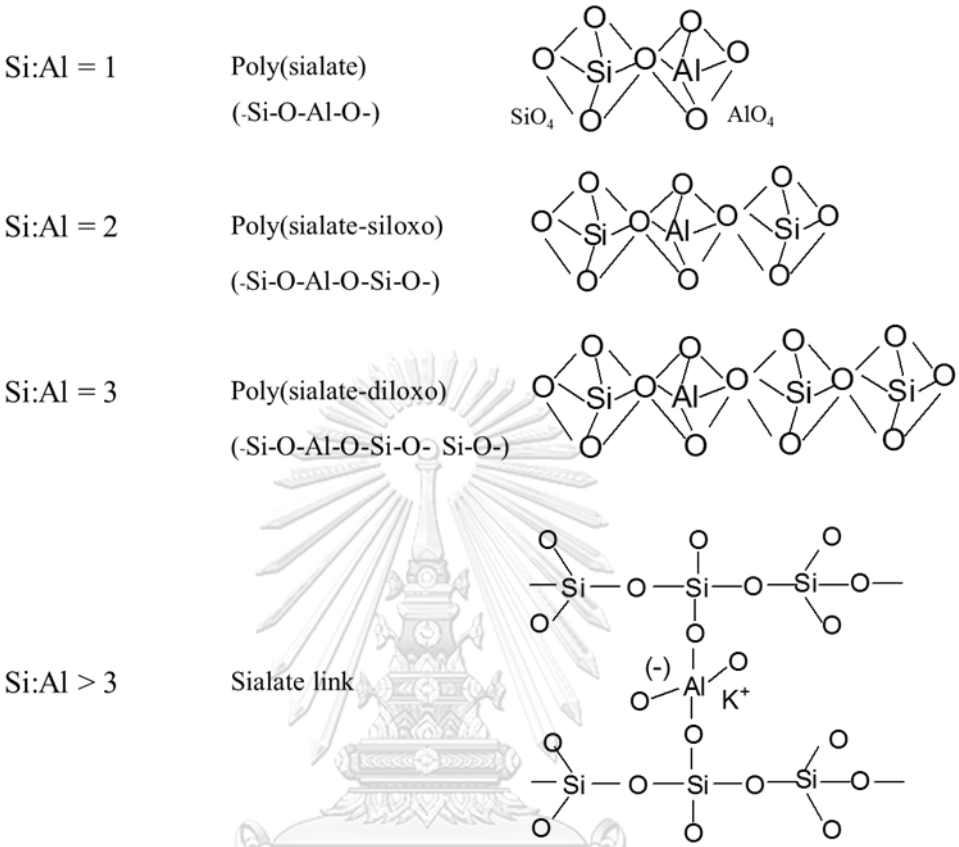

Fig. 2.1 Chemical structure of polysialates

Geopolymer produced by a polymeric reaction of alumino-silicate and alkali activators. Furthermore, geopolymer is able to synthesis at low pressure and low temperature using alumino-silicate sources which can be prepared from natural minerals and industrial wastes such as fly ash, metakaolin, blast furnace slag with a high alkaline concentration solution [6, 7]. Table 2.1 shows summarized experimental reports of geopolymer which have been reported.

Table 2.1 Main classes of currently developed geopolymer

Class of geopolymer materials	References
- Metakaolin MK-750-based geopolymer, poly(sialate-siloxo) Si:Al=2:1	[8, 9]
- Waterglass-based geopolymer, poly(siloxonate), soluble silicate, Si:Al=1:0	[10]
- Rock-based geopolymer, poly(sialate-multisiloxo) 1< Si:Al<5	[11, 12]
- Calcium-based geopolymer, (Ca, K, Na)-sialate, Si:Al=1, 2, 3	[13]
- Fly ash-based geopolymer	[14, 15]
- Silica-based geopolymer, sialate link and siloxo link in poly(siloxonate) Si:Al>5	[16, 17]
- Phosphate-based geopolymer, $AlPO_4$-based geopolymer	[18, 19]

2.1.2 Geopolymer structure

As mentioned before, geopolymer structure composed of sialate (silicon-oxo-aluminate) network in the chemical framework consisting of SiO_4 and AlO_4 tetrahedral linked alternately by sharing all oxygen atoms. Positive ions or alkali cations, for example, Ca^{++} , Na^+ and K^+ are charge-balanced of the negative charge of Al^{3+} in four-fold coordination [20]. A polymeric structure of (poly)sialate formed becomes the main chain of the geopolymeric structure and the formula of polysialates is presented as follow [21]:

$$Mn\ [(-Si\text{-}O_2)z\text{-}Al\text{-}O_2\text{-}]n,\ wH_2O \qquad (1)$$

where M is monovalent cation such as sodium or potassium

n is degree of polycondensation

z is amount of $Si\text{-}O_2$ (1, 2, 3 or higher)

w is amount of water

Geopolymerization starts from oligomer which is a small unit of the three-dimensional macromolecular structure which reacts at room temperature or at curing temperature. Geopolymerization process can be estimated into three stages: (I) deconstruction, (II) polymerization and (III) stabilization [22-24]. In geopolymer, the polymerize linkages are connected together in a type of sialate (Si-O-Al) and siloxo (Si-O-Si). The classified of polysialate in the chemical structure of geopolymer are separated into four units from the term of Si/Al atomic ratio[3, 4, 20]. The first unit is sialate and poly(sialate) at Si: Al = 1. For second units, the ratio of Si: Al at 2 is sialate-siloxo and poly(sialate- siloxo). Third, at Si: Al at 3 is sialate link and poly(sialate-multisiloxo) unit. The last elementary unit is sialate link and poly(sialate- multisiloxo) unit at Si: Al > 3 which are chains from connected Si-O-Al between two poly(siloxonate),

poly(silanol) or poly(sialate). Finally, in geopolymer framework, the elementary units (poly(sialate) chain and ring) are coordinated together with an oxygen atom to build a 3D network.

2.1.3 Geopolymerization reaction

As mentioned before, the geopolymerization process includes 3 steps as shown in Fig. 2.2. At first in (I) deconstruction process, the solid alumino-silicate materials are leached on the surface by alkali hydrolysis which produced aluminate and silicate species [25]. The Al-O-Al, Si-O-Si, and Si-O-Al of alumino-silicates source are dissolved in strong alkali solution [26]. The metal cations from alkali solution could balance the charge of aluminium in form of four-fold coordination with oxygen [27]. After that (II) polymerization process occurs in the solution. The neighboring reactive groups are formed as Si-O-Na and O-H-Al and silicate molecules from alkali silicate are reacted together and further polycondensation reaction to get a 3D framework of geopolymer. The (III) Stabilization is the last step, the formation of the preliminary units via polycondensation reaction at room temperature to 90 °C could form rigid chains or network of oxygen bonded with aluminate and silicate tetrahedral. When curing at a higher temperature, the stronger geopolymers are received, therefore, the hydroxyl groups in macromolecules are more capable of condensing with a neighboring molecules.

.

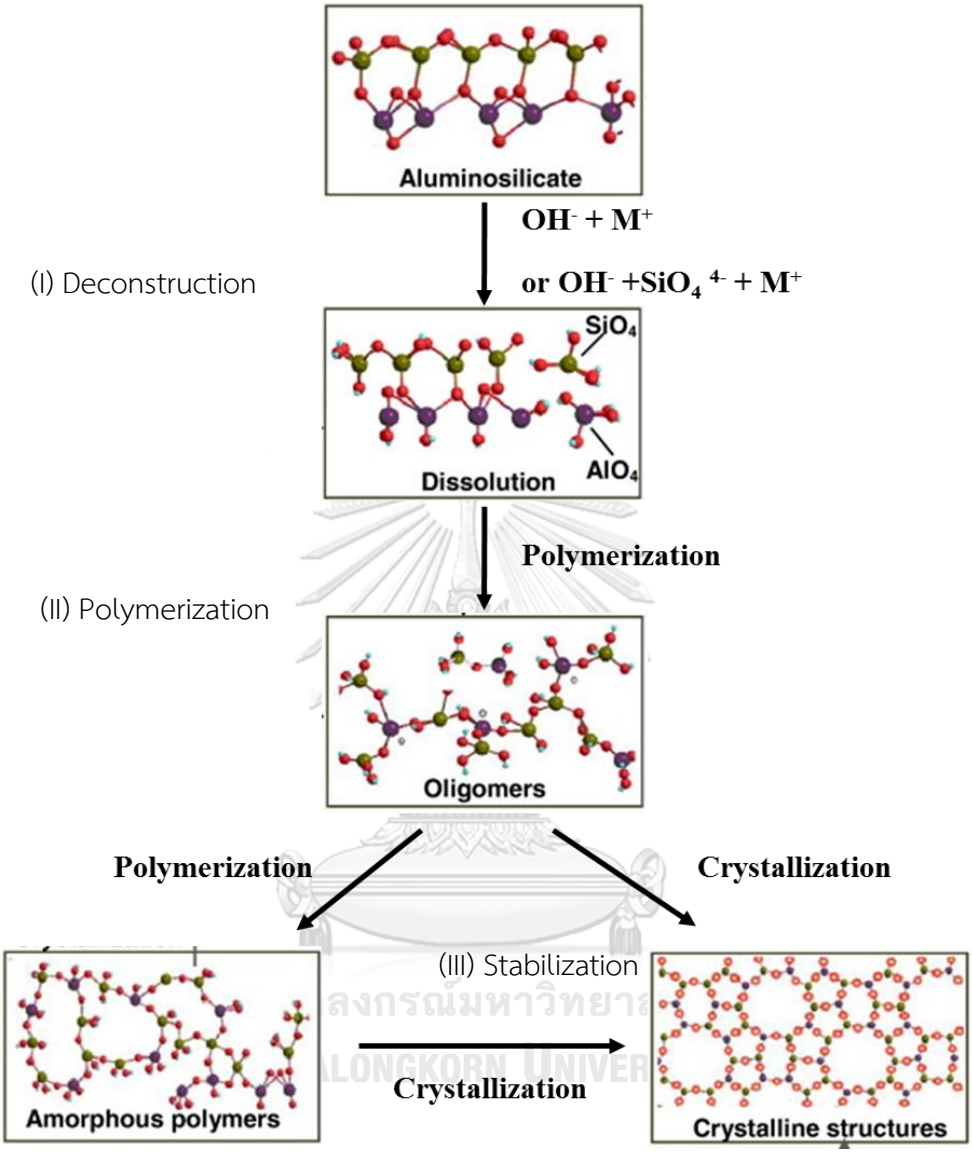

Fig. 2.2 A sketched model of the geopolymerization process. M^+ refers to alkali cations (usually Na^+ and/or K^+). SiO_4^{4-} refers to dissolved silicate

2.1.4 Synthesis of geopolymer

The starting materials are very important in geopolymer preparation. (I) Raw materials and inactive filler and (II) Geopolymer liquor are the sources for synthesis geopolymer. One important property of the suitable raw material and inactive filler are pozzolanic property [28]. Raw materials used for synthesis geopolymer could be alumino-silicate natural minerals or industrial wastes for example slag [29], rice husk ash [30], waste glass [31] and fly ash [32]. Furthermore, kaolinite or metakaolinite [33] is an inactive filler which is used for supply Al^{3+} ions. The main composition of the pozzolanic materials are SiO_2, Al_2O_3, and CaO. Each raw materials contain different oxide composition which affect the potential of the reaction. Moreover, the particle size of raw materials or in active filler also affect the geopolymerization reaction [34]. The (II) Geopolymer liquor is a chemical activator such as alkali hydroxide and/or silicates solutions. An alkali hydroxide solution desired for the dissolution of raw materials and sodium or potassium silicate conducted as an alkali activator, binder and dispersant or plasticizer [35, 36]. The alkali hydroxide solution used as an activator for the geopolymer synthesis is sodium hydroxide solution (NaOH) or potassium hydroxide solution (KOH) with high concentration solution [37-40]. The NaOH solution is the most widely used as hydroxide activator because Si and Al ions from raw materials could be leaching by NaOH solution and getting high reaction rate compared with KOH solution [41]. The geopolymer paste transforms to be solid which has higher strength after the raw materials were mixed with alkali solutions. Many factors affect the strength of geopolymer samples such as alkali concentration and curing temperature. The strength of geopolymer sample increased with an increase of NaOH concentration due to a high concentration of NaOH could increase dissolving rate of Si and Al ions from raw materials [42]. The compressive strength of geopolymer was increased resulting from a dense matrix in microstructure when high concentration of NaOH was used [21, 43].

Geopolymer prepared by using 10 M NaOH as alkali activator has highest compressive strength [44]. However, the strength of geopolymer was decreased when the concentration of NaOH was used over 14 M. The polycondensation was quick reacted in over hydroxide ion concentration [44, 45]. This result confirmed that a high alkali concentration improved the dissolution of Si and Al on the surface of raw material particles and developed the geopolymer strength, however, excess hydroxide ions produced fast alumino-silicate species precipitation at the early stage, resulting in a lower strength on geopolymer sample [27, 46]. In addition, the curing temperature is one of the factor for geopolymerization process. The curing temperature affects the setting time and hardening time of geopolymer sample, the strength increased with an increase in the curing time [47] and the curing temperature [48]. Nevertheless, at a temperature higher than 80 ^{o}C, the strength of geopolymer sample was decreased due to the over hydration and over shrinkage was occurred in geopolymer sample curing at over 100^{o}C [7, 43, 49].

2.1.5 Geopolymer applications

Geopolymer has many attractive properties such as high temperature resistance, high chemical resistance, long durability, low shrinkage and fast solidification with high-strength etc. The geopolymer materials can be used for many applications as shown in Table 2.2. Furthermore, Fig. 2.3 shows the geopolymer applications divided by the Si/Al ratio in the poly (sialate) structure. A higher ratio of Si/Al demonstrated very rigidly in the 3D network. Several reports studied and synthesized geopolymer for a specific application such as P. Pavithra et al. studied the geopolymer for concrete from fly ash [50]. In addition, Y. Park et al. developed the geopolymer concrete from fly ash and crumb rubber [51]. Moreover, geopolymer can be used as an adsorbent for adsorption heavy metal or dye from aqueous solution and wastewaters. Recently, Cu and Pb ions were removed from aqueous solution by fly ash based geopolymer. The adsorption capacity of fly ash based geopolymer for removal reached to 80 mg/g and 92 mg/g of Pb and Cu ions, respectively [52, 53]. L. Li et al. studied the capacity of fly ash based geopolymer for removal dye in solution [54]. Moreover, the geopolymer has been studied and used for immobilization heavy metal and radioactive waste [55]. The fly ash based geopolymer had a high potential for immobilize Pb ions [56] because hazardous waste or ions are locked in a 3D framework of geopolymer. Geopolymer not only used for adsorption or immobilizing hazardous waste or ions but also applied for composites materials. The hybrid composite materials from geopolymer with epoxy melamine resin have been produced, the result showed that this material had high temperature resistant to use for kitchen tools and plates, coatings and flooring [57]. The potassium based geopolymers (K-geopolymer) was formed by mixing ferronickel (FeNi) slag, doped with pure alumina for excellent fire protection material [58].

Table 2.2 Summary of geopolymer applications

Geopolymer applications	References
Concrete and cement	[50] [51]
Adsorbent for heavy metal ion	[54]
Immobilisation of toxic and radioactive waste	[40]
Composites	[57]
Fire resistant and protection matrix	[58]

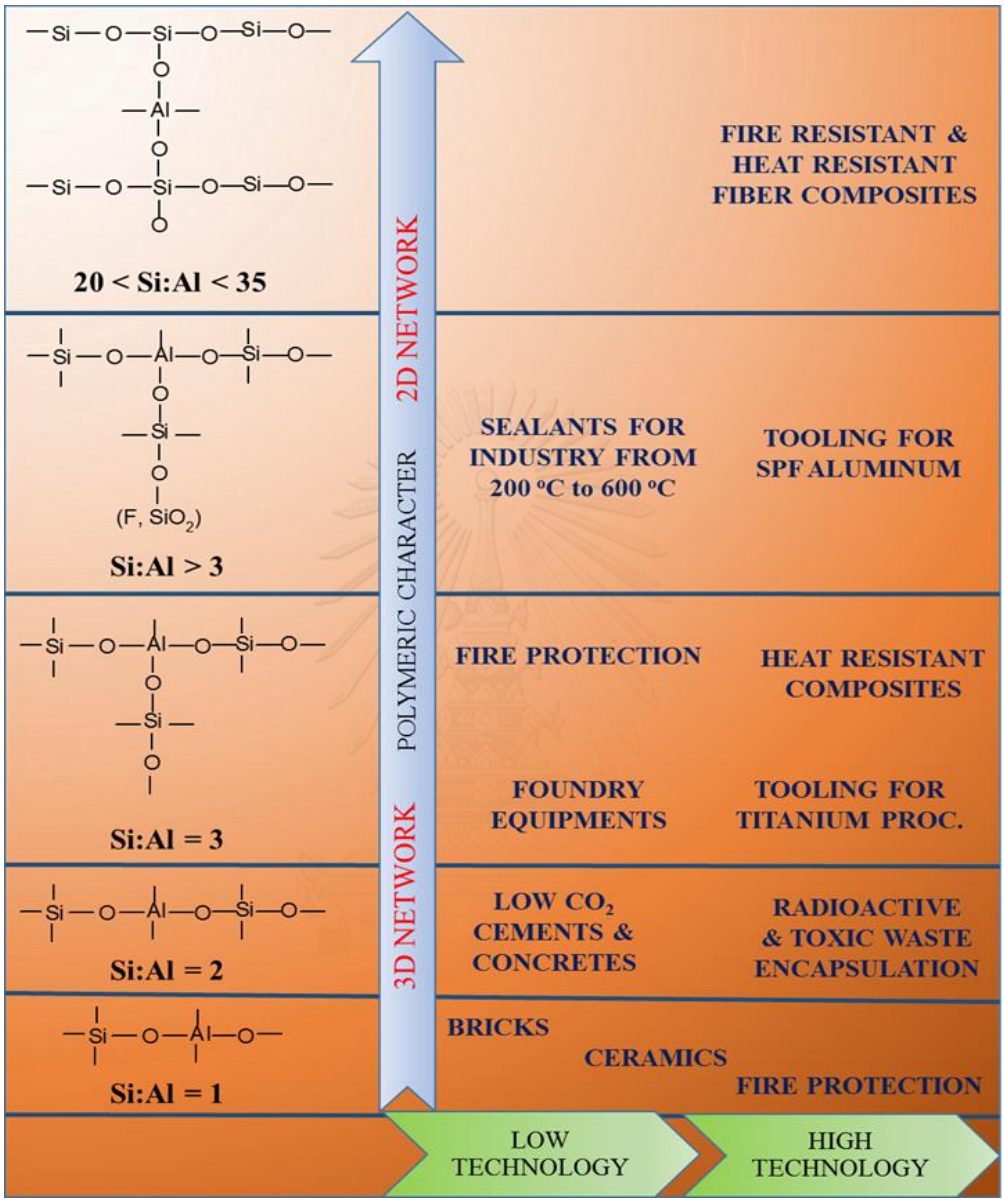

Fig. 2.3 Applications of geopolymer materials based on the Si:Al ratio

2.2 RAW MATERIALS USED TO SYNTHESIS GEOPOLYMER

The various raw materials that can be used for synthesis geopolymer such as mineral clay, fly ash or industrial wastes. The investigation of materials sources for producing geopolymer are shown in Table 2.3

Table 2.3 Raw materials for synthesis geopolymer

Raw materials	References
Metakaolin	[59]
Fly ash	[60]
Rice husk ash	[36]
Blast furnace slag	[61]
Waste glass, waste ceramics	[62, 63]
Mine tailing, Iron ore tailing	[64, 65]
Aluminium and grey cast iron slags	[66]

2.2.1 FLY ASH

From industrial furnaces burning solid fuels, the precipitated of any fine particles materials from the stack gases is used in term of fly ash. Fly ash is generated in a large amount in coal thermal power plant. Fly ash is commonly known as a supplementary cementitious material to enhance rheological properties and reduction of alkali-aggregate reaction in cement industry. Moreover, fly ash has a potential to be a raw material for geopolymer because fly ash composed of silica and alumina which are major constituents for geopolymer reaction [67]. The production, types, microstructure, and properties of are described as following [2]:

2.2.1.1 Production of fly ash

At electricity generating power plants, finely ground coal is high speed injected into the furnace with a stream of hot air. The coal is burnt immediately on entry into the boiler where the temperatures are around 1250-1800 °C. The remaining matter in a coal such as clays and shales which consisting of silica, alumina and iron oxide are rapidly cooled down by the flue gases and then the remaining matter solidifies into fine particles. About 80 % of coal as in the boiler must be removed before the flue gases are discharged to the atmosphere. Generally, the fly ash particles are removed from the flue gases by electrostatic precipitators. This material is called pulverized fuel ash or fly ash. Some matter of the coal ash which sinters to form a coarser materials falls to the bottom of the furnace is called bottom ash. The collection process of fly ash and bottom ash from power station as shown in Fig. 2.4.

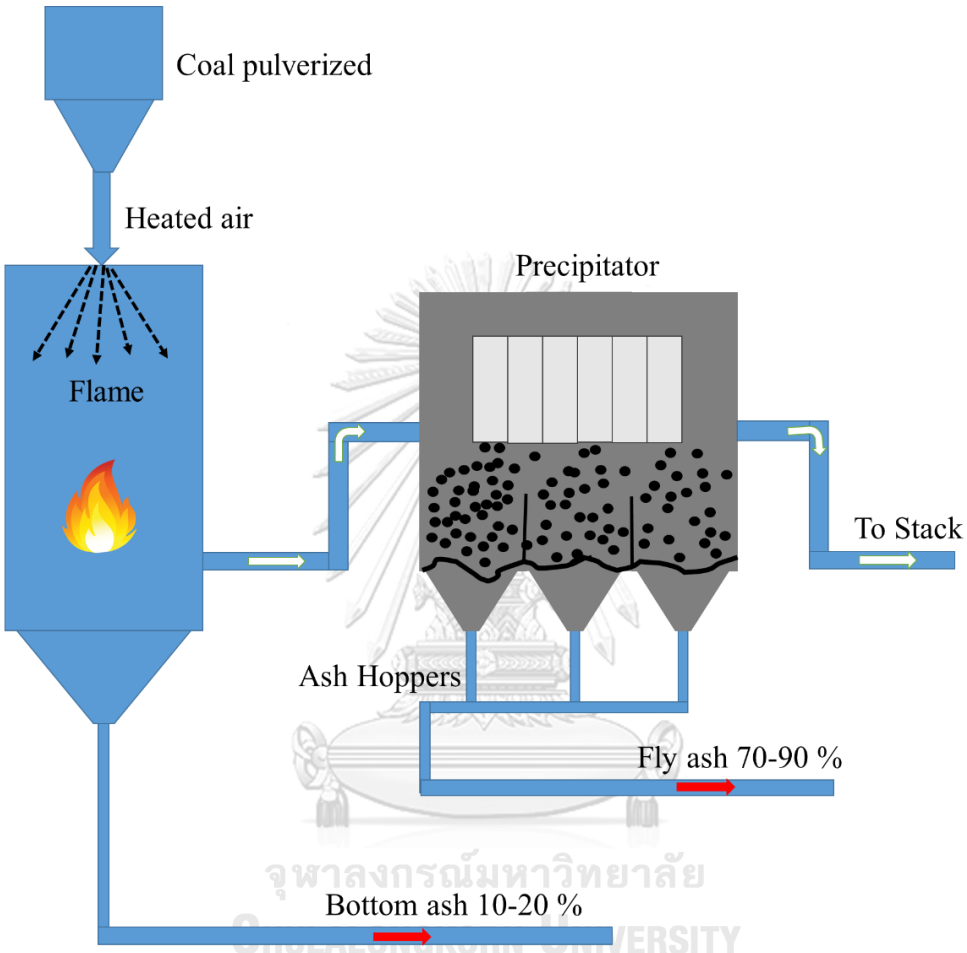

Fig. 2.4 The collection of fly ash and bottom ash from power station

2.2.1.2 Types of fly ash

Type of fly ash is classified based on its chemical composition. American Society for Testing and Materials (ASTM) Specification C 618 defines the chemical composition of Class C and Class F fly ash as following:

- Class C: This is generally derived from sub-bituminous coals and consists primarily of calcium alumino-sulfate glass, as well as quartz, tricalcium aluminate, and free lime (CaO). The class C of fly ash is also referred to as high calcium fly ash because it typically contains more than 10 % CaO.

- Class F: The ashes are typically derived from bituminous and anthracite coals and consist primarily of an alumino-silicate glass, with quartz, mullite, and magnetite also present. The low calcium fly ash is less than 10 % in CaO content.

The oxides values for both types is given in Table 2.4. The composition of fly ash can vary depending on the composition of the coal fuel which stuck after combustion.

Table 2.4 Range of chemical composition for class C and class F of fly ashes.

Composition %	Class C	Class F
SiO_2	18-24.8	47.2-54
Al_2O_3	12.1-14.9	27.7-34.9
Fe_2O_3	6.3-7.8	3.6-11.5
CaO	13.9-49	1.3-4.1
MgO	1.9-2.8	1.4-2.5
SO_3	5.5-9.1	0.1-0.9
Na_2O	0.5-2	0.2-1.6
K_2O	1-3	0.7-5.7

2.2.1.3 Morphology and physical properties of Fly ash

Fly ash consists of glassy, hollow, spherical particles which have thin wall hollow spheres (cenospheres). Fly ash particle occur in round to angular shape, smooth and dense surface. Fly ash consists of silt-sized particles which are generally spherical, typically ranging in size between 10 and 100 μm as shown in Fig. 2.5. The specific gravity of coal fly ash usually ranges from 2.1 to 3.0 and its bulk density is around 0.9-1.6 g/cm^3, while its specific surface area varies from 1 to 2 m^2/g. The color of fly ash is usually dark gray in color, depending on its chemical and mineral constituents. Tan and light colors are typically associated with the high lime content. A brownish color is typically associated with the iron content. A dark gray to black color is typically attributed to an elevated unburned carbon content. Fly ash color is usually very consistent for each power plant and coal source.

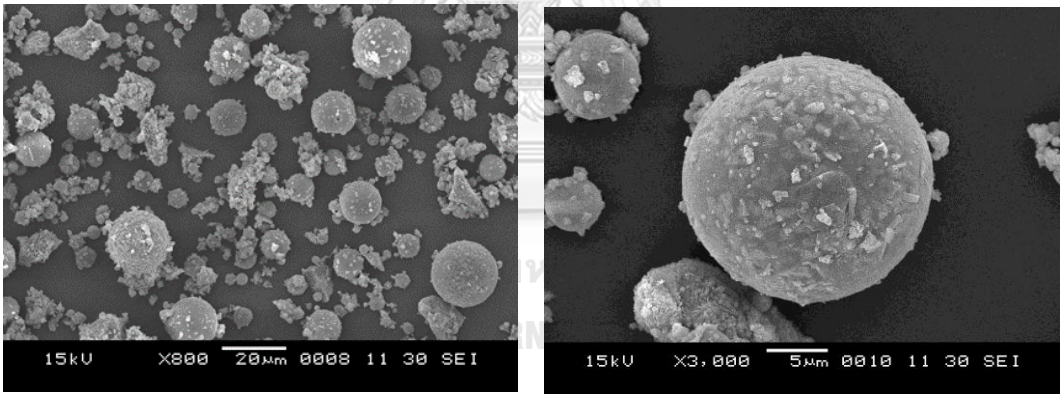

Fig. 2.5 Morphology of fly ash

2.2.1.4 Utilization of fly ash

A large number of technologies have been studied and developed for productive utilization of fly ash. Fly ash can be used as a raw material for many industries and construction. The example of fly ash utilization are presented as follows [68-70]:

- Back filling/stowing of mines: fly ash can be used for stowing of underground mines and backfilling of open cast mines for saving of top fertile soil and precious river sand.

- Building materials such as bricks, blocks, and tiles: fly ash based bricks/blocks/tiles are as well as clay-based conventional building products which result in saving of topsoil. Fly ash bricks are lighter and have higher compressive strength than the clay bricks.

- Cement and concrete: fly ash can enhance the performance of cement and concrete. Moreover, the fly ash improving concrete durability which increase the life of concrete. Portland cement can be replaced by fly ash around 15-30 %.

- Fly ash in agricultural: the advantage of fly ash in agricultural is moisture retaining capacity, soil modifier, nutrients uptake, soil binding, stores carbohydrates and stores carbohydrates. The fly ash is mixed less than 10 % in the soil.

- Water and wastewater treatment: fly ash can be used for adsorbing toxic metal or dyes in domestic and industrial wastewater. Fly ash is able to remove toxic metal by 98-100 %. In addition, fly ash combined with metakaolin can be used to remove chromium in wastewater.

2.2.1.5 Fly ash from Mae Moh coal fired power plant, Lampang, Thailand

Mae Moh coal power plant is a lignite coal-fired thermal power plant generating 2500+ megawatt (MW) per day, consisting of ten 300 MW units. The fly ash and bottom ash are by-products of the process. From total ten of units, six units of the fly ashes are supplied to cement manufacturing companies. Four left units of fly ash are dumped in a disused mine. Summary of consumption and production for the coal power plants is shown in Table 2.5 [71].

Fly ash from Mae Moh Lignite fly ash is class C type following the chemical constituents of ASTM C618 [72]. The maximum sulfur content (SO_4) is 4.0% and the maximum free calcium content is 2.0%. The coal used in power plant is from a natural material which makes the chemical composition of fly ash unstable. The Chemical composition of Mae Moh lignite fly ash from 1985-2001 are presented in Table 2.6 [73-75].

Table 2.5 Summary of consumption and production of Mae Moh coal fired power plant

	units
Energy production (MW)	2500+
Coal consumption	
(tonnes/unit/day)	4100
(thousand tonnes/year)	15000
Fly ash production	
(tonnes/day/unit)	1200
(thousand tonnes/year)	4380

Table 2.6 Chemical composition of Mae Moh lignite fly ash from 1985-2001.

year	composition %								
	SiO_2	Al_2O_3	Fe_2O_3	CaO	MgO	Na_2O	K_2O	SO_3	LOI
1985	12.0	5.9	17.3	39.5	4.6	2.0	0.8	11.5	6.3
1990	37.8	20.5	14.2	17.4	3.3	0.9	2.1	3.9	0.8
1992	40.3	24.0	15.0	11.2	2.8	1.0	2.6	3.1	0.5
1997	41.5	28.1	12.3	10.0	1.2	0.6	3.3	2.0	0.8
2001	39.9	18.2	13.6	17.2	2.4	1.3	2.7	1.5	0.1

2.2.2 METAKAOLIN

Kaolin is a mineral which widely used in paper, filler, and ceramics industries. Kaolin transforms to pozzolanic materials called metakaolin by suitable thermal treatment. Metakaolin can be used to improve mortar and concrete properties. Moreover, metakaolin can be also used for cement in cementitious materials and geopolymer.

2.2.2.1 Dehydroxylation of metakaolin

Metakaolin (MK; $Al_2Si_2O_7$) is a pozzolanic material which is obtained from dehydroxylated of the kaolin clay at temperatures between 500-900 ^{o}C. The clay minerals lose most of the water at temperature around 100-200 ^{o}C and kaolinite becomes calcined due to losing water through dehydroxilization. The dehydroxilization of metakaolin from kaolin is an endothermic process because of the energy required to break the chemically bond of hydroxyl ions. The obtained metakaolin properties and compositions depend on kaolin purities and temperature of the dehydroxylated. To produce a pozzolanic property of metakaolin, the dehydroxilization must be obtained without overheating. Therefore, the temperature for calcined the kaolin is important. The reactions of kaolin clay with different calcined temperature are concluded as following equations [76];

At ~ 500 ^{o}C : $Al_2O_3 \cdot 2SiO_2 \cdot 2H_2O$ (kaolinite) → $Al_2O_3 \cdot 2SiO_2 + 2H_2O$ (MK)

At ~ 925 ^{o}C : $2[Al_2O_3 \cdot 2SiO_2] \rightarrow 2Al_2O_3 \cdot 3SiO_2 + SiO_2$ (silicon-spinel)

At ~ 1100 ^{o}C : $2Al_2O_3 \cdot 3SiO_2 \rightarrow 2[Al_2O_3 \cdot 2SiO_2] + SiO_2$ (1:1 mullite-type phase)

At ~ 1400 ^{o}C : $3[Al_2O_3 \cdot 3SiO_2] \rightarrow 3Al_2O_3 \cdot 2SiO_2 + SiO_2$ (3:2 mullite)

The optimum calcination temperature to produce metakaolin is still different from one research to another. It depends on the raw kaolin for calcination. Normally, the metakaolin prepared by calcination at 500 to 800 °C. The kaolin transforms into metakaolin at a temperature above 500 °C by the structural loss of OH groups and rearrangement of Al and Si atoms. The flakes of kaolinite become more deformed and condensed at 650°C and 800 °C. Metakaolin recrystallizes to octahedral γ-Al_2O_3 and flakes had sintered at a temperature above 900 °C. At 925 °C, kaolin transforms to silicon-spinel and mullite is generated when the temperature above 1400 °C.

2.2.2.2 Morphology and physical properties of metakaolin

The microstructure of metakaolin is plate-like and stacks particle shape. Metakaolin particles size is generally 0.25-5 μm as shown in Fig. 2.6 [76]. Metakaolin color is white to light yellow. Metakaolin contains of 50-55% SiO_2 and 40-45% Al_2O_3 as a major component and other oxides include Fe_2O_3, TiO_2, CaO and MgO are the minor component. The specific gravity of metakaolin is usually 2.6, while its bulk density varies from 0.3-0.4 g/cm^3. The specific surface area of Metakaolin is 15 m^2/g [77].

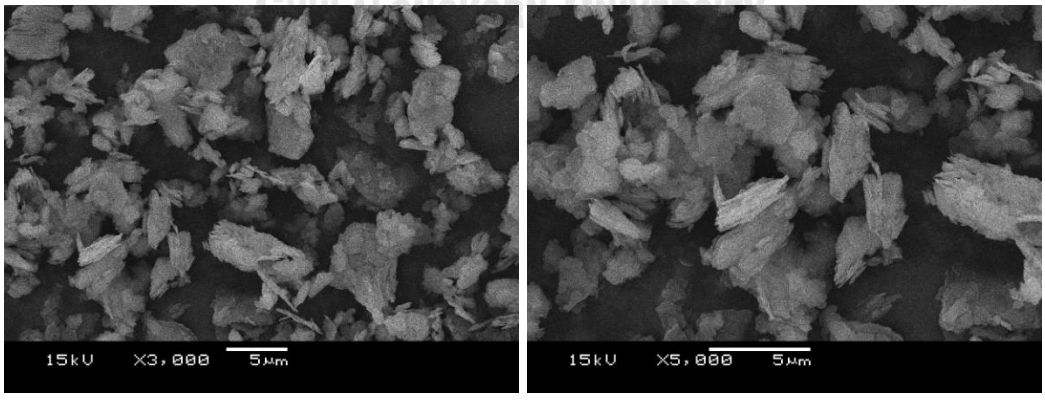

Fig. 2.6 Morphology of Metakaolin

2.2.2.3 Utilization of metakaolin

Metakaolin find its usage in several of concrete applications [77] for example in glass fiber reinforced concrete, in precast concrete for architectural, industrial, civil, and structural purposes, in ferro-cement products and fiber cement, add to improved finish ability, appearance and color, add in pool plasters, mortars, repair material, stuccos and add to get high strength, high performance in lightweight concrete. Furthermore, metakaolin is added in concrete for improved workability, enhanced compressive strength, increased flexural and tensile strengths, improved durability, reduced permeability, increased chemical attack resistance, increased particle packing, reduced efflorescence potential and reduction in alkali–silica reactivity (ASR).

2.2.2.4 Kaolin from Thailand

Kaolin is generally found in mountainous or plateaus from the original source of feldspar. After the rock is eroded from the air, the kaolin is formed in the area. In Thailand, Kaolin is used as raw materials for ceramics industry including pottery, tableware, sanitary ware and refractory. Kaolin resources in many provinces from Thailand such as Ranong, Prachinburi, Lumpang, Narathiwat, Uttaradit, Chiang Rai. Kaolin from each province has different chemical compositions as shown in Table 2.7 [78].

Table 2.7 Chemical compositions of kaolin from various sources in Thailand

Chemical composition (wt %)	Ranong	Narathiwat	Prachinburi	Uttaradit	Chiang Rai	Lumpang
SiO_2	48.75	47.30	48.10	68.56	44.50	59.70
Al_2O_3	34.58	35.72	36.10	19.32	38.20	27.60
Fe_2O_3	0.71	0.38	1.47	2.21	0.80	0.85
TiO_2	0.02	0.20	0.79	0.21	0.20	0.07
CaO	0.07	0.11	0.20	0.05	0.10	0.13
MgO	0.34	1.01	0.14	0.53	-	0.25
K_2O	2.52	1.76	0.16	4.99	0.80	5.85
Na_2O	0.48	0.39	0.13	0.22	-	0.15

2.2.3 POLYETHERSULFONE

In recent years, study of inorganic - polymer composite materials have been developed. Polyethersulfone (PES) was one of polymer to use for fabricate a membrane and fibrous materials with many techniques. In this study, the PES polymer was chosen with phase inversion techniques because it is easily preparation procedure, cheap and use room temperature in the process.

The geopolymer–PES composite is suitable for new adsorbents. It is know that polyethersulfone (PES) [79] is transparent and amorphous in nature. PES is a thermoplastic polymer and classified as a sulfone plastic. In XRD peak of PES, one prominent of amorphous phase shows at $2\theta = 19.9^{o}$. PES polymer has high glass transition temperature (Tg) due to PES has sulfone group in a structure that are so stiff (Tg = 190-230^{o}C). PES structure has a softer ether bond and a harder benzene ring as shown in Fig. 2.7

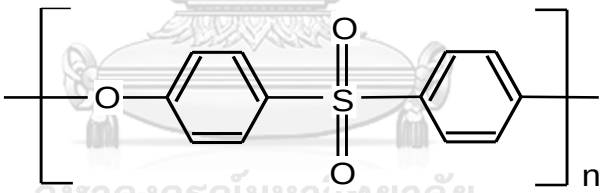

Fig. 2.7 Chemical structure of Polyethersulfone (PES)

Additional properties of PES as following [80, 81]: excellent toughness, thermal stability, dimensional stability, resistance to steam, mineral acids and boiling water, moderate chemical resistance in many alkalis, excellent biology and blood compatibility, good gas permeability and selectivity values, high critical pressure of plasticization, high mechanical strength and low cost and commercially available.

Among the polymers, PES is widely used as a membrane material in many processes for example blood purification, sterilization and pharmaceutical, protein separation, water purification and pre-treatment of reverse osmosis. Nevertheless, PES membrane has limitation about membrane fouling because PES membrane has a high hydrophobic property which can adsorb bacteria and hydrophobic particles or nonpolar solutes onto its surface. Phase inversion method was used for the preparation of membrane. The produced membrane is always symmetric. The membrane structure is related to the composition of PES, solvent and additive, PES solution temperature, and the mixture of non-solvents. The phase inversion method has a variety of general different techniques. Immersion precipitation or non-solvent induced phase inversion is the one of a common method for prepare the PES membrane. In the procedure, the PES was dissolved by a solvent. Then the homogenous polymeric solution was cast or extruded and immersed in a coagulation bath containing methanol or deionized water. The exchange between non-solvent and solvent occurred in the precipitation process. The structure of the membrane is obtained from a combination of phase separation method and mass transfer. This precipitation method can also be called a dry/wet method. The membrane was fabricated in many shapes which used different technique depending on applications such as hollow fiber membrane (extruding, spinning), flat sheet membrane (casting), and composite membrane (dip coating).

2.3 ADSORPTION

Wastewater from domestic household, agricultural and industrial is one of the most pollution which affect environmental factors and humanity [82]. The heavy metals contaminated water has been a serious and long-lasting environmental problem released from a battery, metal plating and smelting manufacturing [83]. Several methods are applied for removal of heavy metal ions including chemical precipitation, reverse osmosis, ion exchange, electrochemical treatment, and adsorption [82]. Adsorption is one of the techniques that are relatively easy and low-cost to use for wastewater treatment [84].

2.3.1 Terms and definitions

Adsorption is one of the basic and main surface phenomena. Adsorption is found to occur in many biological, natural physical, and chemical systems. Adsorption is the adhesion of adsorbate (atoms, ions or molecules) from a gas, liquid or dissolved solid to adsorbent (a surface). The solid which adsorption occurs at the surface is called adsorbent. The adsorbent is usually a porous material with a large specific surface area. The atoms, ions or molecules which adsorbed on an adsorbent surface is called adsorbate. Moreover, desorption is the reverse process of adsorption. The definition of the basic terms of adsorption is shown in Fig. 2.8.

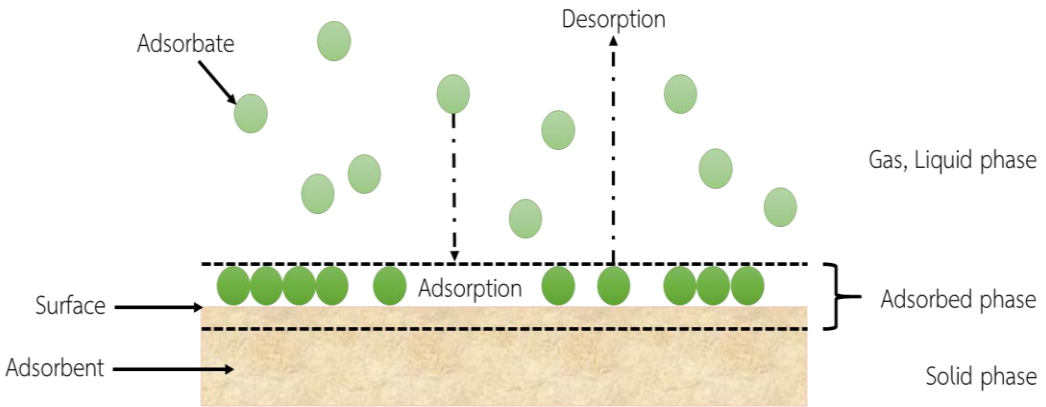

Fig. 2.8 The definition of the basic terms of adsorption

2.3.2 Types of adsorption process

The basic of attractive forces existing between adsorbent and adsorbate, adsorption can be divided into two types: Physical adsorption or Chemical adsorption.

2.3.2.1 Physical adsorption or Physisorption

The force of attraction between adsorbate and adsorbent is intermolecular forces (Van der Waals forces) which is weak and long-range bonding. Physisorption observed multilayer adsorption on a homogeneous surface at equilibrium pressure (Fig. 2.9). BET isotherm can be used to model adsorption equilibrium. This adsorption has low enthalpy about 5-50 kJ/mole and takes place between all molecules on any surface at a lower temperature than the boiling point of adsorbate. Moreover, this adsorption process is reversible and not specific. The process of physisorption decreases when the temperature increases.

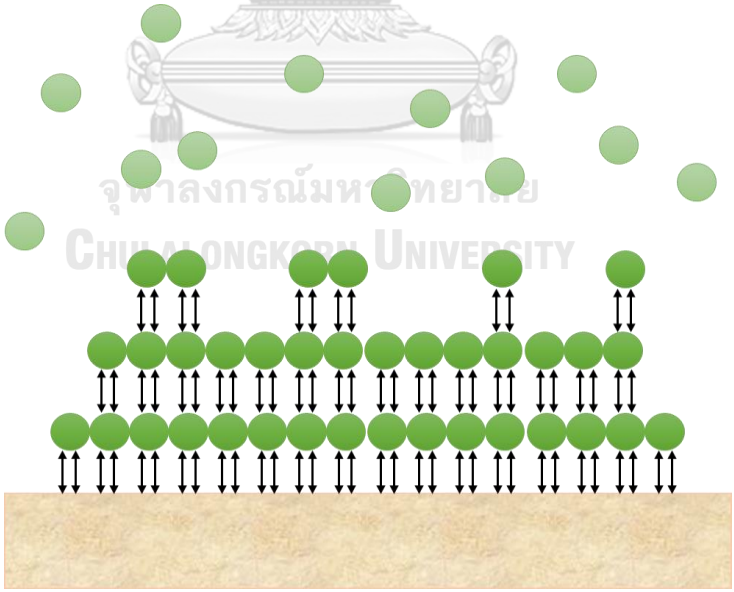

Fig. 2.9 Physical adsorption process

2.3.2.2 Chemical adsorption or Chemisorption

The force of attraction between adsorbate and adsorbent is chemical forces of attraction or chemical bond which has strong and short-range bonding. Chemisorption observed monolayer adsorption on a homogeneous surface at equilibrium pressure (Fig. 2.10). Langmuir isotherm can be used to model adsorption equilibrium. This adsorption has high enthalpy about 50-500 kJ/mole and takes place with the formation of adsorbate monolayer on adsorbent at all temperature. Furthermore, this adsorption process is irreversible and highly specific. The process of chemisorption at first increases and then decreases with the temperature increases.

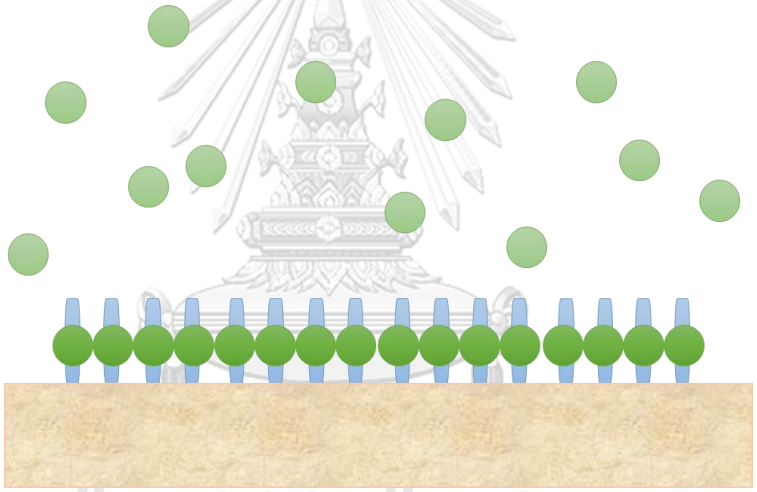

Fig. 2.10 Chemical adsorption process

2.3.3 Factors affecting adsorption

- Surface area

Adsorption occurs on a surface, therefore, the total surface area which is available for adsorption can be defined by the specific surface area of adsorbent. The solid is more finely and more porous make a greater adsorption amount.

- Nature of adsorbate and adsorbent

The number of ions or gas adsorbed depends on the nature of adsorbate and adsorbent. For example, the liquefiable gas (CO_2, NH_3, Cl_2, HCl, SO_2 etc.) are more adsorbed than permanent gases (H_2, O_2, N_2 etc.) because the liquefiable gas has greater Van Der Waals force or attraction of molecule force.

- Pressure or concentration

In the reversible adsorption, the concentration of solute increases or pressure of a gases vapor increase affected higher adsorption in most cases.

- Hydrogen ion concentration

The hydroxide ions and hydrogen ions are quite strongly adsorbed affected the adsorption of other ions.

- Temperature

The removal of heavy metal increases at a higher temperature. Very different temperature affected on adsorption in water and wastewaters.

- Mixed solutes

In purification water and wastewaters, the adsorbed materials will be the mixture of many compounds. The compounds may enhance or may interface or may act independently with each other which effect to adsorption.

2.3.4 Adsorption isotherm

The adsorption technique is generally used for removal of pollutant in aqueous media. The most important information for an understanding of an adsorption process is adsorption equilibrium information. An understanding of adsorption isotherms is important critical to improving adsorption system design and adsorption mechanism pathways. Linearization is created from inherent bias, several error functions have been studied to fix the problems. The evolution of computer technology is also used for nonlinear isotherm modeling [85].

2.3.4.1 Langmuir adsorption isotherm

One of the most common isotherm equations in solid-liquid systems is Langmuir adsorption equation. This equation is valid for monolayer adsorption onto a surface with a finite number of identical sites which are homogeneously distributed over the adsorbent surface. The general form of the Langmuir equation is as follow:

$$qe = \frac{qmK_LCe}{(1+K_LCe)} \quad (1)$$

where C_e is the equilibrium concentration of heavy metal ions (mg/L)

q_e is the amount of heavy metal ions adsorbed per unit mass of the adsorbent (mg/g)

K_L is the Langmuir adsorption constant (L/mg)

q_m is the maximum amount of per unit mass of adsorbent to form a complete monolayer on the surface (mg/g)

The linear form of this equation is as follow:

$$\frac{Ce}{qe} = \frac{1}{qmKL} + \frac{Ce}{qm} \quad (2)$$

Langmuir isotherm can be expressed using a dimensionless constant called the separate factor (R_L) as follow:

$$R_L = \frac{1}{1+K_L C_0} \quad (3)$$

where C_O is initial concentration of adsorbate (mg/g)

K_L is Langmuir adsorption constant (L/mg)

The R_L values indicates the adsorption to be linear when R_L=1, unfavorable when R_L>1, favorable when 0<R_L<1 and irreversible when R_L=0.

2.3.4.2 Freundlich adsorption isotherm

The Freundlich isotherm is an empirical model which is used for non-ideal sorption process and relate to heterogeneous adsorption surface. It can be expressed by the following equation:

$$q_e = K_F C_e^{1/n} \quad (4)$$

where q_e is the quantity of the solute adsorbed per unit weight of adsorbent (mg/g)

C_e is the equilibrium concentration of the adsorbing compound (mg/L)

K_F ($mg^{1-(1/n)} g^{-1} L^{1/n}$) is the adsorption capacity when metal ion equilibrium concentration equals to 1

n is the degree of dependence of adsorption on equilibrium concentration

When this equation is expressed in logarithmic form, a linear relationship is obtained equation:

$$\ln(q_e) = \ln(K_F) + \frac{1}{n} \ln C_e \quad (5)$$

2.3.4.3 Redlich-Peterson (R-P) adsorption isotherm

Redlich-Peterson adsorption isotherm is a combine of Langmuir and Freundlich isotherms. This isotherm model is an empirical isotherm and combines the

element from both Langmuir and Freundlich equations; so the adsorption mechanism is not followed ideal monolayer adsorption. This isotherm is expressed as follow:

$$q_e = \frac{K_{RP}\, C_e}{1+aC_e^g} \qquad (6)$$

where q_e is the quantity of the solute adsorbed per unit weight of adsorbent (mg/g)

C_e is the equilibrium concentration of the adsorbing compound (mg/L)

K_{RP} is Redlich constant (L/g)

a is Redlich constant $[(L/mg)^g]$

g is exponent which lies between 1 and 0

The linear form can be expressed as follow:

$$\ln \frac{Ce}{q_e} = g\ln c_e - \ln K_{RP} \qquad (7)$$

2.3.4.4 Dubinin-Radushkevish (D-R) adsorption isotherm

D-R isotherm is an empirical adsorption model that is generally applied to express adsorption mechanism onto heterogeneous surfaces. D-R isotherm used to describe the physical adsorption and this isotherm is more general than Langmuir isotherm. It rejects the homogeneous surface or constant adsorption potential. Moreover, D-R isotherm is based on Polanyi's potential theory. The form of D-R equation is expressed as follows:

$$\ln q_e = \ln q_m - \beta\varepsilon^2 \qquad (8)$$

$$\varepsilon = RT\ln\left(1+\frac{1}{C_e}\right) \qquad (9)$$

where q_e is the quantity of the solute adsorbed per unit weight of adsorbent (mg/g)

q_m is the adsorption capacity (mol/g)

β is the D-R constant (mol^2/kJ)

ε is the Polanyi potential

R is ideal gas constant (8.31 J/mol-k)

T is absolute temperature (K)

2.3.5 Modelling of kinetic study

The systems of kinetics can reveal the adsorption mechanism. Modelling of kinetic was study of determine the mechanism which is include external diffusion, internal diffusion and chemical reactions. To identify the mechanism, the pseudo first order, pseudo second order and intraparticle diffusion models were used to evaluate of time dependent data [82, 86, 87].

2.3.5.1 Pseudo first order model and Pseudo first order model

The pseudo first order rate equation by the following expression is expressed as:

$$\ln(q_e - q_t) = \ln q_e - k_1 t \qquad (10)$$

Pseudo second order model, if the rate of sorption in linear form is a second order chemisorption mechanism kinetic and equation is expressed as:

$$\frac{t}{q_t} = \frac{1}{k_2 q_e^2} + \frac{1}{q_e} t \qquad (11)$$

where qe is adsorption capacity at equilibrium (mg/g)

qt is adsorption capacity at any time (mg/g)

t is time (min)

k_1 is rate constant of pseudo first order sorption (min^{-1})

k_2 is rate constant of pseudo second order sorption (g/mg min)

2.3.5.2 Intraparticle diffusion model

The intraparticle diffusion model can be written equation as:

$$q_t = K_p t^{1/2} + C \qquad (12)$$

where qt is adsorption capacity at any time (mg/g)

k_p is intraparticle diffusion rate constant (mg/g $h^{1/2}$)

t is time (h)

C is the intercept in linear graph (mg/g)

2.4 RELATED RESEARCH

M.S. Al-Harahshen et al.[87] evaluated the capacity of a highly amorphous geopolymer for removing copper ions from aqueous solution. The amorphous geopolymer was synthesized from waste fly ash. The raw fly ash was collected from Rajhi Cement plant, Jordan. The fly ash powder was mixed with NaOH (14 M) at a mass ratio of FA: NaOH = 4:3. Then the paste was mixed until homogeneity for 5-10 min, poured into a plastic cylinder and cured at 105 °C for 2 h. After that, the synthesized geopolymer was left at room temperature for 3 days. The geopolymer sample was crushed, ground and sieved to particle size less than 200 μm. The phases of geopolymer powder was examined by XRD analysis. The XRD pattern of raw material and geopolymer were shown in Fig. 2.11. From XRD pattern, the original fly ash contained major phases of quartz, hematite and mullite, and cristobolite, plagioclase was found as minor phase. Moreover, the main chemical composition of both fly ash and the geopolymer are silica, alumina, iron oxide, calcium oxide, and magnesium oxide. For study removal of Cu^{2+} ions, the effect of pH, geopolymer dose, contact time, temperature and initial Cu^{2+} concentration were evaluated. For effect of pH (Fig. 2.12-a), when pH was increased from 1 to 6, the geopolymer adsorbed more Cu^{2+} from 5.6% to 88.21%. Furthermore, the dosage amount from 0.03 g to 0.15 showed the removal efficiency increased from 45% to 88.2% as seen in Fig. 2.12-b. The contact time varies from 5 to 180 was considered to study the effect of contact time on Cu^{2+} ions removal. A contact time at 120 min was used in this study. The effect of temperature on Cu^{2+} removal was studied at 25-45 °C. The result indicated that the adsorption of Cu^{2+} on the geopolymer reached to the maximum value at 45 °C. For the last factor that affects removal Cu^{2+} ions was initial concentration of Cu^{2+} ions (Fig. 2.12-c). The result showed that the adsorption efficiency dropped when the initial concentration of Cu^{2+} was increased. Moreover, the kinetics data were fitted well to the pseudo-second order

and Langmuir isotherm model was given to be more applicable than Freundlich isotherm model.

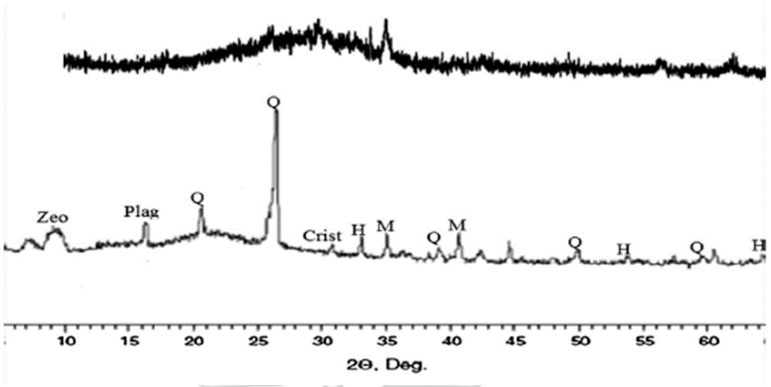

Fig. 2.11 XRD patterns of raw fly ash (upper graph) and fly ash based geopolymer (lower graph)
(Q-quartz, M-mullite, H-hematite, Zeo-zeolite, Plag-plageoglase, Crist-Cristobolite)

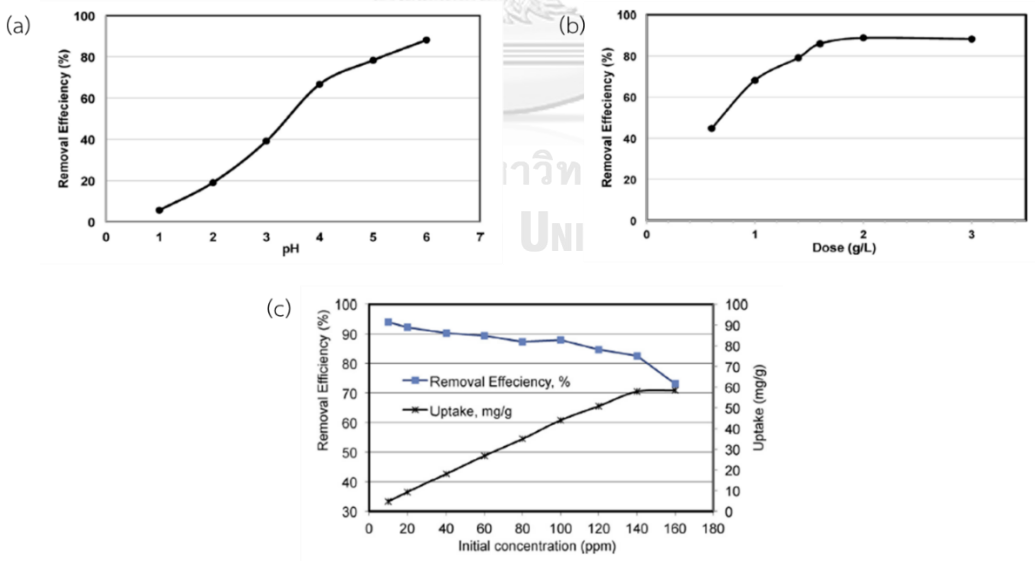

Fig. 2.12 (a) Effect of pH, (b) adsorbent dose, (c) the initial concentration on Cu^{2+} removal efficiency

I. Kara et al.[86] studied metakaolin based geopolymer (MKG) as an adsorbent for removal Zn^{2+} and Ni^{2+} from aqueous solution. Geopolymer with compositions of SiO_2/Al_2O_3 = 3.2, Na_2O/SiO_2 = 0.2, Na_2O/Al_2O_3 = 0.7 and H_2O/Na_2O = 13.8 were synthesized. Metakaolin was added in alkali solution and mixed for 15 min. The geopolymer paste was poured into HDPE mold and cured at 80 °C for 2 days. After that geopolymer sample was left at room temperature for 3 days and kept at 80 °C for 2 days. Then the geopolymer was ground and sieved to obtain particle size at 150 μm. The MKG specific surface area was found to be 39.24 m^2/g by BET analysis. The XRD pattern of MKG is shown in Fig. 2.13. The XRD pattern showed board hump peak which is characteristic of the amorphous material and had a minor peak of quartz. For adsorption tests, the effect of pH, geopolymer dose, contact time, temperature and initial concentration were studied as a parameter. The geopolymer amount affected the adsorption of Zn^{2+} and Ni^{2+} ions onto MKG. The result was seen that the Zn^{2+} and Ni^{2+} ions removal increased with an increase in the dose of MKG (Fig. 2.14). Over 2.0 g/L in Zn^{2+} solution and 3.2 g/L of an amount of MKG, the adsorption efficiency was not significantly changed. The effect of pH on MKG adsorption efficiency was investigated and shown in Fig. 2.15-a. The pH of the solution was varied from 2 to 8. It was seen that the removal of Zn^{2+} and Ni^{2+} ions was increased until pH = 4 and after this value, no significant change was found. In order to determine the effect of temperature, the solution was carried out at 10-25 °C and the adsorption capacity as illustrated in Fig. 2.15-b. The adsorption of Zn^{2+} and Ni^{2+} ions onto MKG slightly increased when the temperature of the solution was increased from 10 to 25 °C. In addition, the adsorption capacity of Zn^{2+} and Ni^{2+} ions on the effect of contact time was determined in Fig. 2.15-c. At the initial stage, the adsorption was rapidly adsorbed and it became slower at neat the equilibrium. For kinetics and model of adsorption, the pseudo-second order kinetics model and the Langmuir isotherm model were fitted well to the equilibrium data for Zn^{2+} and Ni^{2+} ions.

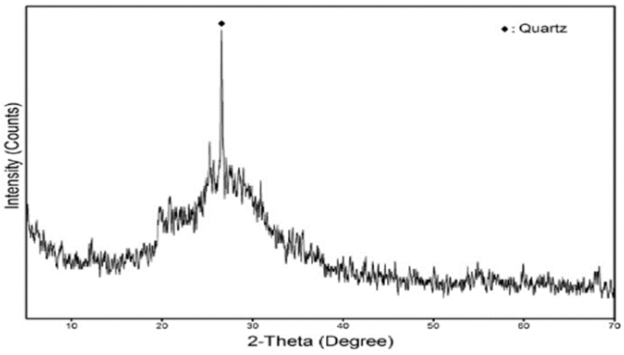

Fig. 2.13 XRD pattern of metakaolin based geopolymer (MKG)

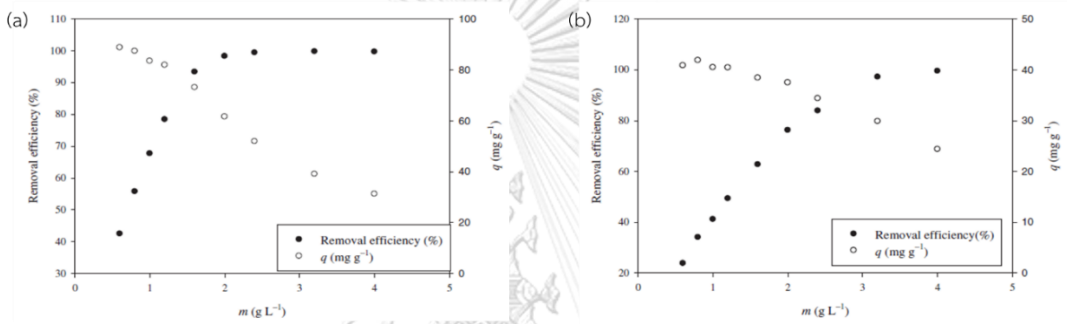

Fig. 2.14 Effect of MKG amount on the adsorption of (a) Zn^{2+} and (b) Ni^{2+} ions

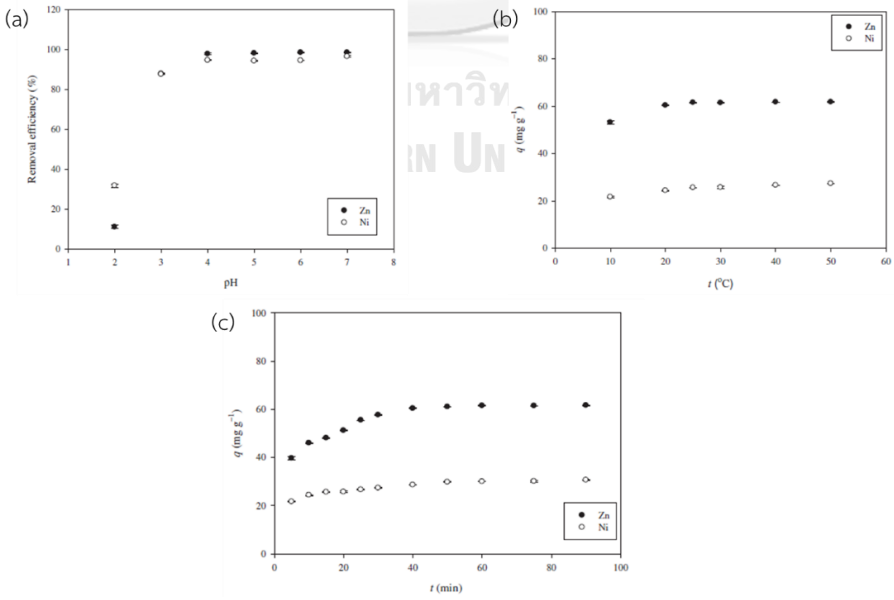

Fig. 2.15 Effect of (a) pH solution, (b) temperature and (c) contact time on the adsorption of Zn^{2+} and Ni^{2+} ions

K. Nakamoto et al.[88] developed mordenite zeolite-polyethersulfone composite fiber. The polyethersulfone (PES) was dissolved by *N*-Methyl-2-pyrrolidone (NMP) as a solvent to prepare the solvent containing 30% of PES. Then, the mordenite zeolite powder was added to PES-NMP solution at concentration 10, 20, 30 and 40 wt%. After the mordenite zeolite-polymer mixed solution was stirred for 24 h, the solution was extruded into a coagulation bath to be a composite fiber. The PES, CF-27, CF-46, CF-59 and CF-69 were used to call the amount of mordenite zeolite powder in fibers at 0, 27.0, 45.5, 58.8 and 69.0 wt%, respectively. The BET surface area of the fibers increased with an increased loading of mordenite zeolite powder. The maximum surface area value (145 m^2/g) was showed in CF-69 fiber. For microstructure of fiber, the finger-like structure appeared in PES fiber and this structure decreased with the higher amount of mordenite zeolite powder. Moreover, the board hump peak indicated an amorphous polymer was seen at 18 deg in 2θ of PES and a crystalline phase of mordenite zeolite following JCPDS: 00-006-0329 was a minor phase in others fiber (Fig. 2.16). A removal of Pb^{2+}, Cd^{2+}, Cu^{2+} and Ni^{2+} ions in aqueous solution on mordenite zeolite powder and composite fibers were measured and shown in Fig. 2.17. The adsorption amount of heavy metal on mordenite zeolite powder was rapidly increased at the early stage and became constant after 6 h (Fig. 2.17-a). The Pb^{2+} ions in aqueous solution were highly adsorbed with mordenite zeolite powder. In composite fiber, the adsorption capacity increased with an increasing amount of mordenite zeolite powder in fiber. The CF-69 fiber was the most excellent adsorbed Pb^{2+}, Cd^{2+}, Cu^{2+} and Ni^{2+} ions in aqueous solution. Furthermore, all of the mordenite zeolite composite fiber adsorbed metal cations in order $Pb^{2+}>Cu^{2+}>Cd^{2+}>Ni^{2+}$. Langmuir adsorption isotherm was fitted well with experimental adsorption isotherms of heavy metal on to mordenite zeolite powder and composite fibers.

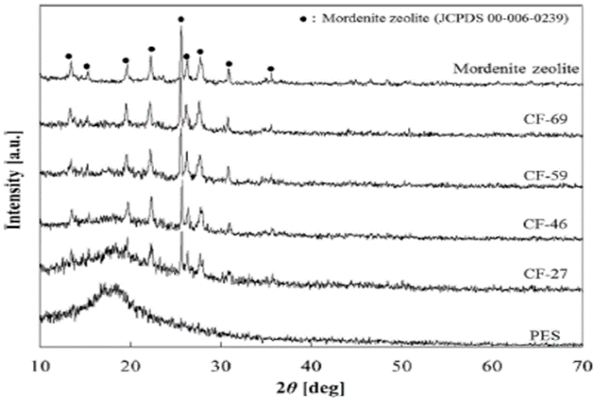

Fig. 2.16 XRD pattern of mordenite zeolite powder and composite fibers

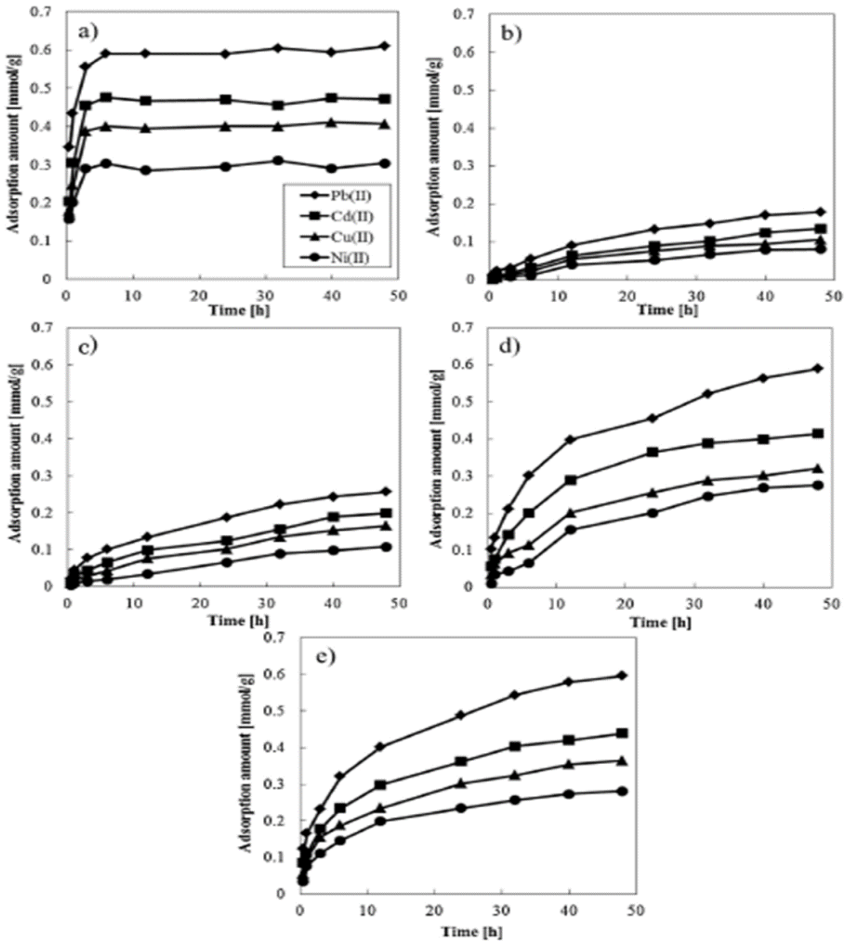

Fig. 2.17 The adsorption capacity of (a) mordenite zeolite powder, (b) CF-27, (c) CF-46, (d) CF-59 and (e) CF-69 for Pb^{2+}, Cd^{2+}, Cu^{2+} and Ni^{2+} ions in aqueous solution

CHAPTER 3

EXPERIMENTAL PROCEDURE

In this study, the fly ash from Mae Moh power plant, Lumpang province and kaolin from Ranong province in Thailand were chosen as a pozzolanic material to synthesize fly ash based geopolymer and metakaolin-based geopolymer. After synthesized geopolymer, fly ash based geopolymer and metakaolin based geopolymer powder were fabricated to be composite fiber with PES polymer. PES polymer was used to form the geopolymer powder to be the fibrous adsorbent materials. The powder and composite fiber geopolymer were studied as an adsorbent for adsorption of heavy metal ions in wastewater. The materials and experimental procedure were explained as the followings:

3.1 MATERIALS AND CHEMICALS

- Fly ash, Mae Moh power plant, EGAT
- Ranong Kaolin, MRD-ECC Co., Ltd.
- Sodium silicate solution- CT-38 (Na_2SiO_3), Chemmin Co. Ltd.
- Sodium hydroxide pellet (NaOH), Ajax Finechem Pty Ltd.
- Polyethersulfone - Ultrason E2010 (PES, MW=50,000), BASF Co. Ltd.
- N-Methyl-2-pyrrolidone (NMP), Nacalai Tesque Inc.
- Lead (II) Nitrate ($Pb(NO_3)_2$)), Nacalai Tesque Inc.
- Copper (II) Nitrate ($Cu(NO_3)_2 \cdot 3H_2O$), Nacalai Tesque Inc.
- Nickel (II) Nitrate Hexahydrate ($Ni(NO_3)_2 \cdot 6H_2O$), Nacalai Tesque Inc.
- Cadmium (II) Nitrate Tetrahydrate ($CdH_8N_2O_{10}$), Nacalai Tesque Inc.
- Distilled water

3.2 PREPARATION OF MATERIALS

- Fly ash

Fly ash is use as received.

- Metakaolin

Metakaolin was obtained by calcination of Ranong kaolin which is from the local kaolin mines in Ranong province, Thailand. Ranong kaolin was ground and then dried at 110 °C to dehydrate water for 24 h. After that, the kaolin was screened through sieve size No.100 (aperture of 150 μm) and calcined at 700 °C for 6 h to transform kaolin to metakaolin completely.

- Alkali Solution

Sodium hydroxide pellet was dissolved in distilled water with a concentration of 10 molars and left the solution for 24 h. Then, sodium hydroxide solution and sodium silicate solution with 31.38% SiO_2, 10.15% Na_2O and 58.47% H_2O were mixed together with the 2.5 ratios of Na_2SiO_3: NaOH and left the solution until reached room temperature.

- PES/NMP solution

The polyethersulfone (PES) was added in N-Methyl-2-pyrrolidone solution (NMP) with containing 30 wt% of PES concentration and stirred for 24 h until PES was clearly dissolved in NMP solution.

3.3 GEPOLYMER PREPARATION FOR HEAVY METAL ADSORPTION

3.3.1 Geopolymer powder

- Fly ash based geopolymer powder

The composition to synthesis geopolymer of this study was related with our previous research [89]. Fly ash was mixed with the prepared alkali solution for 5 mins to achieve good homogeneity. The solid fraction in geopolymer mixture was 65 wt%. After mixing, the liquid paste was poured into a plastic mold. Then the fly ash geopolymer was cured at 60 ^{o}C for 24 h and left at 25 ^{o}C for 6 days. The geopolymer sample was ground, sieved through 100 mesh and washed with distilled water until the pH of wash water was kept at 7±0.5. Afterward, geopolymer powder was cured in a conventional oven at 80 ^{o}C for 24 h.

- Metakaolin based geopolymer powder

Metakaolin and alkali solution were mixed for 5 mins (solid/liquid = 1.86). After that, the obtained paste was cast into cube mold. The geopolymer was formed after curing at 60 ^{o}C for 24 h and keeping at 25 ^{o}C until the 7th curing day. Upon removal from the mold, the geopolymer was crushed and sieved through 100 mesh to control a particle size range. Then the geopolymer powder was washed several times until washed water was reached to pH 7±0.5. The washed geopolymer powder was cured at 80 ^{o}C for 24 h in a conventional oven.

3.3.2 Geopolymer composite fiber

- Fly ash based geopolymer fibers

The phase inversion method was used to fabricate the geopolymer composite fiber. The PES (Polyethersulfone) was dissolved by a NMP (*N*-Methyl-2-prrolidone) which was a solvent and mixed with the powder. Then the homogenous polymeric solution was extruded and immersed in a coagulation bath containing deionized water. The exchange between NMP and water occurred in the precipitation process. The phase of solution was changed from liquid to solid phase. In this study, the Fly ash based geopolymer powder was added at concentrations of 20, 40, and 60 wt% and stirred with PES/NMP solution for 24 h until the slurry was homogeneity. After preparing the fly ash based geopolymer-polymer mixed slurry, the slurry was extruded through a cylindrical needle with 0.6 cm needle diameter of air pressure at 0.42 MPa. The extruded slurry of each batch was dropped into a 25 ^{o}C of water in coagulation bath and then the composite fiber was immersed in water coagulation bath for 24 h. After that, the composite fiber was boiled at 80 ^{o}C for 8 h to remove residual NMP. Finally, the composite fiber was dried vacuum at 60 ^{o}C for 24 h. The fabrication process of geopolymer fiber is shown in Fig. 3.1.

- Metakaolin based geopolymer fibers

Metakaolin based geopolymer composite fibers were also fabricated the same process as fly ash based geopolymer composite fibers. The sample of PES and geopolymer composite fiber as shown in Fig. 3.2.

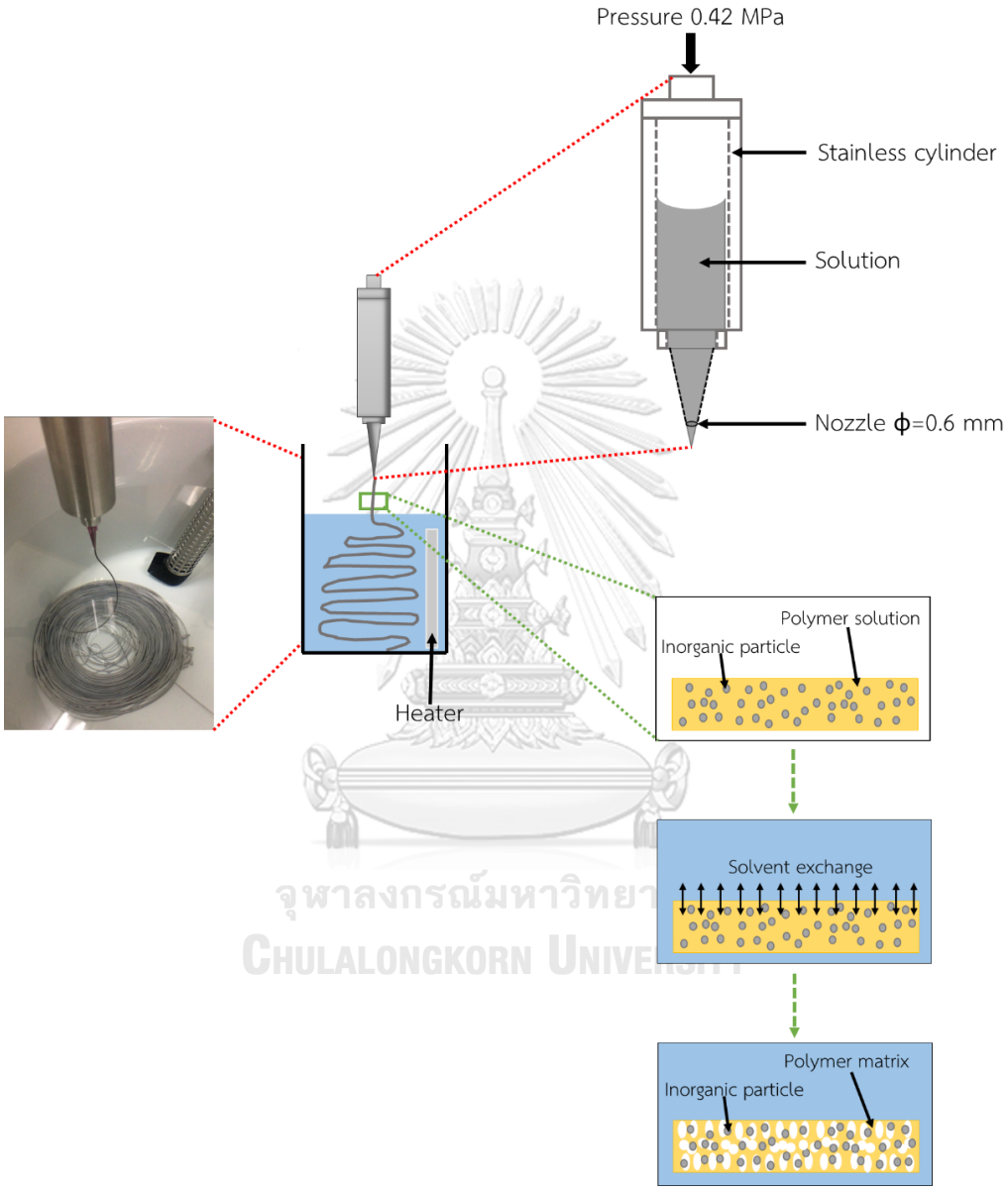

Fig. 3.1 The fabrication process of geopolymer fiber

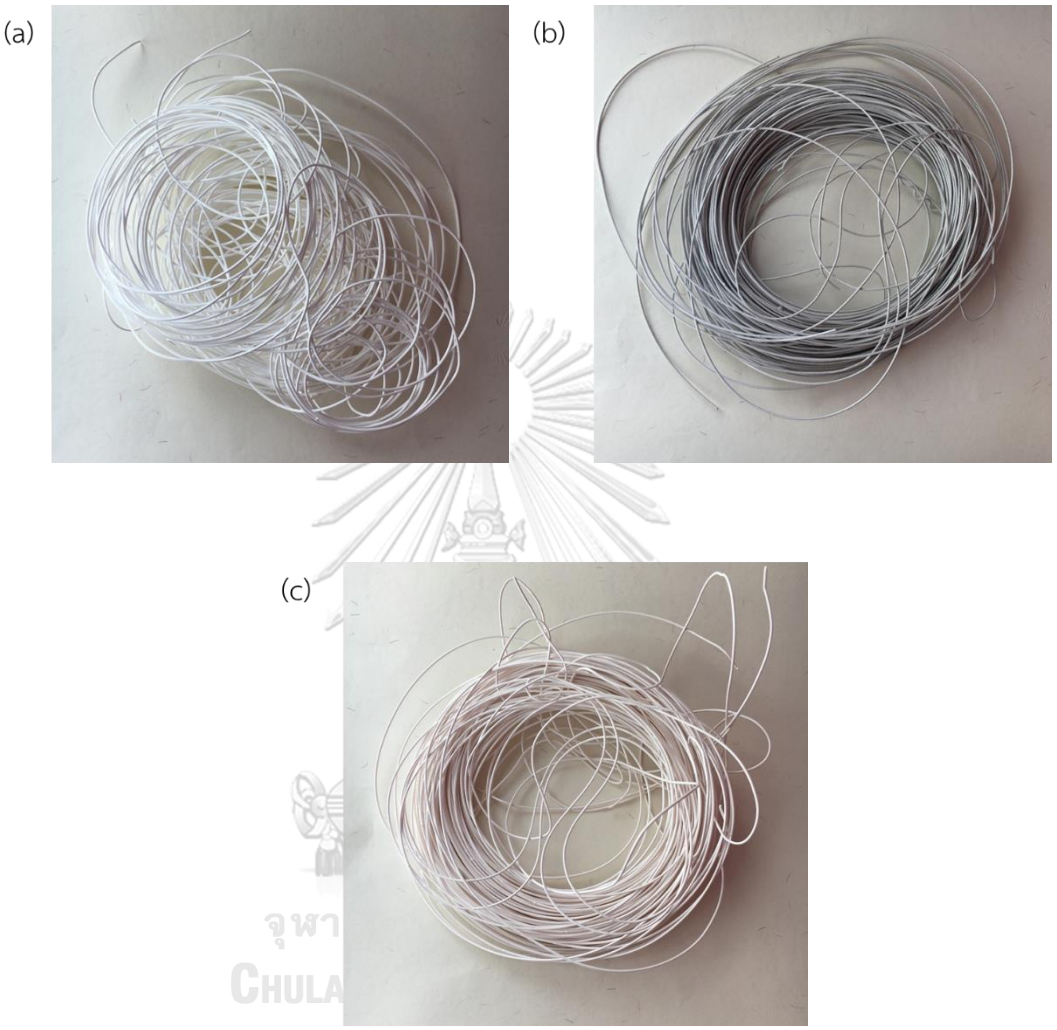

Fig. 3.2 The sample of (a) PES fiber, (b) FAG composite fiber and (c) MKG composite fiber

3.4 CHARACTERIZATION OF RAW MATERIALS AND GEOPOLYMER SAMPLES

3.4.1 Particle size distribution analysis

Laser light scattering technique was used to investigate the particles size of raw materials and geopolymer powder by Mastersizer 2000; Malvern Instruments Corp, United Kingdom. The powder was dispersed in a liquid media before a test. In a media, the laser beam passes through the particles and the angle scatter light of the particles is inversely proportional to their size. The Fraunhofer theory and Mie theory were approximated of large and small particles size, respectively.

3.4.2 Chemical composition analysis

The composition of raw materials and geopolymer powder were performed by X-ray fluorescence (XRF) spectrometer (ZSX Primus II; Rigaku Corp., Japan). The powder was pressed into aluminium ring to be a pellet. XRF spectrometry detects X-ray fluorescence which is released from elements of a sample. X-ray tube generates X-ray and then passes through the sample. The photons discharging (fluoresced) in different energy which can indicate the element occur and detect by a detector.

3.4.3 Phase analysis

The mineral phases were analyzed by X-ray diffraction (Smart lad; Rigaku Corp., Japan) of Cu-K_{α} radiation at 10-60° 2θ deg with 40 kv, 30 mA and a rate of 2 degree/min. X-ray diffraction pattern was recorded by using Bragg's law and matched the peak of each mineral with Joint Committee on Powder Diffraction Standard files (JCPDS).

3.4.4 Morphology

Morphological structures of samples were investigated using scanning electron microscopy (SEM, JSM-6480LV; JEOL Ltd., Japan) at 15 kV of accelerating voltage. The element distribution of fibers was also studied by an Energy dispersive X-ray spectroscopy (EDX, INDA x-sight). The morphology of starting materials and geopolymer powder were observed. For geopolymer composite fiber, the fibers were dipped into liquid nitrogen to freeze it and were broken at a half of fiber to observe the cross-sectional surface.

X-ray computed tomography (X-ray CT) is a 3D imaging technique that has been used to investigate morphology inside of materials. For the high-resolution micro-CT (HRM-CT), the geopolymer fibers were cut to 3 cm and were measured using scanning rotation steps of 0.1 deg. HRM-CT was used to observe morphology in geopolymer fibers.

3.4.5 Tensile strength

For the study the resistance of fibers to breaking while being pulled, the composite fibers were measured by a load measurement device (LTS-500N-S20; Minebea Co. Ltd., Japan). The gauge length of samples was 30 mm with crosshead of 1.5 mm/s. Each sample was tested with five specimens and each specimen had 5mm of length. The diameter of the sample was measured by using a micrometer. The tensile strength is calculated by following;

$$\text{Tensile strength (Pa)} = \frac{\text{Load (N)}}{\text{Area of a cross section } (m^2)}$$

3.4.6 Surface area analysis

The surface area of samples was analyzed by BET analysis (Tristar II 3020; Micromeritics Instrument Corp., Japan) with a nitrogen gas adsorption. The samples were evacuated for 12 h at 80 °C for 24 h before measurements. Measurements were performed at -196 °C and the N_2 gas adsorption data of the samples were evaluated surface area using the Brunauer-Emmett-Teller (BET) equation.

3.5 HEAVY METAL ADSORPTION TEST OF GEOPOLYMER POWDER AND GEOPOLYMER COMPOSITE FIBERS

3.5.1 Preparation of heavy metal ion solutions

Stock solutions of Pb (II), Cu (II), Cd (II) and Ni (II) at concentration of 1000 mg/L were prepared by dissolving appropriated amounts of $Pb(NO_3)_2$, Cu $(NO_3)_2 \cdot 3H_2O$, $CdH_8N_2O_{10}$ and Ni $(NO_3)_2 \cdot 6H_2O$ in distilled water. The concentrations at 10, 20, 40, 60, 80, 100 and 120 mg/L multi- and mono – heavy metal solution were prepared by diluting from the stock solutions. Nitric acid (HNO_3) solution at 0.1 M was used to adjust the pH values for each batch experiments.

3.5.2 Batch adsorption studies

- Effect of geopolymer dosage

Variable geopolymer powder masses (0.02-0.14 g) and geopolymer composite fiber masses (0.05-0.5 g) were added to a 40 ml of 20 mg/L multi- and mono - heavy metal solutions containing Pb^{2+}, Cd^{2+}, Cu^{2+} and Ni^{2+} at a fixed temperature (25 °C), pH of the solution (5) and shaking time (120 min). The uptake percentage and adsorption capacity are calculated for each dose.

- Effect of pH

In order to study effect of pH on the adsorption of heavy metal ions, 40 ml of 20 mg/L multi- and mono - heavy metal solutions containing Pb^{2+}, Cd^{2+}, Cu^{2+} and Ni^{2+} is used at different pH values (1-5) at a temperature of 25 °C, 0.1 g of sample and shaking for 120 min. For each pH, the uptake percentage and adsorption capacity are determined.

- Effect of contact time

The effect of contact time on the adsorption of 20 mg/L multi- and mono - heavy metal ions was investigated by different shaking time of heavy metal solution from 5 to 180 min (geopolymer powder) and 5 min to 72 h (geopolymer fiber) at 5 pH value, 0.1 g of sample and the solution temperature of 25 °C. For each contact time, then the uptake percentage and adsorption capacity are calculated.

- Effect of temperature

A 40 ml of 20 ppm multi- and mono - heavy metal solution containing Pb^{2+}, Cd^{2+}, Cu^{2+} and Ni^{2+} was shaken at a temperature of 25 °C for 120 mins with 0.1 g of sample and at different temperature (25, 35 and 45 °C). The uptake percentage and adsorption capacity are calculated for each temperature.

- Effect of initial concentration

The effect of the different initial concentration (10-120 mg/L) of multi- and mono - heavy metal ions was investigated. The 0.1 g of sample was added to the solution. The solution was then shaken for 120 mins at 5 pH values with a temperature of 25 °C. The uptake percentage and adsorption capacity are determined for each initial concentration.

After tested, the solution was characterized by using atomic absorption spectroscopy (AAS). The removal efficiency (*E*) was calculated using the equation:

$$\text{Removal efficiency } (E, \%) = \frac{C_i - C_{eq}}{C_i} \times 100\%$$

where C_i is initial concentration of the heavy metal solution (mg/L)

C_{eq} is remaining equilibrium concentration (mg/L)

Moreover, the amount of metal ions adsorbed at equilibrium (q_e) was calculated using equation:

$$q_e \text{ (mg/g)} = \frac{(C_i - C_{eq})\, V}{C_i}$$

where C_i is initial concentration of the heavy metal solution (mg/L)

C_{eq} is remaining equilibrium concentration (mg/L)

V is the volume of solution (L)

3.6 EXPERIMENTAL DIAGRAM

3.6.1 Synthesis fly ash based geopolymer powder

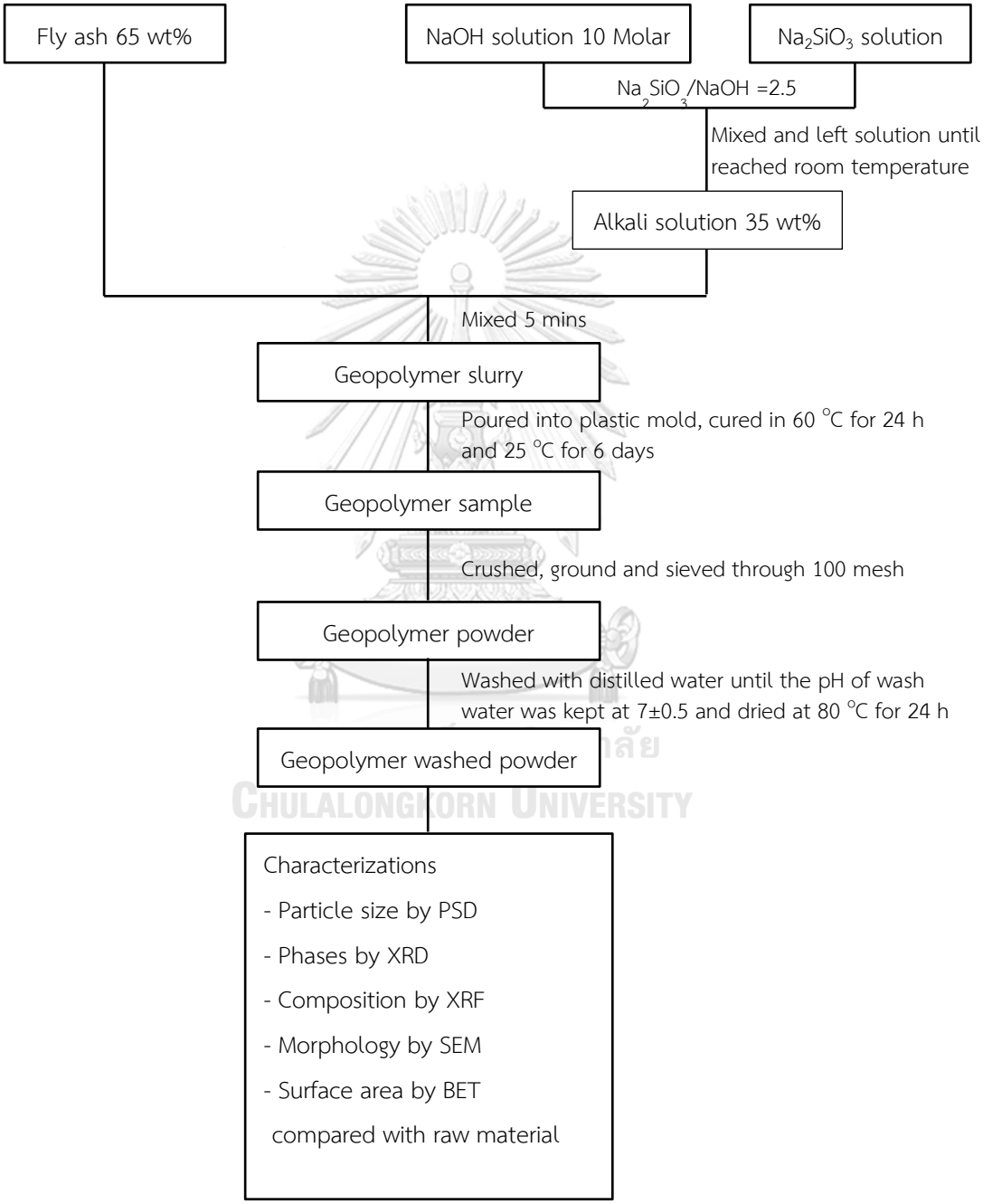

3.6.2 Synthesis metakaolin based geopolymer powder

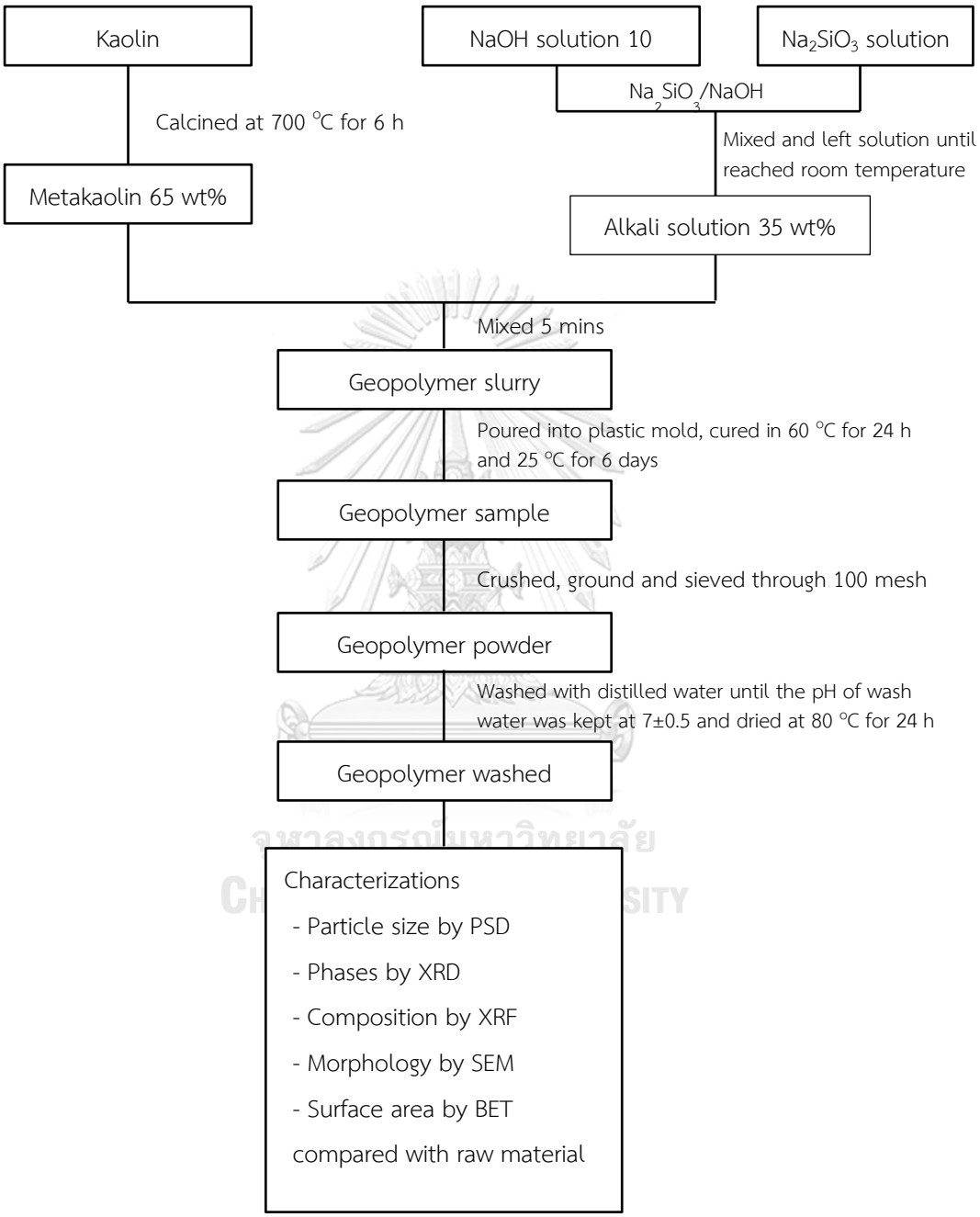

3.6.3 Synthesis fly ash and metakaolin based geopolymer composite fiber

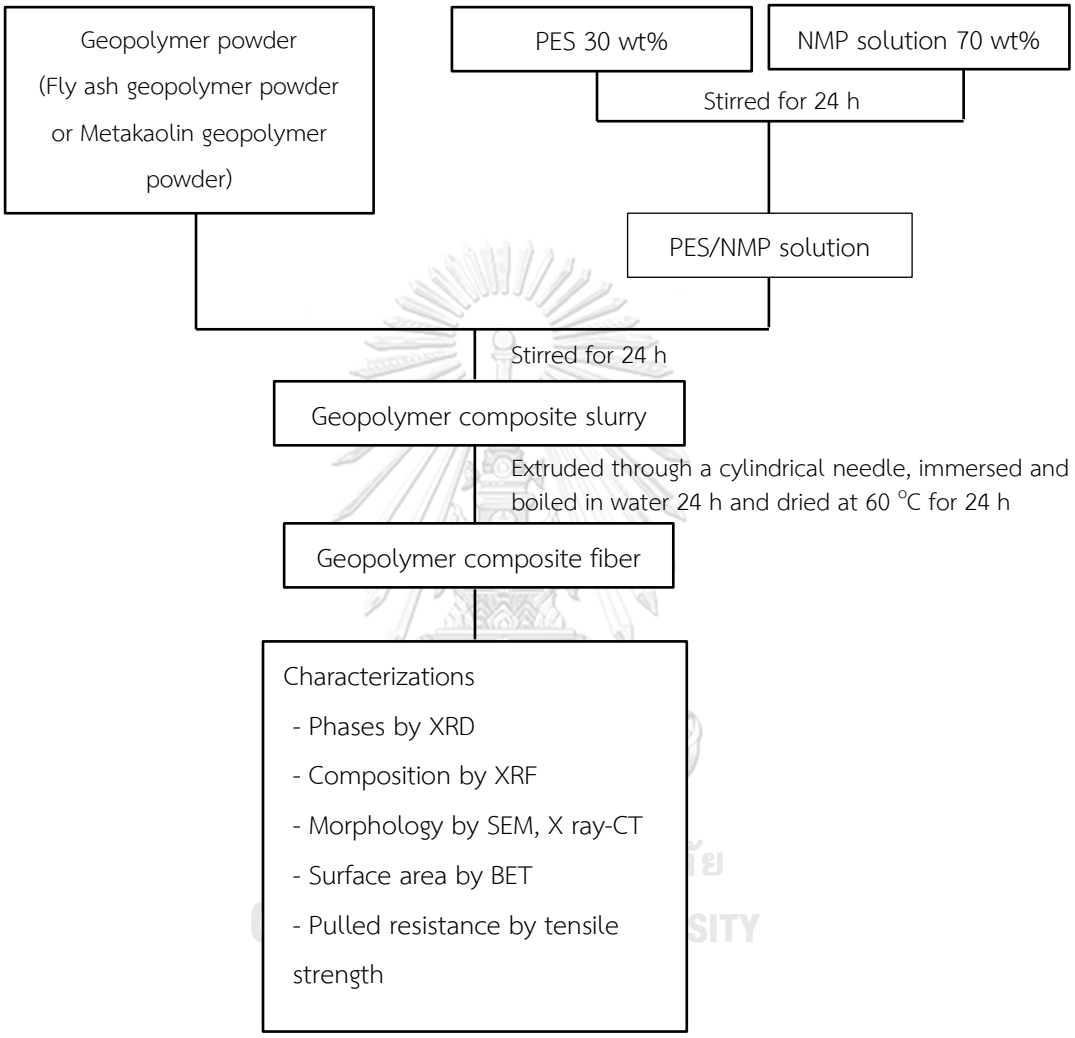

3.6.4 Adsorption test of geopolymer powder and geopolymer composite fiber

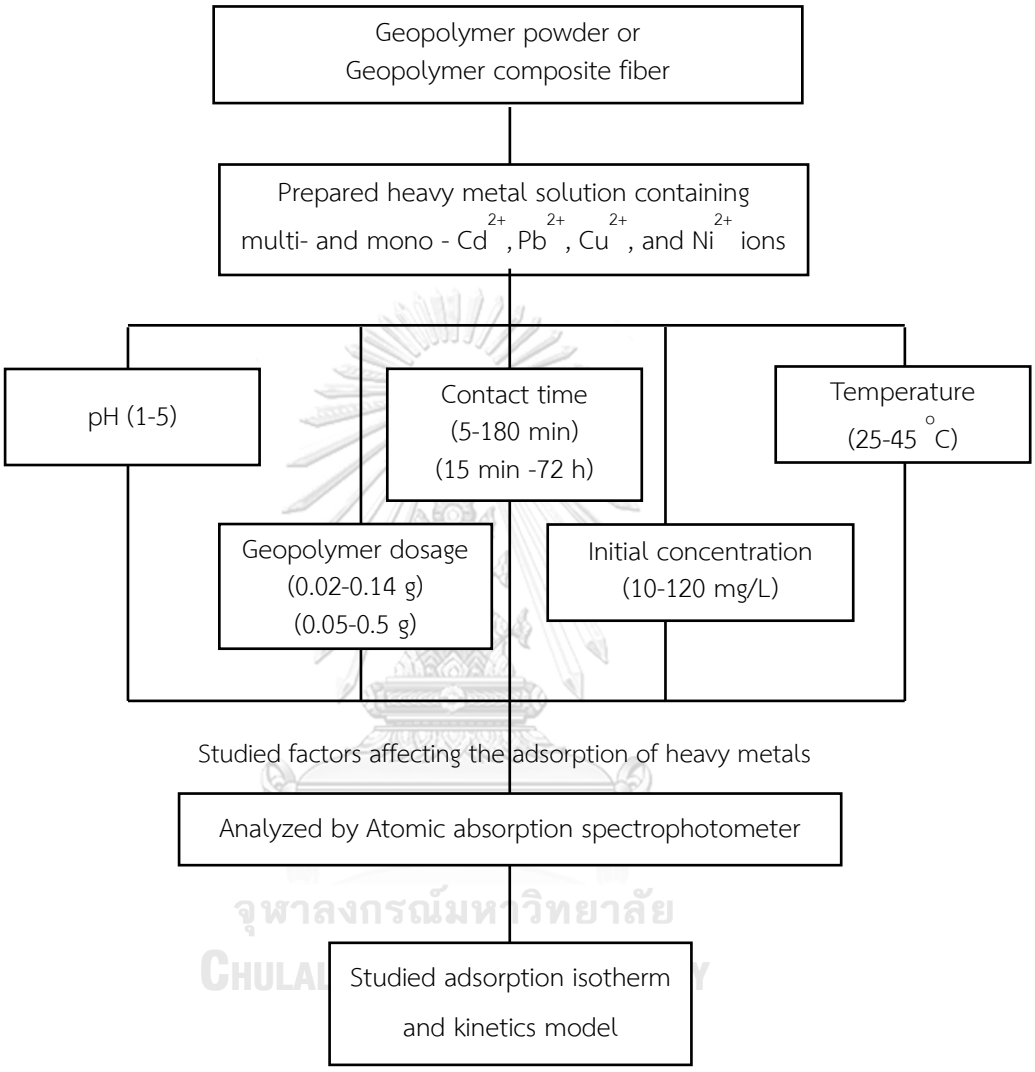

CHAPTER 4

RESULTS AND DISSCUSSION

4.1 FLY ASH BASED GEOPOLYMER POWDER

4.1.1 Characterizations

4.1.1.1 Chemical composition

The chemical compositions of fly ash supplied from Mae Moh power plant and washed fly ash based geopolymer powder are present in Table 4.1. The main compositions of fly ash and fly ash based geopolymer powder are silica (SiO_2), alumina (Al_2O_3), iron oxide (Fe_2O_3) and calcium oxide (CaO). According to the American Society for Testing Materials (ASTM C618) of coal fly ash and raw or calcined natural pozzolan, the total mass of silica, alumina and iron oxide represented 64.20 wt% which can be classified as class C of fly ash. Moreover, the class C is also contained a high calcium oxide component (more than 10 %). In addition, the silica content of washed fly ash based geopolymer powder increased because sodium silicate solution which contains silica content was added for geopolymerization process. However, the other oxide contents of washed fly ash based geopolymer powder was lower than raw fly ash due to oxide contents were released with water in washing geopolymer powder process.

Table 4.1 Chemical compositions of fly ash and fly ash based geopolymer powder

Chemical compound	Fly ash (%)	Washed Fly ash geopolymer (%)
SiO_2	30.80	44.80
Al_2O_3	19.10	16.30
Fe_2O_3	14.30	12.40
CaO	18.40	7.64
MgO	2.31	1.49
SO_3	5.78	0.10
Na_2O	1.39	10.80
K_2O	2.63	1.98

4.1.1.2 Phases

The XRD patterns of fly ash and washed fly ash based geopolymer powder are shown in Fig. 4.1. The crystalline peaks of quartz (JCPDS, 01-087-2096), magnetite (JCPDS, 01-087-0245), mullite (JCPDS, 01-082-0037) and hematite (JCPDS, 00-033-0664) in the XRD patterns of raw fly ash are predominantly displayed. In addition, the non-crystalline phase of the raw fly ash was demonstrated as the broad hump at 2θ = 20-35°. After geopolymerization process, the crystalline phases were decreased and the broad hump peak was increased. This result might indicated that the crystalline phases were transformed to an amorphous structure and some of crystalline phases were released with water through washing process of geopolymer.

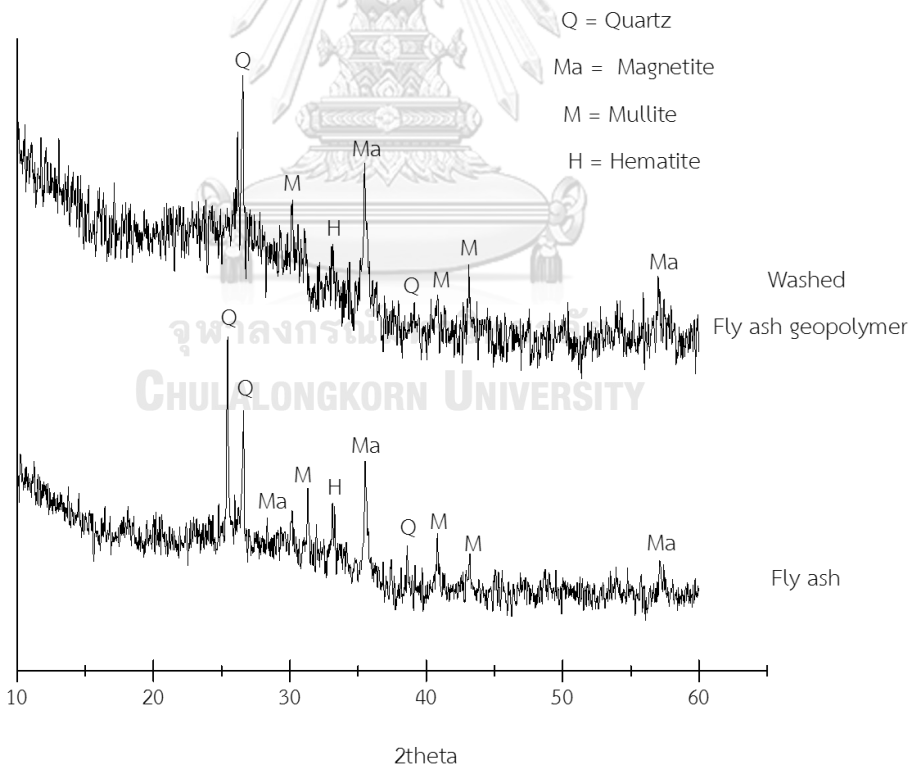

Fig. 4.1 XRD patterns of fly ash and washed fly ash based geopolymer powder

4.1.1.3 Microstructure

Fig. 4.2 showed SEM micrograph of the raw fly ash and washed fly ash based geopolymer powder at 1000× and 3000x magnification. The raw fly ash has spherical particles which occurred in round to angular shape, smooth and dense surface with high ranging in size between 10 and 100 μm (Fig. 4.2 a-b). After geopolymerization process, the surface fly ash particles was dissolved by alkali solution and sodium silicate solution acted as binder to connect between particles. From Fig. 4.2 c-d, fly ash particles has rougher surface than raw fly ash and small and large size of fly ash particles were combined together.

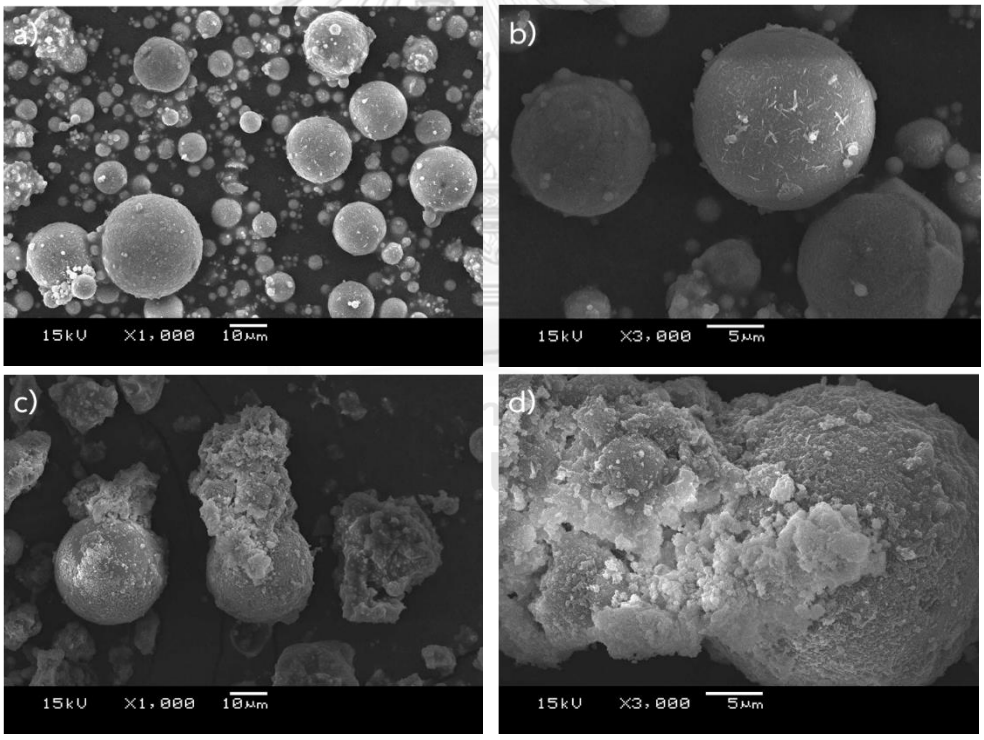

Fig. 4.2 SEM micrograph of (a-b) fly ash and (c-d) washed fly ash based geopolymer powder

4.1.1.4 Particle size distribution and surface area

Particle size distribution of fly ash and washed fly ash based geopolymer powder was measured by laser light scattering technique (Fig. 4.3). The laser-scattered particle distribution of raw fly ash showed the powder size distribution in the range of 0.8–300 μm and showed tri-modal particle size distribution at average particle size of 1.66, 11.48 and 91.20 μm. Moreover, the particle distribution of washed fly ash based geopolymer powder was 1–200 μm. Particle size distributions of fly ash and washed fly ash based geopolymer powder in the median were 41.30 and 45.76, respectively. After geopolymerization process, geopolymer sample was washed and sieved pass through 100 mesh. The particle size of geopolymer powder less than 10 μm was decreased and particle size in the rage of 20-100 μm was increased because the small particle was reacted and agglomerated with a large particles during the reaction.

The raw fly ash powder has lower specific surface area compared to the washed fly ash based geopolymer powder with specific surface area of 0.83 and 85.01 m^2/g, respectively.

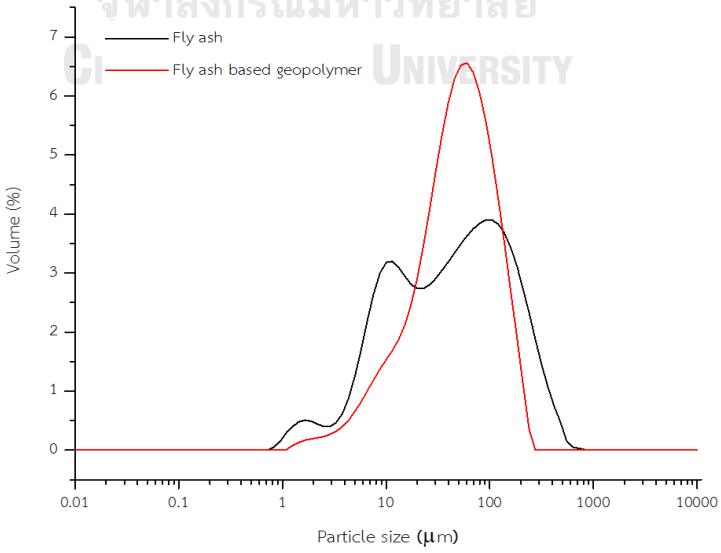

Fig. 4.3 Particle size distribution of fly ash and washed fly ash based geopolymer powder

4.1.2 Adsorption test

4.1.2.1 Effect of contact time

The effect of contact time on heavy metal ions solution (Pb^{2+}, Cu^{2+}, Cd^{2+}, Ni^{2+}) in multi- and mono- cations solution was considered by varying the contact time from 5-180 min and the results are shown in Fig. 4.4 and Fig. 4.5. The initial concentration of each heavy metal ions was fixed at 20 mg/L with 0.1 g of geopolymer in 40 mL of solution and initial pH of 5. Heavy metals of Pb^{2+}, Cu^{2+}, Cd^{2+}, and Ni^{2+} were adsorbed by geopolymer powder. The adsorption efficiency increased with an increase of the contact time in both solution systems (Fig. 4.4).

The removal efficiency of Pb^{2+}, Cu^{2+}, Cd^{2+}, and Ni^{2+} ions at 5 mins of contact time was 87.17, 40.83, 19.90, and 9.43%, respectively in multi-cations solution as shown in Fig. 4.4 (a). Morover, the adsorption efficiency of Pb^{2+}, Cu^{2+}, Cd^{2+}, and Ni^{2+} ions was 95.07, 46.65, 31.92, 24.01% at 120 mins of contact time. For calculate adsorption capacity of geopolymer on different time, FAG geopolymer powder could adsorbed a cations (Pb^{2+}, Cu^{2+}, Cd^{2+}, and Ni^{2+}) up to 7.60, 3.73, 2.55, 1.92 mg/g at 120 mins of contact time as displyed in Fig. 4.5(a).

In mono-cations solution, significant removal efficiency occurred after 5 mins contact time (97.55, 67.97, 67.45, and 54.38%, respectively) and a slightly change in longer contact time Fig. 4.4 (b). After 120 min, the removal efficiency of Pb^{2+}, Cu^{2+}, Cd^{2+}, and Ni^{2+} ions was also slightly increased (99.92, 85.91, 76.33, 56.55%). In addition, the adsorption capacity on Pb^{2+}, Cu^{2+}, Cd^{2+}, and Ni^{2+} ions of FAG powder was 7.99, 6.87, 6.11, 4.52 mg/g (Fig. 4.5 (b)). Therefore, a contact time of 120 min was used in all following tests.

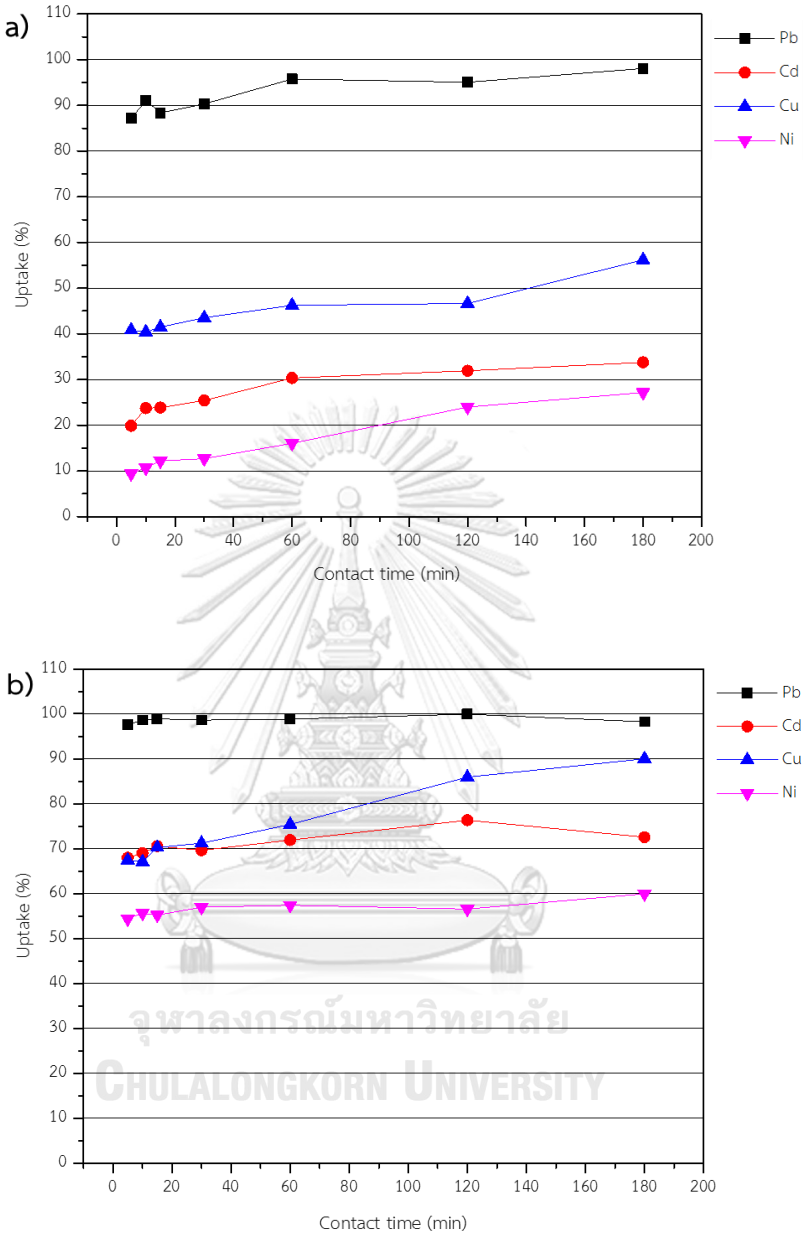

Fig. 4.4 Effect of contact time on heavy metal ions removal efficiency of FAG powder in (a) multi-cations solution and (b) mono-cations solution

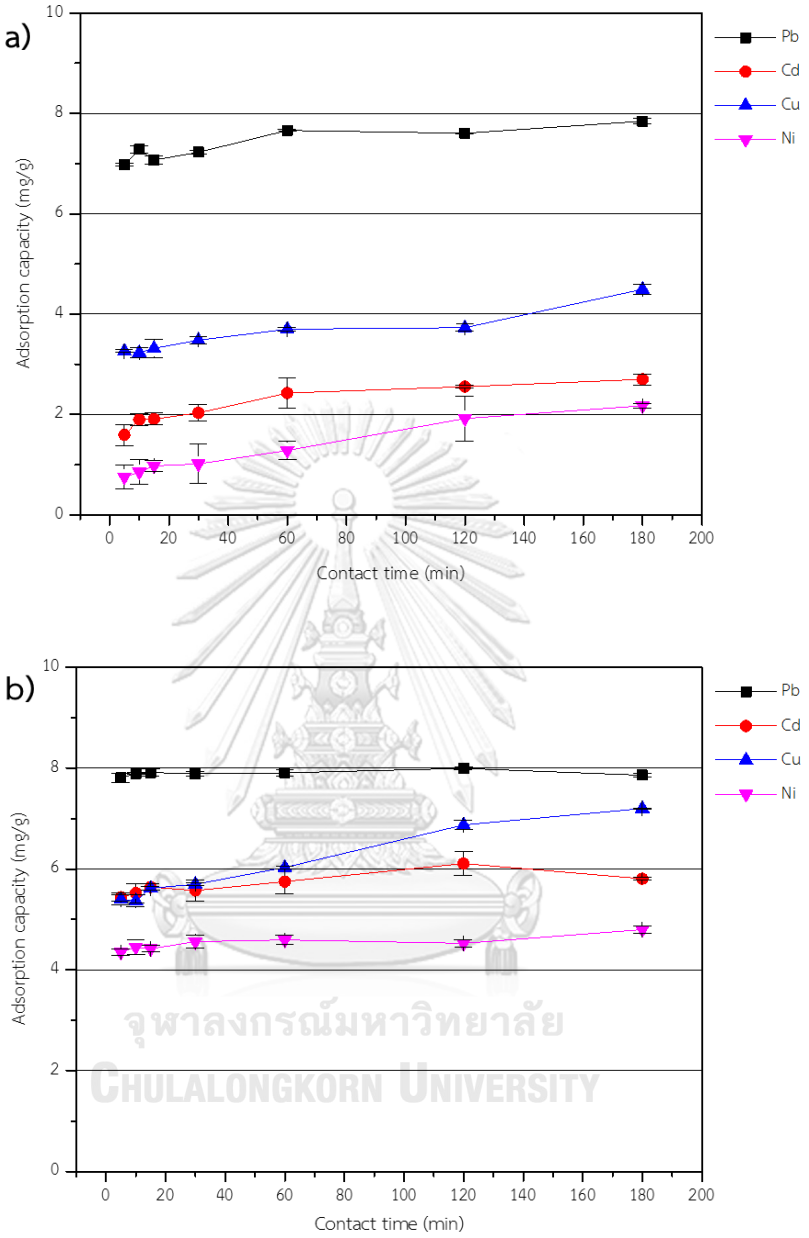

Fig. 4.5 Effect of contact time on adsorption capacity of FAG powder (a) multi-cations solution and (b) mono-cations solution

4.1.2.2 Effect of geopolymer dosage

The effect of geopolymer dosage on the adsorption was considered at 25 °C, initial concentration of Pb^{2+}, Cu^{2+}, Cd^{2+}, and Ni^{2+} of 20 mg/L and a pH value of 6 using the following dosage: 0.02, 0.04, 0.06, 0.08, 0.10, 0.12, and 0.14 g/40 mL (Fig. 4.6 and Fig. 4.7). The results showed that the adsorption efficiency and the adsorption capacity of heavy metal ions increased with an increase of adsorbent dose because the active site for adsorbing ions is increased.

Increasing of geopolymer dosage from 0.02 g to 0.14 g, the adsorption efficiency increased of Pb^{2+}, Cu^{2+}, Cd^{2+}, and Ni^{2+} ions from 46.68, 23.40, 6.51, and 6.20% to 96.60, 56.36, 39.28, and 28.67%, respectively in multi-cations solution as given in Fig. 4.6 (a). Effect of adsorbent dose on adsorption capacity of FAG powder is calculated. Fig. 4.7 (a) showed the adsorption capacity of Pb^{2+}, Cu^{2+}, Cd^{2+}, and Ni^{2+} ions with increasing geopolymer dose from 0.02 g to 0.14 g was changed from 3.83, 1.87, 0.52, and 0.50 mg/g to 7.72, 4.51, 3.14, and 2.29 mg/g.

The adsorption efficiency increased of Pb^{2+}, Cu^{2+}, Cd^{2+}, and Ni^{2+} ions from 84.93, 54.14, 33.51, and 0.25 % to 98.24, 89.98, 72.56, and 59.95 %, respectively with an increasing of geopolymer dosage from 0.02 g to 0.14 g in mono-cations solution (Fig. 4.6 (b)). The adsorption capacity of geopolymer dosage on Pb^{2+}, Cu^{2+}, Cd^{2+}, and Ni^{2+} ions was studied. The adsorption capacity values increasing from 6.79, 4.33, 2.68, and 0.02 mg/g to 7.93, 7.72, 6.75, and 4.93 mg/g with geopolymer dose from 0.02 g to 0.14 g.

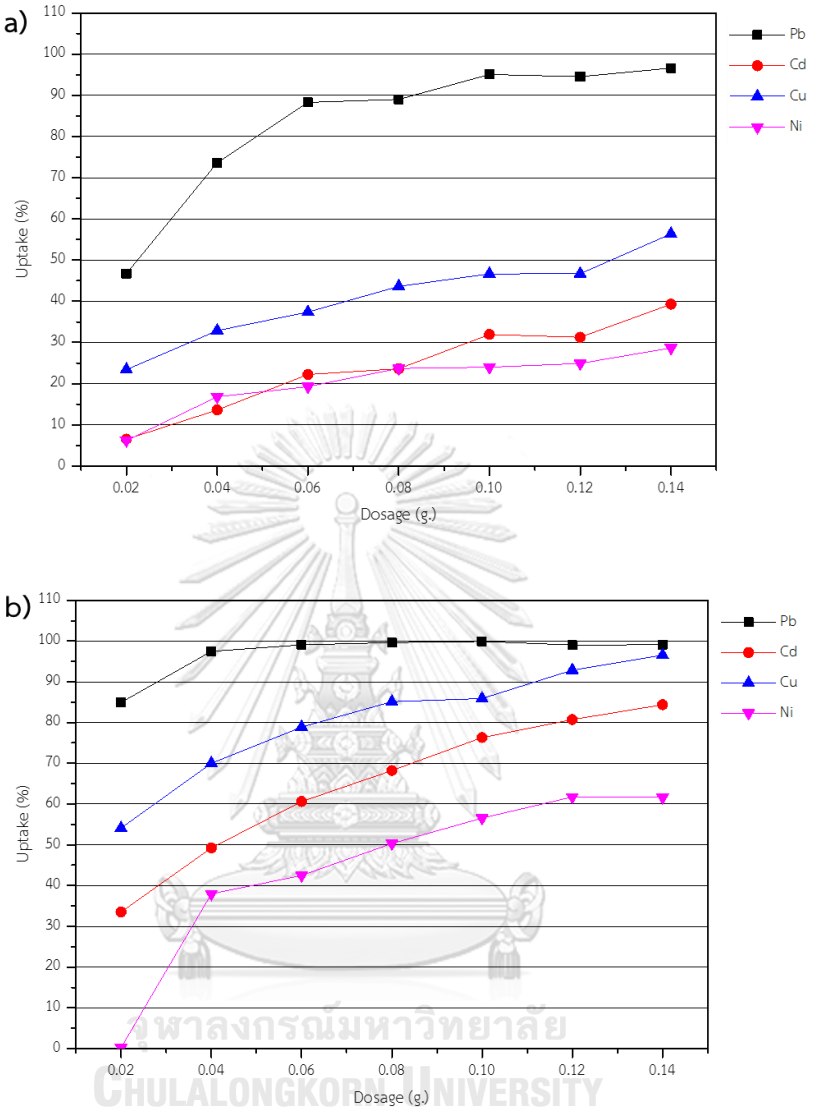

Fig. 4.6 Effect of adsorbent dose on heavy metal ions removal efficiency of FAG powder (a) multi-cations solution and (b) mono-cations solution

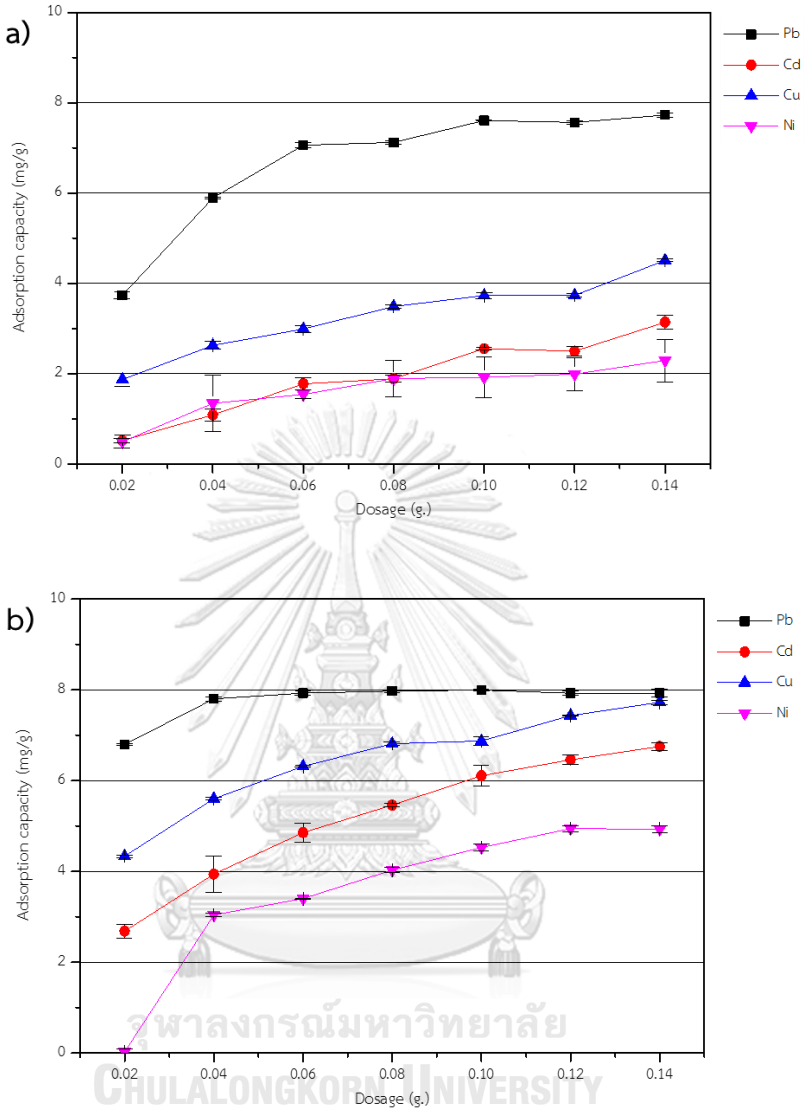

Fig. 4.7 Effect of adsorbent dose on adsorption capacity of FAG powder (a) multi-cations solution and (b) mono-cations solution

4.1.2.3 Effect of solution pH

From Fig. 4.8 and Fig. 4.9, the effect of varying pH values (1-5) of heavy metal ions in solution on removal efficiency was evaluated at a temperature of 25 °C using a geopolymer dosage of 0.1 g/ 40 mL for 120 mins contact time and initial concentration of Pb^{2+}, Cu^{2+}, Cd^{2+}, and Ni^{2+} of 20 mg/L. The adsorption efficiency increased when pH was increased from 1 to 5 because at low pH values, the excess of positive H_3O^+ ions could compete with heavy metal ions on available adsorption geopolymer surface.

The sorption effectiveness of Pb^{2+}, Cu^{2+}, Cd^{2+}, and Ni^{2+} ions increased from 1.05 to 95.07% of Pb^{2+}, 0 to 46.66% of Cu^{2+}, 0 to 31.93% of Cd^{2+}, and 0 to 24.01% of Ni^{2+} when pH of multi-cations solution was increased from 1 to 5 as seen in Fig. 4.8 (a). Moreover, a maximum adsorption capacity values of Pb^{2+}, Cu^{2+}, Cd^{2+}, and Ni^{2+} ions on FAG powder was found to be 7.60, 3.73, 2.55, and 1.92 mg/g at pH 5 (Fig. 4.9 (a)).

Fig. 4.8 (b) and Fig. 4.9 (b) showed the adsorption efficiency and adsorption capacity of FAG powder on Pb^{2+}, Cu^{2+}, Cd^{2+}, and Ni^{2+} ions in mono-cations solution system. When pH of multi- cations solution was increased from 1 to 5, the adsorption efficiency increased up to 95.92% of Pb^{2+}, 85.90% of Cu^{2+}, 76.32% of Cd^{2+}, and 56.55% of Ni^{2+} and adsorption capacity values increased up to 7.99 mg/g of Pb^{2+}, 6.87 mg/g of Cu^{2+}, 6.11 mg/g of Cd^{2+}, and 4.52 mg/g of Ni^{2+}.

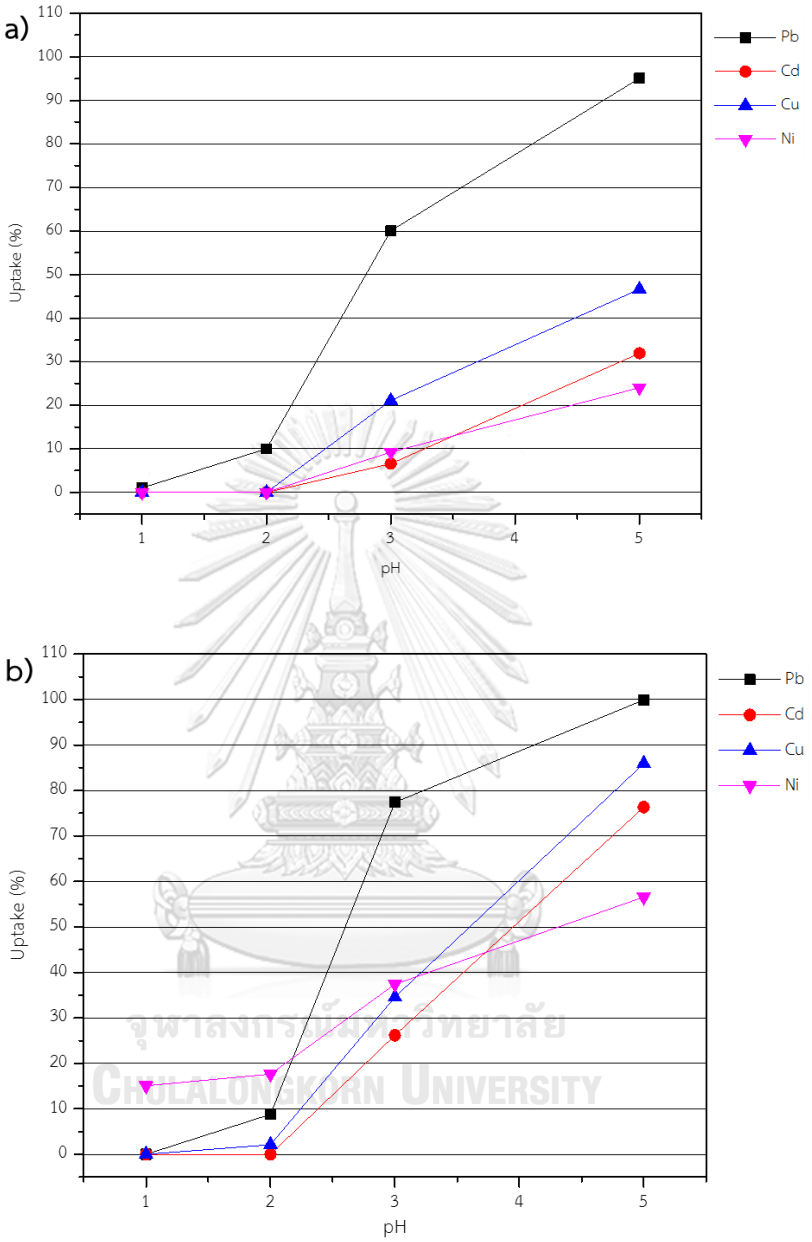

Fig. 4.8 Effect of pH on heavy metal ions removal efficiency of FAG powder (a) multi-cations solution and (b) mono-cations solution

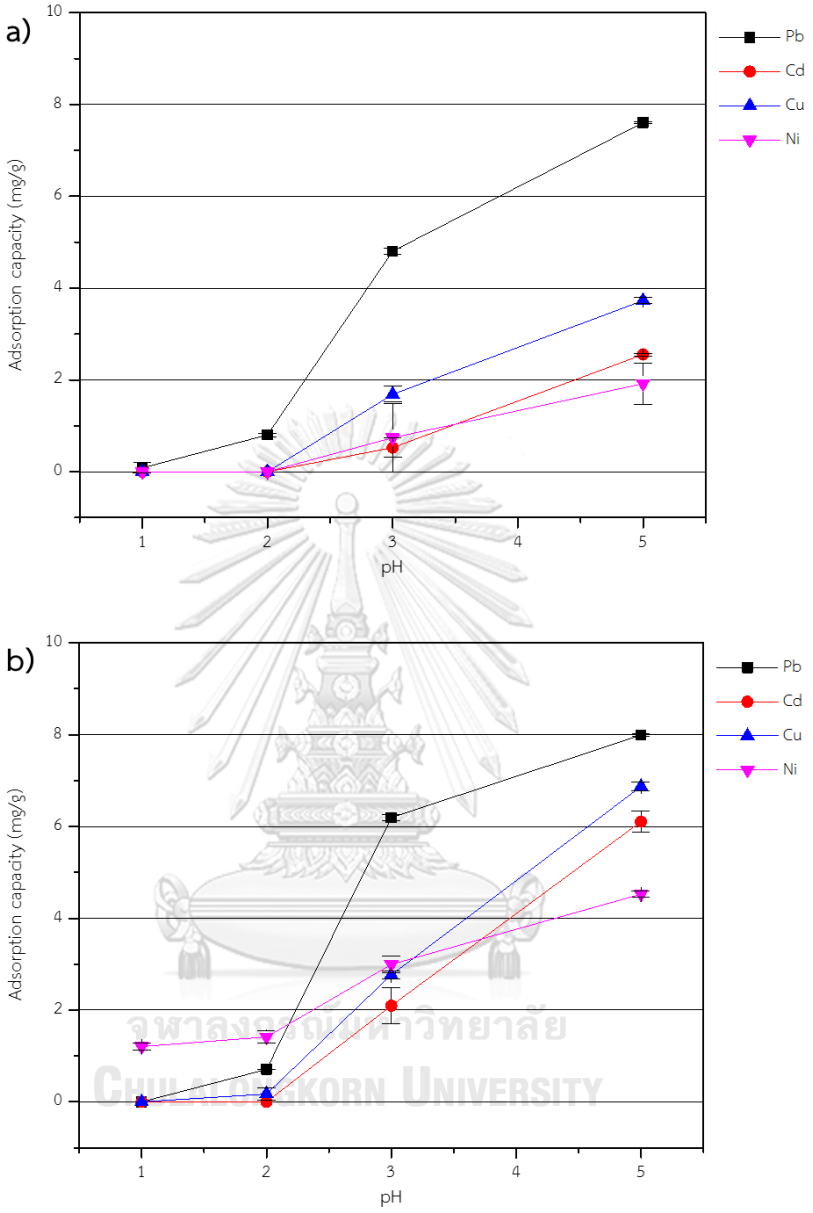

Fig. 4.9 Effect of pH on adsorption capacity of FAG powder (a) multi-cations solution and (b) mono-cations solution

4.1.2.4 Effect of temperature

For the effect of temperature (Fig. 4.10 and Fig. 4.11), the adsorption efficiency was studied at 25, 35, and 45 °C at a pH value of 5, 0.1 g/ 40 mL geopolymer dosage, a contact time of 120 mins and initial concentration of Pb^{2+}, Cu^{2+}, Cd^{2+}, and Ni^{2+} of 20 mg/L. The adsorption of heavy metal ions on geopolymer powder increased with an increasing of temperature in all kind of heavy metal ions. The vaporization of water was found as a result to the micro-cavities was improved in geopolymer powder so adsorption capacity was increased at high temperature.

The removal efficiency values of Pb^{2+}, Cu^{2+}, Cd^{2+}, and Ni^{2+} were found to be 100, 88.68, 79.28, 39.28% at 25 °C, 98.94, 90.14, 80.09, 40.11% at 35 °C, and 99.54, 93.39, 83.30, 46.08% at 45 °C in multi-cations solution as shown in Fig. 4.10 (a). The adsorption capacity of Pb^{2+}, Cu^{2+}, Cd^{2+}, and Ni^{2+} increased up to 7.96, 7.47, 6.66, and 3.69 mg/g when temperature was increased from 25 to 45 °C (Fig. 4.11 (a)).

The removal efficiency values and adsorption capacity values of Pb^{2+}, Cu^{2+}, Cd^{2+}, and Ni^{2+} were found up to 99.68, 96.22, 82.85, 65.18% and 7.97, 7.70, 6.63, 5.21 mg/g at 45 °C in mono-cations solution as shown in Fig. 4.10 (b) and Fig. 4.11 (b), respectively.

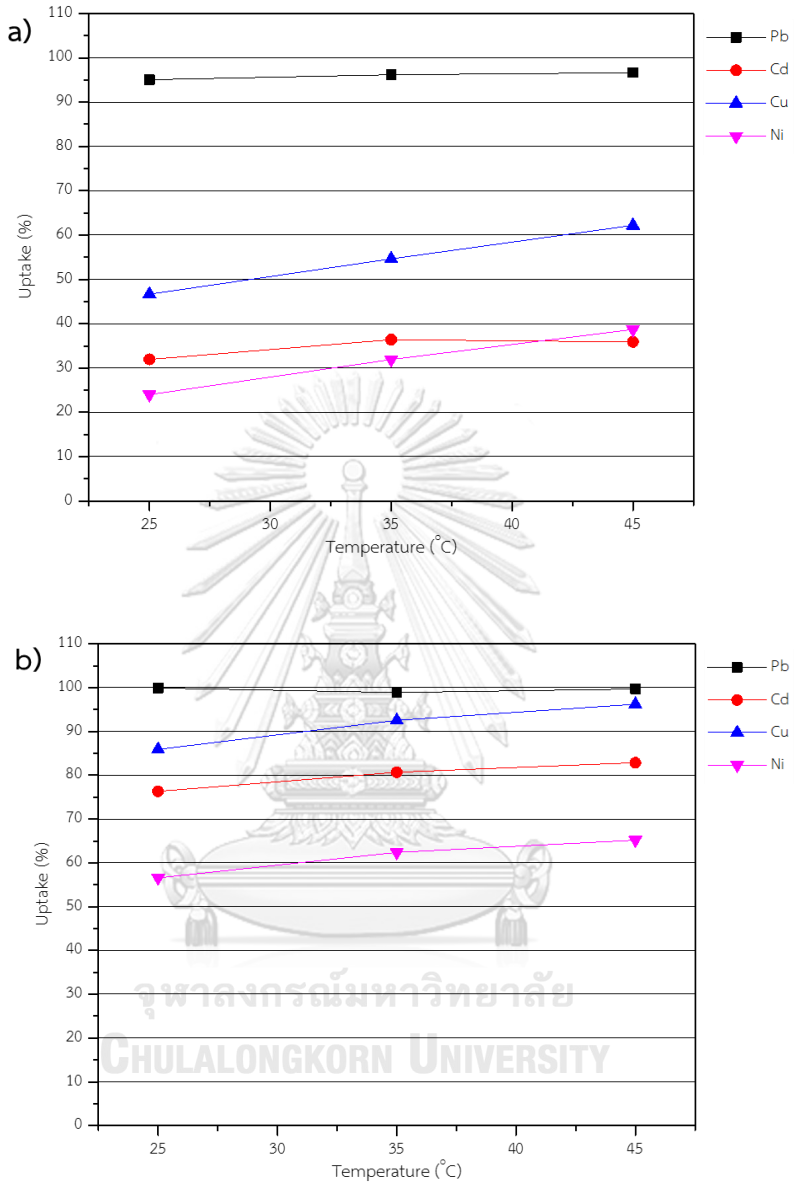

Fig. 4.10 Effect of temperature on heavy metal ions removal efficiency of FAG powder (a) multi-cations solution and (b) mono-cations solution

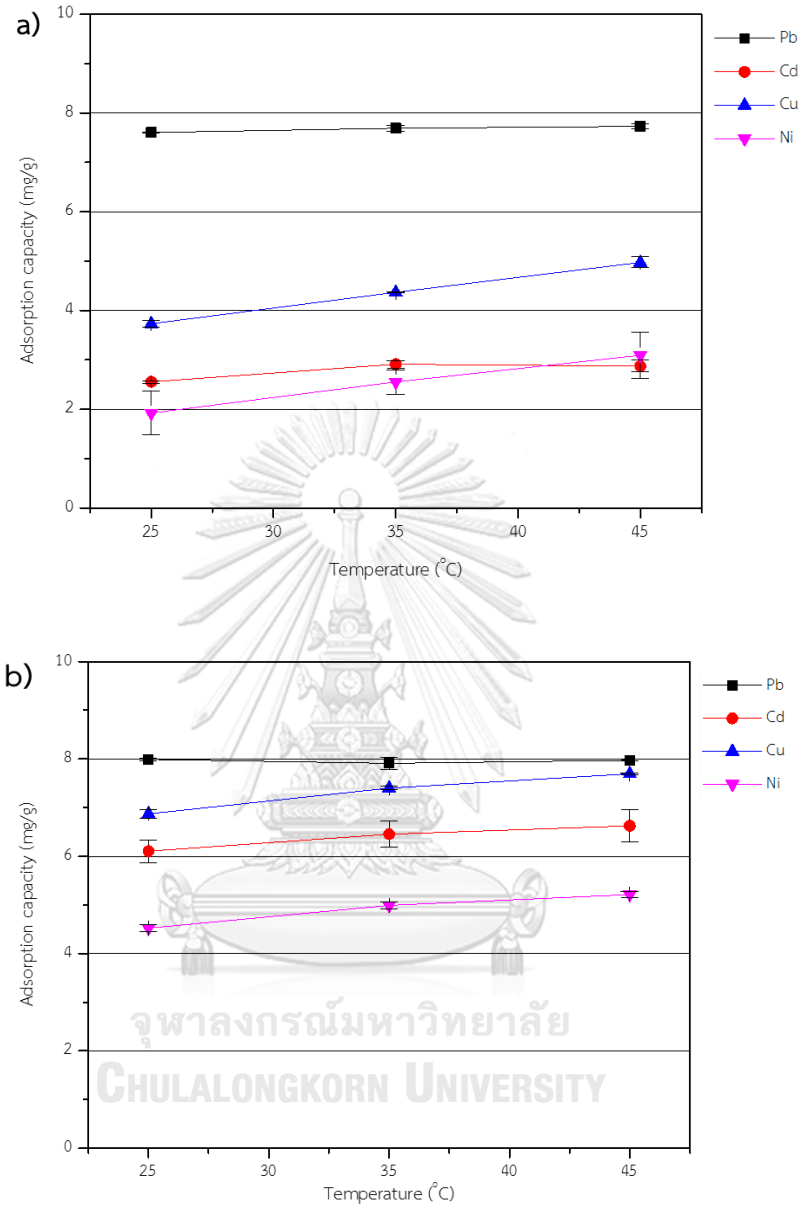

Fig. 4.11 Effect of temperature on adsorption capacity of FAG powder (a) multi-cations solution and (b) mono-cations solution

4.1.2.5 Effect of initial concentration

The initial concentration was studied using a geopolymer dosage of 0.1 g/ 40 mL at pH 5 and a temperature of 25 °C for 120 min contact time. The initial concentration of heavy metal solution was varied from 20-120 mg/L. The results indicated that at low initial concentration, the removal efficiency was increased due to the available pores on adsorbent surface. When the initial concentration of Pb^{2+}, Cu^{2+}, Cd^{2+}, and Ni^{2+} ions increased, the accessible sites become insufficient to adsorb ions, for this reason, some ions still remain in the solution without being sorbed by the adsorbent.

Fig. 4.12 (a) and Fig. 4.13 (a) displayed the adsorption efficiency and adsorption capacity of Pb^{2+}, Cu^{2+}, Cd^{2+}, and Ni^{2+} on FAG powder at various concentrations in multi-cations solution. The initial concentrations less than 20 mg/L, the removal efficiency remained a higher percentage than 95.07, 46.66, 31.92, and 24.11% of Pb^{2+}, Cu^{2+}, Cd^{2+}, and Ni^{2+}. The maximum adsorption capacity values of Pb^{2+}, Cu^{2+}, Cd^{2+}, and Ni^{2+} were found as 47.24 mg/g of Pb^{2+} at 120 mg/L, 9.40 mg/g of Cu^{2+} at 120 mg/L, 8.34 mg/g of Cd^{2+} at 120 mg/L and 4.09 mg/g of Ni^{2+} at 80 mg/L.

The adsorption efficiency and adsorption capacity of Pb^{2+}, Cu^{2+}, Cd^{2+}, and Ni^{2+} on FAG powder at various concentrations in mono-cations solution were presented in Fig. 4.12 (b) and Fig. 4.13 (b). The initial concentrations less than 20 mg/L, the removal efficiency remained a higher percentage than 99.91, 76.33, 85.90, and 56.55 % of Pb^{2+}, Cu^{2+}, Cd^{2+}, and Ni^{2+}. The maximum adsorption capacity values of Pb^{2+}, Cu^{2+}, Cd^{2+}, and Ni^{2+} were found as 42.95 mg/g of Pb^{2+} at 120 mg/L, 12.79 mg/g of Cd^{2+} at 120 mg/L, 14.14 mg/g of Ni^{2+} at 120 mg/L and 9.50 mg/g of Cu^{2+} at 80 mg/L.

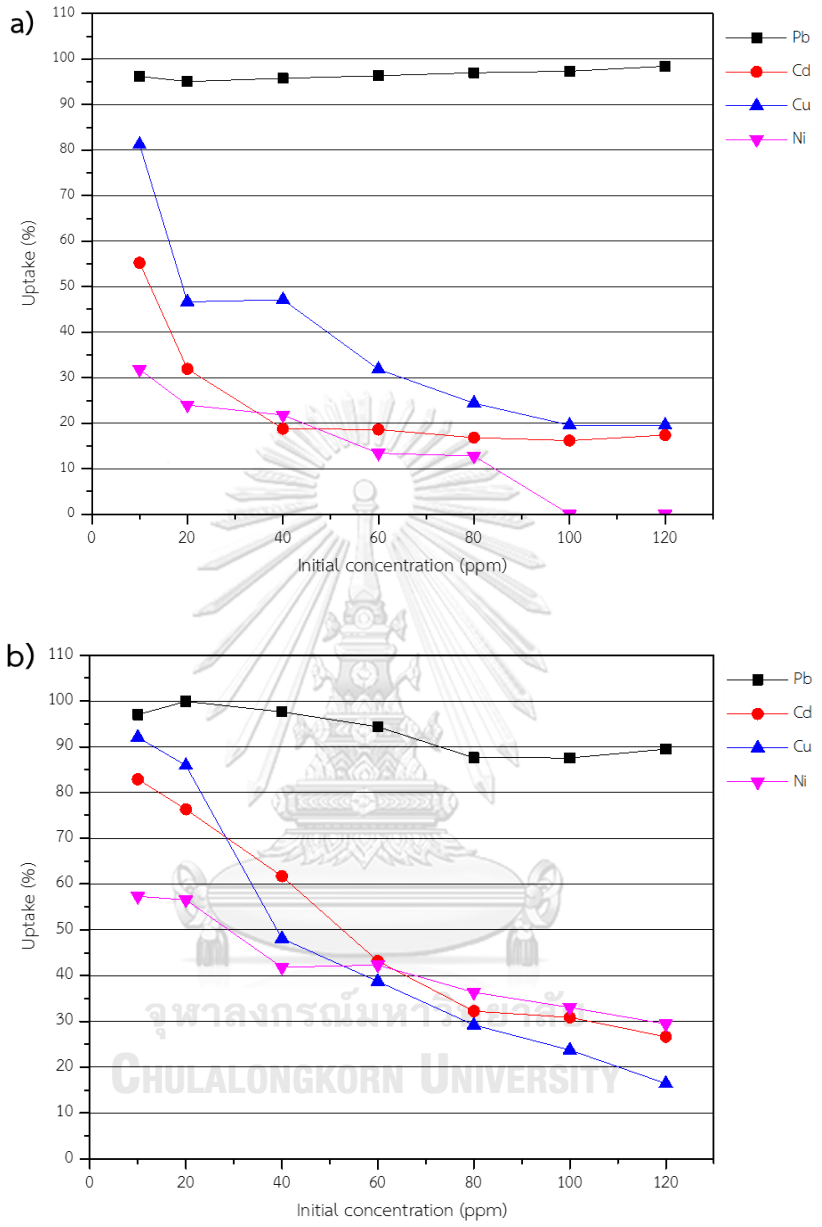

Fig. 4.12 Effect of initial concentration on heavy metal ions removal efficiency of FAG powder (a) multi-cations solution (b) mono-cations solution

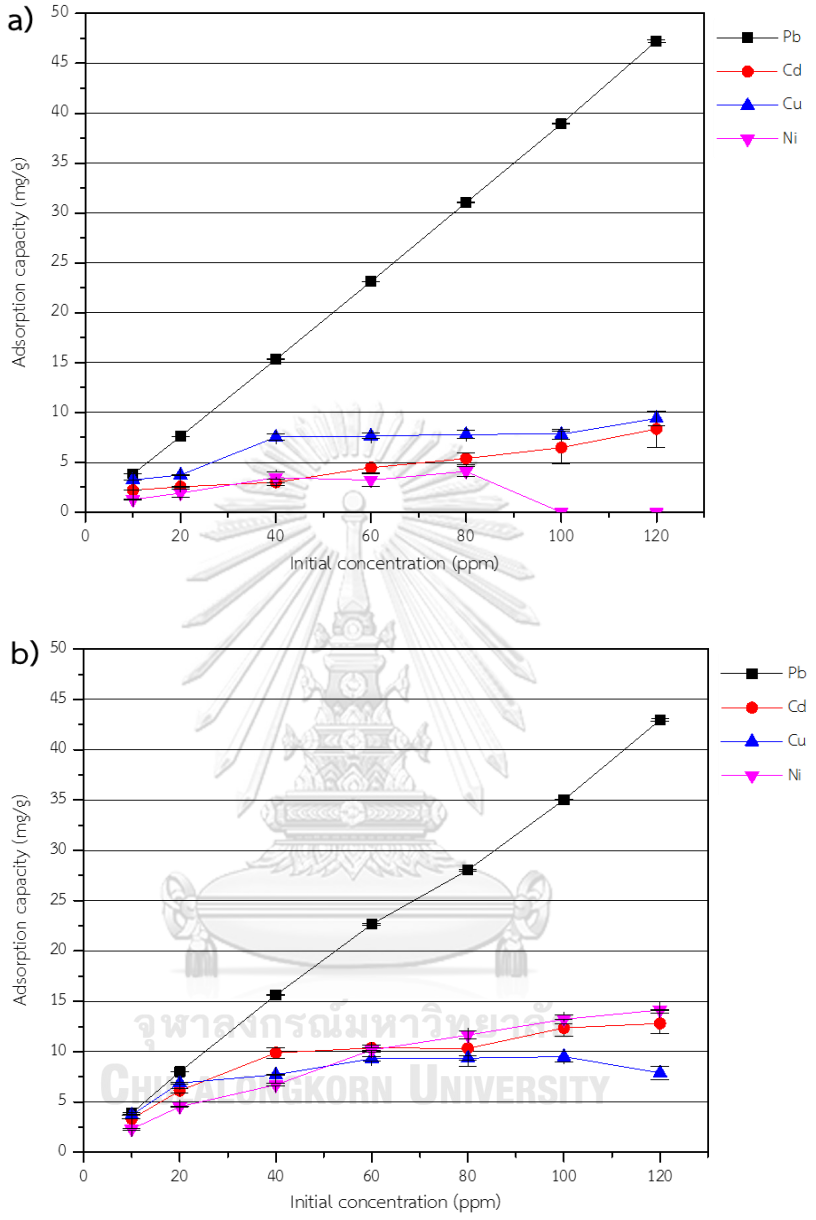

Fig. 4.13 Effect of initial concentration on adsorption capacity of FAG powder (a) multi-cations solution (b) mono-cations solution

4.1.3 Adsorption isotherm

The equilibrium data isotherm analysis for heavy metal adsorption on to FAG powder can be expressed in terms of adsorption isotherm models. Langmuir, Freundlich, Redlich-Peterson and Dubinin-Radushkevish isotherm models were used to describe the adsorption equilibrium. The objective is to evaluate the most appropriate correlations from the curves and then optimize the sorption systems.

The adsorption data of Pb^{2+}, Cu^{2+}, Cd^{2+}, $Ni^{2+}$was fitted with the equation in each isotherm to obtain the graph and affinity of adsorption of the FAG powder in multi- and mono-cations solution as shown in Fig. 4.14 to Fig. 4.17. The model parameters and summary of adsorption isotherm are presented in Table 4.2 and Table 4.3. Moreover, the diagram of adsorption isotherm which were fitted with each ions are shown in Fig. 4.18.

In multi-cations solution, Pb^{2+} and Ni^{2+} were fitted well with Langmuir adsorption isotherm and Cu^{2+} and Cd^{2+} were fitted well with Freundlich adsorption isotherm. The results indicated that Pb^{2+} and Ni^{2+} could adsorb on FAG powder in monolayer and Cu^{2+} and Cd^{2+} could adsorb on FAG powder in multilayer. The maximum capacities of Pb^{2+}, Cu^{2+}, Cd^{2+}, Ni^{2+} on the Langmuir model was in the order $Pb^{2+}>Cu^{2+}>Cd^{2+}>Ni^{2+}$. From the Langmuir model, the value of R_L was indicated the favorability of the adsorption process; unfavorable ($R_L>1$), favorable ($0<R_L<1$) or irreversible ($R_L=0$). The calculated R_L values of Pb^{2+}, Cu^{2+}, Cd^{2+}, Ni^{2+} were 0.886, 0.054, 0.024, and 0.143, indicating that the adsorption process is favorable. Moreover, the values of the Freundlich constant (*1/n*) were between 0.1 and 1, indicating a favorable adsorption.

In mono-cations solution, all of Pb^{2+}, Cu^{2+}, Cd^{2+}, Ni^{2+} were fitted well with Langmuir adsorption isotherm. The results conclude that Pb^{2+}, Cu^{2+}, Cd^{2+}, Ni^{2+}could

adsorb on FAG powder in monolayer. The calculated R_L values of Pb^{2+}, Cu^{2+}, Cd^{2+}, Ni^{2+} were 0.094, 0.051, 0.011, and 0.254, indicating that the adsorption process is favorable.

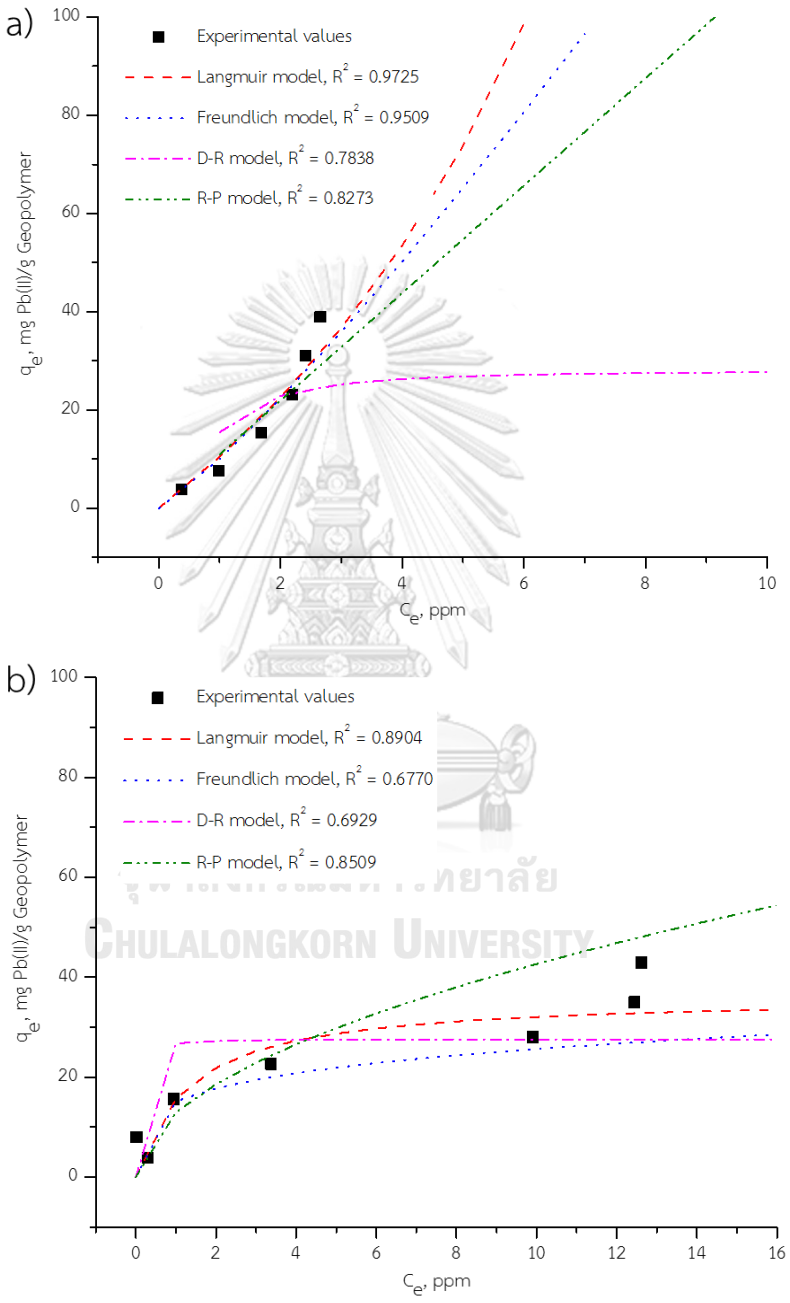

Fig. 4.14 The adsorption isotherms of Pb(II) by applying Langmuir, Freundlich, Redlich-Peterson and Dubinin–Radushkevich isotherm models of FAG adsorbent (a) multi-cations solution (b) mono-cations solution

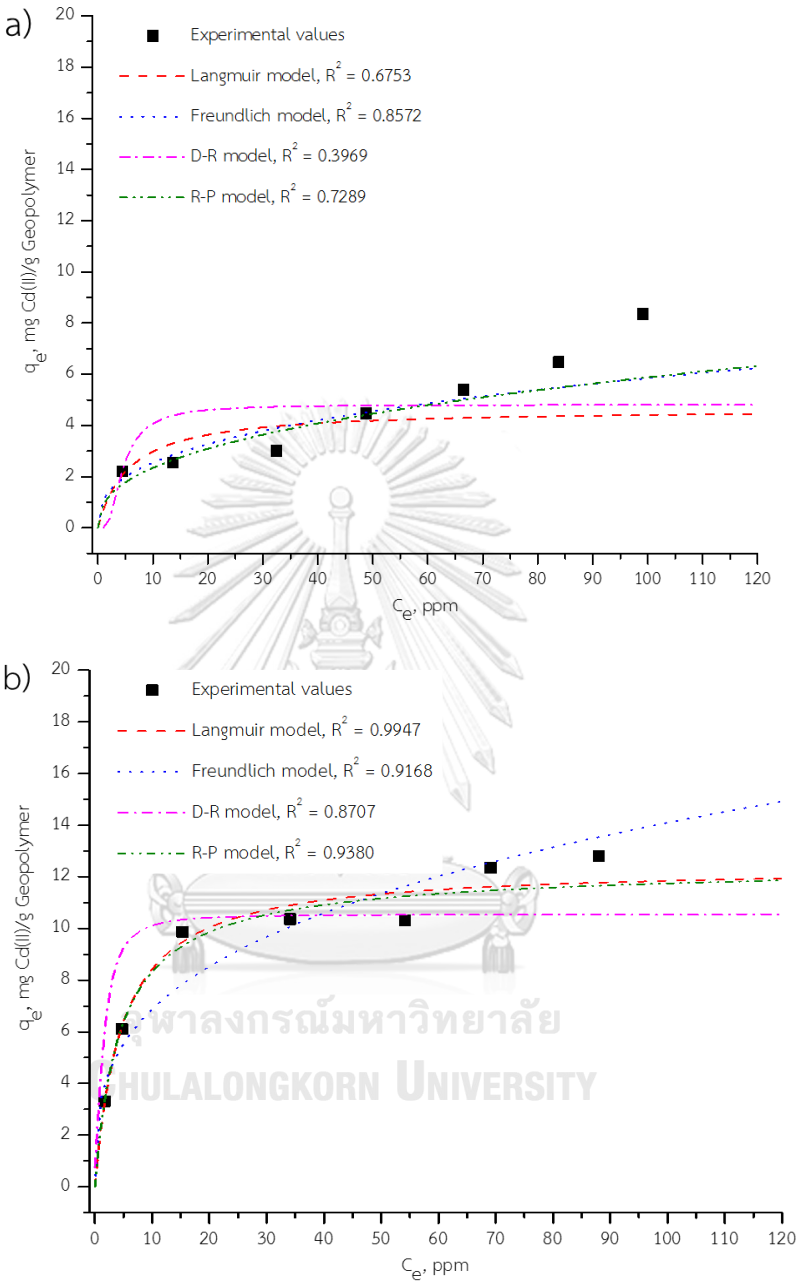

Fig. 4.15 The adsorption isotherms of Cd(II) by applying Langmuir, Freundlich, Redlich-Peterson and Dubinin–Radushkevich isotherm models FAG adsorbent (a) multi-cations solution (b) mono-cations solution

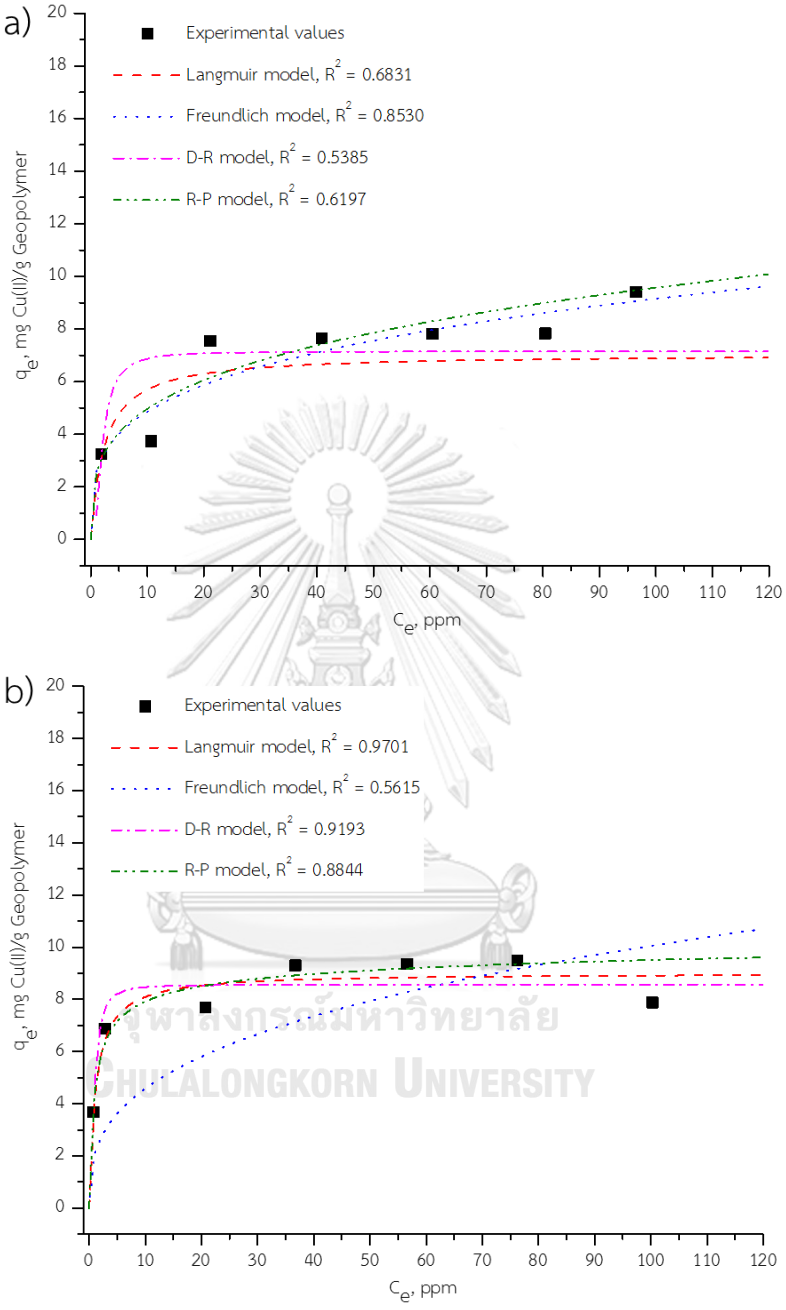

Fig. 4.16 The adsorption isotherms of Cu(II) by applying Langmuir, Freundlich, Redlich-Peterson and Dubinin–Radushkevich isotherm models FAG adsorbent (a) multi-cations solution (b) mono-cations solution

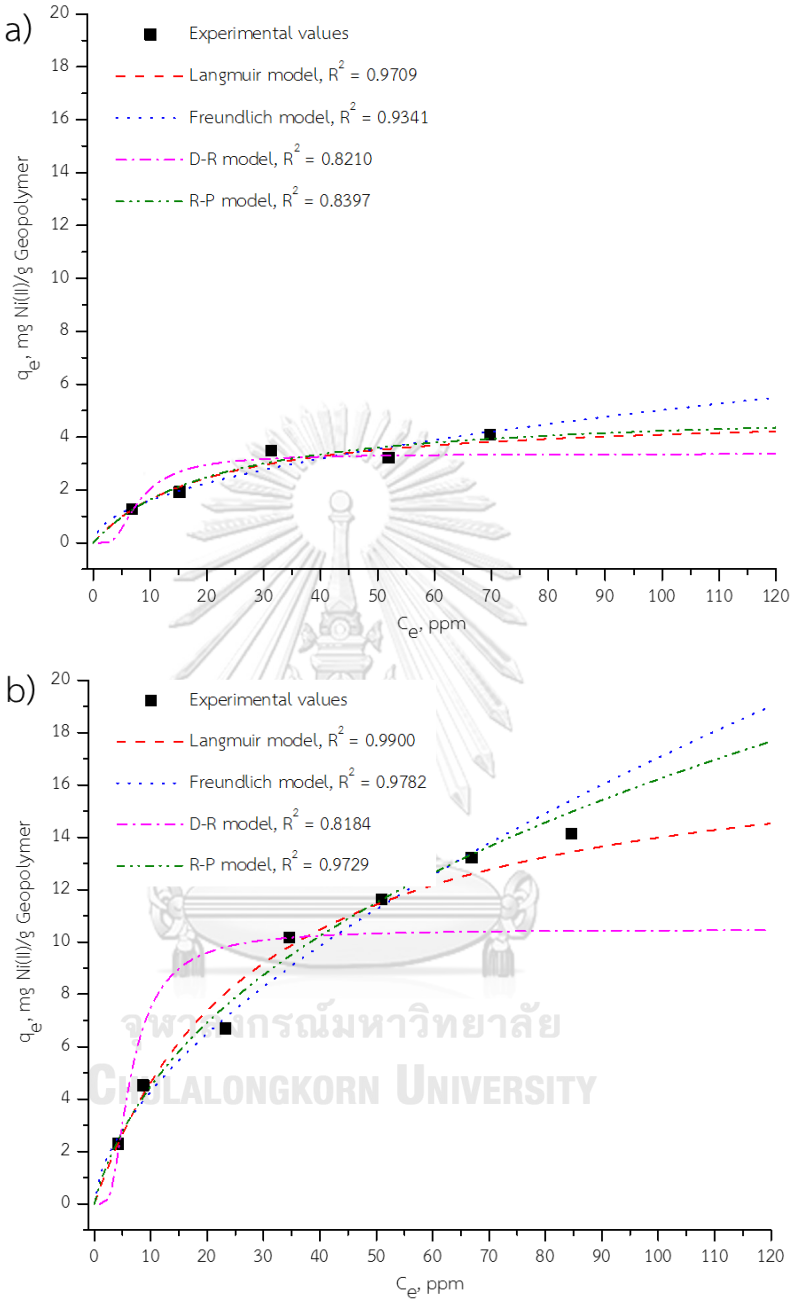

Fig. 4.17 The adsorption isotherms of Ni(II) by applying Langmuir, Freundlich, Redlich-Peterson and Dubinin–Radushkevich isotherm models FAG adsorbent (a) multi-cations solution (b) mono-cations solution

Table 4.2 Summary of adsorption isotherm of metal ions with FAG adsorbent

Solution system	Metal ion	Isotherm model
Multi-cations	Pb^{2+}	Langmuir model
	Cd^{2+}	Freundlich model
	Cu^{2+}	Freundlich model
	Ni^{2+}	Langmuir model
Mono-cations	Pb^{2+}	Langmuir model
	Cd^{2+}	Langmuir model
	Cu^{2+}	Langmuir model
	Ni^{2+}	Langmuir model

Table 4.3 Parameters on Langmuir, Freundlich, Redlich-Peterson and Dubinin-Radushkevish isotherm of FAG adsorbent

Solution system	Isotherm model	Parameter	Metal			
			Pb^{2+}	Cd^{2+}	Cu^{2+}	Ni^{2+}
Multi-cations	Langmuir	q_m	142.857	4.655	7.047	4.914
		K_L	0.068	0.178	0.423	0.050
		R^2	0.9725	0.6753	0.6831	0.9709
		R_L	0.886	0.054	0.024	0.143
	Freundlich	K_F	9.951	10109	2.574	0.512
		$1/n$	1.168	0.361	0.275	0.496
		R^2	0.9509	0.8572	0.8530	0.9341
	Redlich-Peterson	K_{RP}	88.952	3441	97.667	0.240
		a	7.126	36093	37.579	0.047
		g	0	0.600	0.717	1
		R^2	0.8273	0.7289	0.6197	0.8397
	Dubinin–Radushkevich	q_m	27.978	4.810	7.148	3.369
		β	2×10^{-7}	3×10^{-6}	7×10^{-7}	9×10^{-6}
		R^2	0.7838	0.3969	0.5385	0.8210
		E	1581.138	408.248	845.154	235.702
Mono-cations	Langmuir	q_m	36.232	12.407	9.017	18.018
		K_L	0.767	0.212	0.886	0.035
		R^2	0.8904	0.9947	0.9701	0.9900
		R_L	0.094	0.051	0.011	0.254
	Freundlich	K_F	15.170	3.350	2.090	1.080
		$1/n$	0.228	0.312	0.341	0.599
		R^2	0.6770	0.9168	0.5615	0.9782
	Redlich-Peterson	K_{RP}	2.711×10^{6}	7.800	10.593	0.969
		a	0.218×10^{6}	0.244	1.387	0.271
		g	0.483	0.985	0.950	0.632
		R^2	0.8509	0.90380	0.8844	0.9729
	Dubinin–Radushkevich	q_m	27.547	10.548	8.569	10.475
		β	1×10^{-8}	9×10^{-7}	2×10^{-7}	6×10^{-6}
		R^2	0.6929	0.8707	0.9193	0.8184
		E	7071.068	745.356	1581.139	288.675

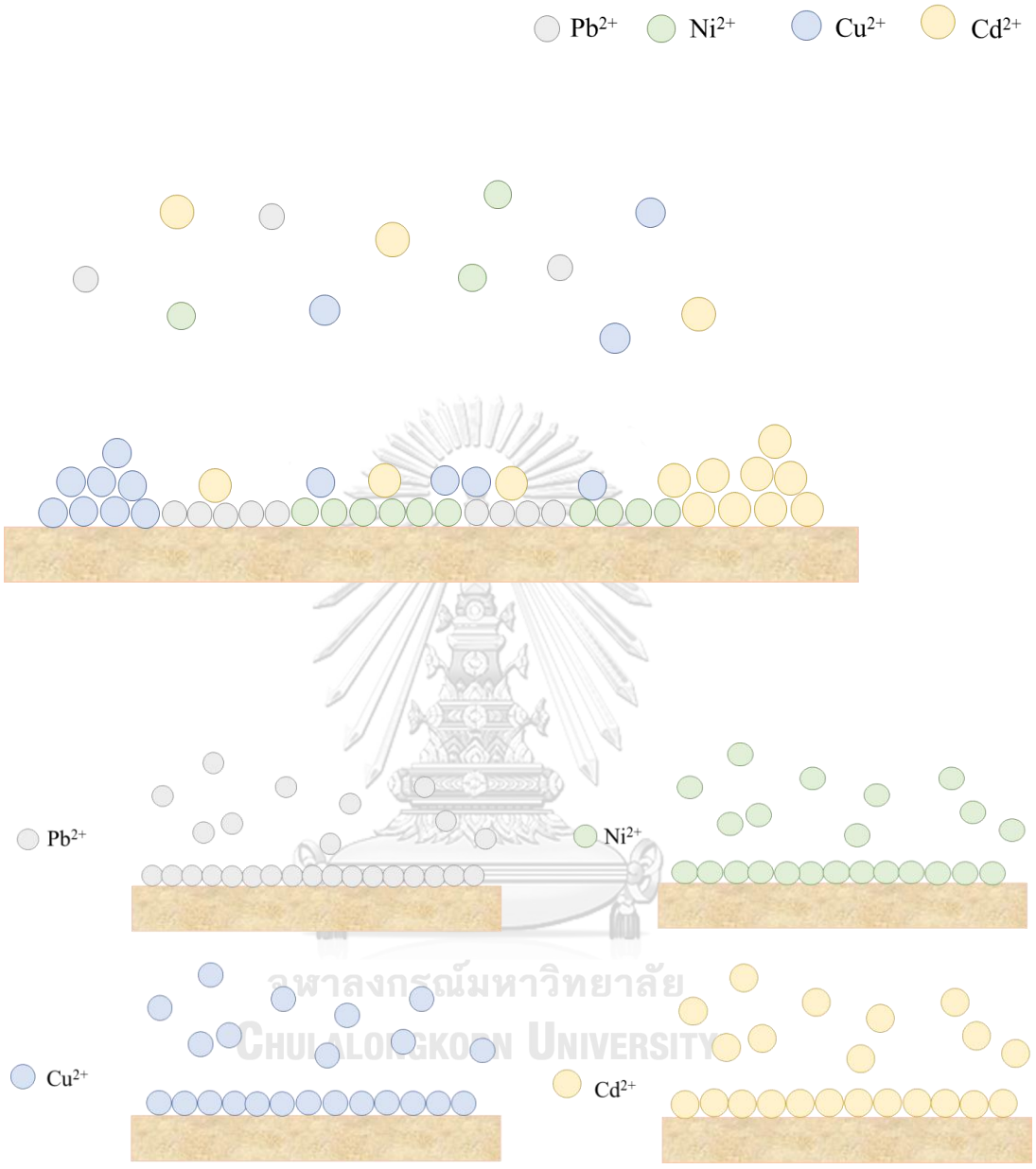

Fig. 4.18 The diagram of adsorption isotherm of metal ions with FAG adsorbent in multi-cations solution (upper) and mono-cations solution (lower)

4.1.4 Kinetics study

4.1.1.1 Pseudo first order model and pseudo second order model

Kinetic adsorption data was model by using the pseudo first order model and pseudo second order model where the aims were determined the best model that describes the adsorption data and understood the mechanism of adsorption. The kinetics of Pb^{2+}, Cd^{2+}, Cu^{2+} and Ni^{2+} by FAG powder in multi- and mono-cations solution are shown in Fig. 4.19. The rate constants of the kinetic models with the regression (R^2) are given in Table 4.4. The results show that the second order model fitted better than first order model with the experimental data based on R^2 and the adsorption capacities (q_e) of calculated values compared with experimental values (q_m). The second order kinetics with respect to availability of surface sites on FAG powder rather than the metal concentration in the solution. Moreover, this model based on assumption that the rate limiting step which might be a chemical adsorption involving the valance forces through exchange or sharing of electrons between the adsorbate and adsorbent [90, 91].

Table 4.4 Parameter values for batch kinetic adsorption models of FAG powder

Solution system	Metal	Pseudo first order			Pseudo second order			Experimental value q_m(mg/g)
		k_1 (min^{-1})	q_e (mg/g)	R^2	k_2 (g/mg min)	q_e (mg/g)	R^2	
Multi-cations	Pb^{2+}	0.012	0.791	0.6597	0.082	7.846	0.9996	7.847
	Cd^{2+}	0.017	1.027	0.9533	0.053	2.760	0.9982	2.701
	Cu^{2+}	0.005	1.227	0.8354	0.035	4.385	0.9856	4.498
	Ni^{2+}	0.014	1.629	0.9481	0.016	2.372	0.9556	2.175
Mono-cations	Pb^{2+}	0.079	0.132	0.7899	1.131	7.893	0.9999	7.993
	Cd^{2+}	0.009	0.643	0.7720	0.262	5.907	0.9989	6.106
	Cu^{2+}	0.015	2.151	0.9475	0.024	7.294	0.9966	7.198
	Ni^{2+}	0.004	0.354	0.3264	0.152	4.750	0.9988	4.796

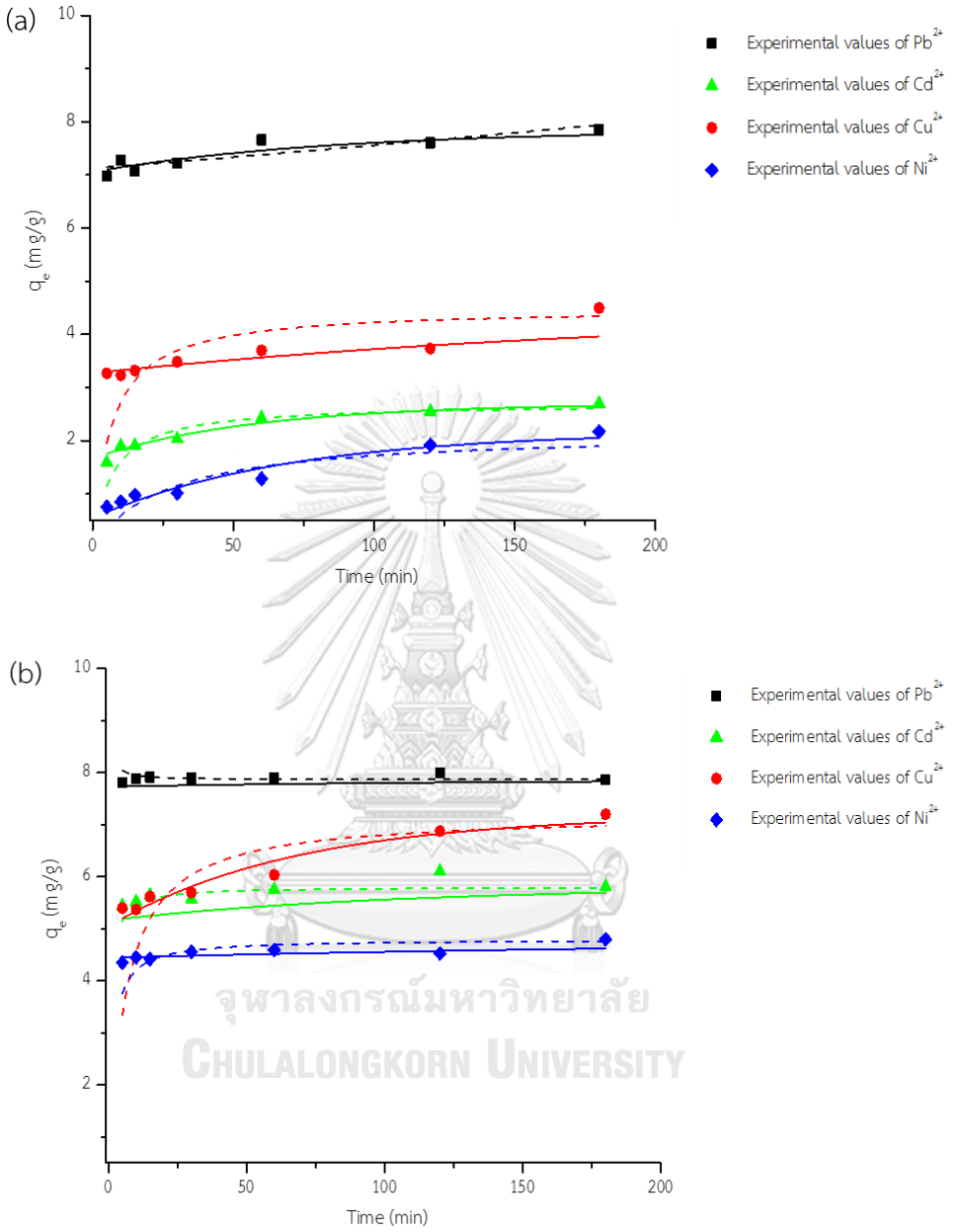

Fig. 4.19 Kinetics of Pb^{2+}, Cd^{2+}, Cu^{2+} and Ni^{2+} adsorption on FAG powder and model's fit to the data (a) multi-cations solution (b) mono-cations solution (Pseudo first order: solid line, Pseudo second order: dash line)

4.1.1.2 Intraparticle diffusion model

From Fig. 4.20, Intraparticle diffusion plots of the adsorption by FAG powder in multi-cations solution and mono-cations solution were seen. Table 4.5 showed Intraparticle diffusion parameters for the adsorption. The fast rate of adsorption occurred in the adsorption process of metal ions and surface of FAG powder, therefore, the trend of the lines had only single line. It is indicated that the intraparticle diffusion was not occurred in the adsorption process of FAG powder and metal ions.

Table 4.5 Intraparticle diffusion parameters for the adsorption by FAG powder

Solution system	Metal	Intraparticle diffusion		
		k_p (mg/g $h^{0.5}$)	C (mg/g)	R^2
Multi-cations	Pb^{2+}	0.555	6.901	0.9214
	Cd^{2+}	0.722	1.536	0.9667
	Cu^{2+}	0.759	2.948	0.9341
	Ni^{2+}	1.004	0.414	0.9878
Mono-cations	Pb^{2+}	0.042	7.856	0.4048
	Cd^{2+}	0.336	5.399	0.8186
	Cu^{2+}	1.325	4.880	0.9864
	Ni^{2+}	0.233	4.325	0.8710

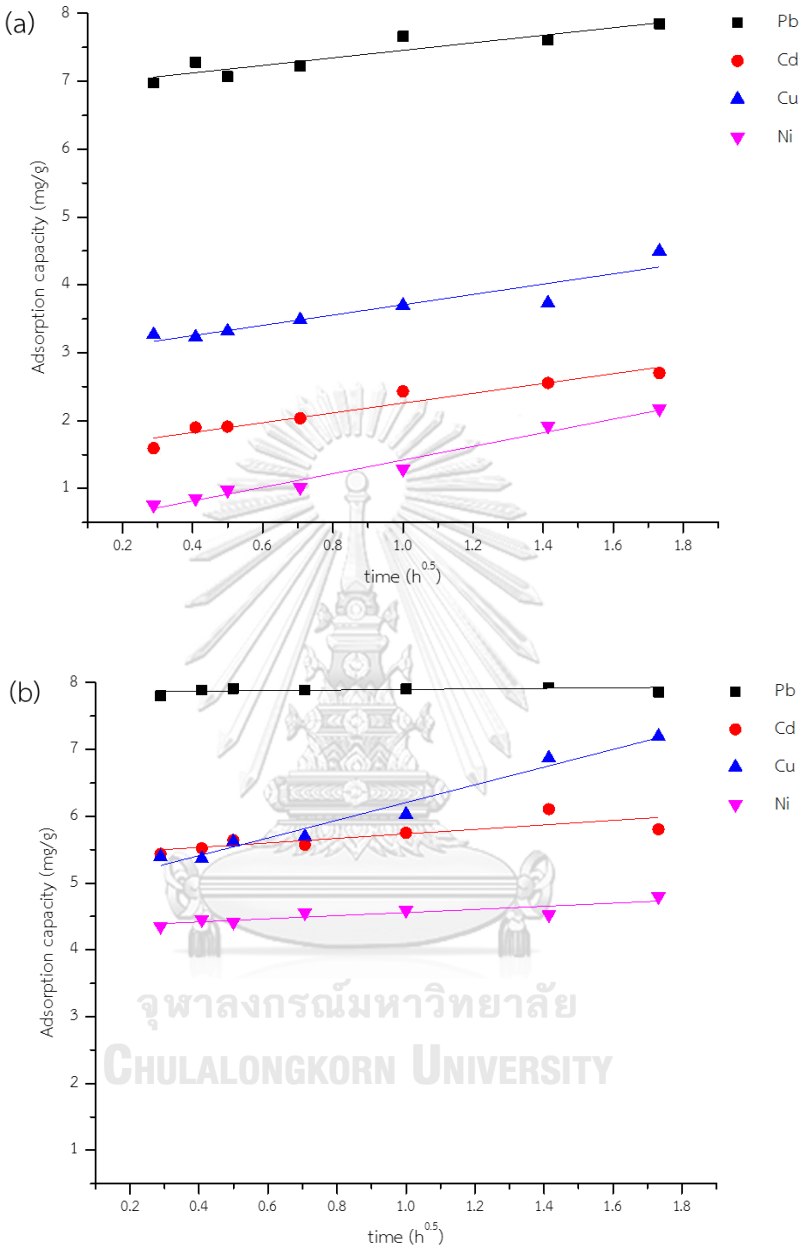

Fig. 4.20 Intraparticle diffusion plots of the adsorption by FAG powder (a) multi-cations solution (b) mono-cations solution

4.2 METAKAOLIN BASED GEOPOLYMER POWDER

4.2.1 Characterizations

4.2.1.1 Chemical composition

From Table 4.6, the chemical composition of metakaolin and washed metakaolin based geopolymer were listed. The results showed that the main composition of metakaolin consisted of 50.30 % SiO_2, 41.60 % Al_2O_3, 1.48 % Fe_2O_3, and 2.80 % K_2O. After geopolymerization process, the main composition of metakaolin geopolymer composed of 47.20 % SiO_2, 31.00 % Al_2O_3, 1.10 % Fe_2O_3, 2.10 % K_2O, and 10.50 % Na_2O. In addition, the amount of SiO_2, Al_2O_3 were decreased when compared with raw metakaolin because metakaolin geopolymer sample was washed with distilled water until pH 7. In the washing process, some of the elements in geopolymer powder could be released with water. Furthermore, the Na_2O in metakaolin geopolymer has high values due to the alkali solution composed of the Na_2O component which uses for reacting with raw materials in geopolymerization reaction.

Table 4.6 Chemical compositions of metakaolin and metakaolin based geopolymer powder

Chemical compound	MK (%)	Washed MK geopolymer (%)
SiO_2	50.30	47.20
Al_2O_3	41.60	31.00
Fe_2O_3	1.48	1.10
CaO	0.05	0.06
MgO	0.10	0.08
Na_2O	0.11	10.50
K_2O	2.80	2.10
MnO	0.12	0.10

4.2.1.2 Phases

The metakaolin and metakaolin geopolymer powder were characterized by XRD as shown in Fig. 4.21. The crystalline minerals of metakaolin and metakaolin geopolymer were muscovite (JCPDS, 00-007-0042), quartz (JCPDS, 01-089-8934), alunite (JCPDS, 00-003-0616) and kaolinite (JCPDS, 01-089-6538). However, the metakaolin geopolymer showed a broad hump peak between 2θ=18 - 32° which provided amorphous phase. The crystalline peaks intensities decreased after geopolymerization process in geopolymer phases as metakaolin was dissolved by alkali solution and transformed to an amorphous structure and some minerals could be released in the washing process. For this reason, it could be confirmed that the geopolymerization of alumino-silicate materials was successfully synthesized.

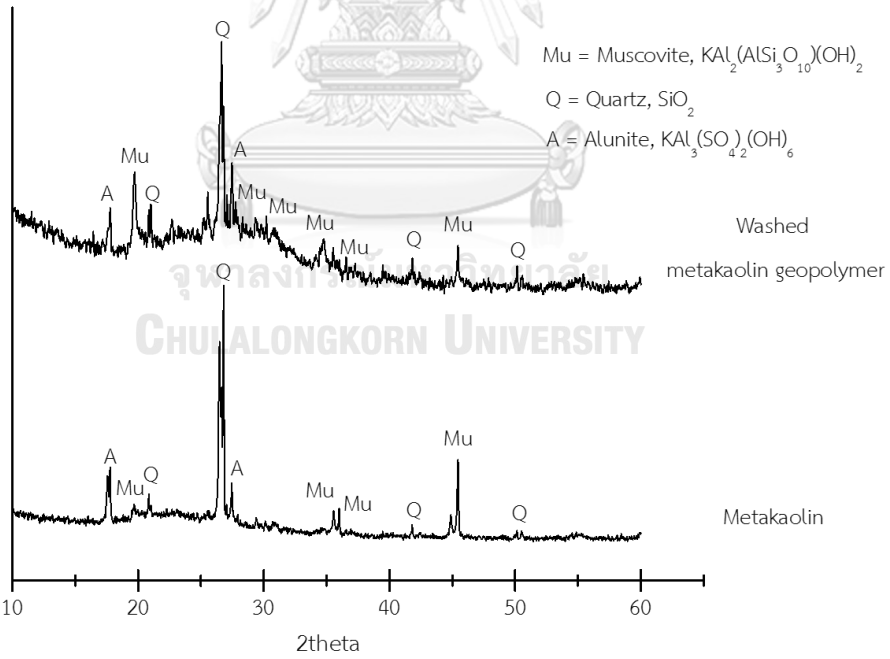

Fig. 4.21 XRD patterns of metakaolin and washed metakaolin based geopolymer powder

4.2.1.3 Microstructure

SEM micrograph of metakaolin and washed metakaolin based geopolymer powder at 1000× and 3000x magnification as shown in Fig. 4.22. The metakaolin showed the coarser aggregates with irregular particles in the range size of 10-100 μm (Fig. 4.22 a-b). The surface metakaolin particles after geopolymerization process was rougher surface than unreacted metakaolin because the surface of particles was dissolved by alkali solution and sodium silicate solution to produced aluminate and silicate species for geopolymerization reaction (Fig. 4.22 c-d).

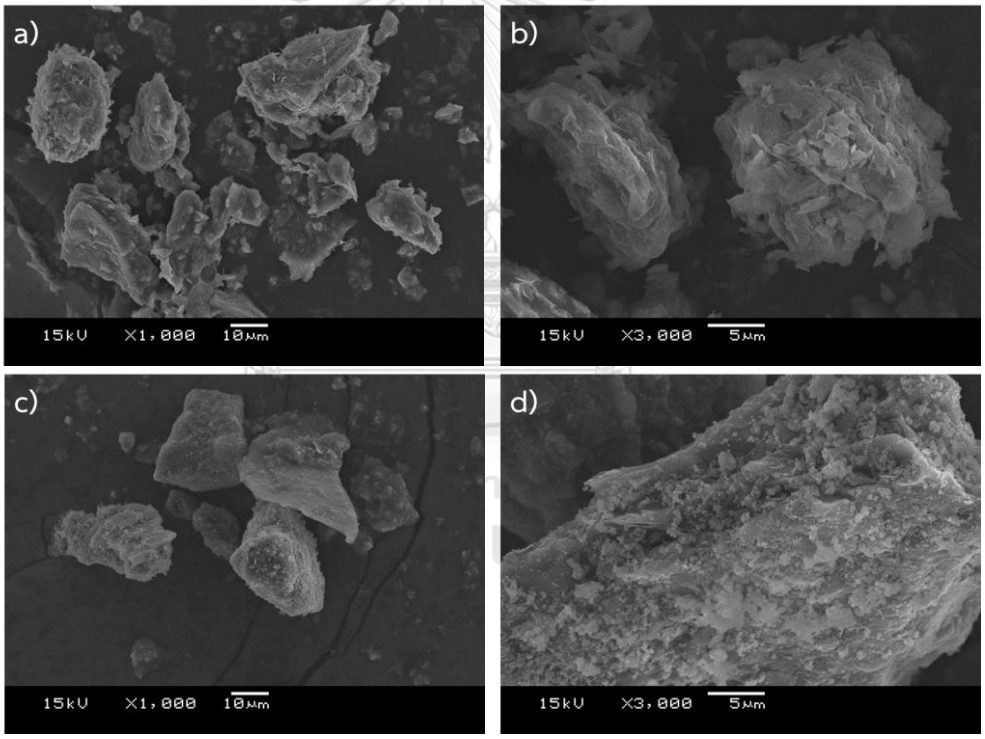

Fig. 4.22 SEM micrograph of (a-b) metakaolin and (c-d) washed metakaolin based geopolymer powder

4.2.1.4 Particle size distribution and surface area

Particle size distribution of metakaolin and washed mtakaolin based geopolymer powder was measured by laser light scattering technique (Fig. 4.23). The laser-scattered particle distribution of metakaolin showed the powder size distribution in the range of 1–100 μm. Moreover, the particle distribution of washed metakaolin based geopolymer powder was 1–200 μm. and showed bi-modal particle size distribution at average particle size of 11.48 and 52.48 μm. Particle size distributions of metakaolin and washed metakaolin based geopolymer powder in the median were 20.97 and 29.43, respectively. The particle size of geopolymer powder in the range 10-80 μm was decreased and particle size higher than 100 μm was increased because the small particle was reacted and agglomerated to be a large particles during the reaction.

The metakaolin powder has lower specific surface area compared to the washed metalakolin based geopolymer powder with specific surface area of 9.84 and 20.36 m^2/g, respectively.

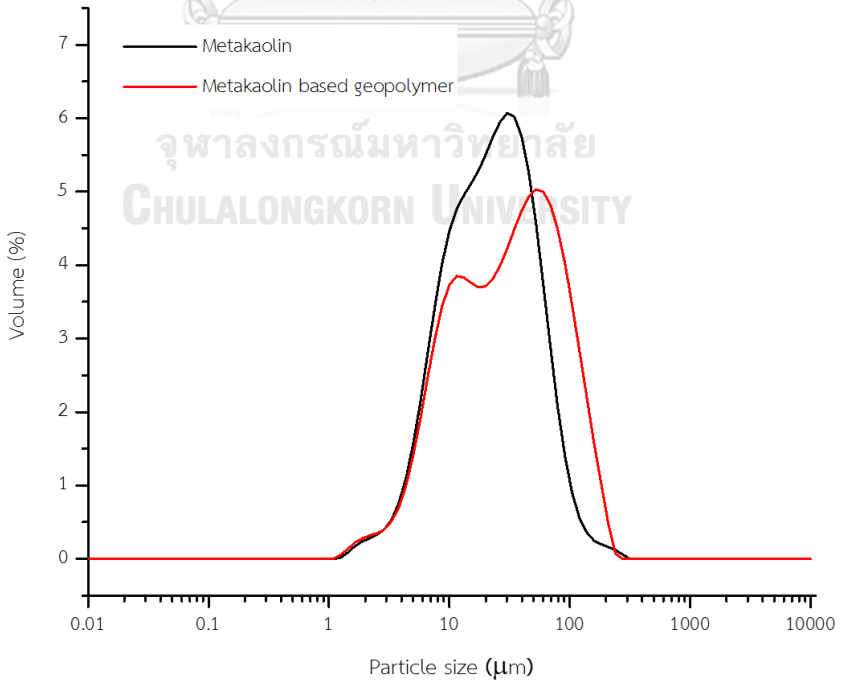

Fig. 4.23 Particle size distribution of metakaolin and washed metakaolin based geopolymer powder

4.2.2 Adsorption test

4.2.2.1 Effect of contact time

The effect of contact time of Pb^{2+}, Cu^{2+}, Cd^{2+}, Ni^{2+} in multi- and mono-cations solutions was determined between 5-180 min and the results were presented in Fig. 4.24 and Fig. 4.25. The initial concentration of each heavy metal ions was fixed at 20 mg/L with 0.1 g of geopolymer in 40 mL of solution and initial pH of 5. Heavy metals of Pb^{2+}, Cu^{2+}, Cd^{2+}, and Ni^{2+} were adsorbed by geopolymer powder. The results showed that the adsorption was fast at initial stage of contact period and it became slower near equilibrium. Therefore, 120 and 180 min were determined as the equilibrium time with the adsorption efficiency of and the adsorption capacity values of 100, 88.67, 79.27 and 39.08% and 8, 7.09, 6.34 and 3.13 mg/g for Pb^{2+}, Cu^{2+}, Cd^{2+}, Ni^{2+}, respectively in multi-cations solution. Moreover, the adsorption efficiency of and the adsorption capacity values of 97.17, 85.12, 80.22 and 72.21% and 7.77, 6.81, 6.41 and 5.77 mg/g for Pb^{2+}, Cu^{2+}, Cd^{2+}, Ni^{2+}, respectively in mono-cations solution were shown.

4.2.2.2 Effect of geopolymer dosage

Adsorbent dosage is an important parameters due to it determines the adsorption capacity of an adsorbent for given initial concentration of the adsorbate. Therefore, the effect of geopolymer amount on the adsorption of Pb^{2+}, Cu^{2+}, Cd^{2+}, Ni^{2+} ions onto MKG powder is investigated and the results are shown in Fig. 4.26 and Fig. 4.27. It was seen that the percentage of metal removal increased with an increase in the adsorbent dose. Pb^{2+}, Cu^{2+}, Cd^{2+}, Ni^{2+} removal efficiency from 75.23% (6.01 mg/g), 23.41% (1.87 mg/g), 18.19% (1.45 mg/g) and 1.55% (0.12 mg/g) to 100% (8 mg/g), 88.67% (7.09 mg/g), 79.27% (6.34 mg/g) and 39.08% (3.13 mg/g), respectively when the adsorbent dose was increase from 0.02 to 0.10 g/ 40mL in multi-cations solution. In addition, the percentage of metal removal increased with an increase in the adsorbent

dose. Pb^{2+}, Cu^{2+}, Cd^{2+}, Ni^{2+} removal efficiency from 77.61% (6.21 mg/g), 73.92% (5.91 mg/g), 68.11% (5.45 mg/g) and 52.47% (4.20 mg/g) to 97.17% (7.77 mg/g), 85.12% (6.81 mg/g), 80.22% (6.41 mg/g) and 72.21% (5.77 mg/g), respectively when the adsorbent dose was increase from 0.02 to 0.10 g/ 40mL in the case of mono-cations solution. Further increase in the adsorbent up to 0.12 g/ 40mL, the removal efficiency and the adsorption capacity was not significantly changed. It might be explain by the increase surface area and active sites on the adsorbent surface with increased adsorbent dose. Accordingly, the optimum dose of MKG powder to achieve the highest removal efficiency and highest adsorption capacity for Pb^{2+}, Cu^{2+}, Cd^{2+}, Ni^{2+} was determined as 0.1 g/ 40mL.

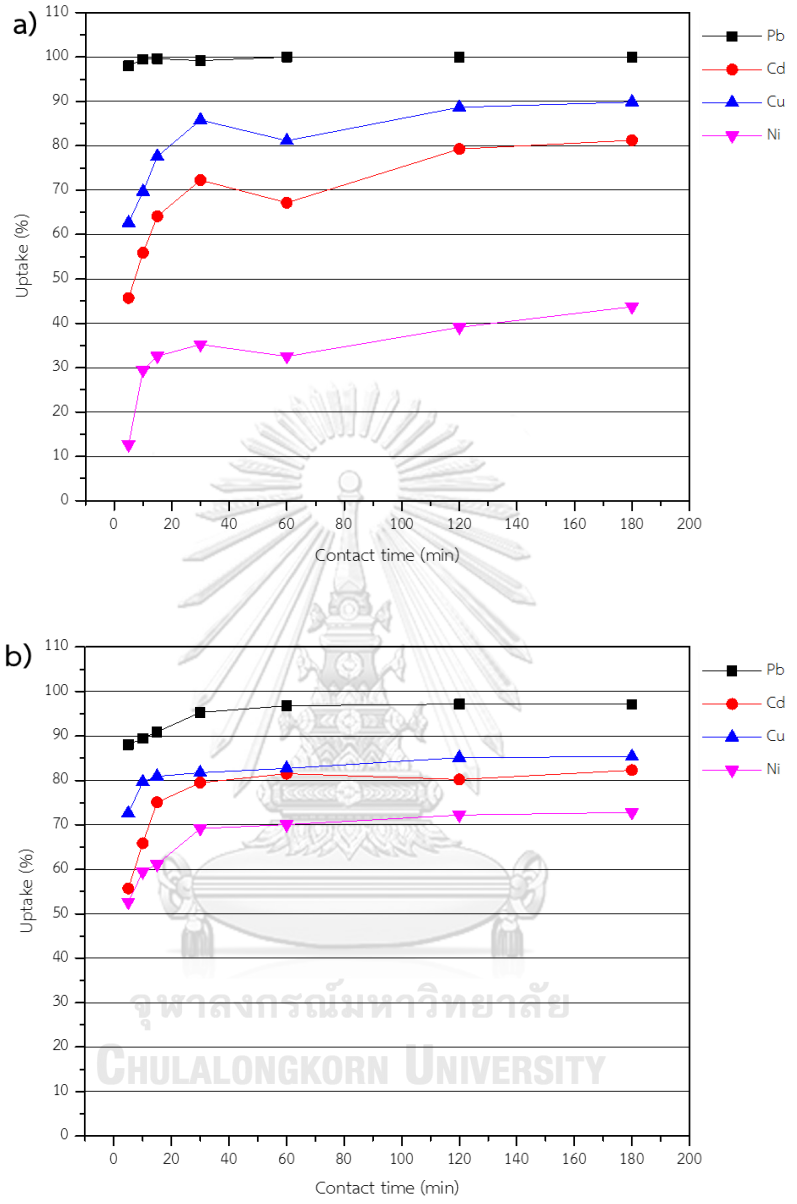

Fig. 4.24 Effect of contact time on heavy metal ions removal efficiency of MKG powder (a) multi-cations solution (b) mono-cations solution

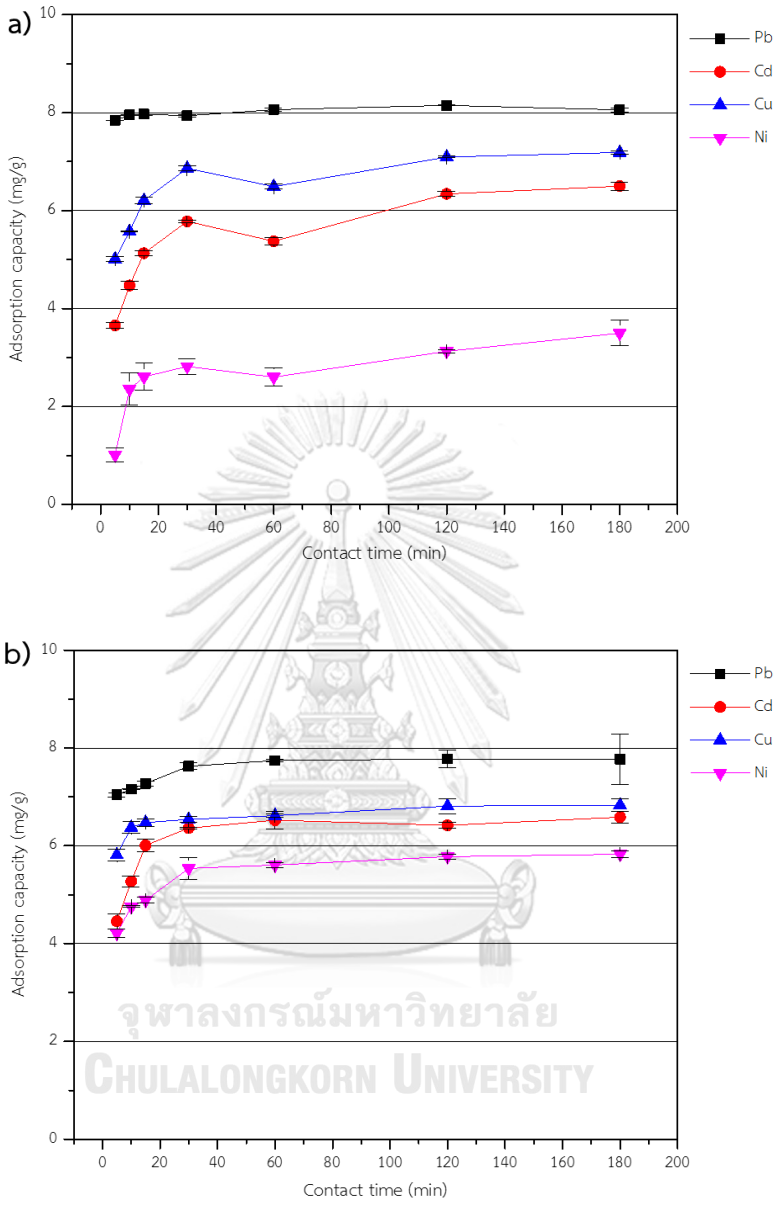

Fig. 4.25 Effect of contact time on adsorption capacity of MKG powder (a) multi-cations solution (b) mono-cations solution

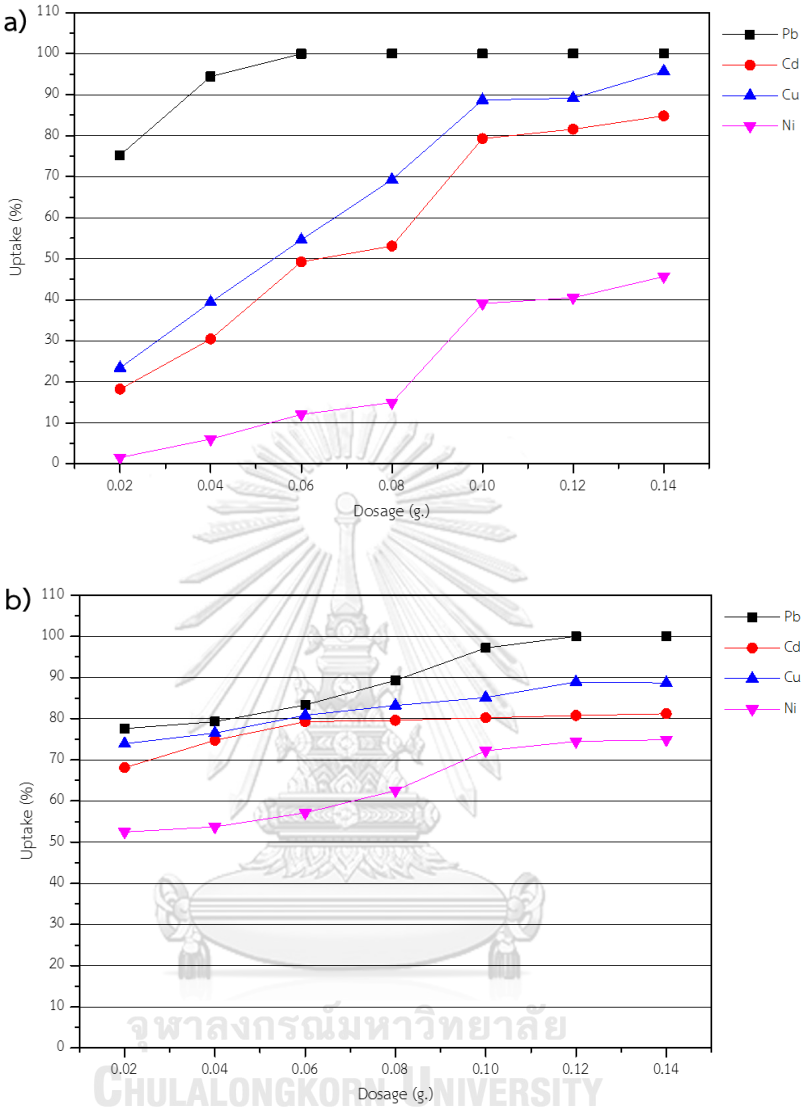

Fig. 4.26 Effect of adsorbent dose on heavy metal ions removal efficiency of MKG powder (a) multi-cations solution (b) mono-cations solution

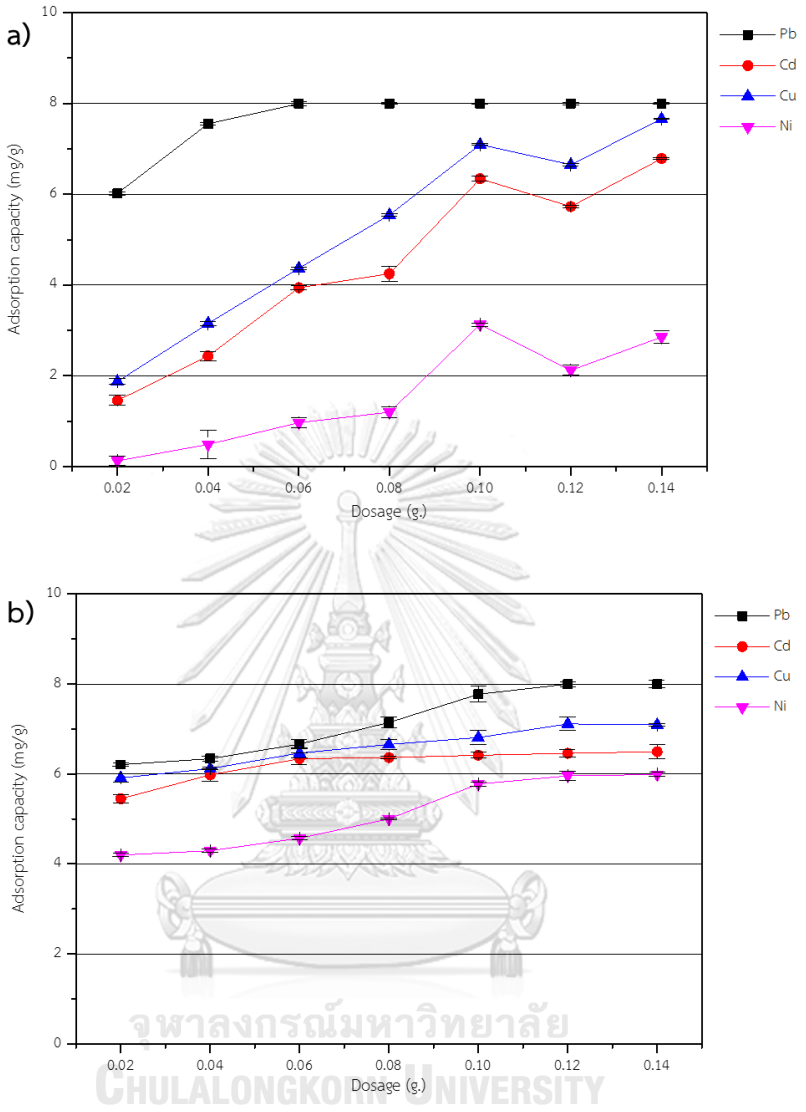

Fig. 4.27 Effect of adsorbent dose on adsorption capacity of MKG powder (a) multi-cations solution (b) mono-cations solution

4.2.2.3 Effect of solution pH

The pH of aqueous solution is one of parameter for controlling an adsorption process. The effect of pH on Pb^{2+}, Cu^{2+}, Cd^{2+}, Ni^{2+} adsorption onto MKG powder was investigated by ranging the solution pH from 1 to 5 at 25 ^{o}C and the removal efficiency and the adsorption capacity of MKG powder with multi- and mono-cations solution as a function of pH are plotted in Fig. 4.28 and Fig. 4.29. An apparent increase in Pb^{2+}, Cu^{2+}, Cd^{2+}, Ni^{2+} removal effiecncy and adsorption capacity of MKG powder was observed until pH 5. The adsorbent tends to select H^{+} when the concentration of H^{+} ions in solution is higher. Therefore, the adsorption efficiency and the adsorption capacity of heavy metals decresed in low pH. As a results, the removal efficiency and the adsorption capacity of MKG powder were carried out at original pH values of the metal solution (pH around 5).

4.2.2.4 Effect of temperature

In order to investigate the effect of temperature on the adsorption efficiency and the adsorption capacity of Pb^{2+}, Cu^{2+}, Cd^{2+}, Ni^{2+} onto MKG powder, the experiments were carried out at different temperatures. The relationship between the temperature and adsorption efficiency and the adsorption capacity values are illustrated in Fig. 4.30 and Fig. 4.31. Adsorption efficiency and the adsorption capacity values were slightly increased when the temperature was increase from 25 to 45 ^{o}C. It can also be seen from the figures that adsorption efficiency and the adsorption capacity values were not significantly changed by the temperature after 25 ^{o}C. Accordingly, further adsorption studies were conducted at 25 ^{o}C for Pb^{2+}, Cu^{2+}, Cd^{2+} and Ni^{2+} ions.

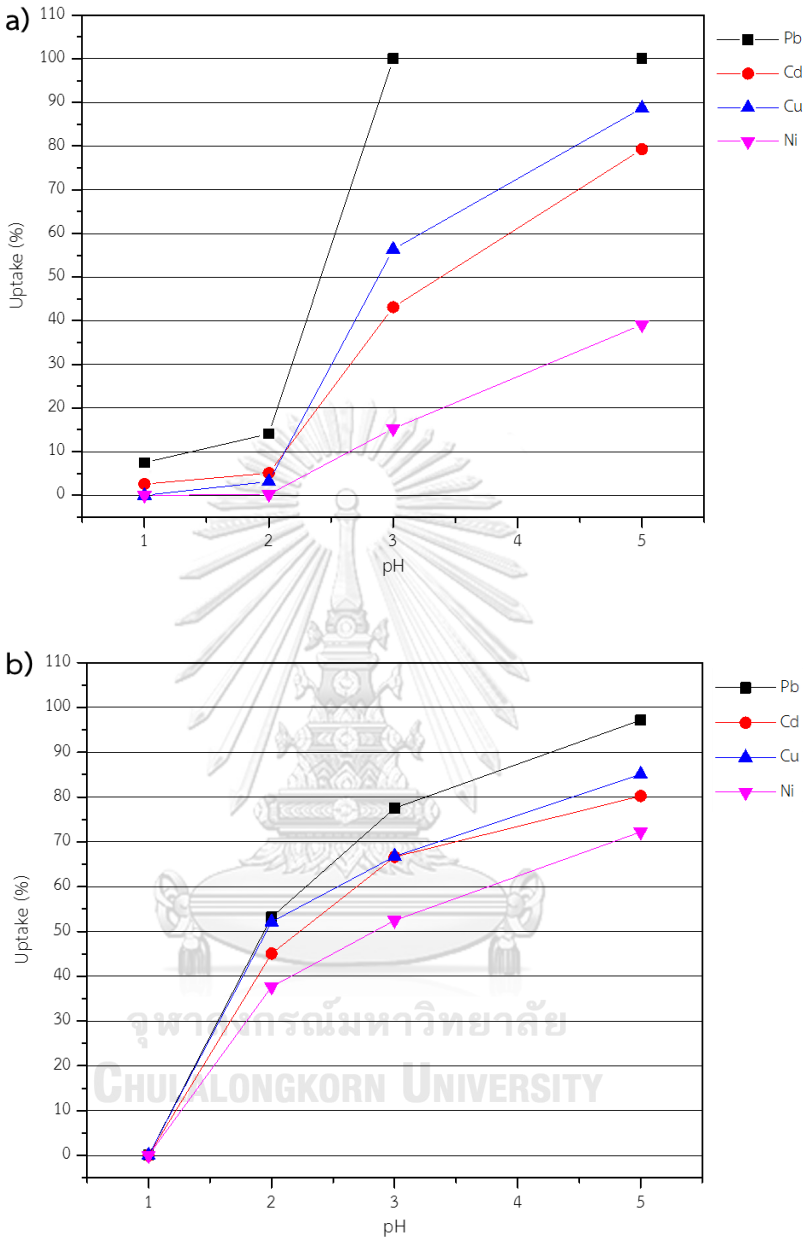

Fig. 4.28 Effect of pH on heavy metal ions removal efficiency of MKG powder (a) multi-cations solution (b) mono-cations solution

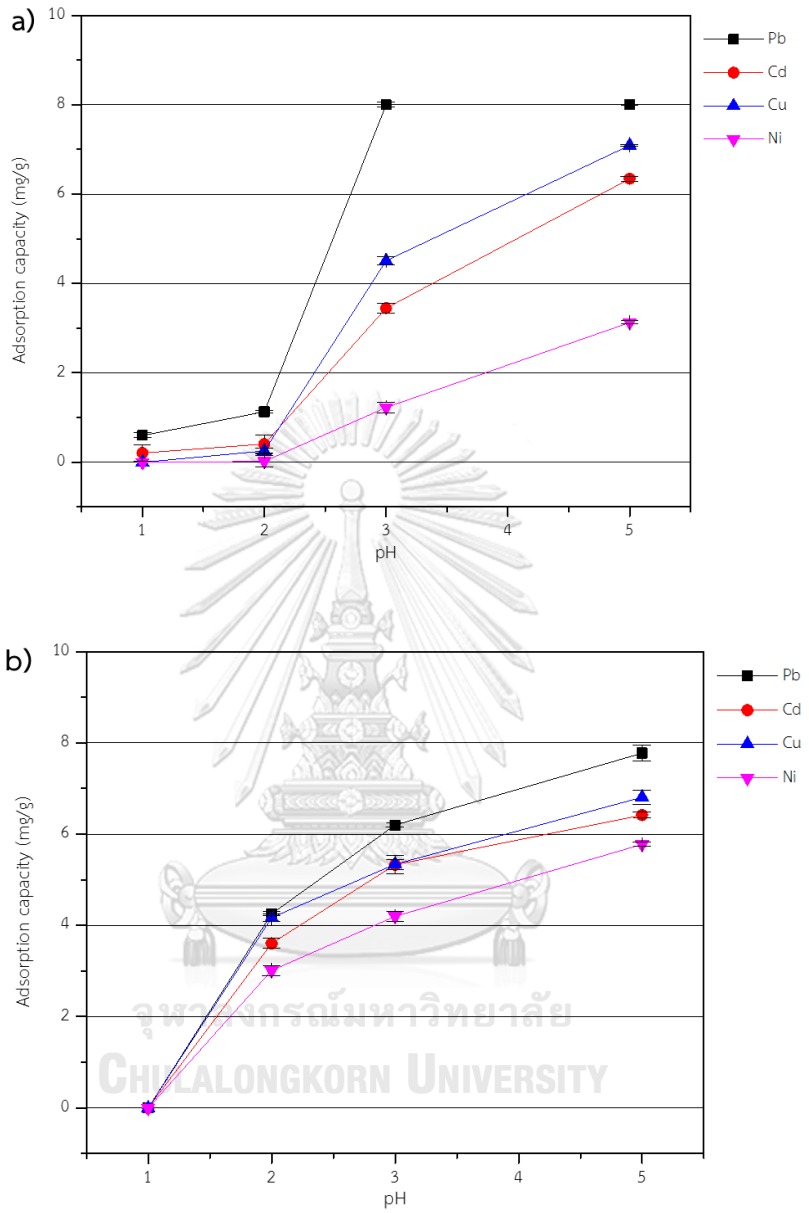

Fig. 4.29 Effect of pH on adsorption capacity of MKG powder (a) multi-cations solution (b) mono-cations solution

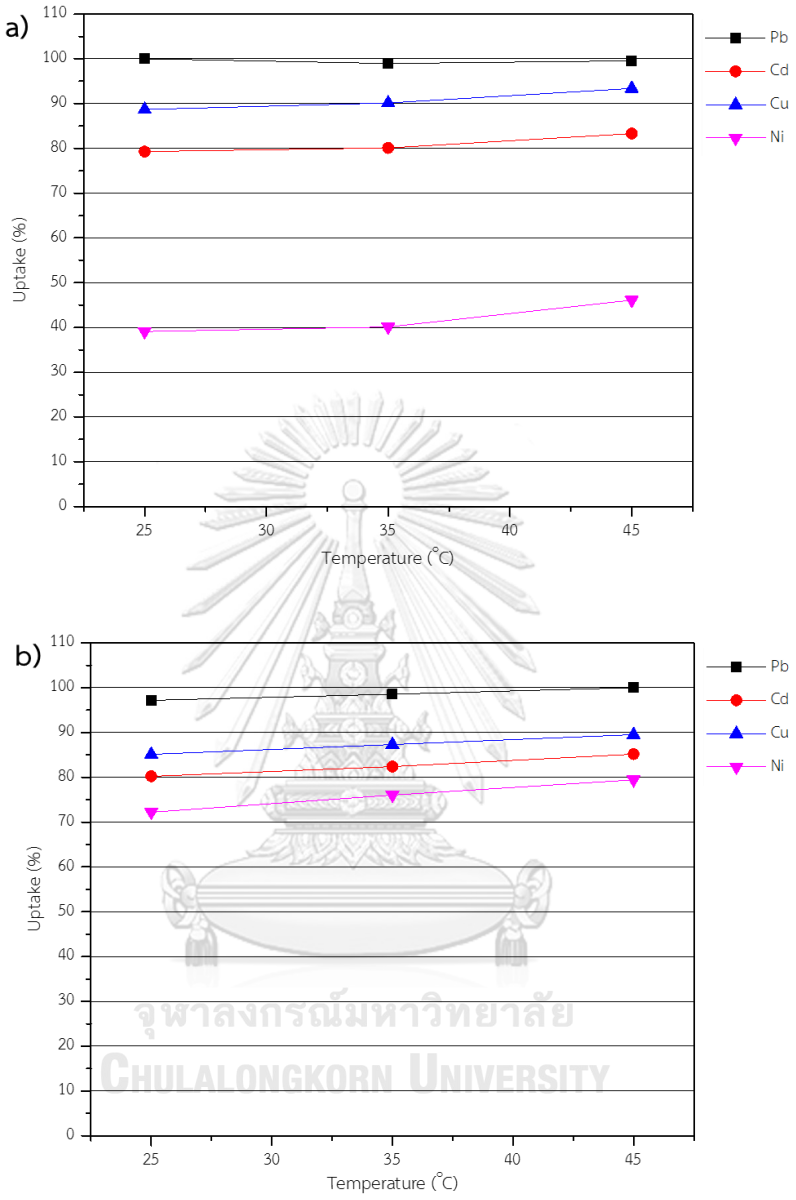

Fig. 4.30 Effect of temperature on heavy metal ions removal efficiency of MKG powder (a) multi-cations solution (b) mono-cations solution

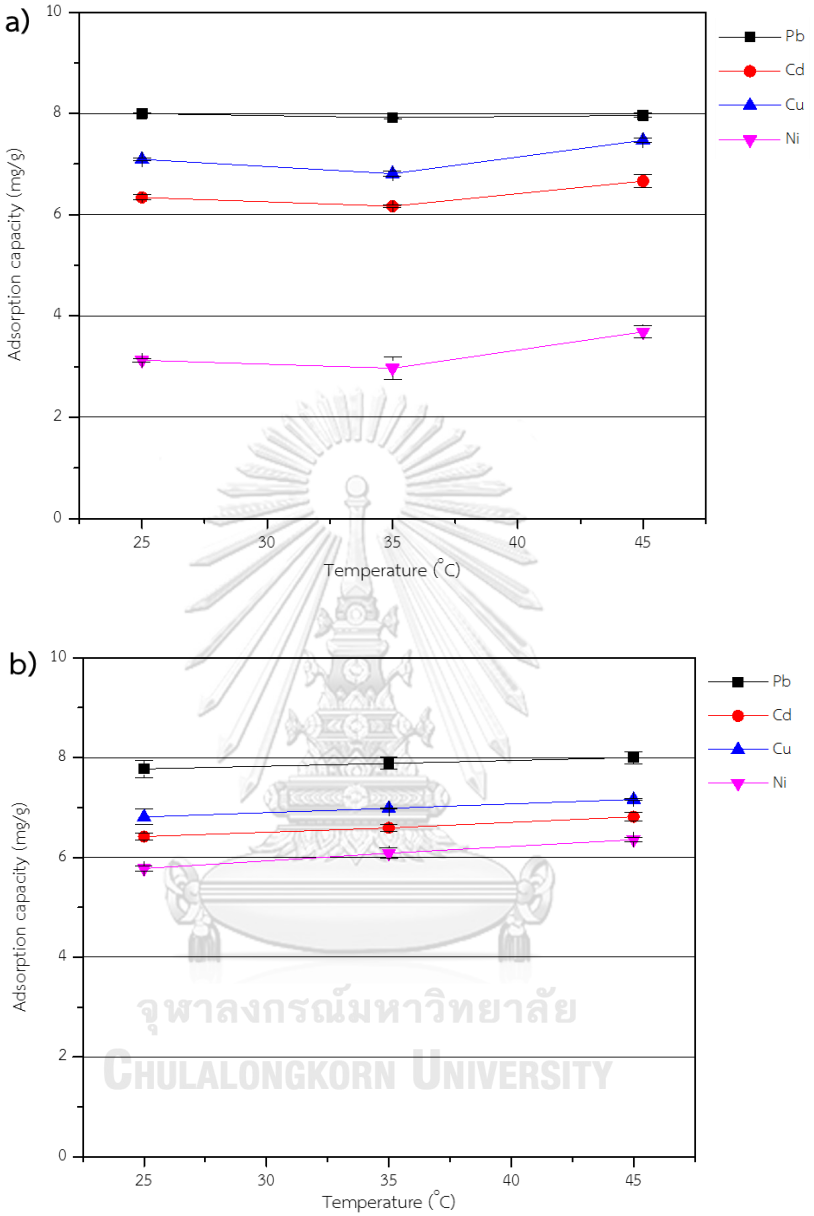

Fig. 4.31 Effect of temperature on adsorption capacity of MKG powder (a) multi-cations solution (b) mono-cations solution

4.2.2.5 Effect of initial concentration

The initial concentration was studied using a geopolymer dosage of 0.1 g/ 40 mL at pH 5 and a temperature of 25 ^{o}C for 120 min contact time. The initial concentration of heavy metal solution was varied from 20-120 mg/L. the removal efficiency and the adsorption capacity of MKG powder with multi- and mono-cations solution as a function of initial concentration are plotted in Fig. 4.32 and Fig. 4.33. The removal efficiency decreased with an increase of initial concentration. The maximum adsorption capacity values of Pb^{2+}, Cu^{2+}, Cd^{2+}, and Ni^{2+} were found as 39.49 mg/g of Pb^{2+} at 120 mg/L, 9.38 mg/g of Cu^{2+} at 60 mg/L, 7.03 mg/g of Cd^{2+} at 40 mg/L and 3.18 mg/g of Ni^{2+} at 10 mg/L in multi-cations solution. Moreover, the maximum adsorption capacity values of Pb^{2+}, Cu^{2+}, Cd^{2+}, and Ni^{2+} were seen as 42.67 mg/g of Pb^{2+} at 120 mg/L, 31.62 mg/g of Cu^{2+} at 120 mg/L, 29.83 mg/g of Cd^{2+} at 120 mg/L and 29.33 mg/g of Ni^{2+} at 100 mg/L in mono-cations solution.

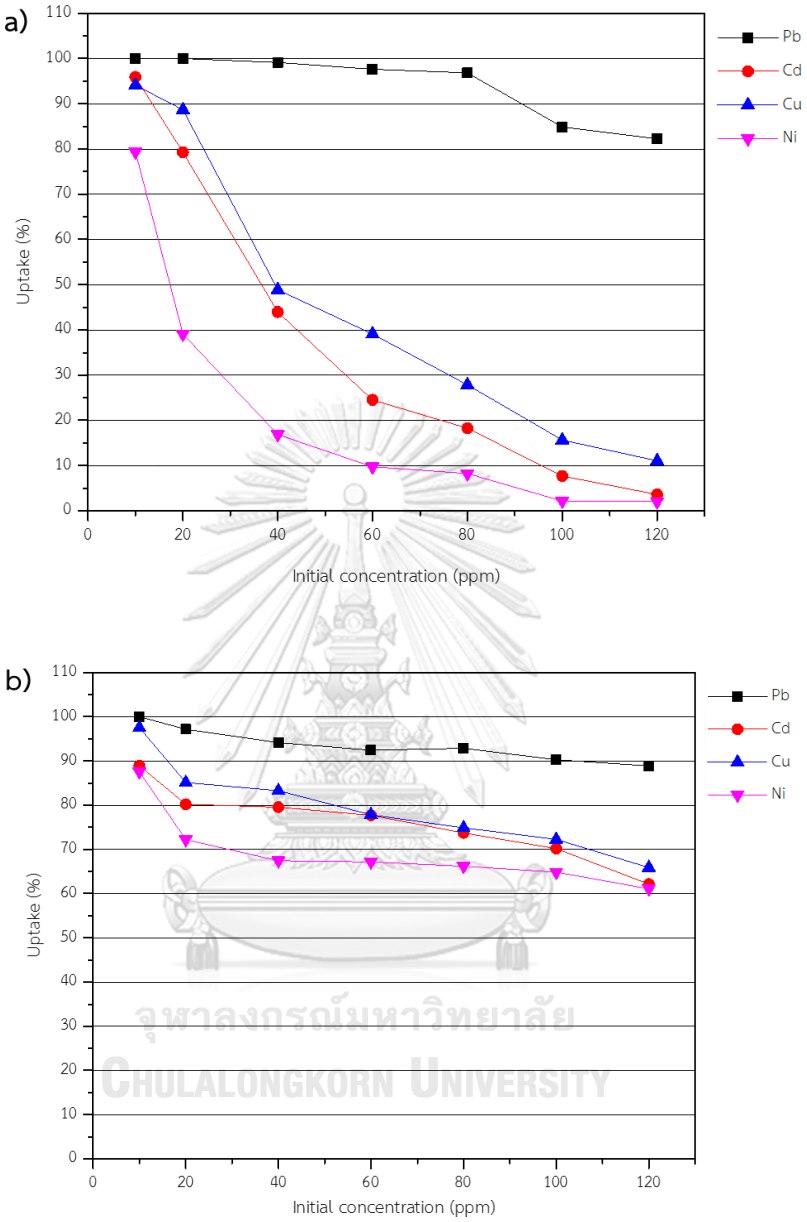

Fig. 4.32 Effect of initial concentration on heavy metal ions removal efficiency of MKG powder (a) multi-cations solution (b) mono-cations solution

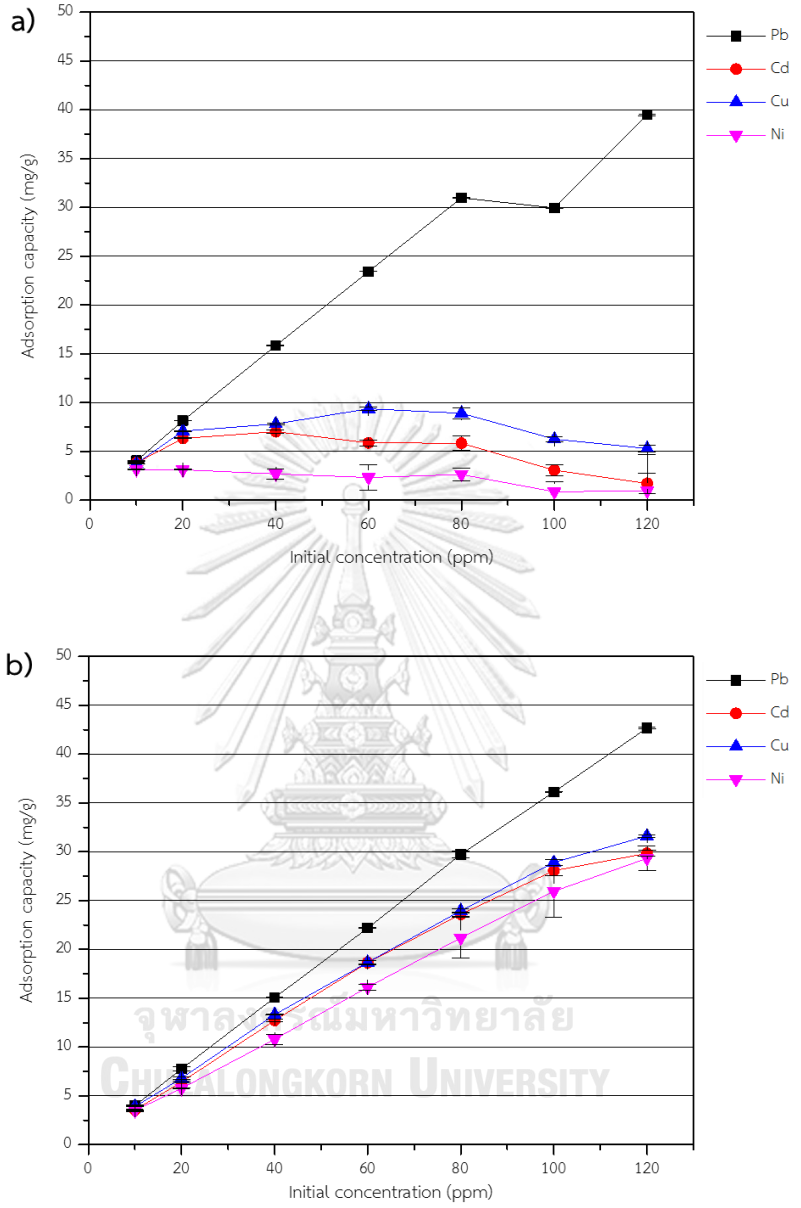

Fig. 4.33 Effect of initial concentration on adsorption capacity of MKG powder (a) multi-cations solution (b) mono-cations solution

4.2.3 Adsorption isotherm

The isotherm analysis on MKG powder of Pb^{2+}, Cu^{2+}, Cd^{2+}, Ni^{2+} is shown in Fig. 4.34 to Fig. 4.37. The four model as Langmuir, Freundlich, Redlich-Peterson and Dubinin-Radushkevish isotherm models were adopted to fit for the experimental data and the fitting results are given in Table 4.7. In addition, the model parameters of adsorption isotherm is presented in Table 4.8. Moreover, the diagram of adsorption isotherm which were fitted with each ions are shown in Fig. 4.38.

In multi-cations solution, the isotherms of Pb^{2+}, Cd^{2+}, Cu^{2+}, and Ni^{2+} by MKG powder were Langmuir isotherm, Redilich-Peterson isotherm, Freundlich isotherm and Redilich-Peterson isotherm, respectively. Pb^{2+} was fitted well with Langmuir adsorption isotherm. The results indicated that Pb^{2+} could adsorb on MKG powder in monolayer. Cd^{2+} and Ni^{2+} was fitted well with Redilich-Peterson isotherm which is combined the Langmuir and Freundlich isotherm. Cu^{2+} was fitted well with Freundlich adsorption isotherm. It meant that Cu^{2+} was adsorbed on MKG powder in multilayer on heterogeneous surface.

In mono-cations solution, all of Pb^{2+}, Cu^{2+}, Cd^{2+}, Ni^{2+} were fitted well with Redilich-Peterson adsorption isotherm. The results concluded that Pb^{2+}, Cu^{2+}, Cd^{2+}, Ni^{2+} were adsorbed on MKG powder in multi- and mono-layer on heterogeneous which is combined the Langmuir and Freundlich isotherm.

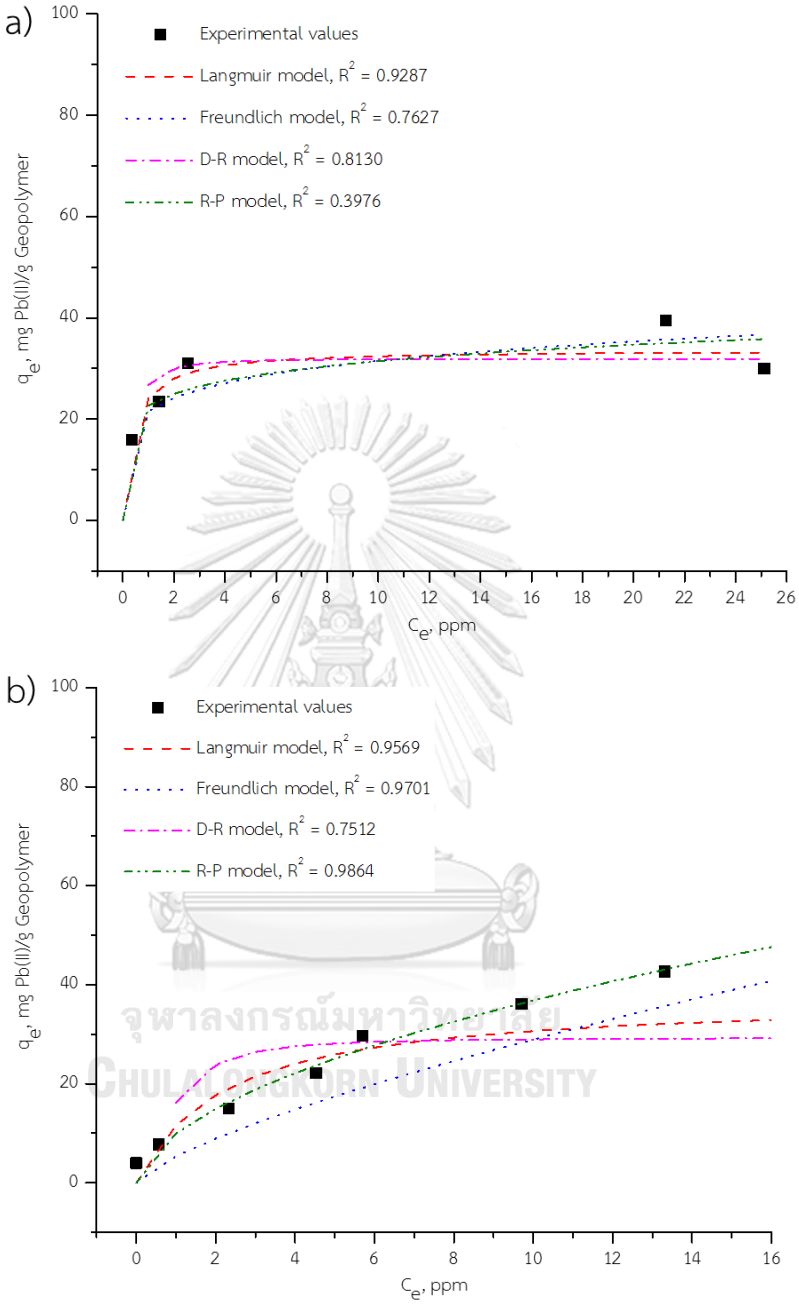

Fig. 4.34 The adsorption isotherms of Pb(II) by applying Langmuir, Freundlich, Redlich-Peterson and Dubinin–Radushkevich isotherm models MKG adsorbent (a) multi-cations solution (b) mono-cations solution

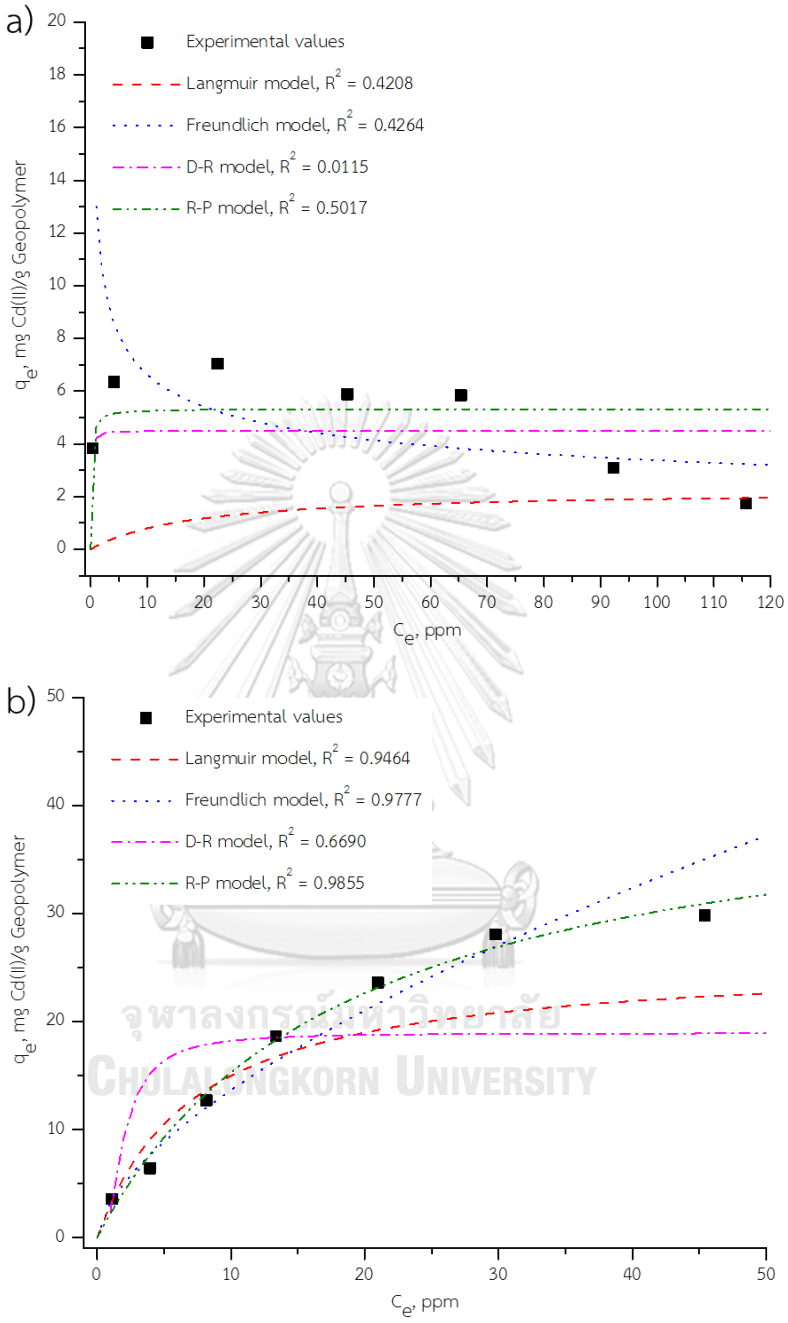

Fig. 4.35 The adsorption isotherms of Cd(II) by applying Langmuir, Freundlich, Redlich-Peterson and Dubinin–Radushkevich isotherm models MKG adsorbent (a) multi-cations solution (b) mono-cations solution

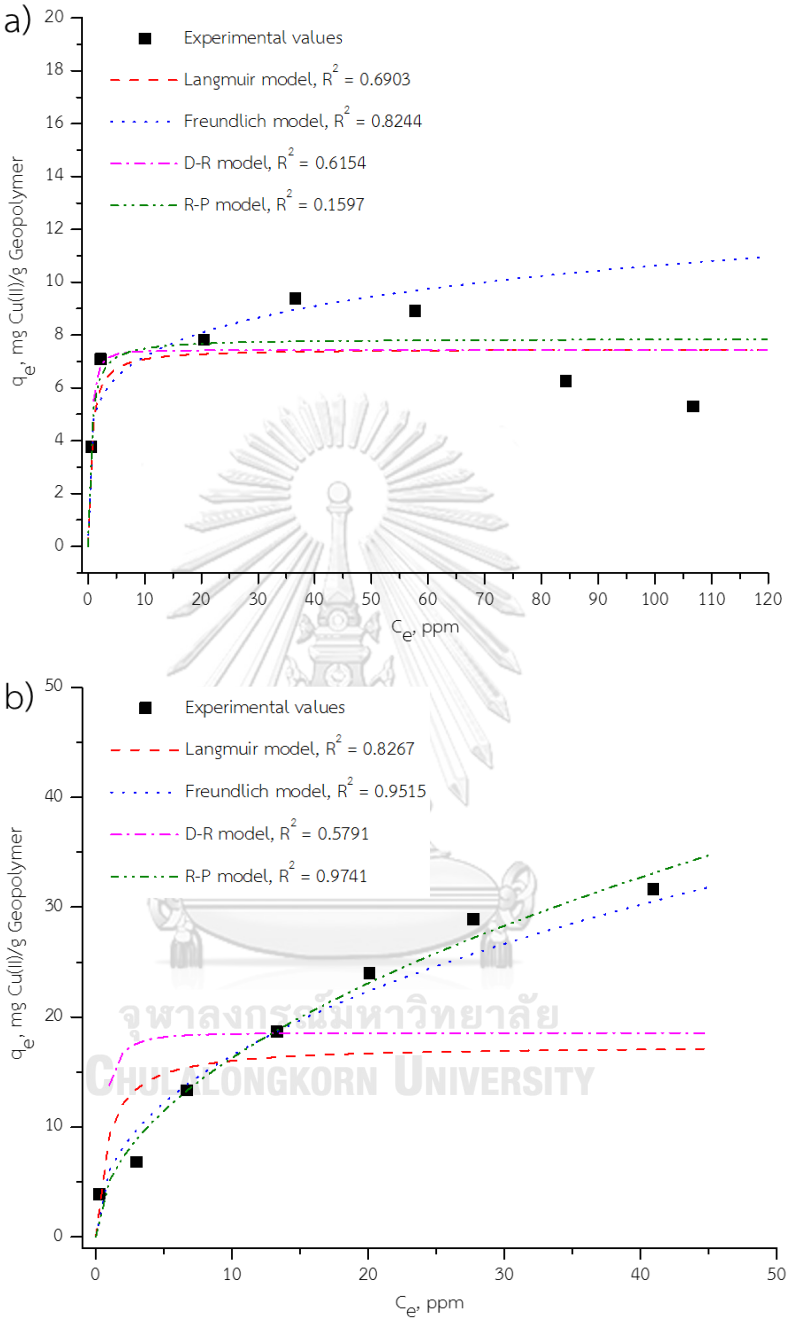

Fig. 4.36 The adsorption isotherms of Cu(II) by applying Langmuir, Freundlich, Redlich-Peterson and Dubinin–Radushkevich isotherm models MKG adsorbent (a) multi-cations solution (b) mono-cations solution

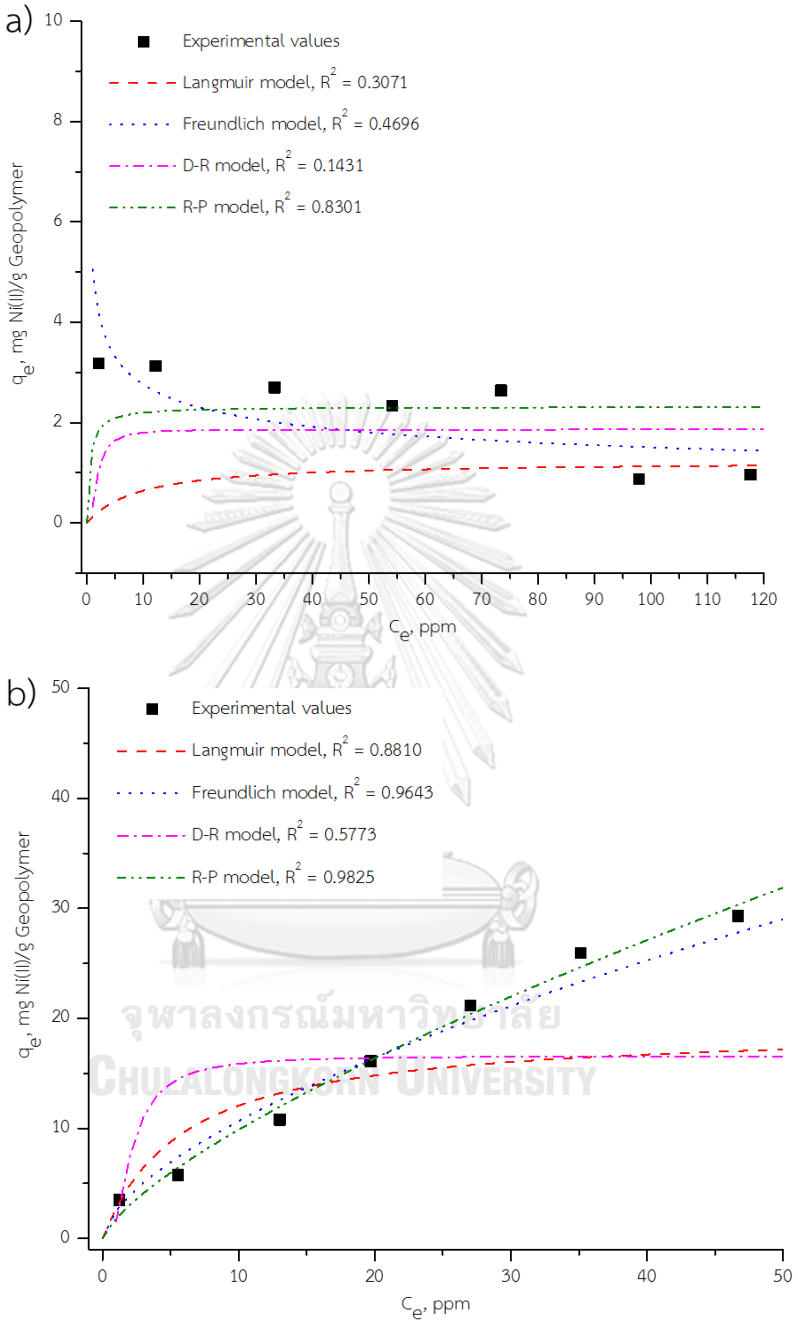

Fig. 4.37 The adsorption isotherms of Ni(II) by applying Langmuir, Freundlich, Redlich-Peterson and Dubinin–Radushkevich isotherm models MKG adsorbent (a) multi-cations solution (b) mono-cations solution

Table 4.7 Summary of adsorption isotherm of metal ions with MKG adsorbent

Solution system	Metal ion	Isotherm model
Multi-cations	Pb^{2+}	Langmuir model
	Cd^{2+}	Redlich-Peterson model
	Cu^{2+}	Freundlich model
	Ni^{2+}	Redlich-Peterson model
Mono-cations	Pb^{2+}	Redlich-Peterson model
	Cd^{2+}	Redlich-Peterson model
	Cu^{2+}	Redlich-Peterson model
	Ni^{2+}	Redlich-Peterson model

Table 4.8 Parameters on Langmuir, Freundlich, Redlich-Peterson and Dubinin-Radushkevish isotherm of MKG adsorbent

Solution system	Isotherm model	Parameter	Metal			
			Pb^{2+}	Cd^{2+}	Cu^{2+}	Ni^{2+}
Multi-cations	Langmuir	q_m	33.670	2.256	7.479	1.230
		K_L	2.517	0.045	1.819	0.110
		R^2	0.9287	0.4208	0.6903	0.3071
		R_L	0.018	0.137	0.005	0.071
	Freundlich	K_F	21.565	13.007	4.860	5.054
		$1/n$	0.165	0.293	0.170	0.263
		R^2	0.7627	0.4264	0.8244	0.4696
	Redlich-Peterson	K_{RP}	-1.4×10^{8}	37..549	15.673	4.329
		a	-4.58×10^{6}	7.051	1.992	1.870
		g	0.858	1	1	1
		R^2	0.3976	0.5017	0.1599	0.8301
	Dubinin–Radushkevich	q_m	31.900	4.482	7.428	1.863
		β	6×10^{-8}	2×10^{-8}	1×10^{-7}	6×10^{-7}
		R^2	0.8130	0.0115	0.6154	0.1431
		E	2886.751	5000	2236.067	912.870
Mono-cations	Langmuir	q_m	37.453	25.907	17.422	19.194
		K_L	0.450	0.137	1.150	0.169
		R^2	0.9569	0.9464	0.8267	0.8810
		R_L	0.143	0.139	0.021	0.112
	Freundlich	K_F	5.384	3.253	6.045	2.546
		$1/n$	0.731	0.623	0.436	0.622
		R^2	0.9701	0.9777	0.9515	0.9643
	Redlich-Peterson	K_{RP}	79.935	2.359	488577	4544.74
		a	6.981	0.054	95524	5457.450
		g	0.472	1	0.497	0.272
		R^2	0.986	0.9855	0.9741	0.9825
	Dubinin–Radushkevich	q_m	29.294	18.948	18.571	16.595
		β	2×10^{-7}	7×10^{-7}	1×10^{-7}	8×10^{-7}
		R^2	0.7512	0.6690	0.5791	0.5773
		E	1581.139	845.154	2236.068	790.570

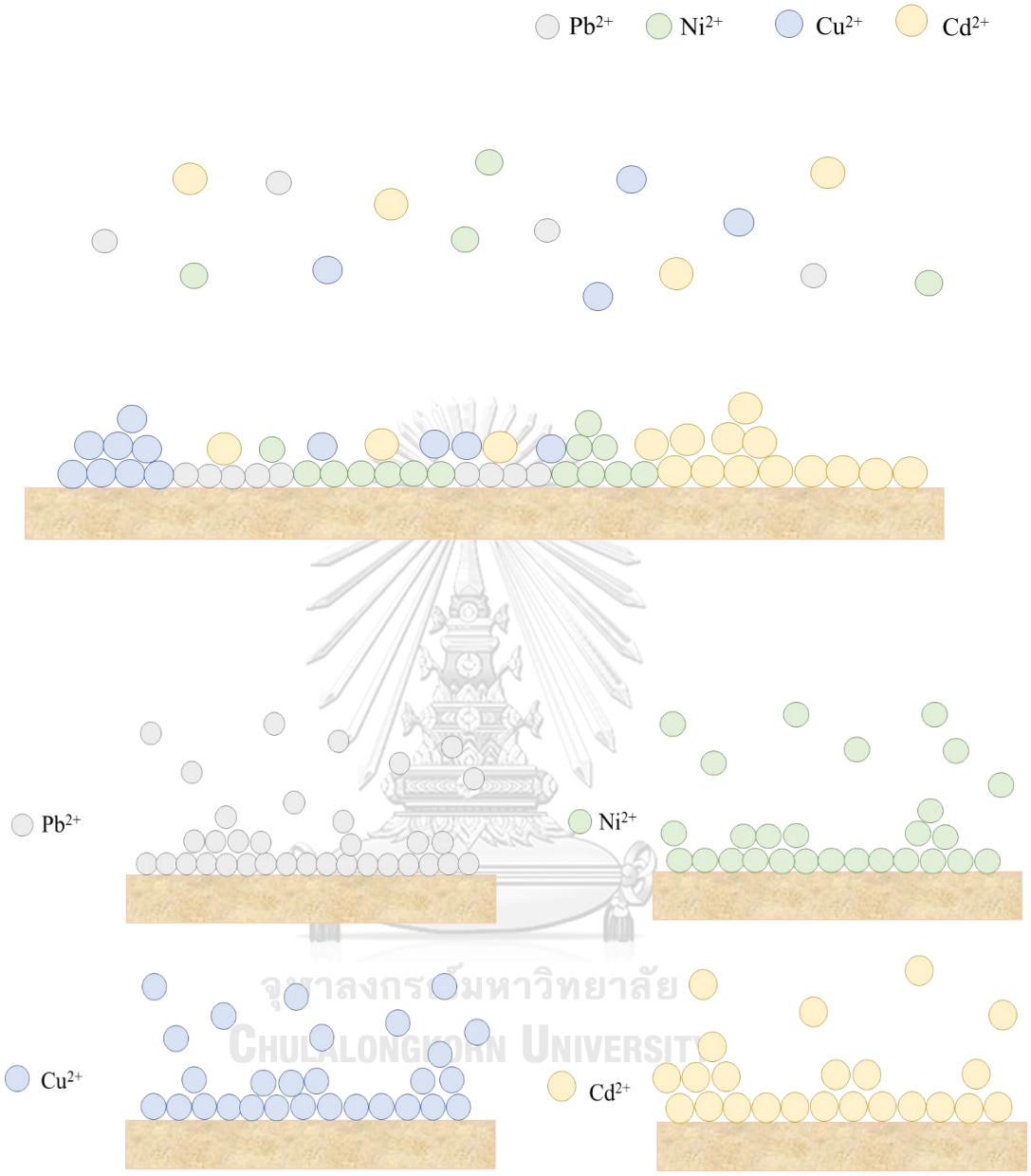

Fig. 4.38 The diagram of adsorption isotherm of metal ions with MKG adsorbent in multi-cations solution (upper) and mono-cations solution (lower)

4.2.4 Kinetics study

4.2.4.1 Pseudo first order model and pseudo second order model

For multi- and mono-cations solutions, the kinetic parameters are presented in Table 4.9. The kinetics of Pb^{2+}, Cd^{2+}, Cu^{2+} and Ni^{2+} by MKG powder in multi- and mono-cations solution are shown Fig. 4.39. Adsorption cations of multi- and mono-cations systems could be modelled using pseudo second order model. This mechanism indicated a comparable concentration of metal ions in solution with high energy which was important of interaction between MKG surface and metal ions species [82, 90].

Table 4.9 Parameter values for batch kinetic adsorption models of MKG powder

Solution system	Metal	Pseudo first order			Pseudo second order			Experimental value q_m(mg/g)
		k_1 (min^{-1})	q_e (mg/g)	R^2	k_2 (g/mg min)	q_e (mg/g)	R^2	
Multi-cations	Pb^{2+}	0.013	0.152	0.1398	0.630	8.094	0.9999	8.149
	Cd^{2+}	0.021	2.371	0.8559	0.151	6.637	0.9970	6.500
	Cu^{2+}	0.023	1.649	0.7925	0.137	7.275	0.9992	7.188
	Ni^{2+}	0.011	1.441	0.6488	0.026	3.567	0.9891	3.498
Mono-cations	Pb^{2+}	0.063	1.153	0.9928	0.169	7.810	1	7.688
	Cd^{2+}	0.212	0.919	0.4864	0.076	6.625	0.9997	6.584
	Cu^{2+}	0.029	0.780	0.9321	0.122	6.866	0.9999	6.830
	Ni^{2+}	0.029	1.307	0.9319	0.068	5.900	0.9999	5.825

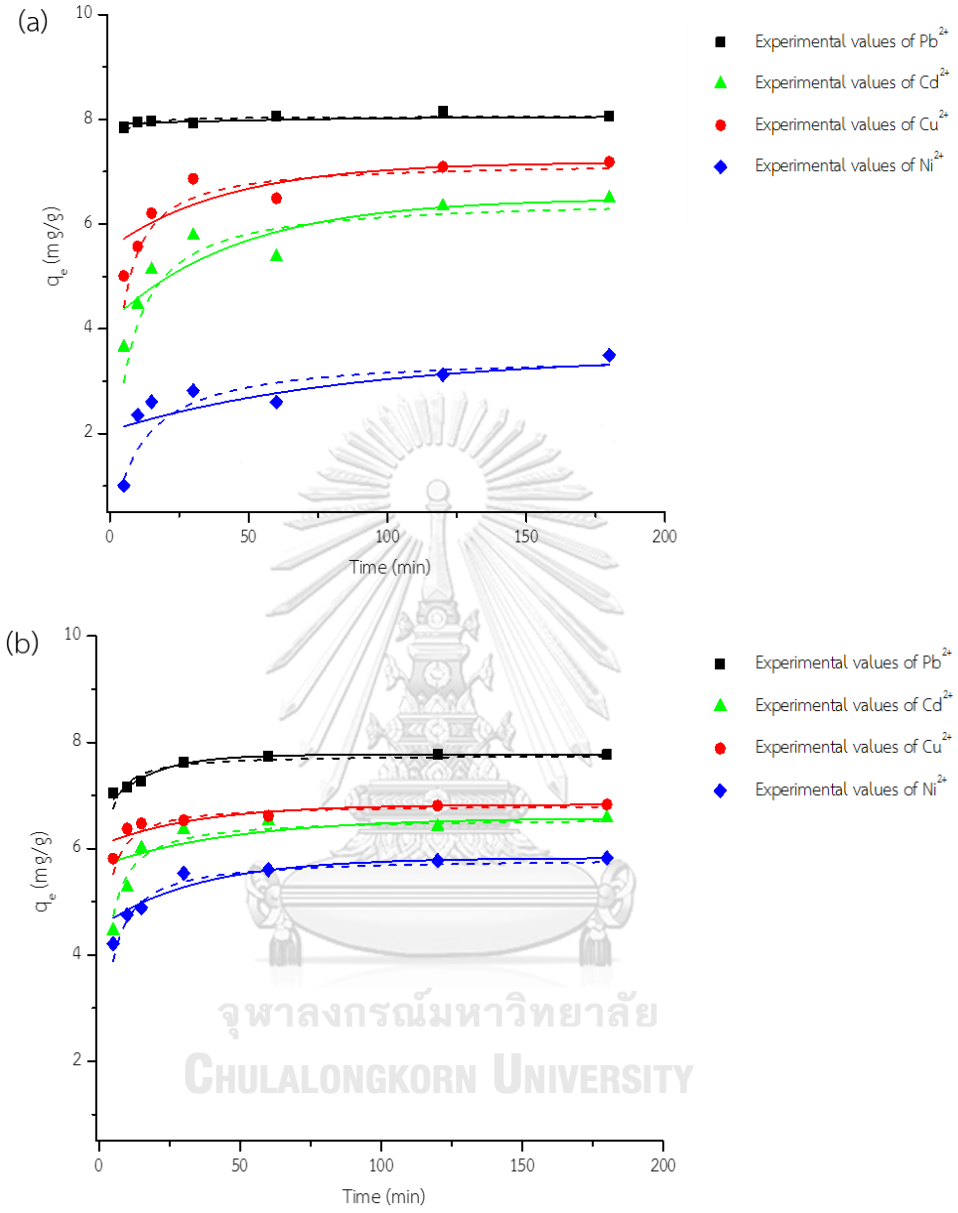

Fig. 4.39 Kinetics of Pb^{2+}, Cd^{2+}, Cu^{2+} and Ni^{2+} adsorption on MKG powder and model's fit to the data (a) multi-cations solution (b) mono-cations solution (Pseudo first order: solid line, Pseudo second order: dash line)

4.2.4.2 Intraparticle diffusion model

From Fig. 4.40, Intraparticle diffusion plots of the adsorption by MKG powder in multi-cations solution and mono-cations solution were seen. Table 4.10 showed Intraparticle diffusion parameters for the adsorption. The fast rate of adsorption occurred in the adsorption process of Pb^{2+}metal ions and surface of MKG powder in multi-cations solution, only single line are observed. For other metal ions with multi- and mono-cations solution system, two portion lines were observed. The first portion lines are attributed the diffusion of metal ions onto the surface of MKG powder. The second region lines are the intraparticle diffusion of metal ions. It is indicated that the metal ions diffused into the MKG powder pores.

Table 4.10 Intraparticle diffusion parameters for the adsorption by MKG powder

Solution system	Metal	Intraparticle diffusion		
		k_p (mg/g $h^{0.5}$)	C (mg/g)	R^2
Multi-cations	Pb^{2+}	0.074	7.894	0.1406
	Cd^{2+}	2.327	3.530	0.7801
	Cu^{2+}	2.109	4.806	0.7981
	Ni^{2+}	1.706	1.289	0.6559
Mono-cations	Pb^{2+}	1.049	6.759	0.9705
	Cd^{2+}	2.685	4.163	0.8766
	Cu^{2+}	0.888	5.848	0.7745
	Ni^{2+}	1.925	3.880	0.9276

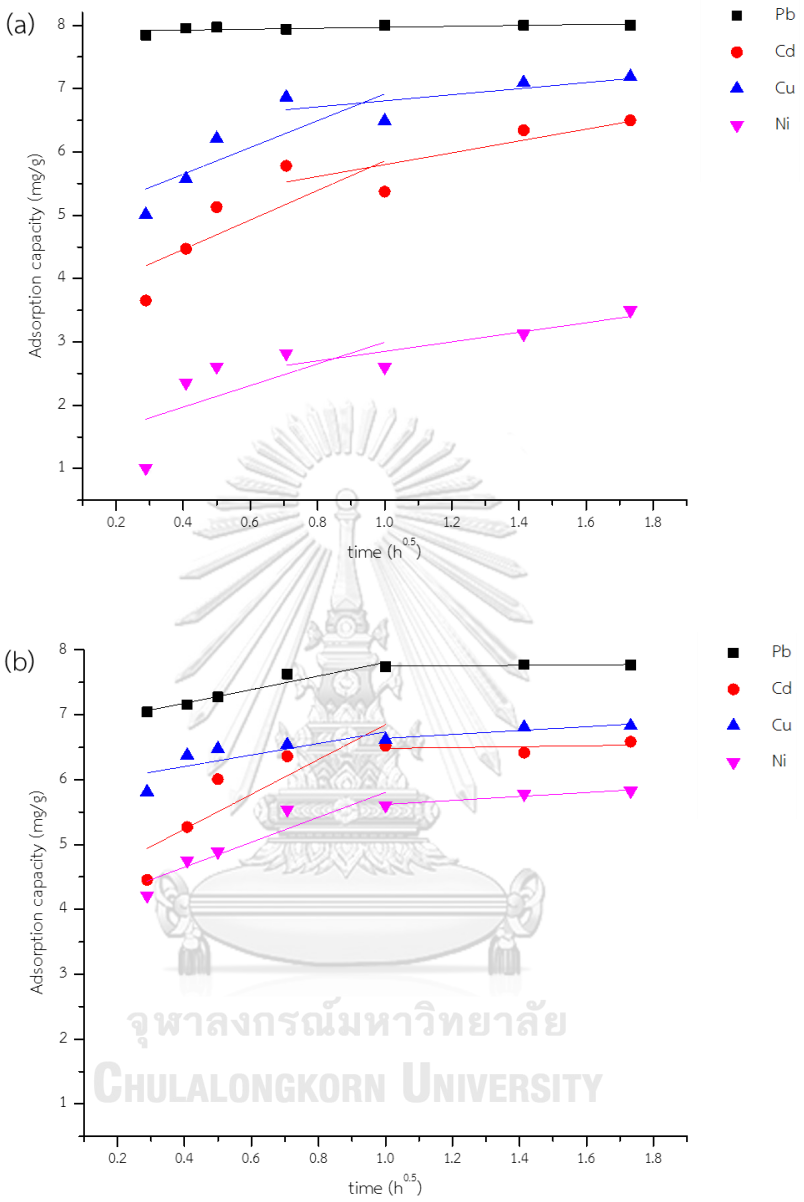

Fig. 4.40 Intraparticle diffusion plots of the adsorption by MKG powder (a) multi-cations solution (b) mono-cations solution

4.3 FLY ASH BASED GEOPOLYMER COMPOSITE FIBER

4.3.1 Characterizations

4.3.1.1 Chemical composition

In Table 4.11, PES fiber and fly ash based geopolymer composite fibers with different fly ash based geopolymer powder amount were characterized by XRF. PES fiber composed of SO_3 and CO_2 because PES structure has sulfone group and a benzene ring. The amount of fly ash based geopolymer powder increased in composite fibers, the compositions of SiO_2, Al_2O_3, Fe_2O_3, CaO, MgO and Na_2O were increased.

Table 4.11 Chemical compositions of PES fiber and fly ash based geopolymer composite fibers

Chemical compound (%)	PES	Washed Fly ash Geopolymer powder	20 wt% FAG fiber	40 wt% FAG fiber	60 wt% FAG fiber
SiO_2	-	44.80	5.44	25.30	52.40
Al_2O_3	-	16.30	2.13	6.36	9.89
Fe_2O_3	-	12.40	1.15	3.89	6.39
CaO	-	7.64	0.44	1.65	2.65
MgO	-	1.49	0.16	0.57	0.77
SO_3	20.70	0.10	20.30	18.10	13.20
Na_2O	-	0.80	0.12	0.23	0.42
CO_2	79.10	13.80	69.90	52.40	40.00

4.3.1.2 Phases

XRD patterns of fly ash based geopolymer powder, PES and the composite fibers are presented in Fig. 4.41. The board hump peak indicating amorphous of PES polymer is presented at 2θ = 12-25°. The sharp crystalline peaks attributed to quartz (JCPDS, 01-087-2096), magnetite (JCPDS, 01-087-0245), mullite (JCPDS, 01-082-0037) and hematite (JCPDS, 00-033-0664) were observed for fly ash based geopolymer powder and in composite fibers. The crystalline peaks were apparently seen in composite fibers and was not shift peaks. This result indicated that the crystalline structure and phases not changed in composite fibers.

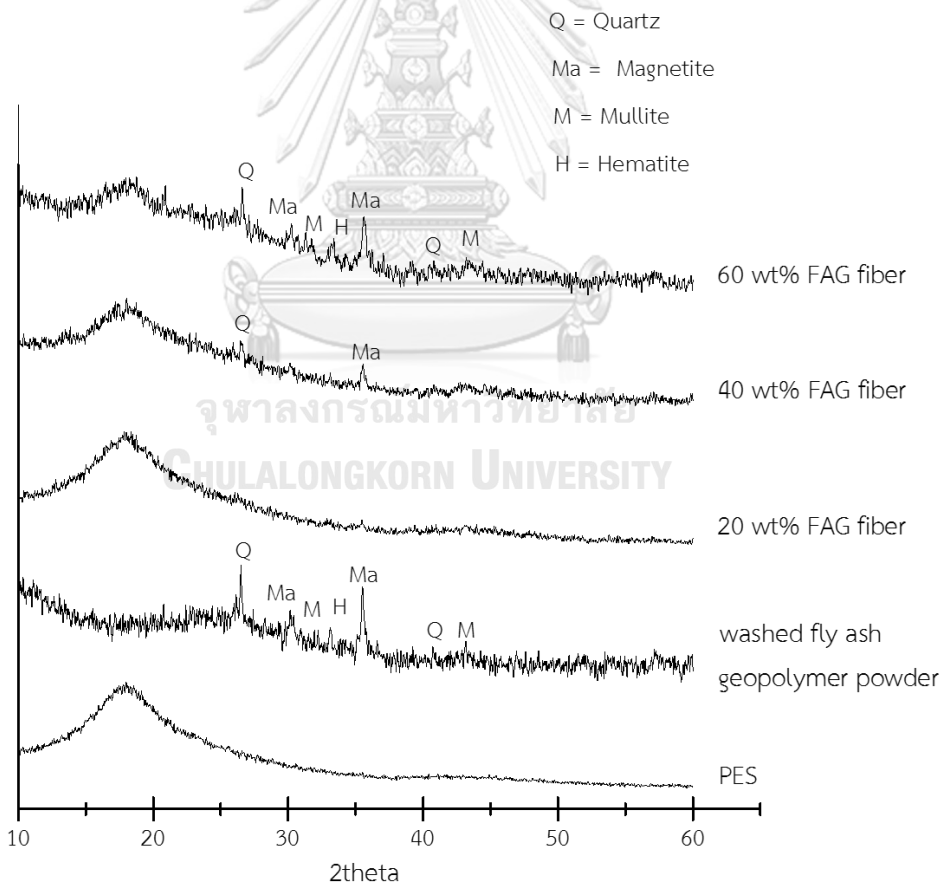

Fig. 4.41 XRD patterns of PES fiber and fly ash based geopolymer composite fibers

4.3.1.3 Microstructure

The porous morphology of fiber in microstructure was compared in each sample with different amount of fly ash based geopolymer powder amount. Fig. 4.42 showed cross section of PES and composite fibers. The PES fiber (Fig. 4.42 (a)) and 20wt% of FAG composite fiber (Fig. 4.42 (d)) had diameter about 500 μm. In addition, the cross section of composite fiber a little decreased when increased the FAG powder amount more 40wt% in the composite fiber. The cross section of 40 and 60wt% of FAG composite fiber (Fig. 4.42 (g, j)) had diameter about 400-450 μm. Geopolymer composite fiber composed of porous structure and fly ash geopolymer powder was surrounded by PES. The outer round of geopolymer fiber appeared the finger-like structure of pore. When FAG powder amount increased, the finger like structure was disappeared. Moreover, the core of geopolymer fiber are shown the sponge structure of pore.

The micro X-ray CT technique was applied to observe inside of the fibers. Fig. 4.43 showed the structure of PES and composite fiber with different amounts of FAG powder. The FAG powder was uniformly distributed in the fiber network with a sponge structure. The fiber was denser when added more amount of FAG powder. In addition, when FAG powder was added more amount than 40 wt%, some FAG powder was agglomerated in the fiber.

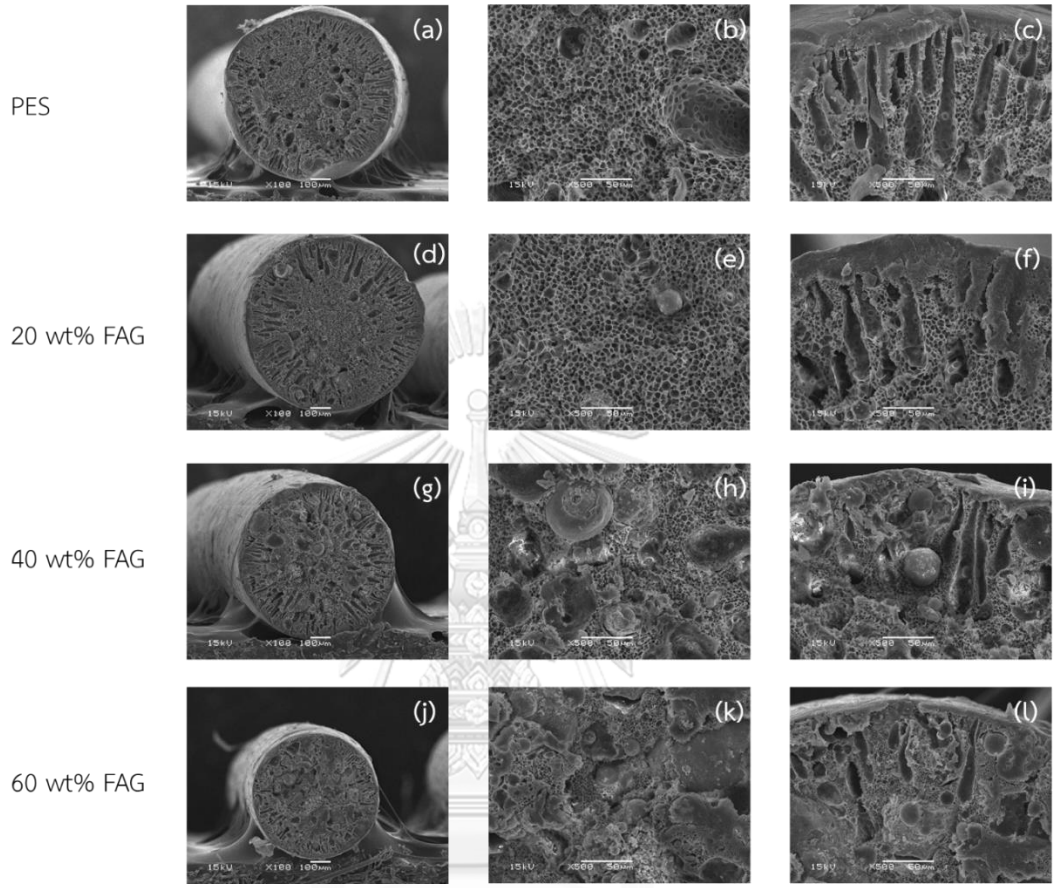

Fig. 4.42 Microstructure of PES fiber and fly ash based geopolymer composite fibers

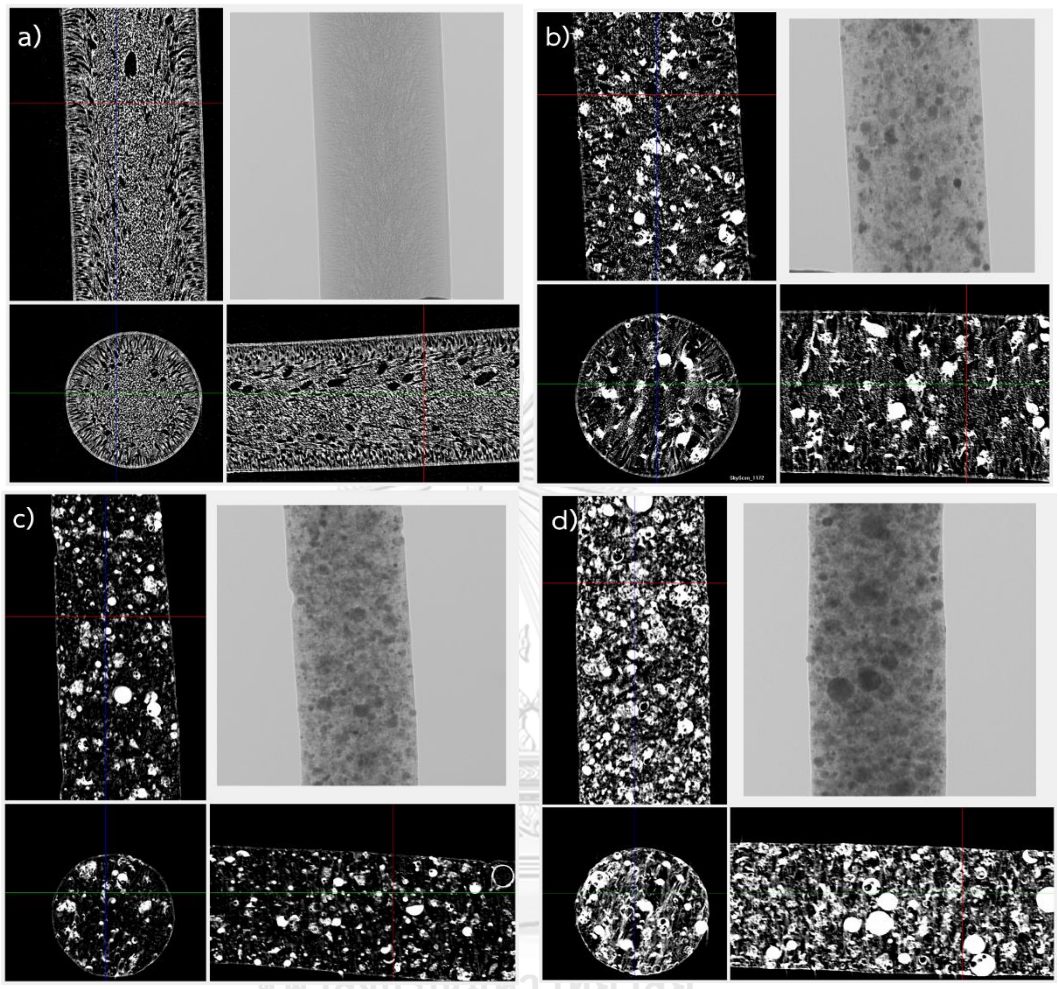

Fig. 4.43 X-ray micro CT images of PES fiber and fly ash based geopolymer composite fibers: (a) PES (b) 20wt% FAG (c) 40wt% FAG and (d) 60wt% FAG

4.3.1.4 Tensile strength and surface area

The tensile strength of PES fiber and fly ash based geopolymer composite fibers is shown in Table 4.12. The tensile strength values decreased with increased FAG powder loading due to the FAG powder was obstructed the connecting of PES polymer in the fibers.

Table 4.12 also listed the specific surface area of the fibers. The values of BET surface area of PES, 20, 40 and 60wt% of FAG powder in composite fiber were 27.39, 50.05, 57.50 and 71.67 m^2/g, respectively. From the results, the FAG powder loading increased, the increased of surface area values occurred because the FAG powders has the rough surface which has higher surface area than flat surface. Form the specific surface area results, the 60wt% of FAG powder in composite fiber was chosen for adsorption test.

Table 4.12 Tensile strength and surface area of PES fiber and fly ash based geopolymer composite fibers

Samples	Tensile strength (MPa)	Surface area (m^2/g)
PES	5.83	27.39
20wt% FAG	4.17	50.05
40w% FAG	2.35	57.50
60wt% FAG	1.40	71.67
FAG powder	-	85.01

4.3.2 Adsorption test

4.3.2.1 Effect of contact time

The time dependence behavior of Pb^{2+}, Cu^{2+}, Cd^{2+}, Ni^{2+} adsorption was studied in the range of 5 min – 72 h and concentration of Pb^{2+}, Cu^{2+}, Cd^{2+}, Ni^{2+} was kept at 20 mg/L at fixed geopolymer fiber dose (0.1 g) and pH of 5 at 25 ^{o}C in multi- and mono-cations solution systems and the results are illustrated in Fig. 4.44 and Fig. 4.45. It can be seen that the adsorption efficiency and the adsorption capacity of Pb^{2+}, Cu^{2+}, Cd^{2+}, Ni^{2+} on FAG geopolymer composite fiber increases with increasing of contact time. The rate for adsorption of geopolymer composite fiber was slower than FAG powder because the metal ions could adsorbed by powder directly. The adsorption efficiency and the adsorption capacity of metal ions increased rapidly in early stage of contact time. In multi-cations solution, the adsorption of Cu^{2+}, Cd^{2+}, and Ni^{2+} became equilibrium after 12 h and the adsorption of Pb^{2+} became equilibrium after 48 h. Moreover, the adsorption of Pb^{2+} became equilibrium after 48 h and the adsorption of other metal ions still increasing with an increase of contact time in mono-cations solution. A contact time of 120 min still was used in all following tests because the results of adsorption efficiency and adsorption capacity at 120 min were used to compare with FAG powder adsorbent in the same of contact time.

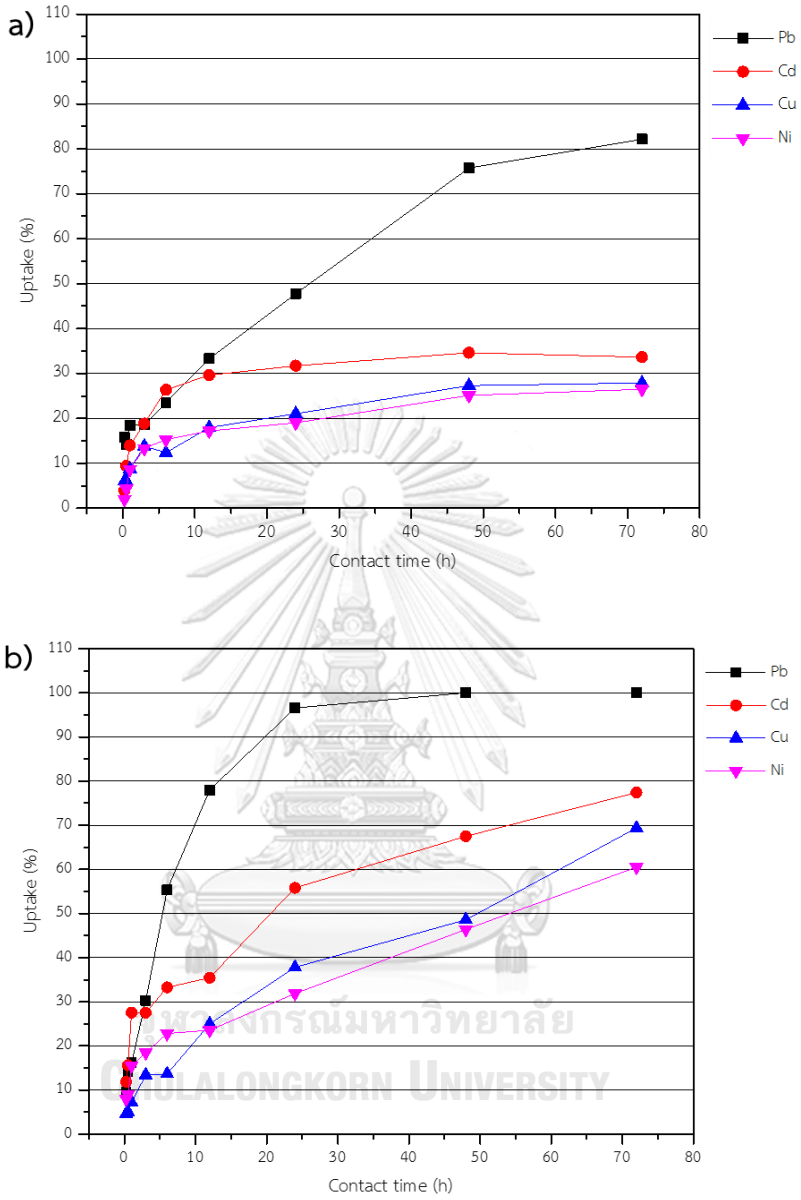

Fig. 4.44 Effect of contact time on heavy metal ions removal efficiency of FAG composite fiber (a) multi-cations solution (b) mono-cations solution

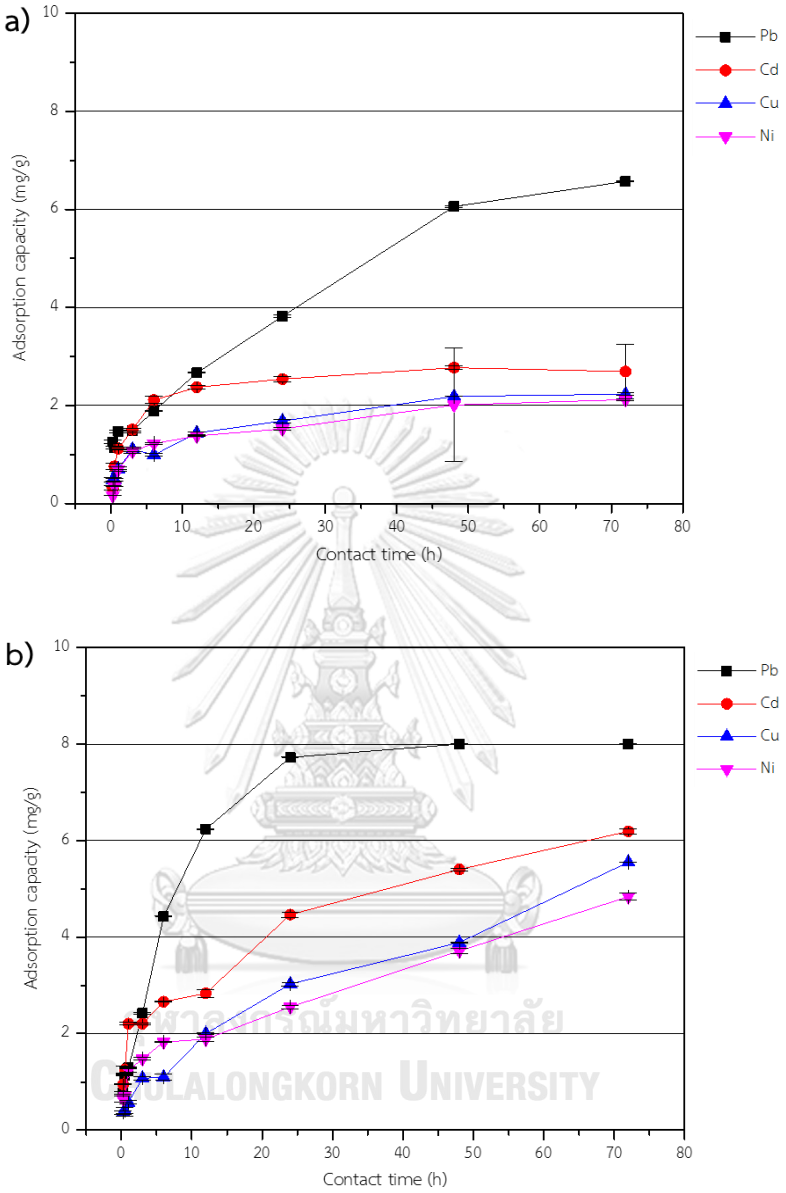

Fig. 4.45 Effect of contact time on adsorption capacity of FAG composite fiber (a) multi-cations solution (b) mono-cations solution

4.3.2.2 Effect of geopolymer dosage

The effect of FAG composite fiber dosage on the adsorption efficiency and the adsorption capacity of Pb^{2+}, Cu^{2+}, Cd^{2+}, and Ni^{2+} was investigated at 25 ^{o}C with pH=5, initial concentration 20 mg/L and contact time 120 min and the results are shown in Fig. 4.46 and Fig. 4.47. The results showed that the adsorption efficiency increased up to 74.09, 45.95, 54.81, and 32.40 for Pb^{2+}, Cu^{2+}, Cd^{2+}, and Ni^{2+} as the dose increase at 0.5g/ 40mL with multi-cations solution. The results in mono-cations solution showed that the adsorption efficiency increased up to 100, 56.88, 63.22, and 52.75 for Pb^{2+}, Cu^{2+}, Cd^{2+}, and Ni^{2+} as the dose increase at 0.5g/ 40mL with multi-cations solution. From the results meant that the available active site at low dosage are not enough to adsorb all of metal ions in solution.

4.3.2.3 Effect of solution pH

The results provided in Fig. 4.48 and Fig. 4.49 presents the effect of pH values of metal ions solution on the adsorption efficiency and the adsorption capacity of FAG composite fiber with initial concentration of 20 mg/L at 25 ^{o}C with geopolymer dosage 0.1 g/40 mL and contacting time of 120 min. The results suggest that the sorption effectiveness increased when pH values of solution increase from 1 to 5. The adsorption efficiency and the adsorption capacity of FAG composite fiber decreased in lower pH values of solution because the concentration of H^{+} is high in solution, the H^{+} could competition with metal ions on available site adsorption on geopolymer composite fiber.

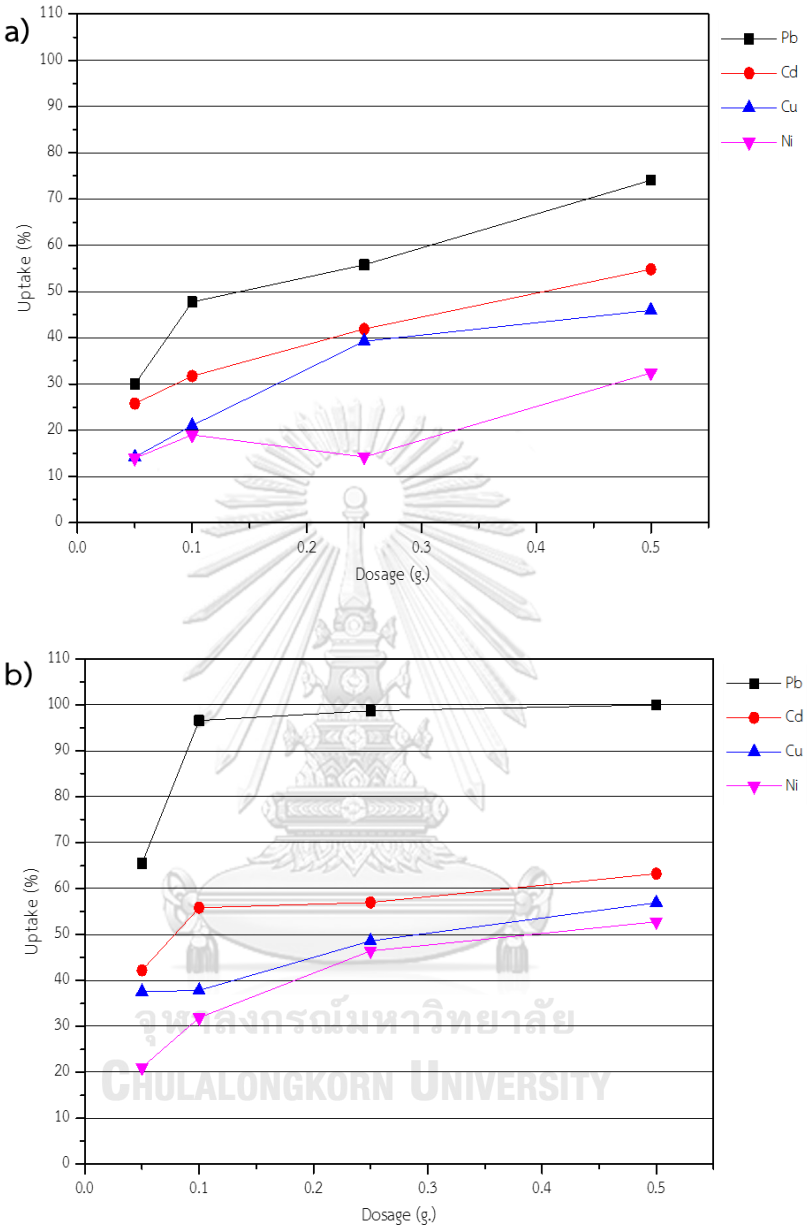

Fig. 4.46 Effect of geopolymer dosage on heavy metal ions removal efficiency of FAG composite fiber (a) multi-cations solution (b) mono-cations solution

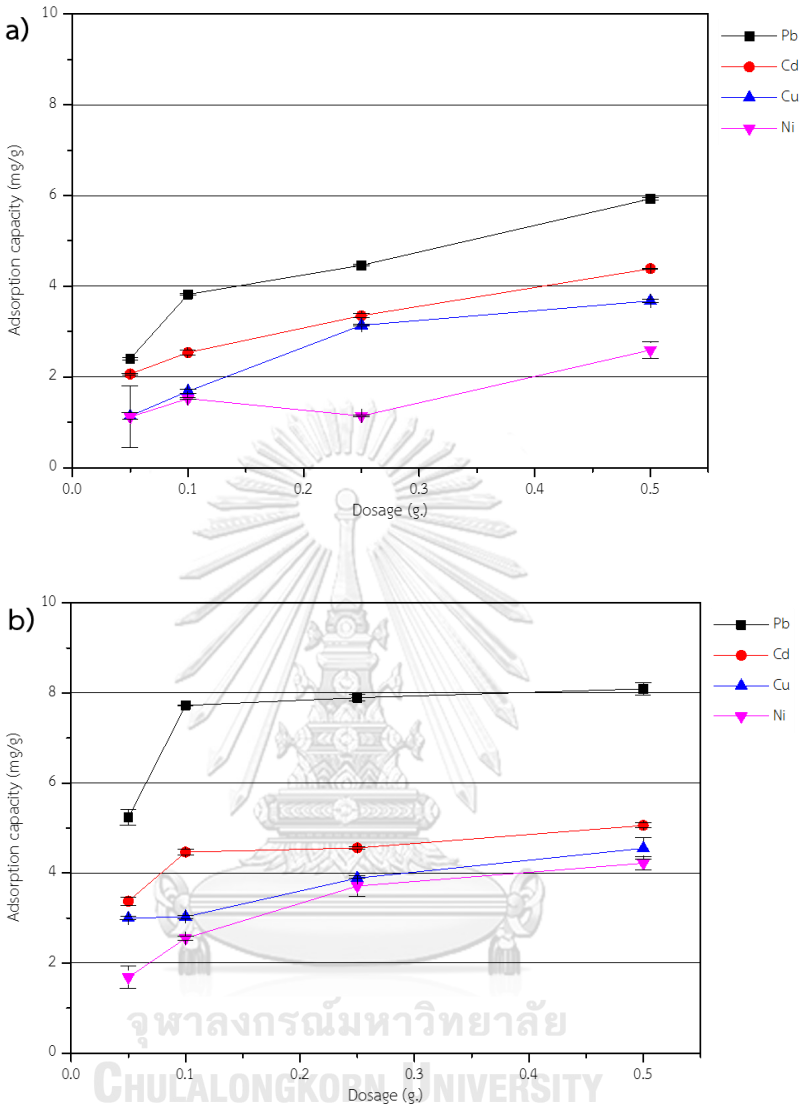

Fig. 4.47 Effect of geopolymer dosage on adsorption capacity of FAG composite fiber (a) multi-cations solution (b) mono-cations solution

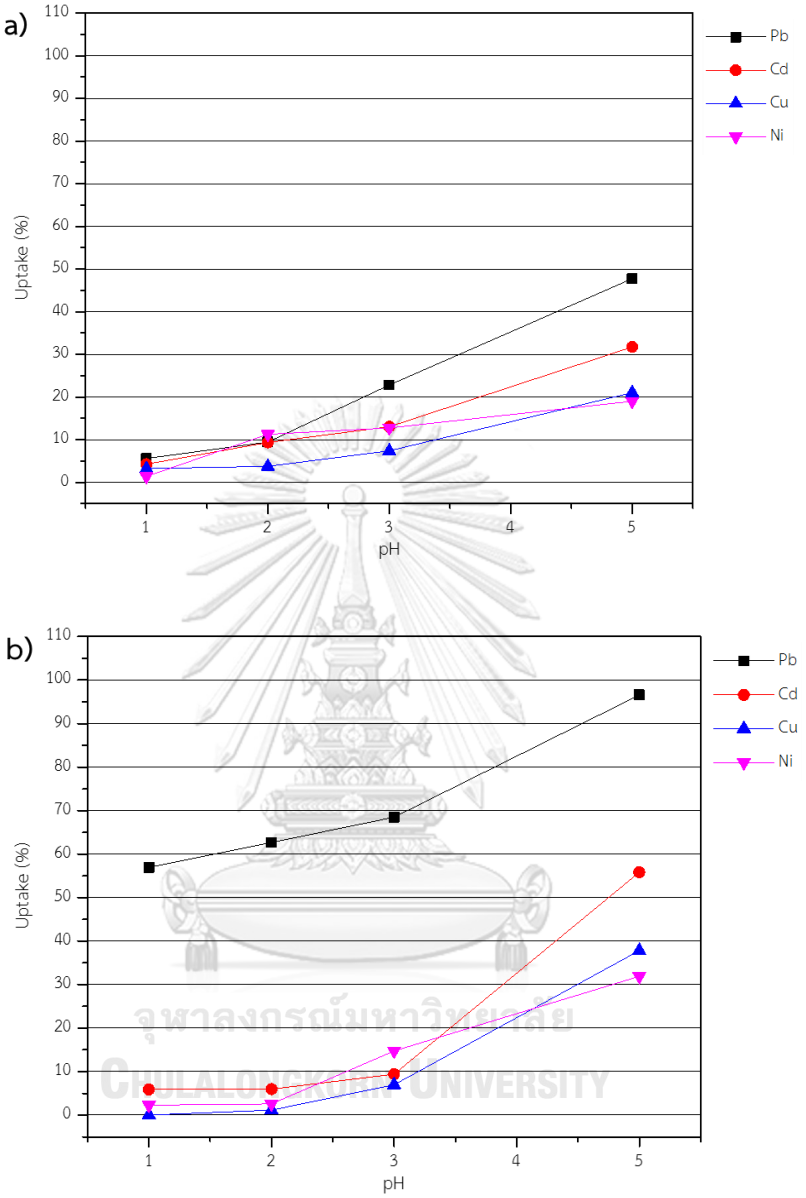

Fig. 4.48 Effect of pH on heavy metal ions removal efficiency of FAG composite fiber (a) multi-cations solution (b) mono-cations solution

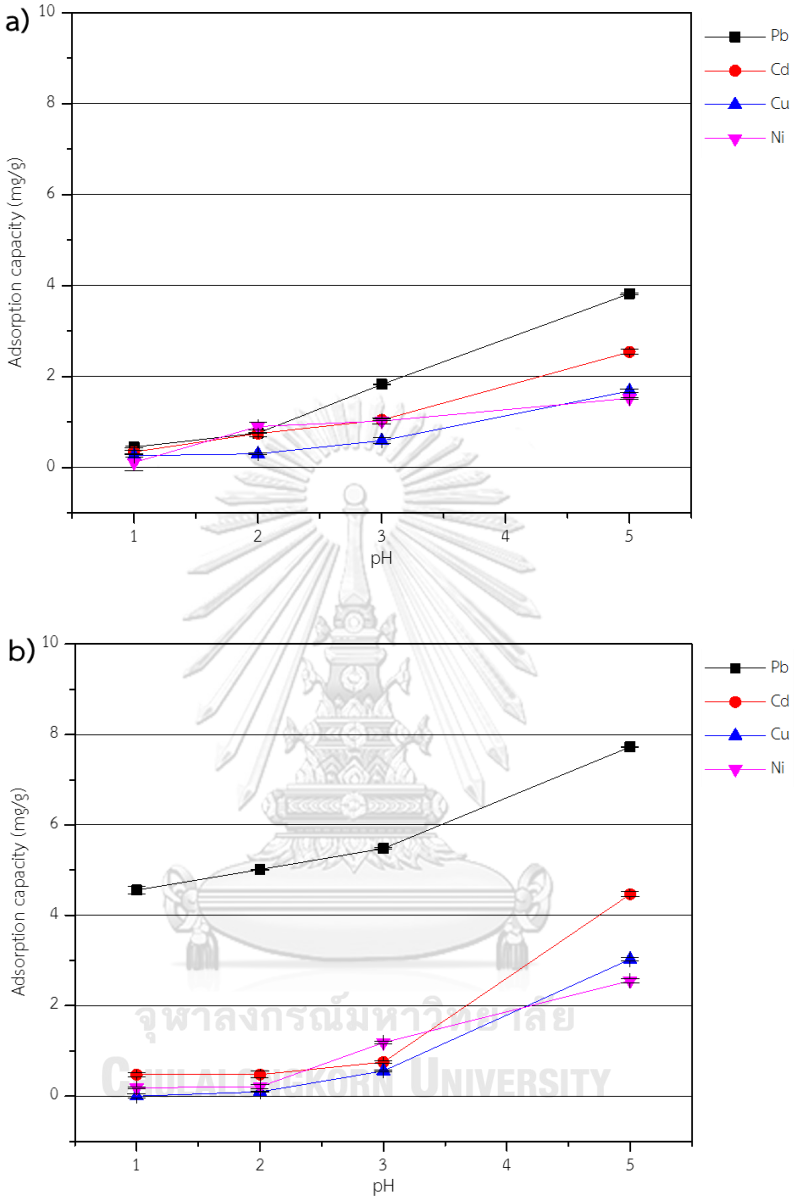

Fig. 4.49 Effect of pH on adsorption capacity of FAG composite fiber (a) multi-cations solution (b) mono-cations solution

4.3.2.4 Effect of temperature

The temperature dependence behavior of Pb^{2+}, Cu^{2+}, Cd^{2+}, and Ni^{2+} adsorption was studied by changing the temperature in the range of 25-45 ^{o}C and the concentration of metal ions was kept at 20 mg/L at fixed geopolymer composite fiber dosage (0.1 g) with contact time of 120 min at pH value of 5 and the results are list in Fig. 4.50 and Fig. 4.51. It can be noticed that the adsorption efficiency and the adsorption capacity of Pb^{2+}, Cu^{2+}, Cd^{2+}, and Ni^{2+} on FAG composite fiber increased with an increasing temperature. The uptake efficiency values for FAG composite fiber in multi-cations solution increased up to 60.43, 23.89, 36.11, and 22.20% with adsorption capacity as 4.83, 1.91, 2.88, and 1.78 mg/g of Pb^{2+}, Cu^{2+}, Cd^{2+}, and Ni^{2+}, respectively. The uptake efficiency values for FAG composite fiber in mono-cations solution increased up to 100, 69.14, 80.34, and 42.79% with adsorption capacity as 8, 5.53, 6.40, and 3.42 mg/g of Pb^{2+}, Cu^{2+}, Cd^{2+}, and Ni^{2+}, respectively. The uptake of Pb^{2+}, Cu^{2+}, Cd^{2+}, and Ni^{2+} on FAG composite fiber in both solution systems reaches a maximum values at 45 ^{o}C. Evaluating the temperature of solution increased the extent and rate of adsorption, shown through increased in pore volume which enhance adsorption process because the water vaporization and formation of micro-cavities inside the fiber in high temperature.

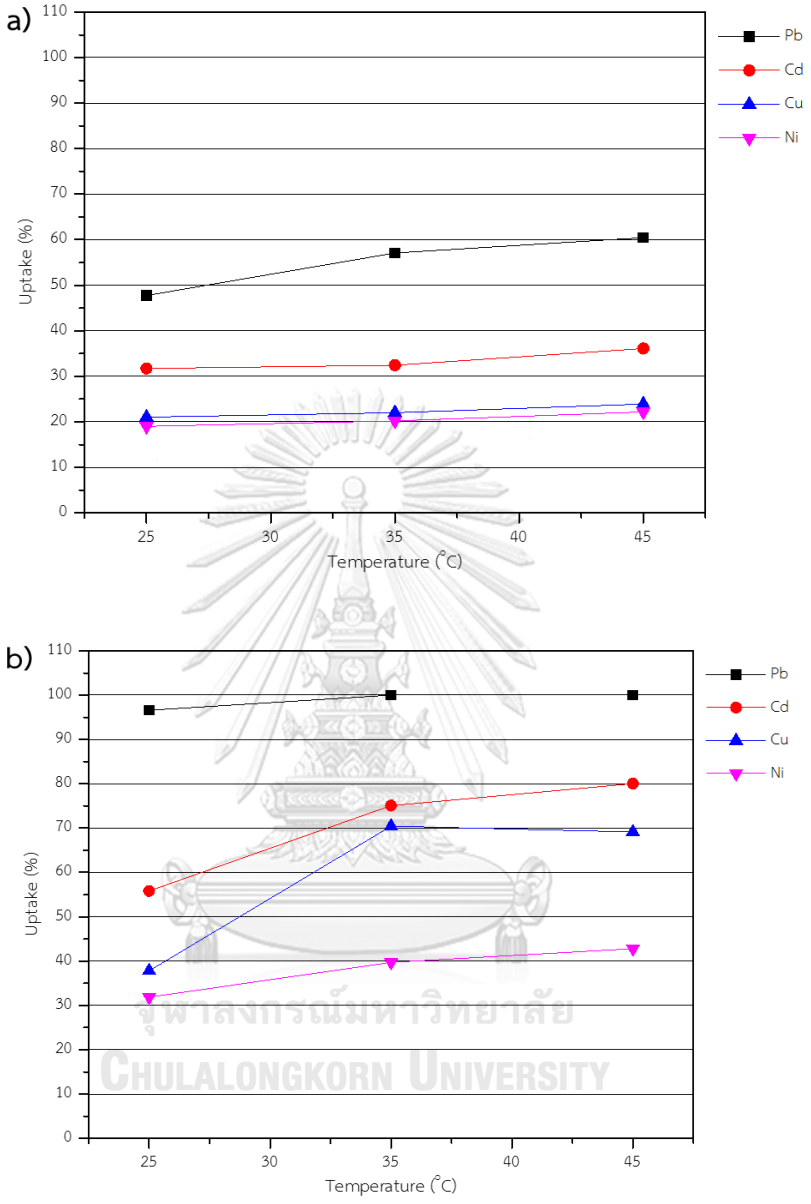

Fig. 4.50 Effect of temperature on heavy metal ions removal efficiency of FAG composite fiber (a) multi-cations solution (b) mono-cations solution

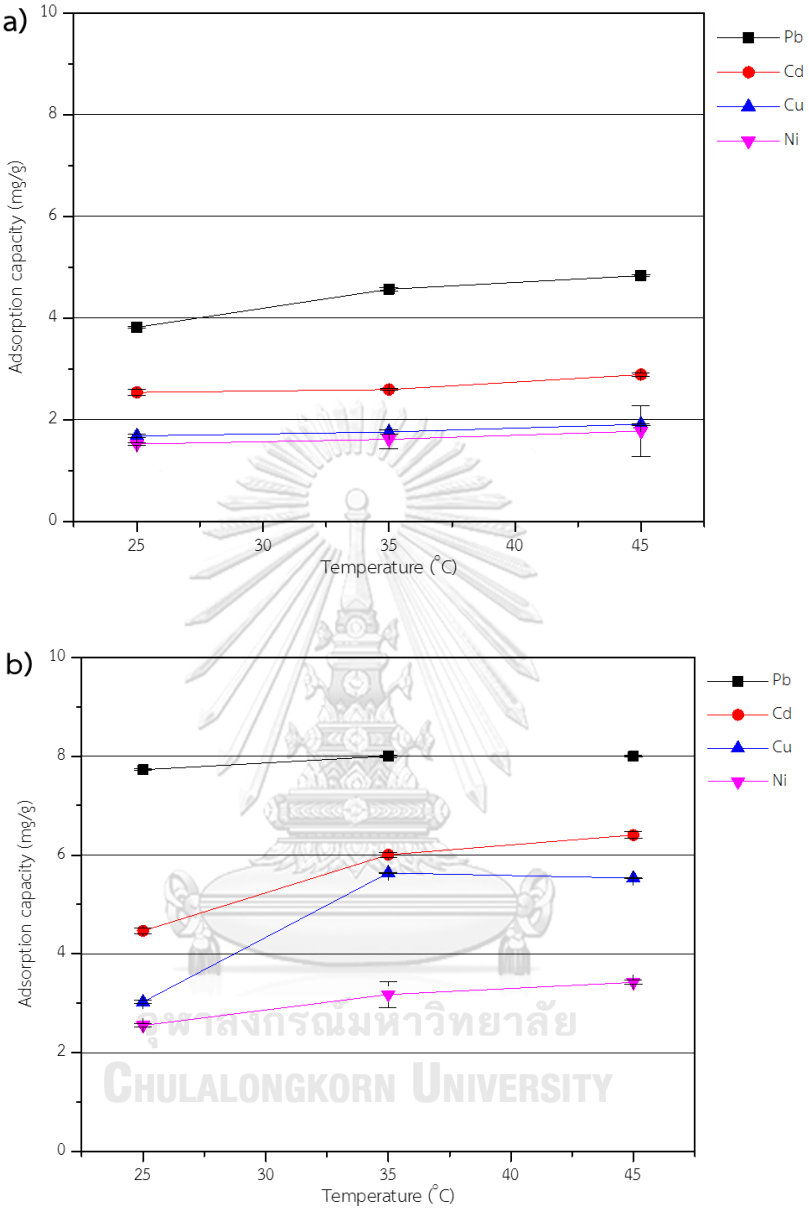

Fig. 4.51 Effect of temperature on adsorption capacity of FAG composite fiber (a) multi-cations solution (b) mono-cations solution

4.3.2.5 Effect of initial concentration

Fig. 4.52 and Fig. 4.53 presented the adsorption efficiency and adsorption capacity of FAG composite fiber at different initial Pb^{2+}, Cu^{2+}, Cd^{2+}, and Ni^{2+} concentration at 25 °C with pH=5, geopolymer dosage of 0.1 g/40mL and contacting time of 120 min. As it was expected, the removal efficiency of Pb^{2+}, Cu^{2+}, Cd^{2+}, and Ni^{2+} declined as the initial concentration increased. The uptake efficiency is about 57.90, 38.27, 52.74, and 35.70% in multi-cations solution and about 100, 51.45, 63.13, and 48.25% in mono-cations solution when the initial concentration of Pb^{2+}, Cu^{2+}, Cd^{2+}, and Ni^{2+} is 10 mg/L. After tested, the adsorption capacity also was calculated. The results showed that The maximum adsorption capacity values of Pb^{2+}, Cu^{2+}, Cd^{2+}, and Ni^{2+} were found as 7.70 mg/g of Pb^{2+}, 4.39 mg/g of Cu^{2+}, 5.93 mg/g of Cd^{2+} and 2.91 mg/g of Ni^{2+} at 120 mg/L in multi-cations solution. Moreover, the maximum adsorption capacity values of Pb^{2+}, Cu^{2+}, Cd^{2+}, and Ni^{2+} were seen as 11.78 mg/g of Pb^{2+} at 100 mg/L, 9.64 mg/g of Cu^{2+}, 10.50 mg/g of Cd^{2+} and 8.42 mg/g of Ni^{2+} at 120 mg/L in mono-cations solution.

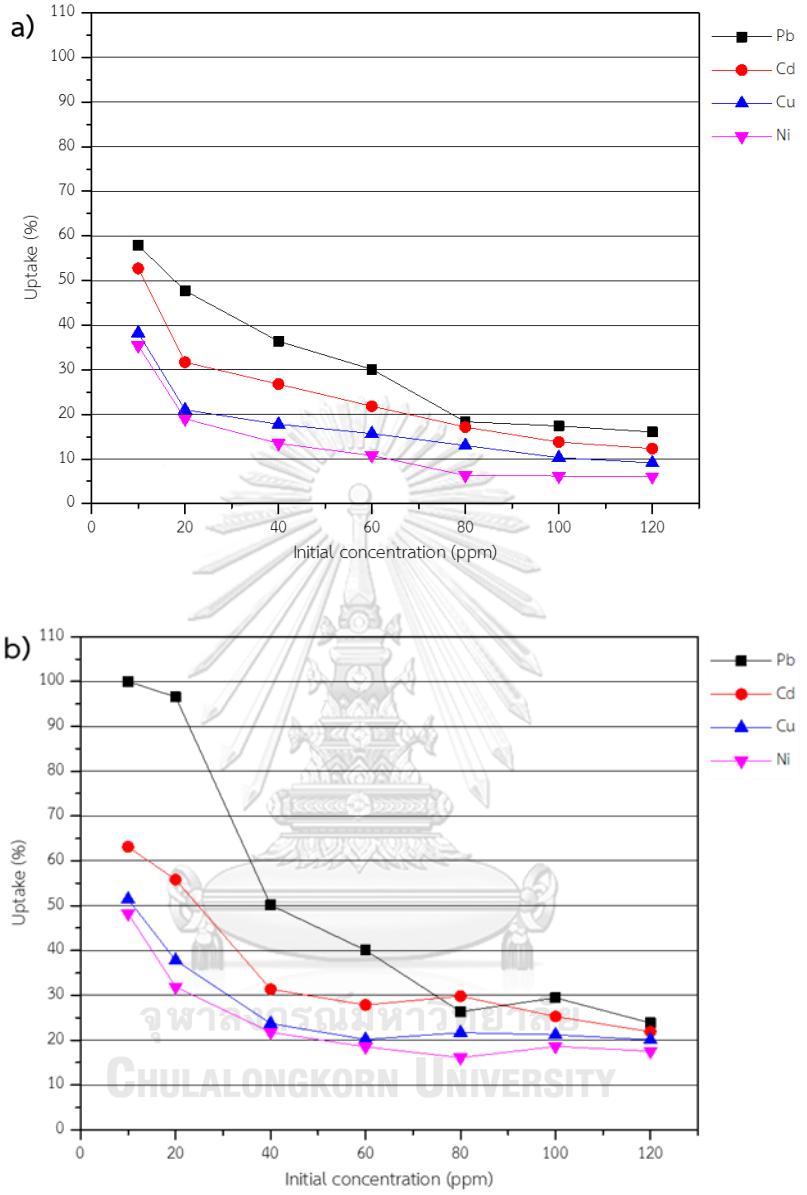

Fig. 4.52 Effect of initial concentration on heavy metal ions removal efficiency of FAG composite fiber (a) multi-cations solution (b) mono-cations solution

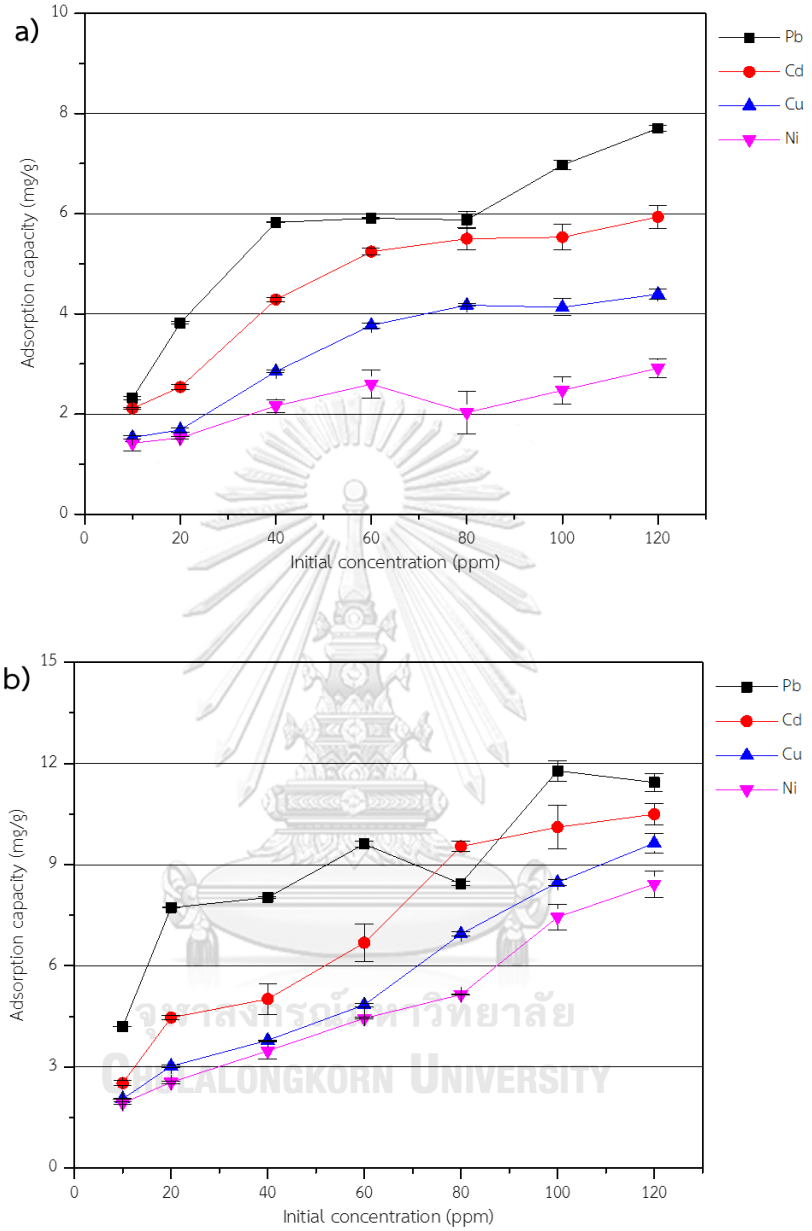

Fig. 4.53 Effect of initial concentration on adsorption capacity of FAG composite fiber (a) multi-cations solution (b) mono-cations solution

4.3.3 Adsorption isotherm

The adsorption data of Pb^{2+}, Cu^{2+}, Cd^{2+}, Ni^{2+} was fitted with the equation in each isotherm to obtain the graph and affinity of adsorption of the FAG composite fiber in multi- and mono-cations solution as shown in Fig. 4.54 to Fig. 4.57. The model parameters and summary of adsorption isotherm are presented in Table 4.13 and Table 4.14. Moreover, the diagram of adsorption isotherm which were fitted with each ions are shown in Fig. 4.58.

In multi-cations solution, Pb^{2+} and Ni^{2+} were fitted well with Langmuir adsorption isotherm and Cu^{2+} and Cd^{2+} were fitted well with Freundlich adsorption isotherm. The results indicated that Pb^{2+} and Ni^{2+} were adsorbed on FAG composite fiber in monolayer and Cu^{2+} and Cd^{2+} were adsorbed on FAG composite fiber in multilayer. The maximum capacities of Pb^{2+}, Cu^{2+}, Cd^{2+}, Ni^{2+} on the Langmuir model was in the order $Pb^{2+}>Cd^{2+}>Cu^{2+}>Ni^{2+}$. From the Langmuir model, the calculated R_L values of Pb^{2+}, Cd^{2+}, Cu^{2+}, Ni^{2+} were 8.299, 5.650, 4.216 and 2.519, indicating that the adsorption process is favorable. Moreover, the values of the Freundlich constant (1/n) were between 0.1 and 1, indicating a favorable adsorption.

In mono-cations solution, Pb^{2+} was fitted well with Redlich-Peterson adsorption isotherm which is combined with Langmuir and Freundlich adsorption isotherm model on FAG composite fiber. Cu^{2+}, Cd^{2+}, Ni^{2+} were fitted well with Freundlich adsorption isotherm. The results concluded that Cu^{2+}, Cd^{2+}, Ni^{2+} could adsorb on FAG composite fiber in multilayer.

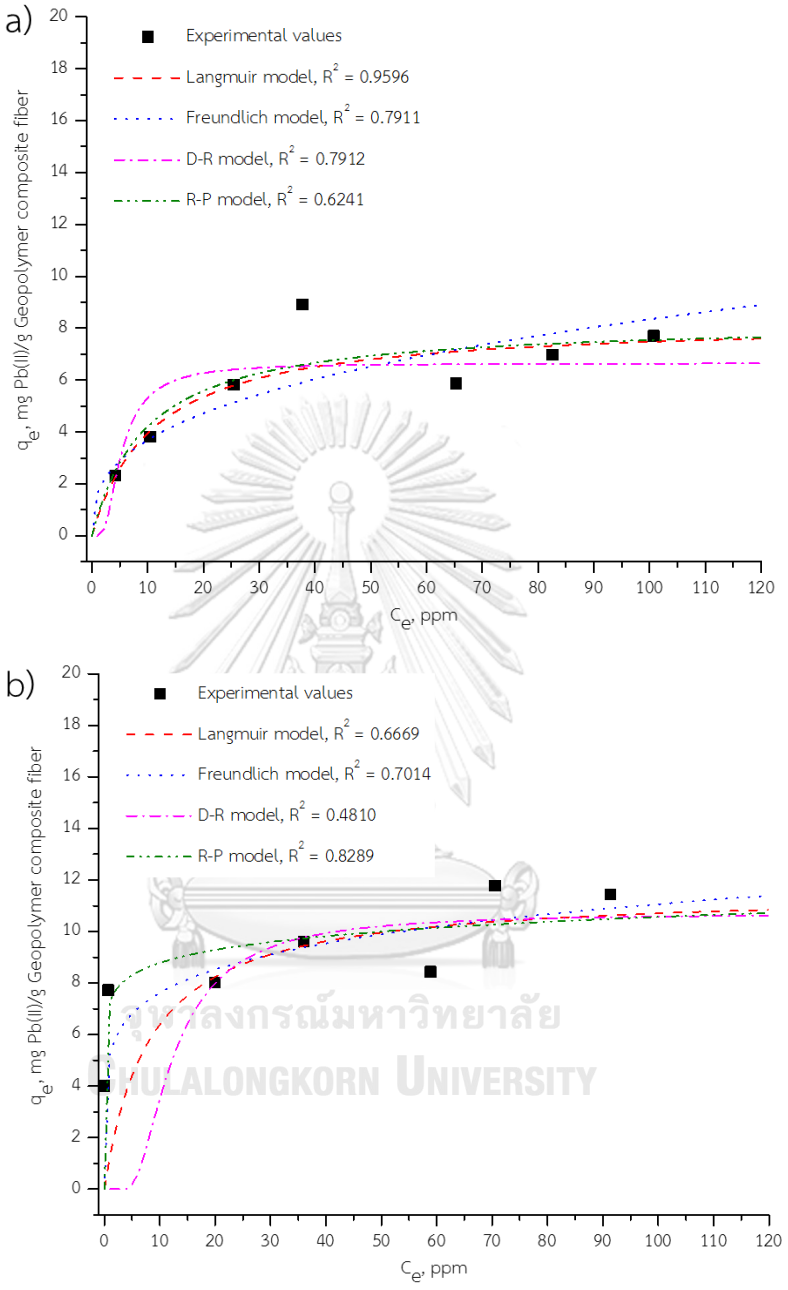

Fig. 4.54 The adsorption isotherms of Pb(II) by applying Langmuir, Freundlich, Redlich-Peterson and Dubinin–Radushkevich isotherm models FAG composite fiber adsorbent (a) multi-cations solution (b) mono-cations solution

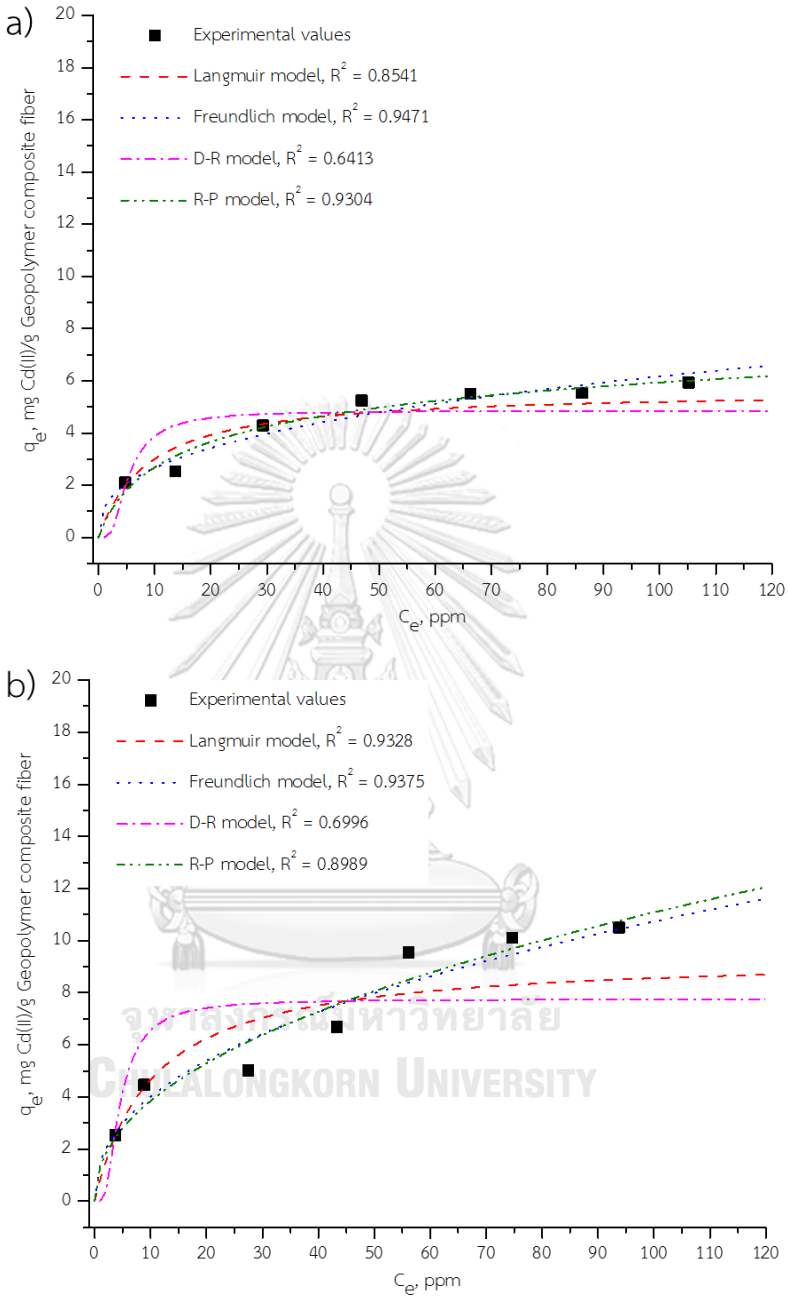

Fig. 4.55 The adsorption isotherms of Cd(II) by applying Langmuir, Freundlich, Redlich-Peterson and Dubinin–Radushkevich isotherm models FAG composite fiber adsorbent (a) multi-cations solution (b) mono-cations solution

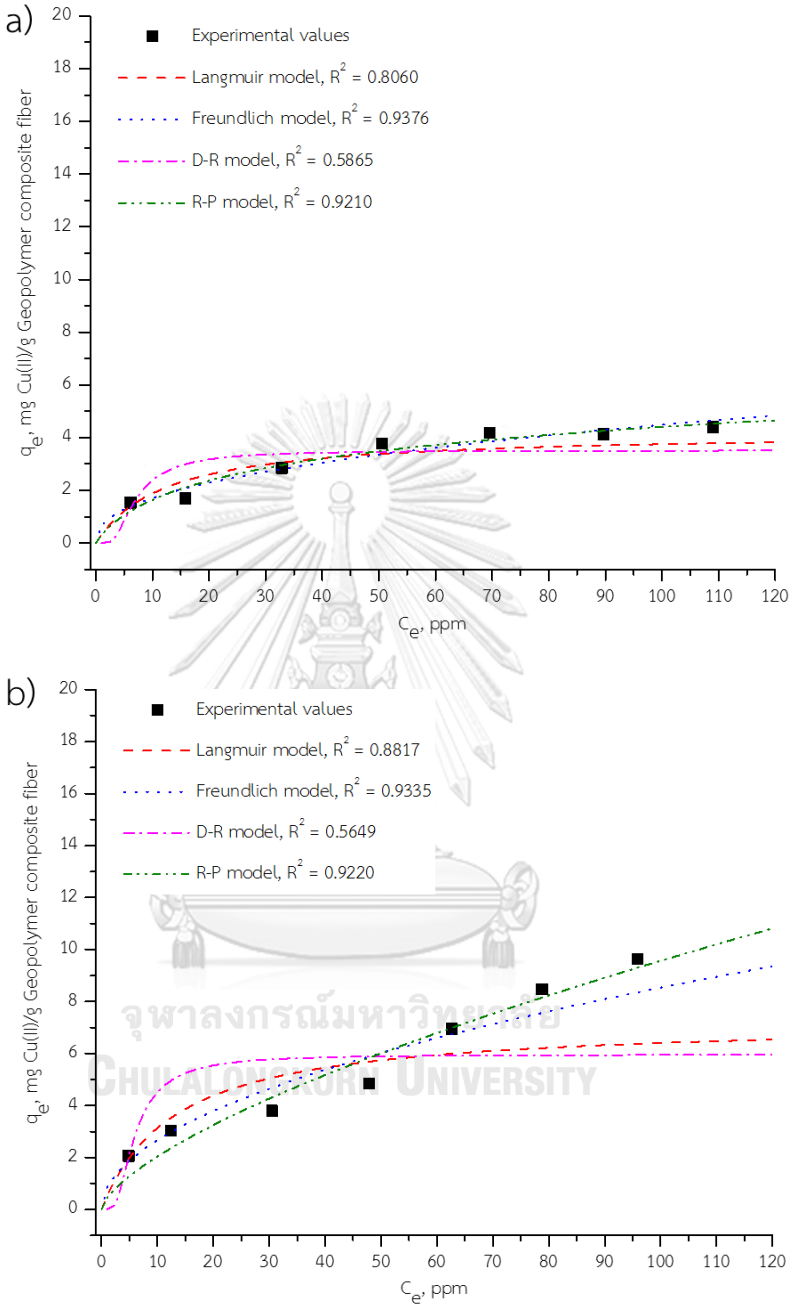

Fig. 4.56 The adsorption isotherms of Cu(II) by applying Langmuir, Freundlich, Redlich-Peterson and Dubinin–Radushkevich isotherm models FAG composite fiber adsorbent (a) multi-cations solution (b) mono-cations solution

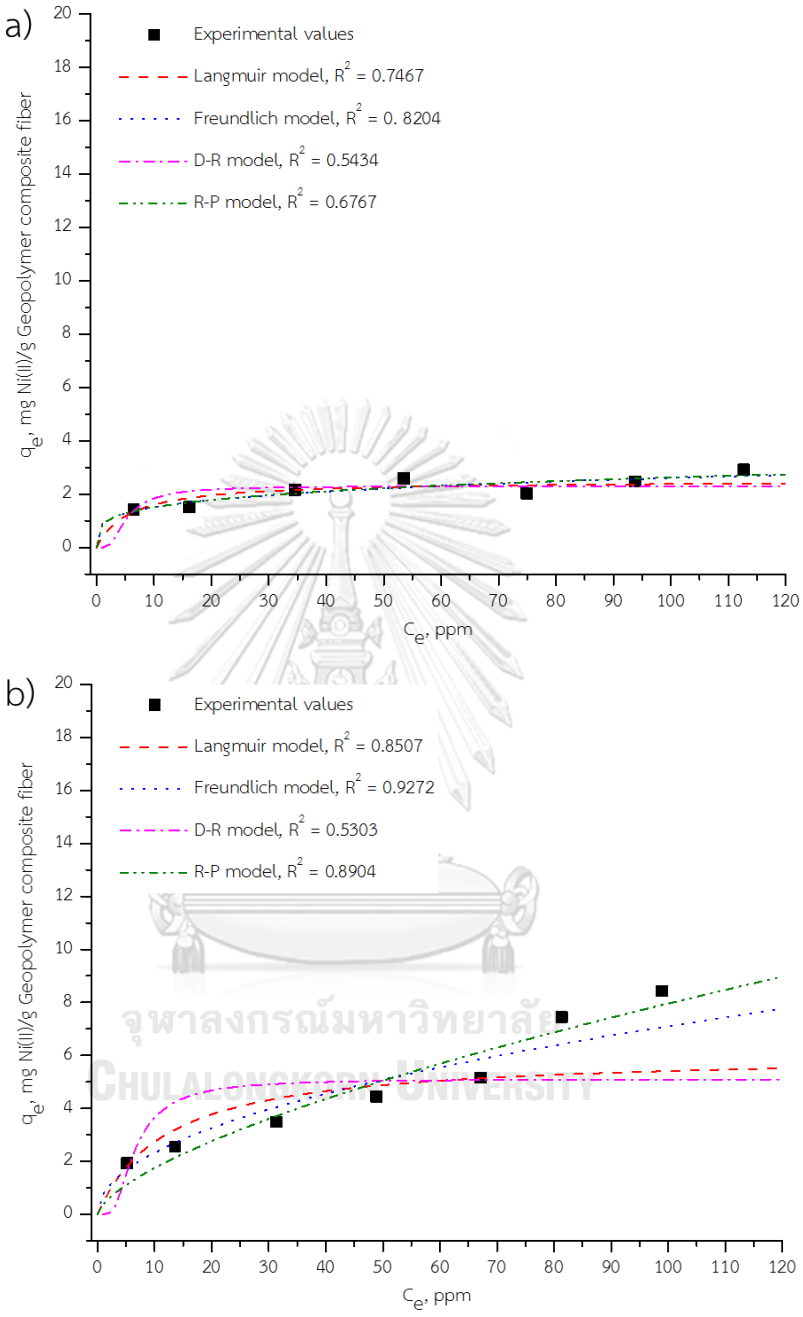

Fig. 4.57 The adsorption isotherms of Ni(II) by applying Langmuir, Freundlich, Redlich-Peterson and Dubinin–Radushkevich isotherm models FAG composite fiber adsorbent (a) multi-cations solution (b) mono-cations solution

Table 4.13 Summary of adsorption isotherm of metal ions with FAG composite fiber adsorbent

Solution system	Metal ion	Isotherm model
Multi-cations	Pb^{2+}	Langmuir model
	Cd^{2+}	Freundlich model
	Cu^{2+}	Freundlich model
	Ni^{2+}	Langmuir model
Mono-cations	Pb^{2+}	Redlich-Peterson model
	Cd^{2+}	Freundlich model
	Cu^{2+}	Freundlich model
	Ni^{2+}	Freundlich model

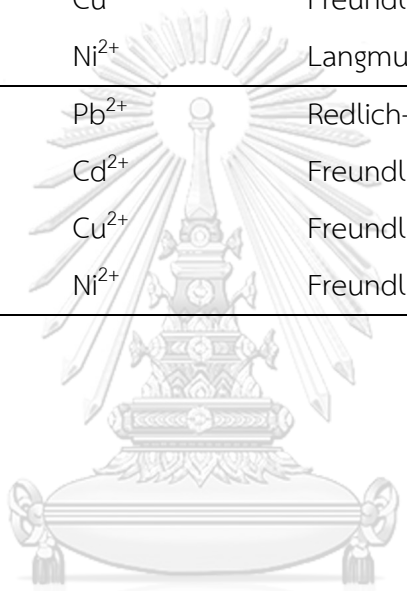

Table 4.14 Parameters on Langmuir, Freundlich, Redlich-Peterson and Dubinin-Radushkevish isotherm of FAG composite fiber adsorbent

Solution system	Isotherm model	Parameter	Metal			
			Pb^{2+}	Cd^{2+}	Cu^{2+}	Ni^{2+}
Multi-cations	Langmuir	q_m	8.299	5.650	4.216	2.519
		K_L	0.091	0.114	0.081	0.175
		R^2	0.9596	0.8541	0.8060	0.7467
		R_L	0.098	0.077	0.102	0.048
	Freundlich	K_F	1.634	1.150	0.650	0.877
		$1/n$	0.354	0.365	0.419	0.237
		R^2	0.7911	0.9471	0.9376	0.8204
	Redlich-Peterson	K_{RP}	0.861	0.651	0.346	1806.190
		a	0.104	0.202	0.180	2072.850
		g	1	0.846	0.790	0.760
		R^2	0.6241	0.9304	0.9210	0.6767
	Dubinin–Radushkevich	q_m	6.652	4.858	3.519	2.307
		β	4×10^{-6}	4×10^{-6}	7×10^{-6}	4×10^{-6}
		R^2	0.7912	0.6413	0.5865	0.5434
		E	353.553	353.553	267.261	353.553
Mono-cations	Langmuir	q_m	11.574	9.343	7.246	6.068
		K_L	0.123	0.098	0.076	0.082
		R^2	0.6669	0.9328	0.8817	0.8507
		R_L	0.082	0.098	0.120	0.110
	Freundlich	K_F	5.249	1.497	00.835	0.762
		$1/n$	0.162	0.428	0.505	0.485
		R^2	0.7014	0.6996	0.9335	0.9272
	Redlich-Peterson	K_{RP}	8.40×10^{6}	27493.8	11319.9	5640.06
		a	1.15×10^{6}	20586.1	26018	14686.6
		g	0.920	0.540	0.329	0.342
		R^2	0.8289	0.8989	0.9220	0.8904
	Dubinin–Radushkevich	q_m	10.710	7.752	5.964	5.105
		β	2×10^{-5}	3×10^{-6}	5×10^{-6}	6×10^{-6}
		R^2	0.4810	0.6996	0.5649	0.5303
		E	158.114	408.248	316.228	288.675

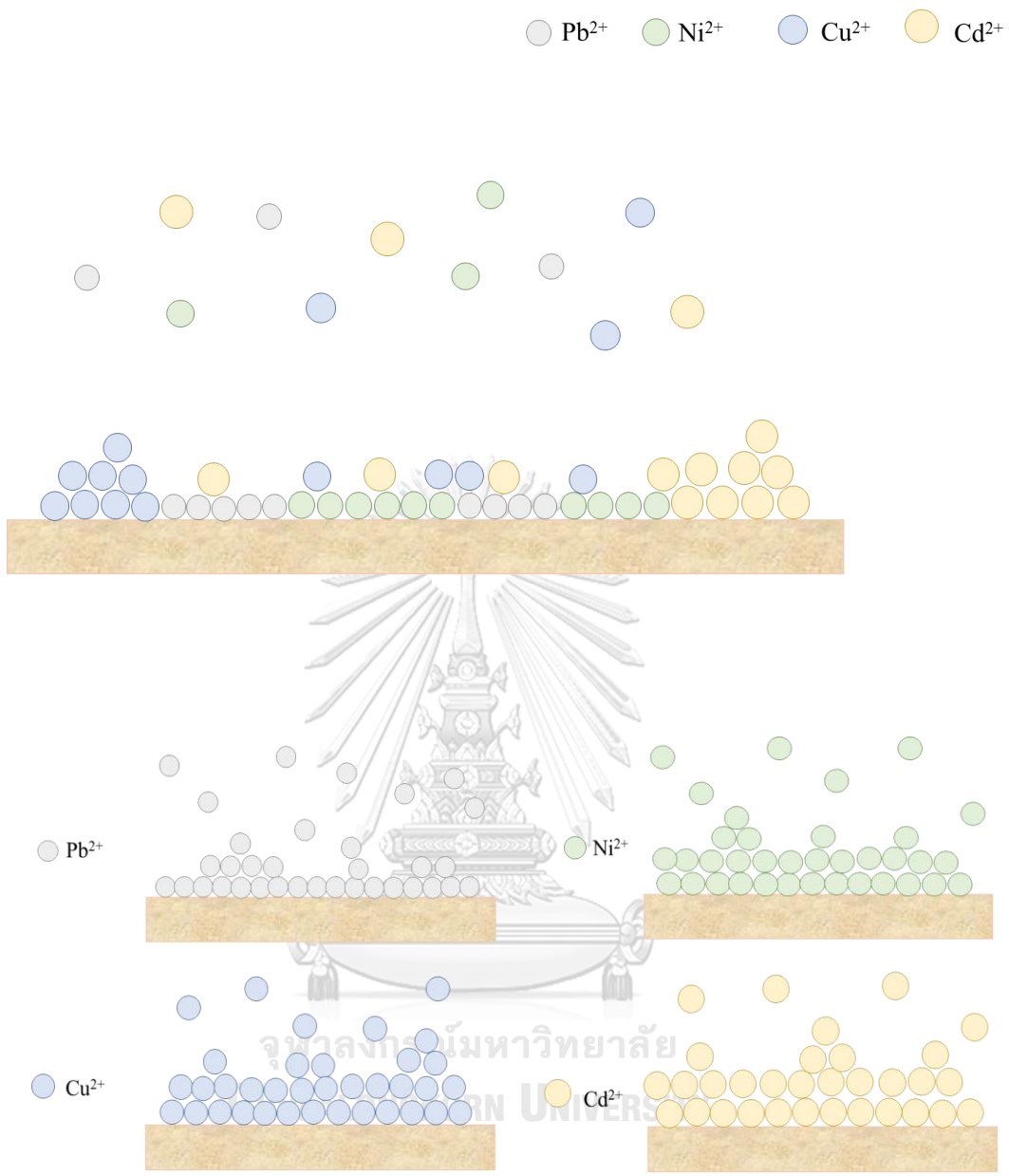

Fig. 4.58 The diagram of adsorption isotherm of metal ions with FAG fiber adsorbent in multi-cations solution (upper) and mono-cations solution (lower)

4.3.4 Kinetics study

4.3.4.1 Pseudo first order model and pseudo second order model

The kinetic parameters and the correlation coefficients calculated from the linear form for heavy metal adsorption of both solution systems are presented in Table 4.15. The kinetics of Pb^{2+}, Cd^{2+}, Cu^{2+} and Ni^{2+} by FAG composite fiber in multi- and mono-cations solution are shown in Fig. 4.59. In multi-cations solution, the linearization (R^2) proved that the pseudo second order model well described the adsorption mechanism of Cd^{2+}, Cu^{2+} and Ni^{2+} , while the pseudo first order model could described the adsorption mechanism of Pb^{2+}. In addition, the linearization (R^2) proved that the pseudo second order model well described the adsorption mechanism of Pb^{2+} and Cd^{2+}, while the pseudo first order model could described the adsorption mechanism of Cu^{2+} and Ni^{2+} in mono-cations solution. However, the model predicted values for the adsorption capacities were close to the experimental values only for pseudo second order model. In the pseudo first order model, the differences between model predicted and experimental values were approximately 10-20%. Therefore, the pseudo second order model is better predicator of the adsorption kinetics than pseudo first order model for Pb^{2+}, Cd^{2+}, Cu^{2+} and Ni^{2+} ions.

Table 4.15 Parameter values for batch kinetic adsorption models of FAG composite fiber

Solution system	Metal	Pseudo first order			Pseudo second order			Experimental value
		k_1 (min^{-1})	q_e (mg/g)	R^2	k_2 (g/mg min)	q_e (mg/g)	R^2	q_m(mg/g)
Multi-cations	Pb^{2+}	0.0007	5.767	0.9501	0.0003	6.826	0.9354	6.571
	Cd^{2+}	0.0015	1.615	0.8253	0.0040	2.772	0.9993	2.769
	Cu^{2+}	0.0012	1.700	0.9531	0.0021	2.286	0.9892	2.230
	Ni^{2+}	0.0008	1.493	0.9239	0.0020	2.158	0.9877	2.118
Mono-cations	Pb^{2+}	0.0001	6.794	0.9501	0.0004	9.327	0.9977	8.899
	Cd^{2+}	0.0001	3.856	0.8960	0.0005	6.208	0.6878	6.192
	Cu^{2+}	0.0003	4.908	0.9775	0.0002	5.550	0.9125	5.551
	Ni^{2+}	0.0004	3.806	0.9506	0.0005	4.670	0.9157	4.840

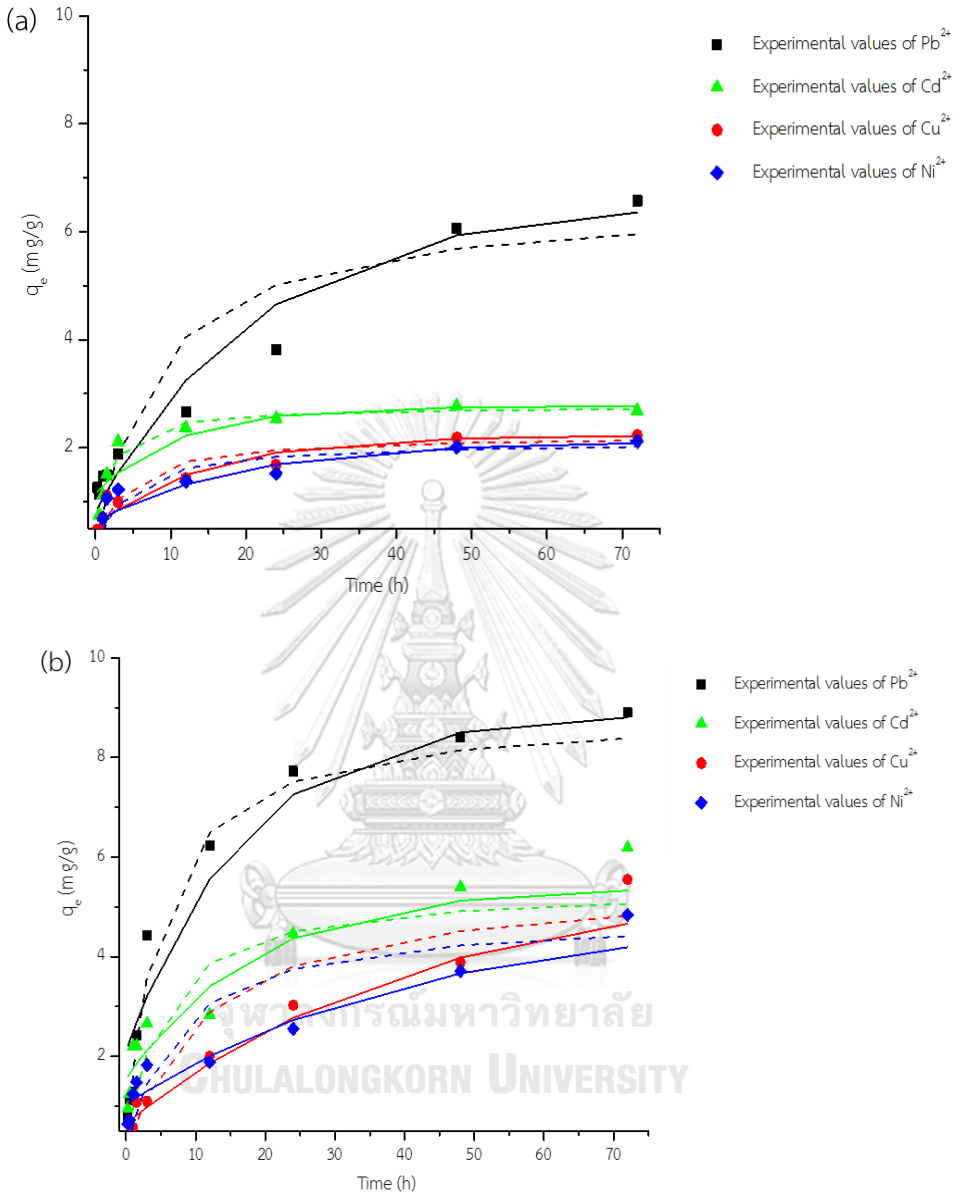

Fig. 4.59 Kinetics of Pb^{2+}, Cd^{2+}, Cu^{2+} and Ni^{2+} adsorption on FAG composite fiber and model's fit to the data (a) multi-cations solution (b) mono-cations solution (Pseudo first order: solid line, Pseudo second order: dash line)

4.3.4.2 Intraparticle diffusion model

From Fig. 4.60, Intraparticle diffusion plots of the adsorption by FAG composite fiber in multi-cations solution and mono-cations solution were shown. Table 4.16 listed Intraparticle diffusion parameters for the adsorption. The fast rate of adsorption still occurred in the adsorption process of Pb^2 ions in multi-cations solution, only single line are observed. It was conclude that diffusion of Pb^{2+} to FAG powder in the fiber through PES scaffold was rate limiting step. For other metal ions with multi- and mono-cations solution system, two portion lines were observed. The first portion lines showed the diffusion of metal ions onto the surface of FAG powder through PES. The next region lines attributed diffusion of metal ions into FAG pores.

Table 4.16 Intraparticle diffusion parameters for the adsorption by FAG composite fiber

Solution system	Metal	Intraparticle diffusion		
		k_p (mg/g $h^{0.5}$)	C (mg/g)	R^2
Multi-cations	Pb^{2+}	0.723	0.506	0.9868
	Cd^{2+}	0.665	0.270	0.9660
	Cu^{2+}	0.314	0.345	0.9499
	Ni^{2+}	0.350	0.287	0.9344
Mono-cations	Pb^{2+}	1.684	0.1204	0.9907
	Cd^{2+}	0.681	0.932	0.9527
	Cu^{2+}	0.596	0.034	0.9869
	Ni^{2+}	0.404	0.063	0.9618

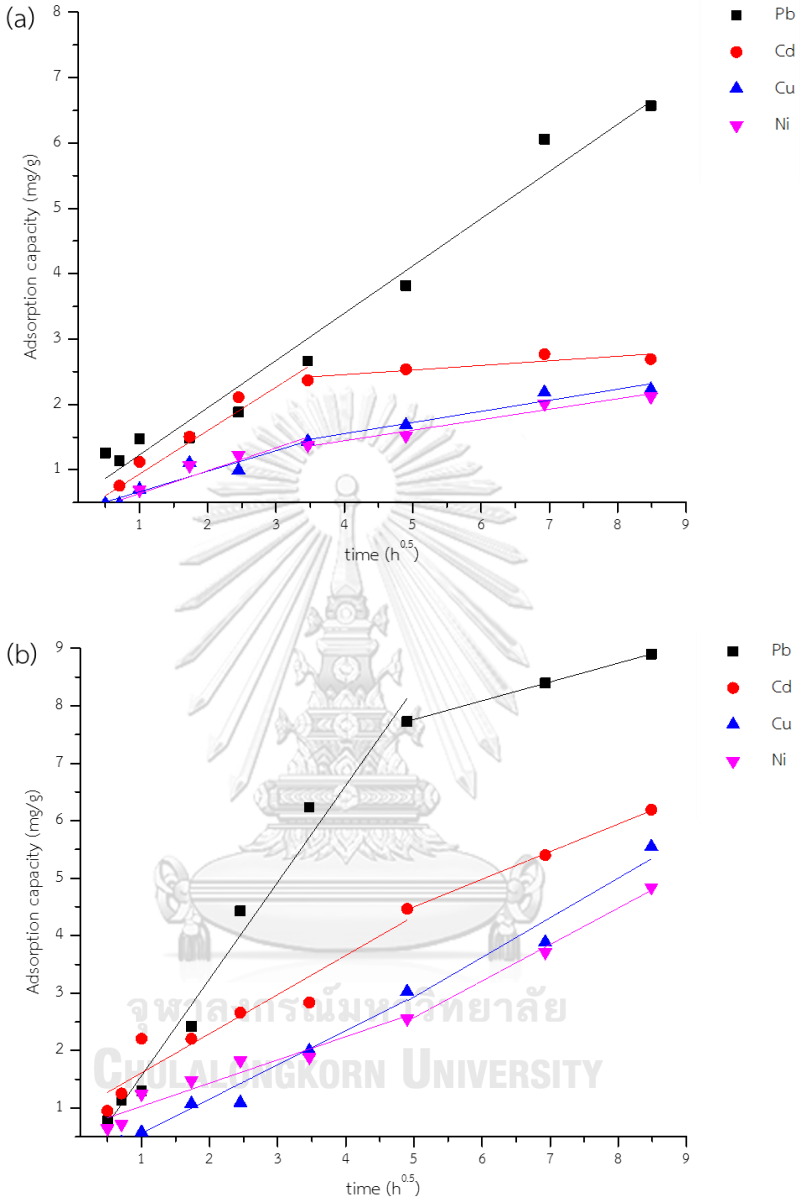

Fig. 4.60 Intraparticle diffusion plots of the adsorption by FAG composite fiber (a) multi-cations solution (b) mono-cations solution

4.4 METAKAOLIN BASED GEOPOLYMER COMPOSITE FIBER

4.4.1 Characterizations

4.4.1.1 Chemical composition

PES fiber and fly ash based geopolymer composite fibers with different fly ash based geopolymer powder amount were characterized by XRF as shown in Table 4.17. PES fiber composed of SO_3 and CO_2 because PES structure has sulfone group and a benzene ring. The compositions of SiO_2, Al_2O_3, Fe_2O_3, CaO, MgO and Na_2O were increased when the amount of metakaolin based geopolymer powder increased in composite fibers.

Table 4.17 Chemical compositions of PES fiber and metakaolin based geopolymer composite fibers

Chemical compound (%)	PES	Washed MK Geopolymer powder	20 wt% MKG fiber	40 wt% MKG fiber	60 wt% MKG fiber
SiO_2	-	47.20	7.67	19.30	24.50
Al_2O_3	-	31.00	5.78	14.20	18.10
Fe_2O_3	-	1.10	0.17	0.43	0.73
CaO	-	0.07	0.32	0.33	0.41
MgO	-	0.08	0.10	0.14	0.14
SO_3	20.70	-	24.10	19.40	12.80
Na_2O	-	10.50	0.76	2.60	3.11
K_2O	-	2.10	0.31	0.89	1.30
MnO	-	0.10	0.01	0.04	0.06
CO_2	79.10	7.79	60.60	42.60	38.60

4.4.1.2 Phases

In Fig. 4.61, XRD patterns of metakaolin based geopolymer powder, PES and the composite fibers are displayed. The board hump peak indicating amorphous of PES polymer is presented at 2θ = 12-25°. The sharp crystalline peaks composed with muscovite (JCPDS, 00-007-0042), quartz (JCPDS, 01-089-8934), alunite (JCPDS, 00-003-0616) and kaolinite (JCPDS, 01-089-6538) were component in metakaolin based geopolymer powder. The crystalline peaks of metakaolin based geopolymer powder showed in composite fibers and the peaks was not shift. It meant that the crystalline structure and phases not changed after added to fabricate composite fibers.

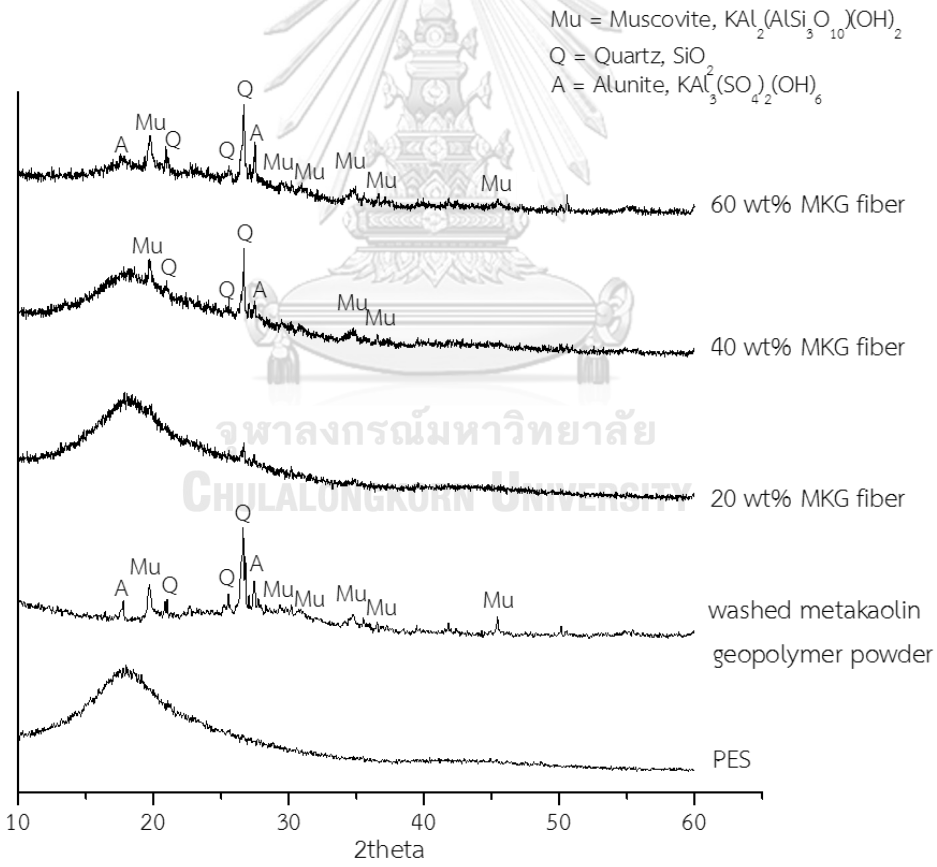

Fig. 4.61 XRD patterns of PES fiber and metakaolin based geopolymer composite fibers

4.4.1.3 Microstructure

The morphology of the fibers with different amount of metakaolin based geopolymer powder amount were compared in Fig. 4.62. The PES fiber (Fig. 4.62 (a)) had diameter about 500 μm. Moreover, when increased the MKG powder amount more 20wt% in the composite fiber, the cross section of composite fiber decreased due to the fibers was close packed when added more MKG powder. The cross section of 20, 40 and 60wt% of MKG composite fiber (Fig. 4.62 (c, g, j)) had diameter about 400-450 μm. The composite fibers had porous structure with finger-like structure of pore (outer) and sponge structure of pore (core). The finger like structure was disappeared after increased geopolymer amount.

The micro X-ray CT technique was used to observe structure inside of the PES and MKG composite fibers as shown in Fig. 4.63. The FAG powder was uniformly dispersed in the fiber network with a finger-like and sponge pore structure. MKG powder in the fibers was agglomerated, therefore, the varying from small to big particles of MKG powder in fibers was seen. Furthermore, the fiber was denser when added more amount of MKG powder.

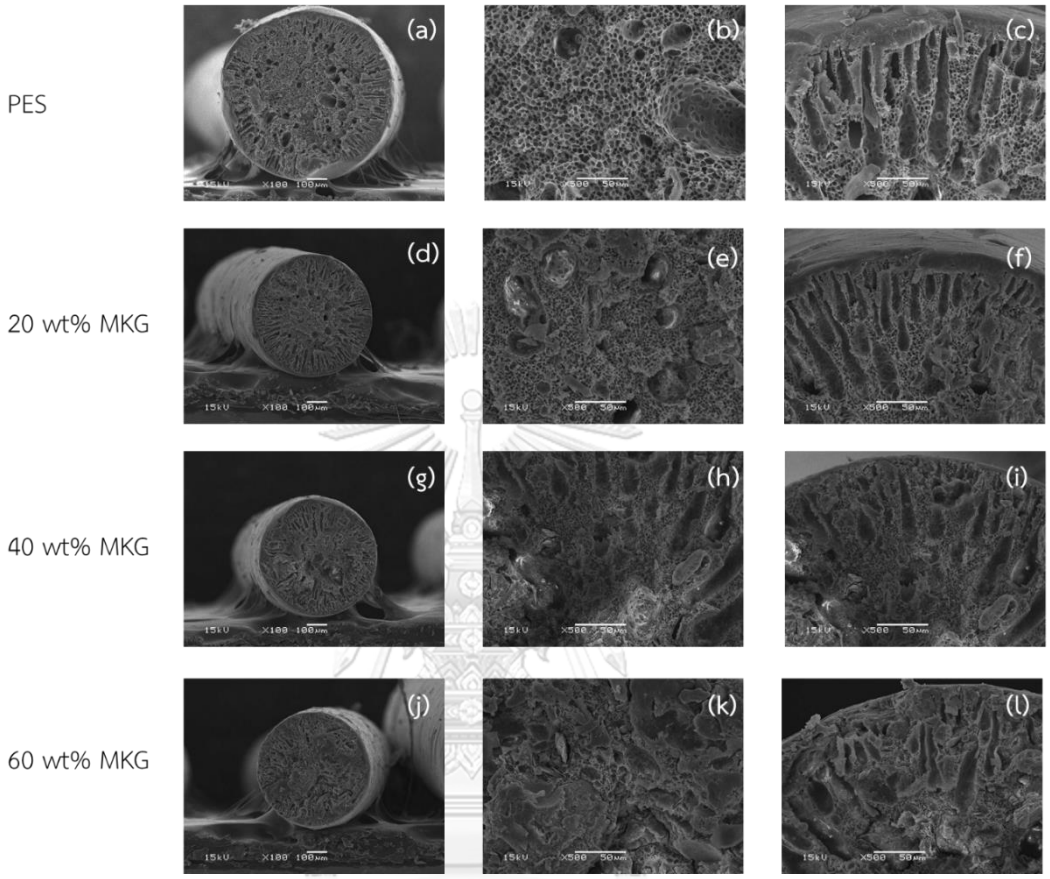

Fig. 4.62 Microstructure of PES fiber and metakaolin based geopolymer composite fibers

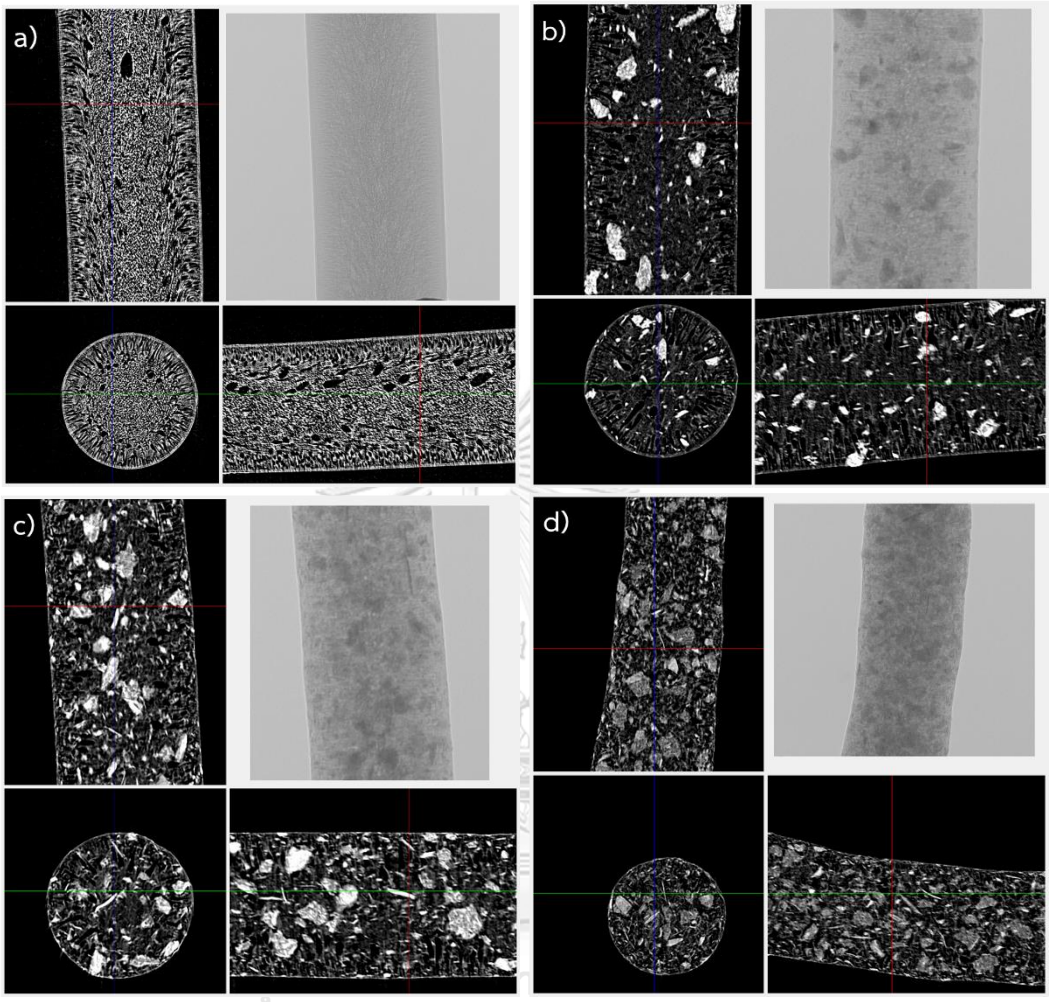

Fig. 4.63 X-ray micro CT images of PES fiber and metakaolin based geopolymer composite fibers: (a) PES (b) 20wt% MKG (c) 40wt% MKG and (d) 60wt% MKG

4.4.1.4 Tensile strength and surface area

Table 4.18 showed, the tensile strength of PES fiber and metakaolin based geopolymer composite fibers. The tensile strength values decreased with increased MKG powder amount because the MKG powder was inserted in the middle of the bonding of PES polymer in the fibers.

From Table 4.18, the surface area values of PES and 20, 40 and 60wt% of MKG powder composite fibers were 27.39, 15.74, 32.11 and 53.11 m^2/g, respectively. The surface area of MKG composite fiber was higher than PES fiber resulted from metakaolin geopolymer powders having small particle and the surface of powder was a rough surface. Form the specific surface area results, the 60wt% of MKG powder in composite fiber was chosen for adsorption test.

Table 4.18 Tensile strength and surface area of PES fiber and metakaolin based geopolymer composite fibers

Samples	Tensile strength (MPa)	Surface area (m^2/g)
PES	5.83	27.39
20 wt% MKG	2.68	15.74
40 w% MKG	1.56	32.11
60 wt% MKG	1.43	53.11
MKG powder	-	20.36

4.4.2 Adsorption test

4.4.2.1 Effect of contact time

The effect of contact time of Pb^{2+}, Cu^{2+}, Cd^{2+}, Ni^{2+} in multi- and mono-cations solutions was determined between 5 min – 72 h and the results were displayed in Fig. 4.64 and Fig. 4.65. The initial concentration of each heavy metal ions was fixed at 20 mg/L with 0.1 g of MKG composite geopolymer fiber in 40 mL of solution and initial pH of 5 and heavy metals of Pb^{2+}, Cu^{2+}, Cd^{2+}, Ni^{2+} were adsorbed. The results showed that the adsorption efficiency increased with increasing of contact time. In multi-cations solution, the adsorption of Cu^{2+}, Cd^{2+}, and Ni^{2+} became equilibrium after 12 h and the adsorption of Pb^{2+} still increased with an increasing of contact time. Moreover, the adsorption of Pb^{2+}, Cu^{2+}, Cd^{2+}, Ni^{2+} also increasing with an increase of contact time in mono-cations solution.

4.4.2.2 Effect of geopolymer dosage

Adsorbent dosage is an important parameters due to it determines the adsorption capacity of an adsorbent for given initial concentration of the adsorbate. Therefore, the effect of geopolymer amount on the adsorption of Pb^{2+}, Cu^{2+}, Cd^{2+}, Ni^{2+} ions onto MKG composite fiber is investigated and the results are shown in Fig. 4.66 and Fig. 4.67. It was seen that the percentage of metal removal increased with an increase in the adsorbent dose. Pb^{2+}, Cu^{2+}, Cd^{2+}, Ni^{2+} removal efficiency up to 46.84% (3.74 mg/g), 25.89% (2.07 mg/g), 33.60% (2.69 mg/g) and 19.72% (1.58 mg/g), respectively when the adsorbent dose was increase up to 0.5 g/ 40mL in multi-cations solution. In addition, the percentage of metal removal increased with an increase in the adsorbent dose. Pb^{2+}, Cu^{2+}, Cd^{2+}, Ni^{2+} removal efficiency up to 66.28% (5.30 mg/g),

57.57% (4.60 mg/g), 61.92% (4.95 mg/g) and 48.50% (3.88 mg/g), respectively when the adsorbent dose was increase up to 0.5 g/ 40mL in the case of mono-cations solution.

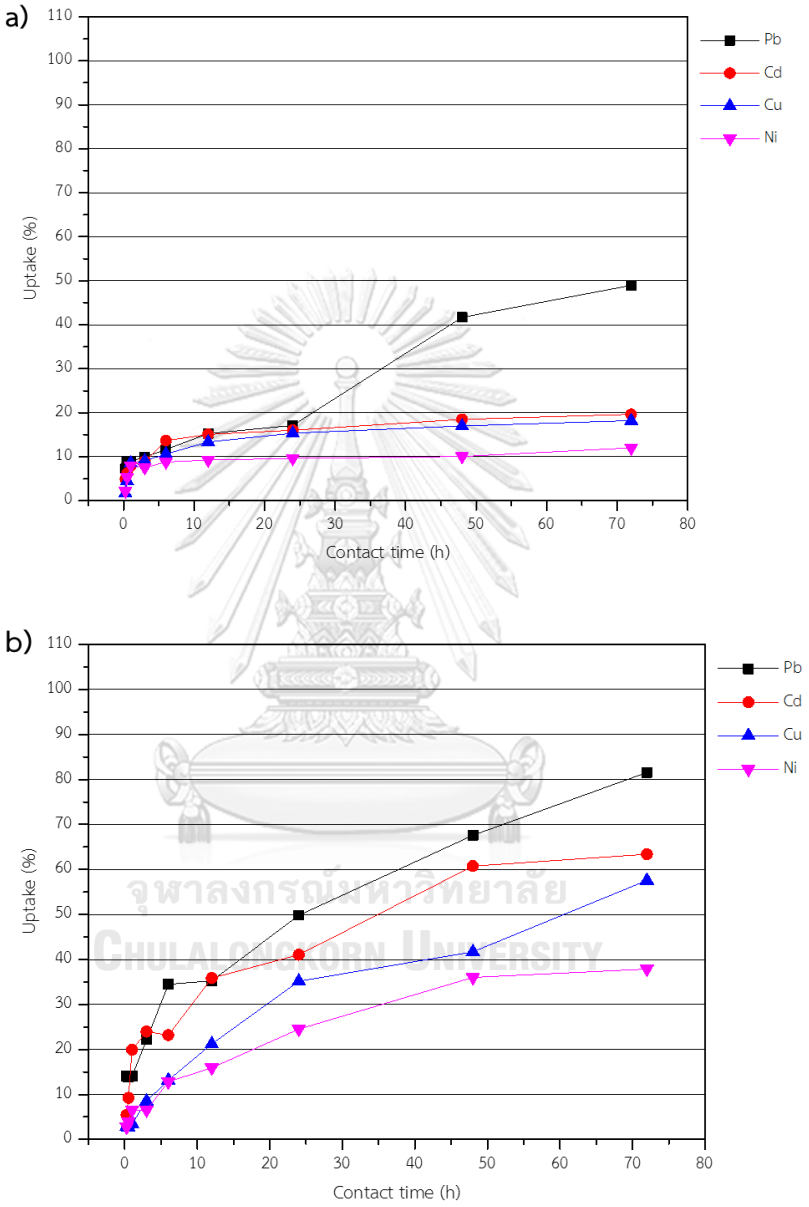

Fig. 4.64 Effect of contact time on heavy metal ions removal efficiency of MKG composite fiber (a) multi-cations solution (b) mono-cations solution

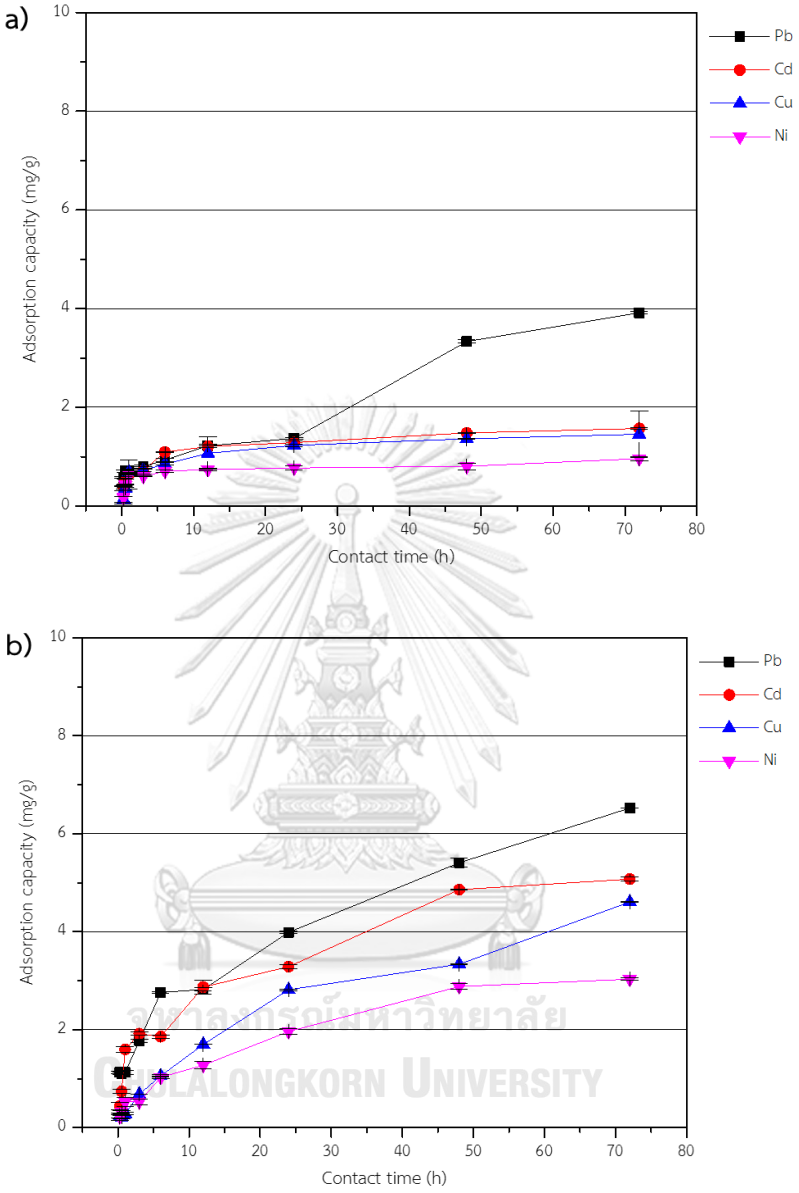

Fig. 4.65 Effect of contact time on adsorption capacity of MKG composite fiber (a) multi-cations solution (b) mono-cations solution

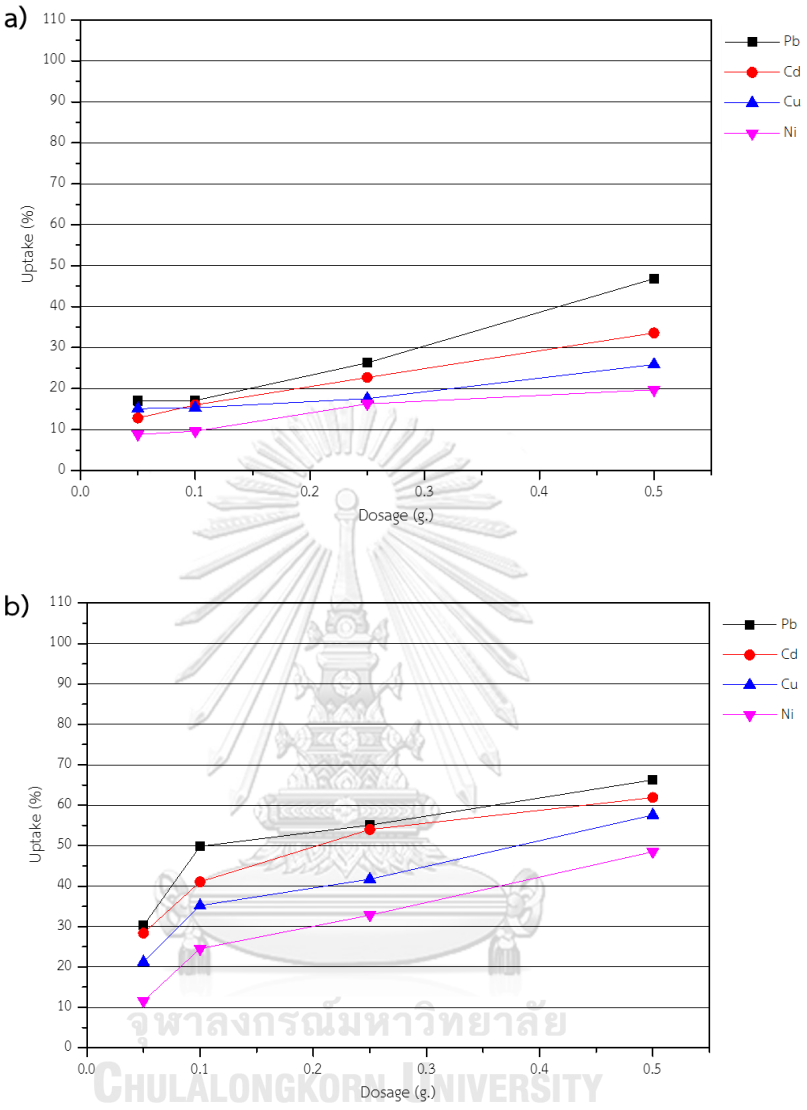

Fig. 4.66 Effect of geopolymer dosage on heavy metal ions removal efficiency of MKG composite fiber (a) multi-cations solution (b) mono-cations solution

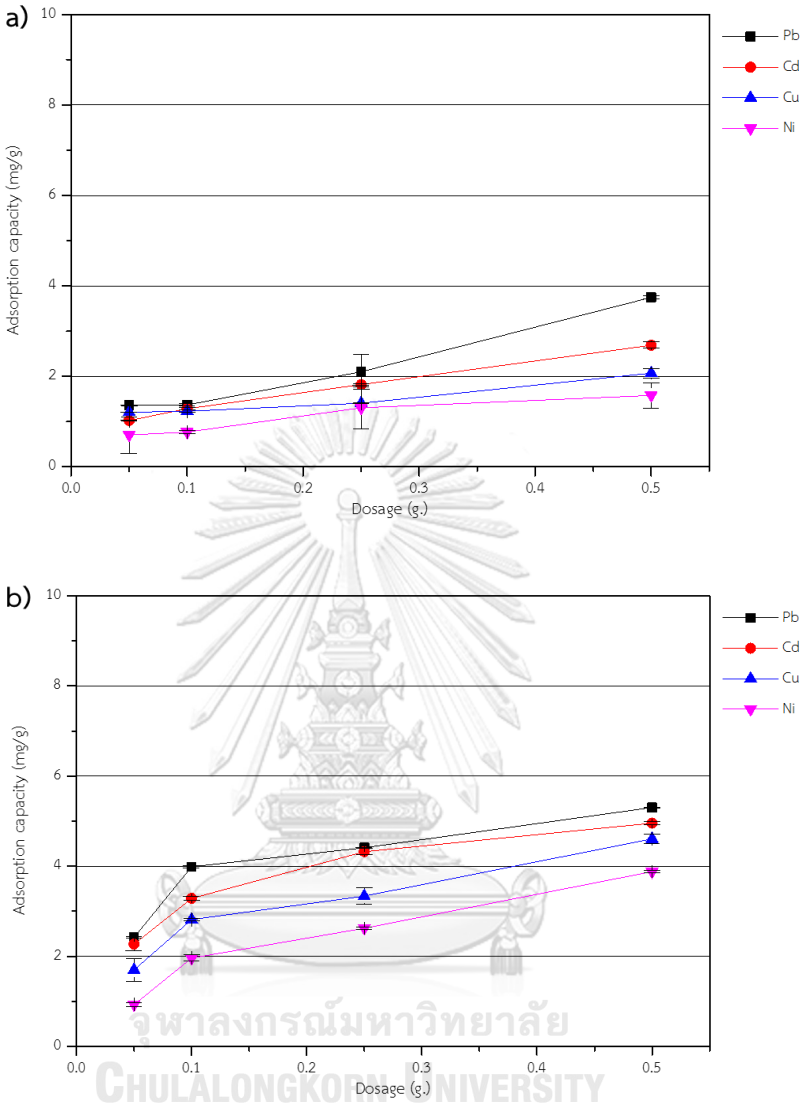

Fig. 4.67 Effect of geopolymer dosage on adsorption capacity of MKG composite fiber (a) multi-cations solution (b) mono-cations solution

4.4.2.3 Effect of solution pH

The pH of aqueous solution is one of parameter for controlling an adsorption process. The effect of pH on Pb^{2+}, Cu^{2+}, Cd^{2+}, Ni^{2+} adsorption onto MKG composite fiber was investigated by ranging the solution pH from 1 to 5 at 25 ^{o}C and the removal efficiency and the adsorption capacity of MKG composite fiber with multi- and mono-cations solution as a function of pH are plotted in Fig. 4.68 and Fig. 4.69. An apparent increase in Pb^{2+}, Cu^{2+}, Cd^{2+}, Ni^{2+} removal efficacy and adsorption capacity of MKG composite fiber was observed until pH 5. The adsorption efficiency and the adsorption capacity of heavy metals decreased in low pH. As a results, the removal efficiency and the adsorption capacity of MKG composite fiber were carried out at original pH values of the metal solution (pH around 5).

4.4.2.4 Effect of temperature

In order to investigate the effect of temperature on the adsorption efficiency and the adsorption capacity of Pb^{2+}, Cu^{2+}, Cd^{2+}, Ni^{2+} onto MKG composite fiber, the experiments were carried out at different temperatures. The relationship between the temperature and adsorption efficiency and the adsorption capacity values are illustrated in Fig. 4.70 and Fig. 4.71. Adsorption efficiency and the adsorption capacity values were increased when the temperature increased from 25 to 45 ^{o}C. It can also be seen from the results that adsorption efficiency and the adsorption capacity values were not significantly changed by the temperature after 25 ^{o}C in the case of multi-cations solution. Nevertheless, the adsorption efficiency and the adsorption capacity values were significantly changed when the temperature increased in the case of mono-cations solution.

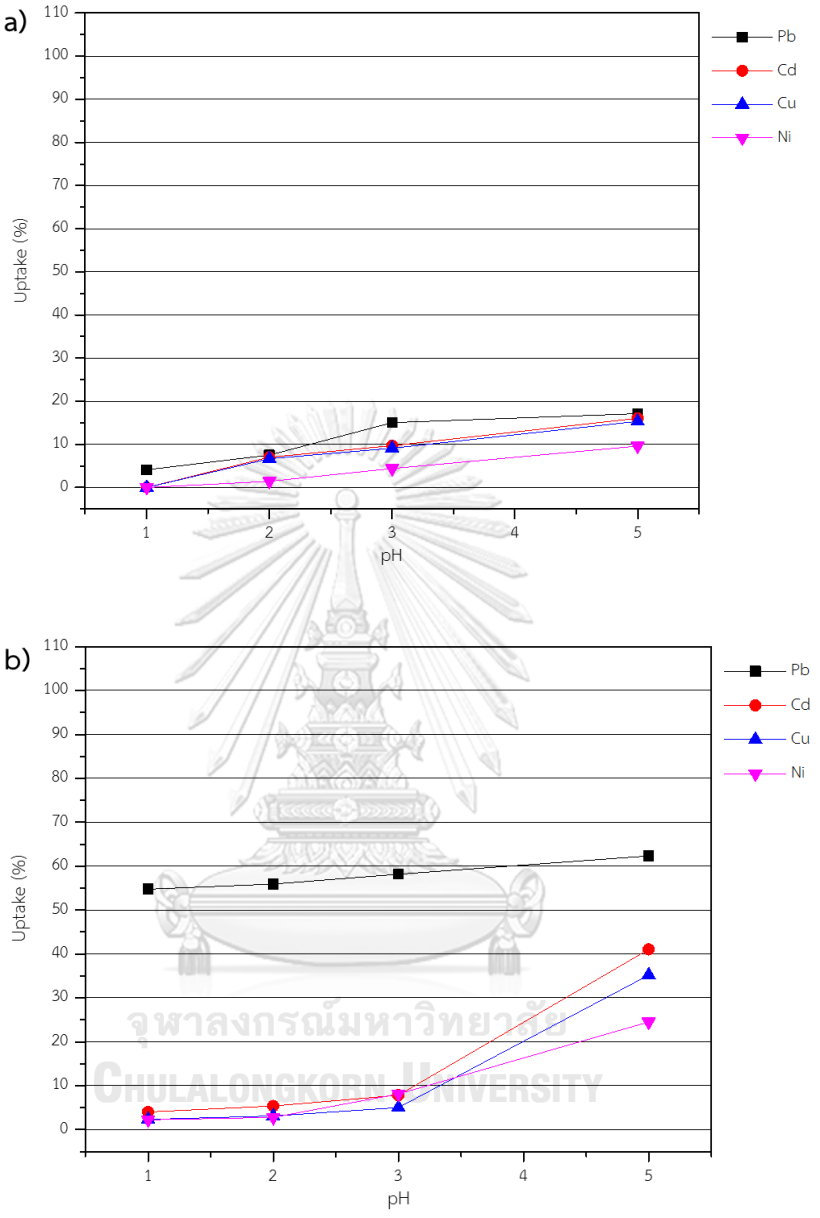

Fig. 4.68 Effect of pH on heavy metal ions removal efficiency of MKG composite fiber (a) multi-cations solution (b) mono-cations solution

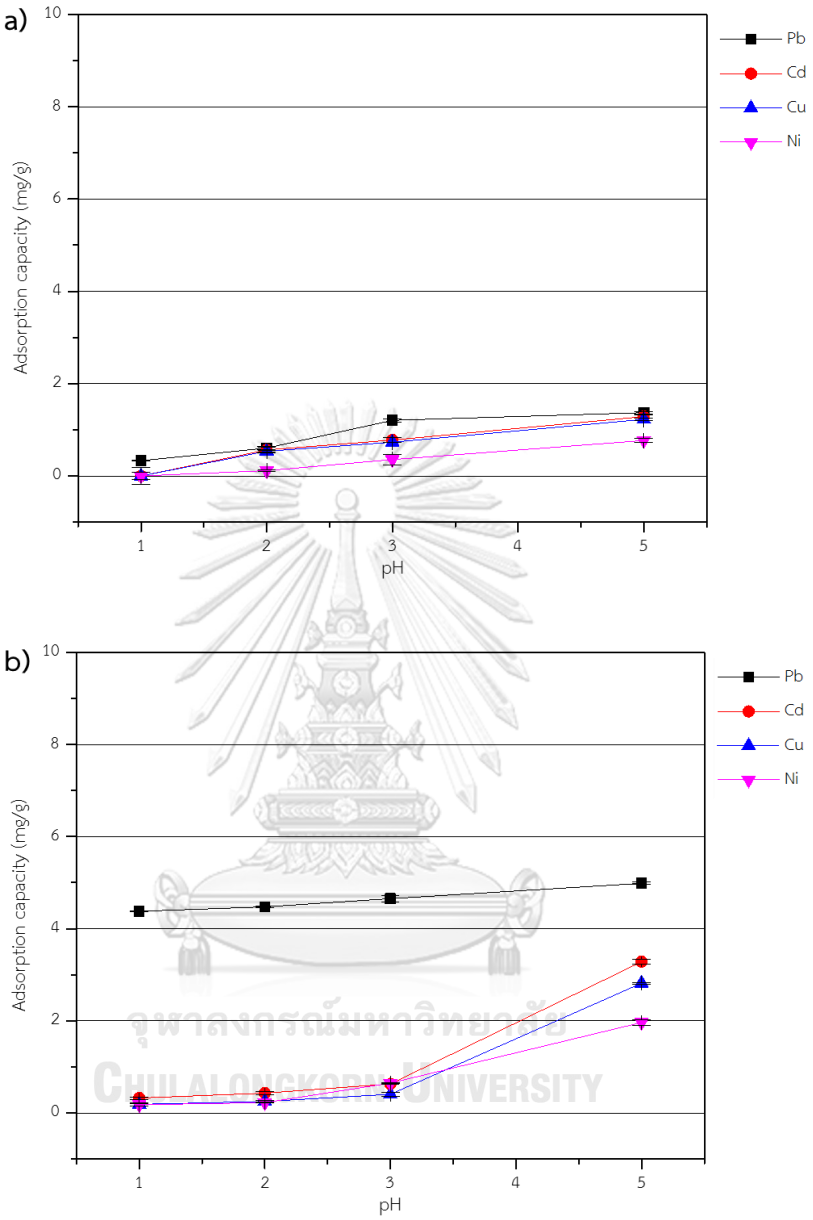

Fig. 4.69 Effect of pH on adsorption capacity of MKG composite fiber (a) multi-cations solution (b) mono-cations solution

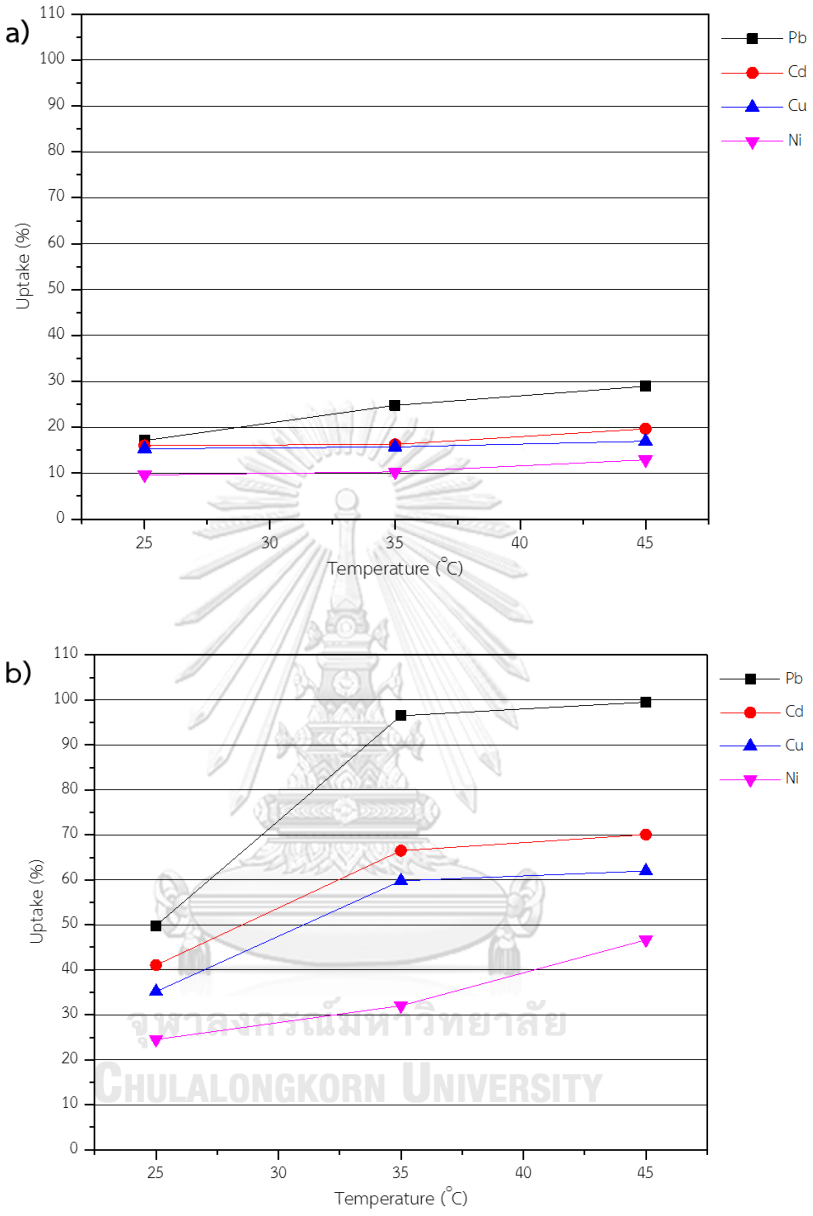

Fig. 4.70 Effect of temperature on heavy metal ions removal efficiency of MKG composite fiber (a) multi-cations solution (b) mono-cations solution

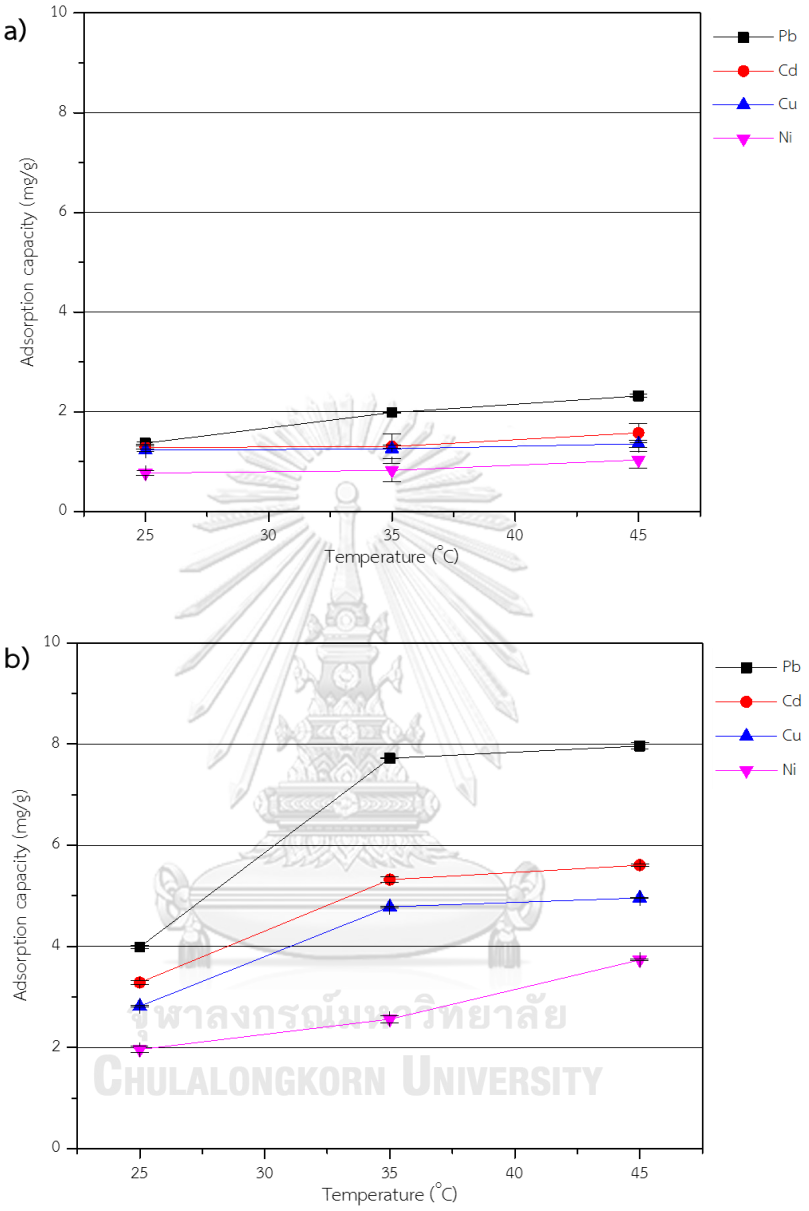

Fig. 4.71 Effect of temperature on adsorption capacity of MKG composite fiber (a) multi-cations solution (b) mono-cations solution

4.4.2.5 Effect of initial concentration

The initial concentration was studied using a geopolymer dosage of 0.1 g/ 40 mL at pH 5 and a temperature of 25 ^{o}C for 120 min contact time. The initial concentration of heavy metal solution was varied from 20-120 mg/L. the removal efficiency and the adsorption capacity of MKG composite fiber with multi- and mono-cations solution as a function of initial concentration are plotted in Fig. 4.72 and Fig. 4.73. The removal efficiency decreased with an increase of initial concentration. The maximum adsorption capacity values of Pb^{2+}, Cu^{2+}, Cd^{2+}, Ni^{2+} were found as 5.76 mg/g of Pb^{2+} at 120 mg/L, 4.15 mg/g of Cu^{2+}, 4.33 mg/g of Cd^{2+}, 3.56 mg/g of Ni^{2+} at 100 mg/L in multi-cations solution. Moreover, the maximum adsorption capacity values of Pb^{2+}, Cu^{2+}, Cd^{2+}, Ni^{2+} were seen as 4.17 mg/g of Pb^{2+}, 3.97 mg/g of Cu^{2+}, 4.07 mg/g of Cd^{2+} and 3.69 mg/g of Ni^{2+} at 120 mg/L in mono-cations solution. From the Fig. 4.73, it was found that the adsorption capacity of Cu^{2+} and Cd^{2+} remained constant values after 100 mg/L in multi-cations solution and the adsorption capacity of Pb^{2+}, Cu^{2+}, Cd^{2+}, Ni^{2+} remained constant values after 100 mg/L in mono-cations solution. This suggested that the geopolymer composite fiber reached the saturation level at initial concentration above 100 mg/L.

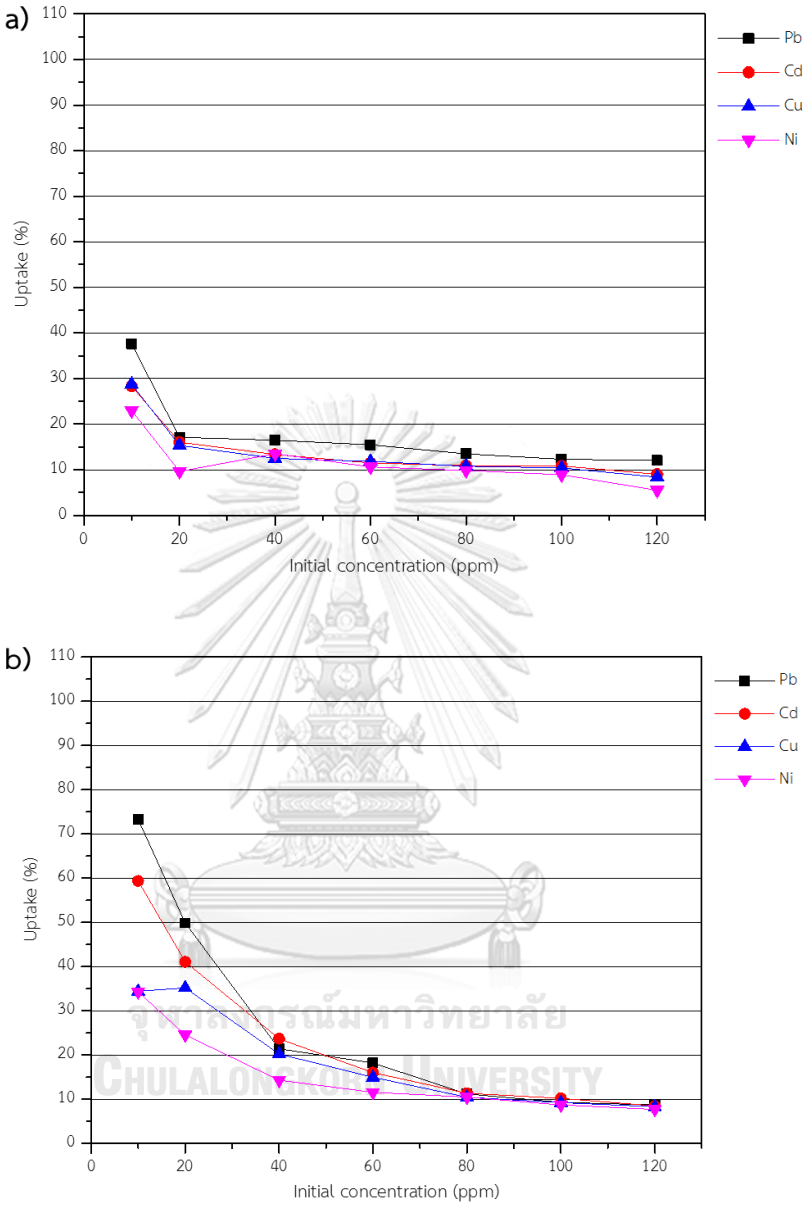

Fig. 4.72 Effect of initial concentration on heavy metal ions removal efficiency of MKG composite fiber (a) multi-cations solution (b) mono-cations solution

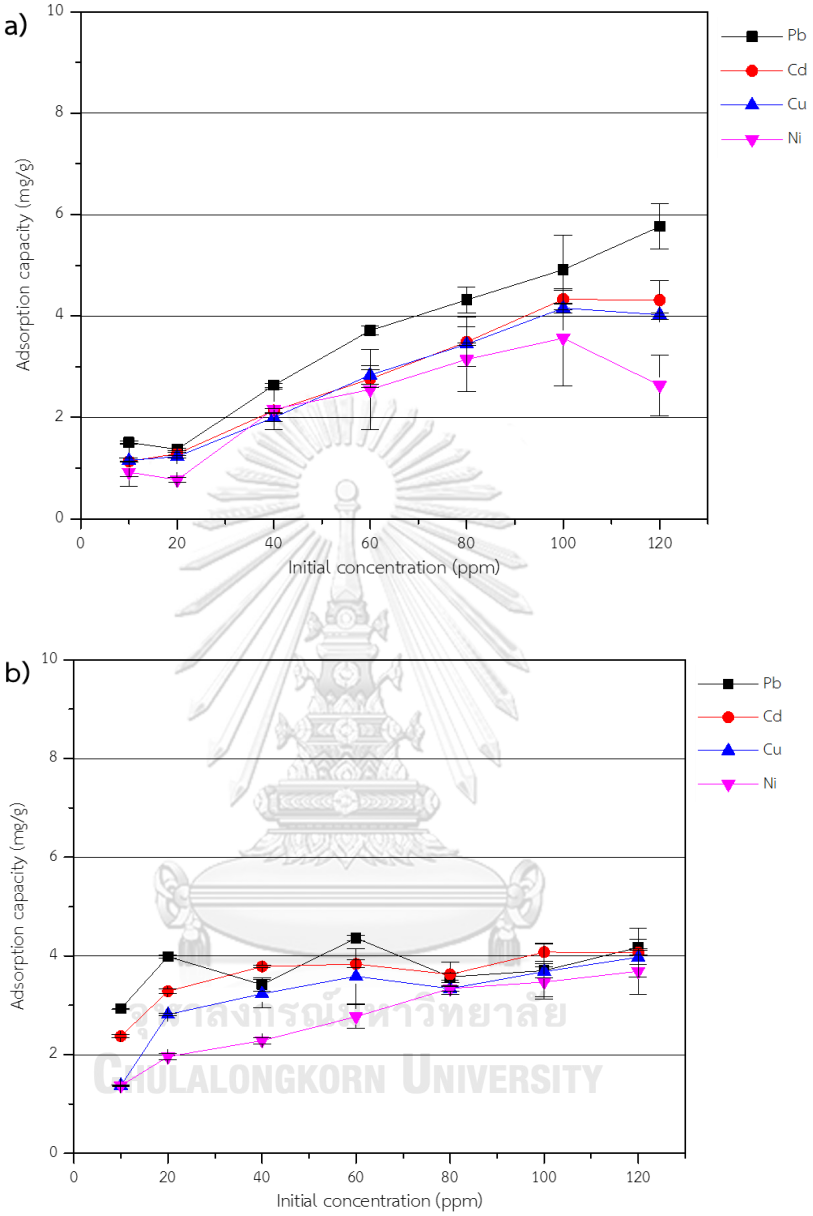

Fig. 4.73 Effect of initial concentration on adsorption capacity of MKG composite fiber (a) multi-cations solution (b) mono-cations solution

4.4.3 Adsorption isotherm

The isotherm analysis on MKG composite fiber of Pb^{2+}, Cu^{2+}, Cd^{2+}, Ni^{2+} is shown in Fig. 4.74 to Fig. 4.77. The four model as Langmuir, Freundlich, Redlich-Peterson and Dubinin-Radushkevish isotherm models were adopted to fit for the experimental data and the fitting results are given in Table 4.19. In addition, the model parameters of adsorption isotherm is presented in Table 4.20. Moreover, the diagram of adsorption isotherm which were fitted with each ions are shown in Fig. 4.78.

In multi-cations solution, the isotherms of Pb^{2+}, Cu^{2+}, Cd^{2+}, Ni^{2+} by MKG composite fiber were Redilich-Peterson adsorption isotherm. The results indicated that all of metal ions was adsorbed in monolayer and multilayer on heterogeneous surface.

In mono-cations solution, the isotherms of Pb^{2+}, Cd^{2+}, Cu^{2+}, and Ni^{2+} by MKG composite fiber were Langmuir isotherm, Langmuir isotherm, Dubinin-Radushkevish isotherm, Freundlich isotherm, respectively. Pb^{2+}, Cd^{2+} was fitted well with Langmuir adsorption isotherm. The results indicated that Pb^{2+}, Cd^{2+}could adsorb on MKG composite fiber in monolayer. $Cu^{2+}$was fitted well with Dubinin-Radushkevish isotherm which is occurred physical adsorption on heterogeneous surface of MKG composite fiber. Ni^{2+} was fitted well with Freundlich adsorption isotherm. It meant that Ni^{2+} was adsorbed on MKG composite fiber in multilayer on heterogeneous surface.

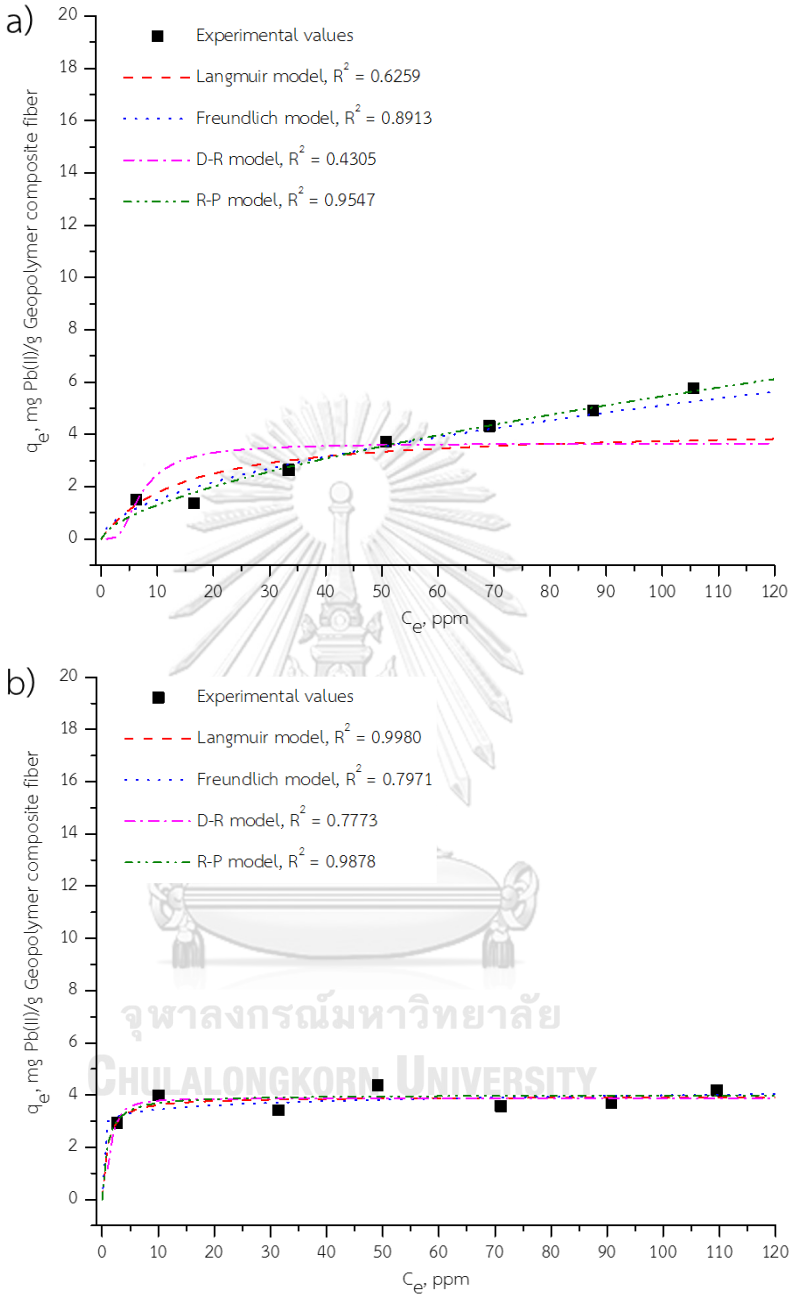

Fig. 4.74 The adsorption isotherms of Pb(II) by applying Langmuir, Freundlich, Redlich-Peterson and Dubinin–Radushkevich isotherm models MKG composite fiber adsorbent (a) multi-cations solution (b) mono-cations solution

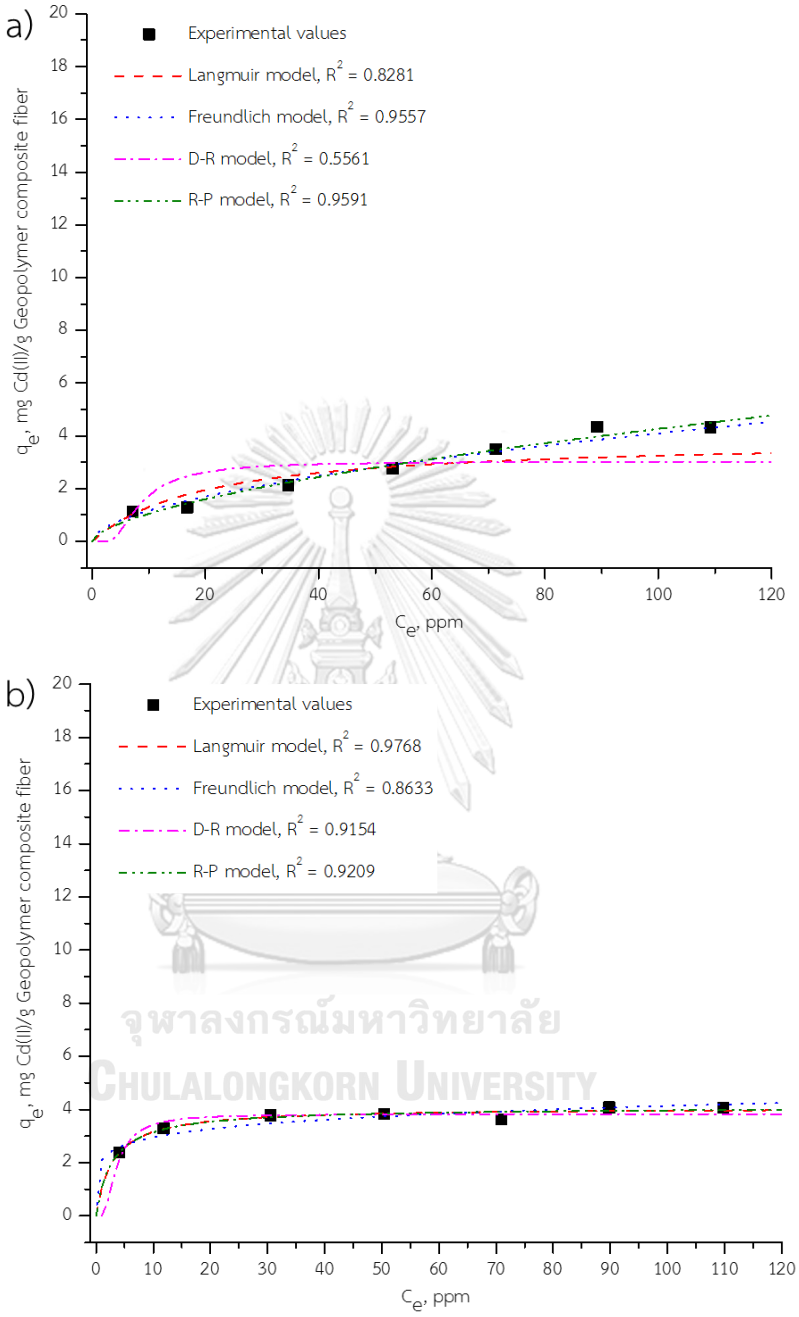

Fig. 4.75 The adsorption isotherms of Cd(II) by applying Langmuir, Freundlich, Redlich-Peterson and Dubinin–Radushkevich isotherm models MKG composite fiber adsorbent (a) multi-cations solution (b) mono-cations solution

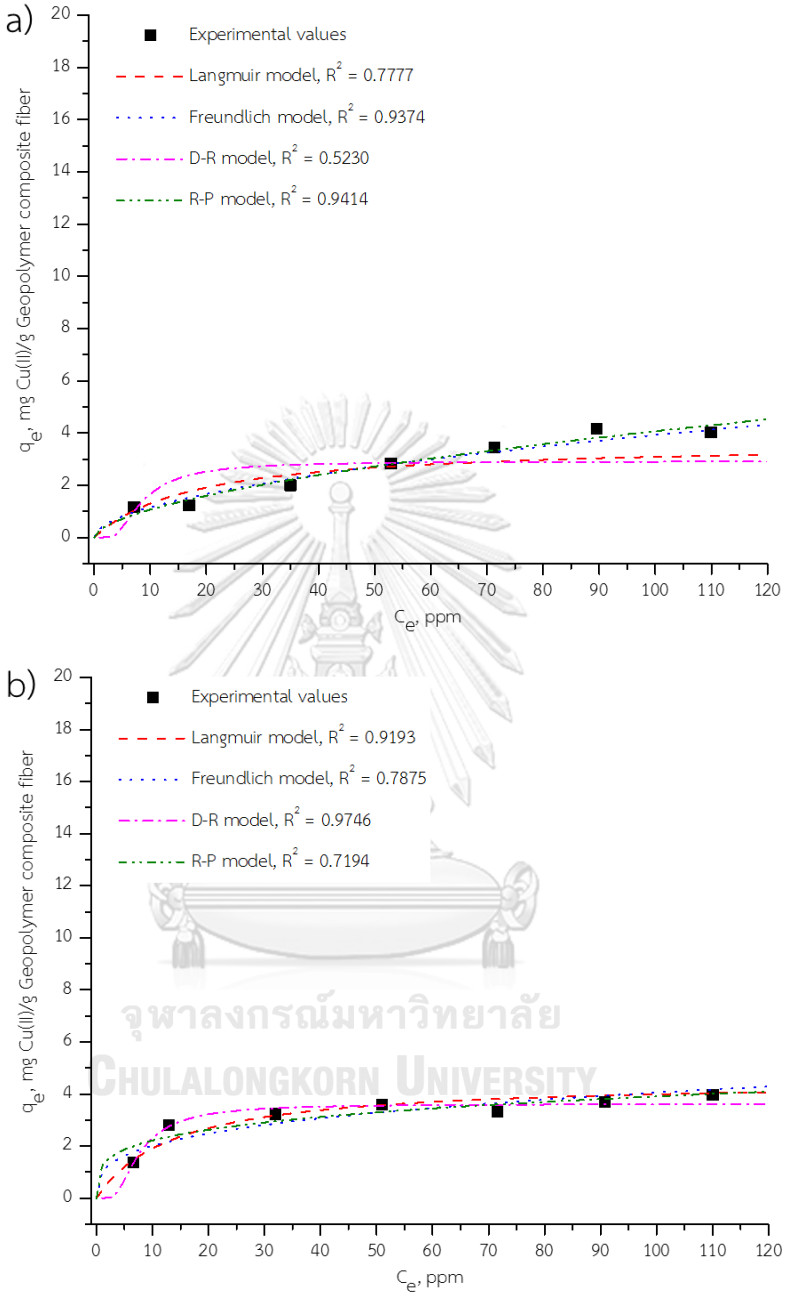

Fig. 4.76 The adsorption isotherms of Cu(II) by applying Langmuir, Freundlich, Redlich-Peterson and Dubinin–Radushkevich isotherm models MKG composite fiber adsorbent (a) multi-cations solution (b) mono-cations solution

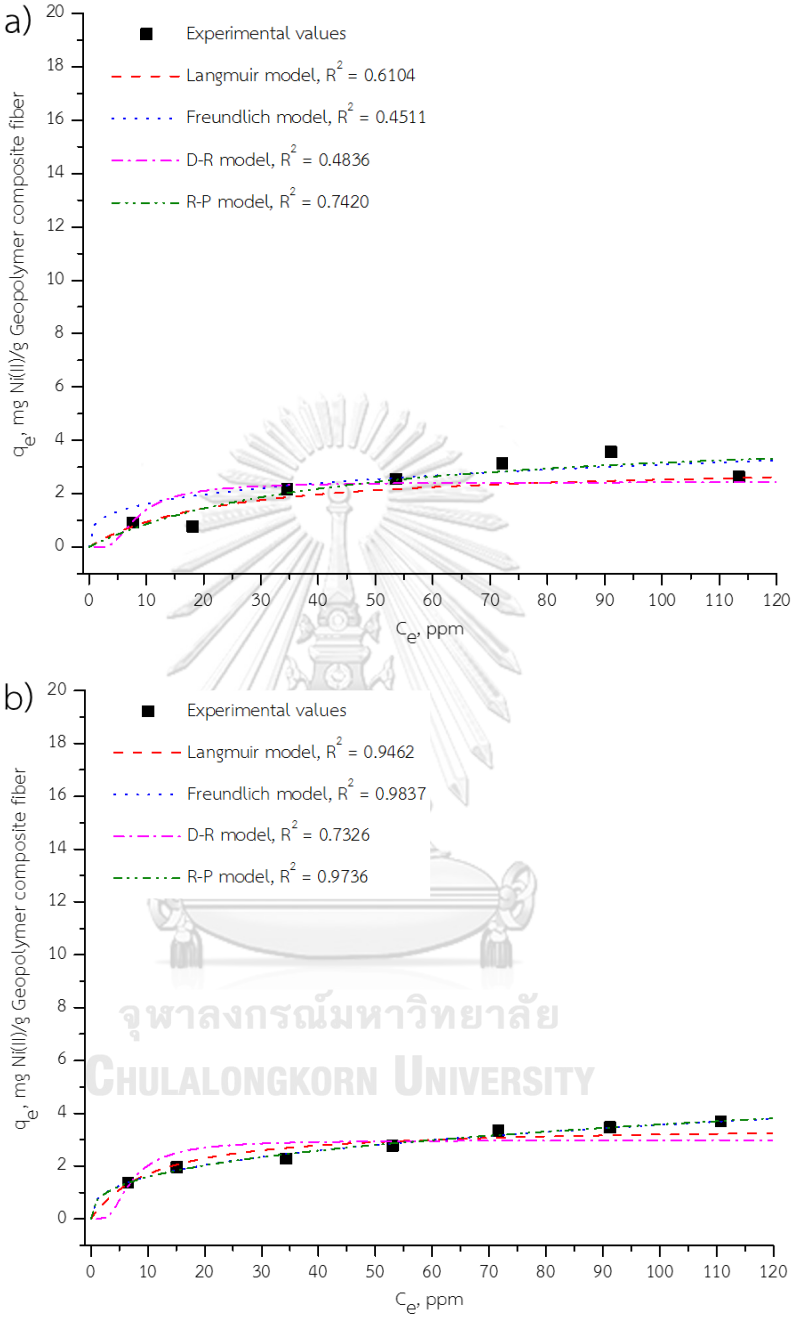

Fig. 4.77 The adsorption isotherms of Ni(II) by applying Langmuir, Freundlich, Redlich-Peterson and Dubinin–Radushkevich isotherm models MKG composite fiber adsorbent (a) multi-cations solution (b) mono-cations solution

Table 4.19 Summary of adsorption isotherm of metal ions with MKG composite fiber adsorbent

Solution system	Metal ion	Isotherm model
Multi-cations	Pb^{2+}	Redlich-Peterson model
	Cd^{2+}	Redlich-Peterson model
	Cu^{2+}	Redlich-Peterson model
	Ni^{2+}	Redlich-Peterson model
Mono-cations	Pb^{2+}	Langmuir model
	Cd^{2+}	Langmuir model
	Cu^{2+}	Dubinin-Radushkevish model
	Ni^{2+}	Freundlich model

Table 4.20 Parameters on Langmuir, Freundlich, Redlich-Peterson and Dubinin-Radushkevish isotherm of MKG composite fiber adsorbent

Solution system	Isotherm model	Parameter	Metal			
			Pb^{2+}	Cd^{2+}	Cu^{2+}	Ni^{2+}
Multi-cations	Langmuir	q_m	4.273	3.894	3.643	3.112
		K_L	0.070	0.050	0.055	0.043
		R^2	0.6259	0.8281	0.7777	0.6104
		R_L	0.118	0.155	0.141	0.169
	Freundlich	K_F	0.442	0.330	0.340	0.850
		$1/n$	0.5316	1.828	1.882	3.565
		R^2	0.8913	0.9557	0.9374	0.4511
	Redlich-Peterson	K_{RP}	18996	2040.79	1548.79	0.106
		a	61795.7	7943.11	5549.23	0.024
		g	0.375	0.390	0.418	1
		R^2	0.9547	0.9591	0.9414	0.7420
	Dubinin–Radushkevich	q_m	3.651	3.032	2.919	2.437
		β	7×10^{-6}	1×10^{-5}	1×10^{-5}	1×10^{-5}
		R^2	0.4305	0.5561	0.5230	0.4836
		E	267.261	223.607	223.607	223.607
Mono-cations	Langmuir	q_m	3.932	4.068	4.539	3.545
		K_L	1.159	0.346	0.073	0.092
		R^2	0.9980	0.9768	0.9133	0.9462
		R_L	0.008	0.026	0.111	0.089
	Freundlich	K_F	2.986	2.105	0.998	0.722
		$1/n$	0.0629	0.1467	0.3044	0.3466
		R^2	0.7971	0.8633	0.7875	0.9837
	Redlich-Peterson	K_{RP}	4.601	1.488	-319882	3181.35
		a	1.145	0.380	-254502	4504.48
		g	1	0.991	0.753	0.647
		R^2	0.7773	0.9209	0.7194	0.9736
	Dubinin–Radushkevich	q_m	3.813	3.832	3.623	2.991
		β	4×10^{-7}	2×10^{-6}	8×10^{-6}	7×10^{-6}
		R^2	0.9878	0.9154	0.9746	0.7326
		E	1118.034	500	250	267.231

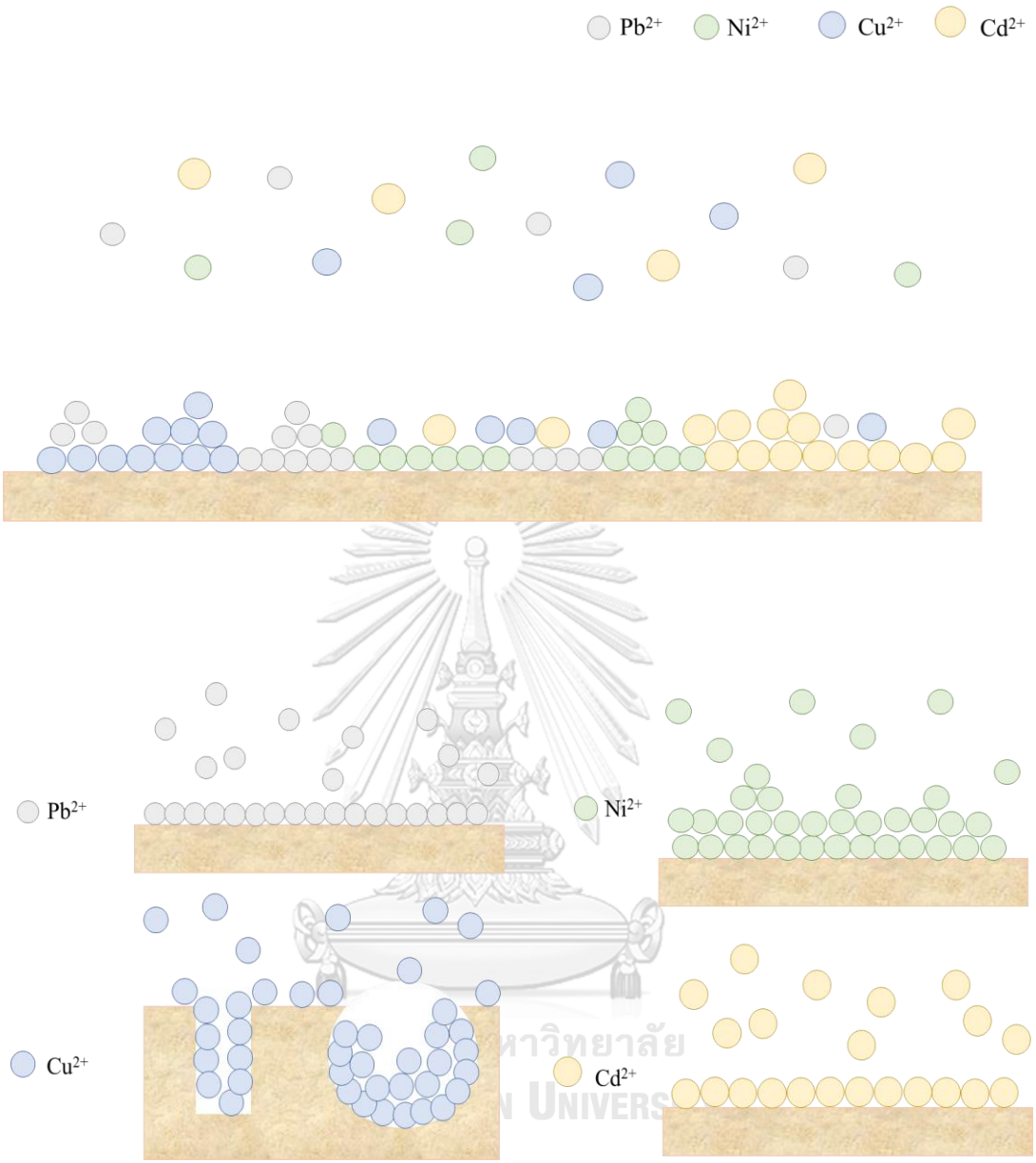

Fig. 4.78 The diagram of adsorption isotherm of metal ions with MKG fiber adsorbent in multi-cations solution (upper) and mono-cations solution (lower)

4.4.4 Kinetics study

4.4.4.1 Pseudo first order model and pseudo second order model

The kinetic parameters and the correlation coefficients calculated from the linear form for heavy metal adsorption of both solution systems are presented in Table 4.21. The kinetics of Pb^{2+}, Cd^{2+}, Cu^{2+} and Ni^{2+} by MKG composite fiber in multi- and mono-cations solution are shown in Fig. 4.79. In multi-cations solution, the linearization (R^2) showed that the pseudo second order model was fitted well with the adsorption mechanism of Cd^{2+}, Cu^{2+} and Ni^{2+}, while the pseudo first order was fitted the adsorption mechanism of Pb^{2+}. In addition, the linearization (R^2) also proved that the pseudo second order model was the best described the adsorption mechanism of Cd^{2+}, while the pseudo first order model could described the adsorption mechanism of Pb^{2+}, $Cu^{2+}$and Ni^{2+} in mono-cations solution. However, the model predicted values for the adsorption capacities were close to the experimental values only for pseudo second order model. In the pseudo first order model, the differences between model predicted and experimental values were approximately 5-20%. Therefore, the pseudo second order model is better predicator of the adsorption kinetics than pseudo first order model for Pb^{2+}, Cd^{2+}, Cu^{2+} and Ni^{2+} ions.

Table 4.21 Parameter values for batch kinetic adsorption models of MKG composite fiber

Solution system	Metal	Pseudo first order			Pseudo second order			Experimental value
		k_1 (min^{-1})	q_e (mg/g)	R^2	k_2 (g/mg min)	q_e (mg/g)	R^2	q_m(mg/g)
Multi-cations	Pb^{2+}	0.0005	3.521	0.8749	0.0003	3.935	0.7516	3.916
	Cd^{2+}	0.0011	0.821	0.7972	0.0005	1.574	0.9958	1.571
	Cu^{2+}	0.0008	0.880	0.9241	0.0045	1.469	0.9966	1.456
	Ni^{2+}	0.0003	0.403	0.5553	0.0104	0.921	0.9878	0.960
Mono-cations	Pb^{2+}	0.0005	5.167	0.9673	0.0004	6.502	0.9508	6.526
	Cd^{2+}	0.0006	3.635	0.8498	0.0006	5.241	0.9741	5.072
	Cu^{2+}	0.0004	4.141	0.9546	0.0002	4.888	0.9348	4.605
	Ni^{2+}	0.0009	2.868	0.9589	0.0006	3.256	0.9591	3.029

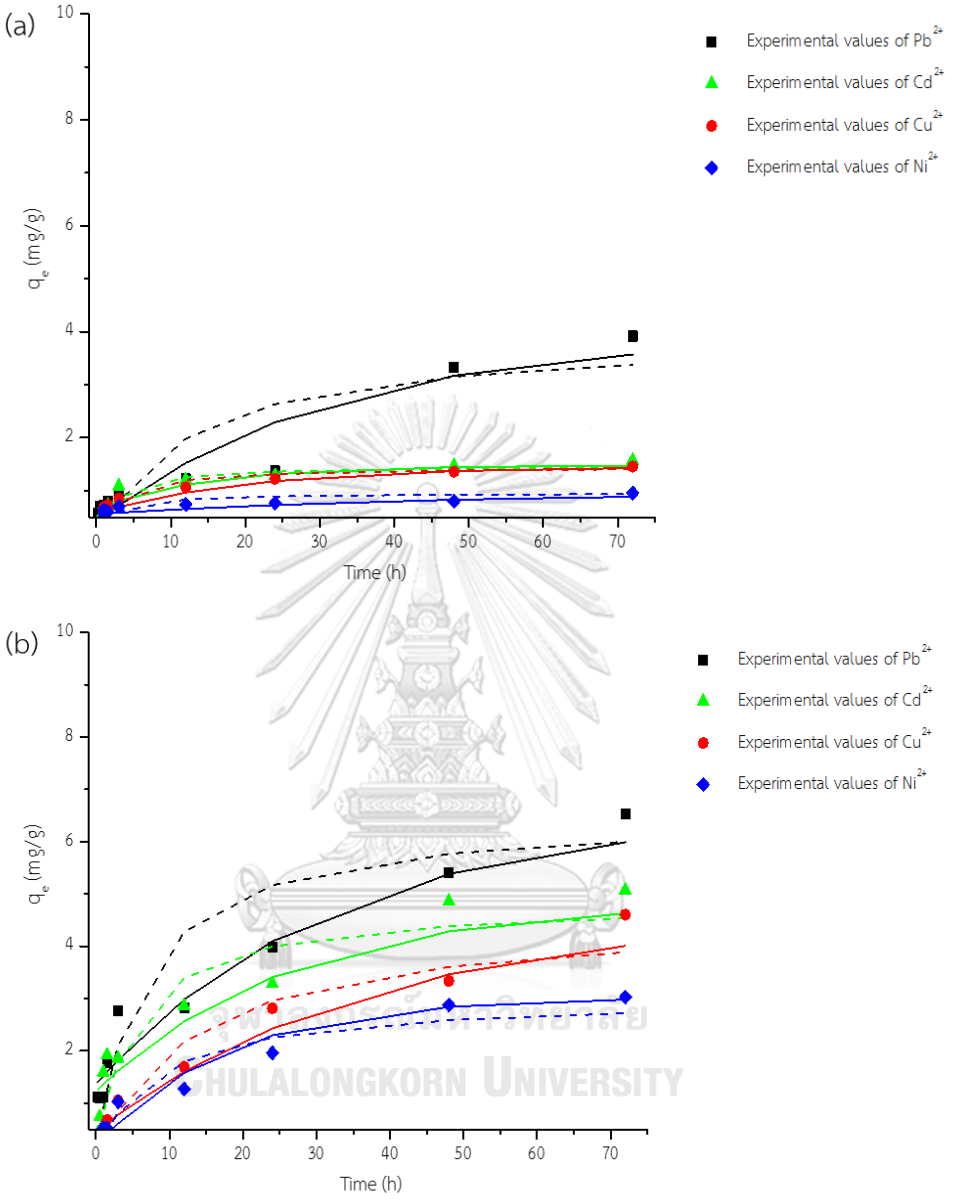

Fig. 4.79 Kinetics of Pb^{2+}, Cd^{2+}, Cu^{2+} and Ni^{2+} adsorption on MKG composite fiber and model's fit to the data (a) multi-cations solution (b) mono-cations solution (Pseudo first order: solid line, Pseudo second order: dash line)

4.4.4.2 Intraparticle diffusion model

From Fig. 4.80, Intraparticle diffusion plots of the adsorption by MKG composite fiber in multi-cations solution and mono-cations solution were presented. Table 4.22 summarized Intraparticle diffusion parameters for the adsorption. The intraparticle diffusion occurred only adsorption of Pb^{2+} in multi-cations solution system. For other metal ions with multi- and mono-cations solution system, only single line are observed. It was conclude that diffusion of metal ions to MKG powder in the fiber through PES scaffold was rate limiting step. It might be because of MKG powder was agglomerated in the fiber during fiber fabrication process which made adsorption rate is slower and less adsorption capacity.

Table 4.22 Intraparticle diffusion parameters for the adsorption by MKG composite fiber

Solution system	Metal	Intraparticle diffusion		
		k_p (mg/g $h^{0.5}$)	C (mg/g)	R^2
Multi-cations	Pb^{2+}	0.178	0.527	0.9867
	Cd^{2+}	0.173	0.506	0.9416
	Cu^{2+}	0.144	0.392	0.9220
	Ni^{2+}	0.066	0.425	0.8221
Mono-cations	Pb^{2+}	0.688	0.652	0.9952
	Cd^{2+}	0.565	0.620	0.9790
	Cu^{2+}	0.551	0.190	0.9941
	Ni^{2+}	0.374	0.051	0.9919

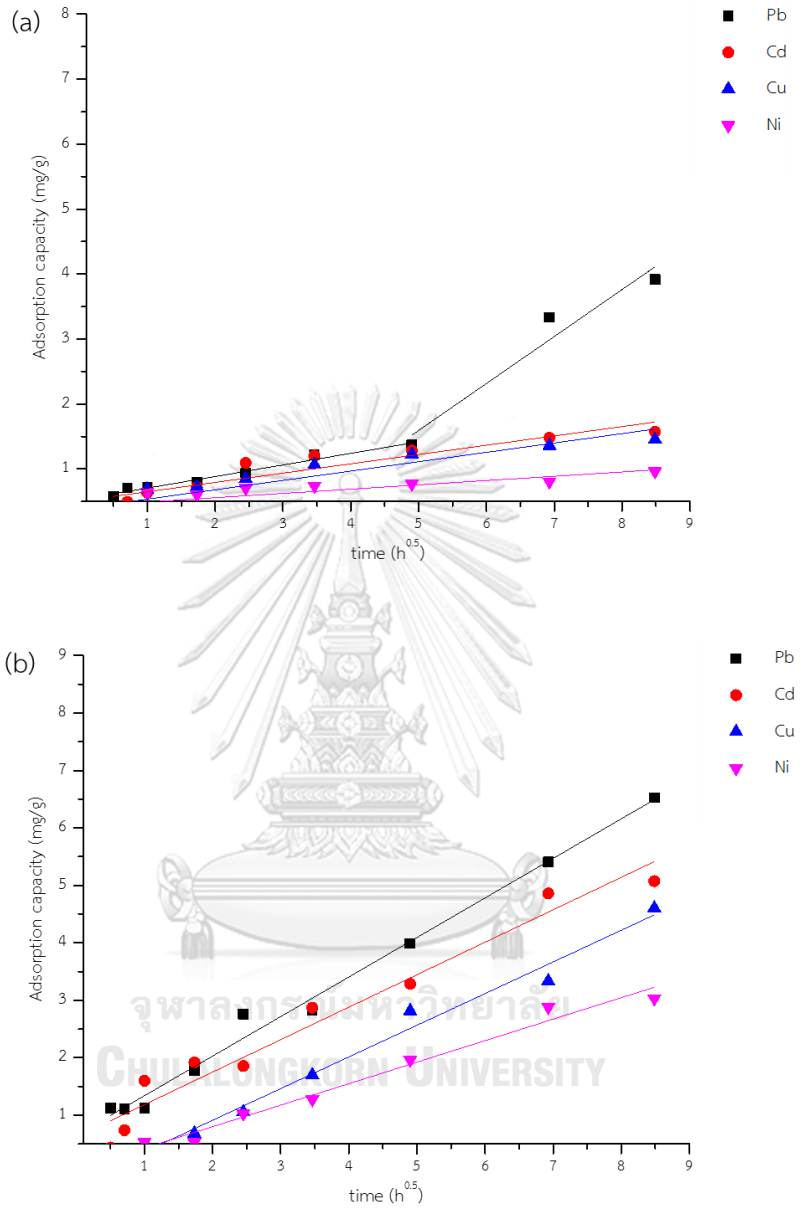

Fig. 4.80 Intraparticle diffusion plots of the adsorption by MKG composite fiber (a) multi-cations solution (b) mono-cations solution

4.5 COMPARISON OF ADSORPTION CAPACITIES FOR Pb^{2+}, Cu^{2+}, Cd^{2+} and Ni^{2+} ONTO DIFFERENT ASORBENTS

From Table 4.23 to Table 4.26, comparison between this published adsorption capacity of various powder adsorbents and highest metal ions adsorption in this work for Pb^{2+}, Cu^{2+}, Cd^{2+} and $Ni^{2+}$are summarized. The geopolymer powder and geopolymer composite fiber obtained in this study had the higher and lower adsorption capacity with the other adsorbents. In this study, the geopolymer powder adsorbed metal ions higher than geopolymer composite fiber because the metal ions were directly adsorbed with the powder. For adsorption Pb^{2+}, Cu^{2+}, Cd^{2+} and Ni^{2+}, the fly ash based geopolymer powder lower adsorbed metal ions than metakaolin based geopolymer powder because metakaolin had smaller size than fly ash therefore, in same weight metakaolin geopolymer had higher surface area than fly ash geopolymer. However, in fly ash based geopolymer composite fiber could adsorb more values than metakaolin based geopolymer composite fiber because the agglomerated of metakaolin in the fiber occurred which could effect to the adsorption capacity of the fiber. To compare with other adsorbents, the initial concentration, the amount of adsorbent and the solution volume should be focus because the adsorption capacity values depended on the conditions for adsorption study to calculate the adsorption capacity values. Considering the availability and cost of raw materials in this study, as well as the ease and the cost and the process of geopolymer preparation, it can be modified, applied and can be used geopolymer powder and geopolymer composite fiber in packed beds in the future.

Table 4.23 Lead adsorption capacity of various adsorbents

Material	q_m (mg/g)	Ref.
Coconut	4.4	[92]
Bagasse fly ash	3.8	[93]
Cashew nut shell	17.8	[94]
Chitosan	8.3	[95]
Corn chaff	6.7	[96]
Cereal chaff	12.5	[97]
Rice husk	5.7	[95]
Natural hen egg shell	1.5	[98]
Natural duck egg shell	1.6	[98]
Biomass FA-geopolymer monolith	6.3	[99]
Mordenite zeolite	151.1	[88]
Fly ash based geopolymer (powder)	118.6	[100]
Metakaolin based geopolymer (powder)	58	[101]
Fly ash based geopolymer (powder)	42.9	This work
Metakaolin based geopolymer (powder)	42.7	This work
Fly ash based geopolymer composite fiber	11.8	This work
Metakaolin based geopolymer composite fiber	4.2	This work

Table 4.24 Copper adsorption capacity of various adsorbents

Material	q_m (mg/g)	Ref.
Activated carbon	54	[102]
Modified activated carbon	12.1	[103]
Chitosan flakes	21	[104]
Anatase-type titanium	1.5	[105]
Prawn shell	16.9	[106]
Blast furnace residue	34	[107]
Lignite	6.4	[108]
Phosphate rock	10.8	[109]
Sewage sludge ash	3.8	[110]
Kaolinite	10.8	[111]
Mordenite zeolite	31.8	[88]
Fly ash based geopolymer (powder)	96.8	[87]
Metakaolin based geopolymer (powder)	45	[101]
Fly ash based geopolymer (powder)	9.5	This work
Metakaolin based geopolymer (powder)	31.6	This work
Fly ash based geopolymer composite fiber	9.6	This work
Metakaolin based geopolymer composite fiber	4	This work

Table 4.25 Cadmium adsorption capacity of various adsorbents

Material	q_m (mg/g)	Ref.
Modified sewage sludge	14.7	[112]
Magnetic chlorapatite nanoparticles	73.1	[113]
Biochar from biogas residues	76.3	[114]
Alkaline treated algae waste	41.8	[115]
Nalco Plant Sand	58.1	[116]
Waste FGD gypsum	43.1	[117]
Mesoporous calcium-silicate material	5.52	[118]
Hydrothermally modified fly ash	87.7	[119]
Sodium tetraborate-modified kaolinite clay	44.1	[120]
Zeolite-based geopolymer from coal fly ash	26.3	[121]
Mordenite zeolite	61.6	[88]
modified circulating fluidized bed fly ash	183.7	[122]
Metakaolin based geopolymer (powder)	12	[101]
Fly ash based geopolymer (powder)	12.8	This work
Metakaolin based geopolymer (powder)	29.8	This work
Fly ash based geopolymer composite fiber	10.5	This work
Metakaolin based geopolymer composite fiber	4.1	This work

Table 4.26 Nickel adsorption capacity of various adsorbents

Material	q_m (mg/g)	Ref.
Orange peel	62.8	[123]
Composite chitosan	78.1	[124]
Black carrot residue	5.7	[125]
Natural clinoptilolite	6.9	[126]
Natural bentonite	25	[127]
Montmorillonite	28.4	[128]
Modification kaolinite	8.4	[128]
Kaolin	1.67	[111]
Zeolite	1.9	[129]
Kaolinite	7.1	[130]
Mordenite zeolite	21.4	[88]
Modified ash (powder)	30.3	[131]
Metakaolin based geopolymer (powder)	42.6	[86]
Fly ash based geopolymer (powder)	14.1	This work
Metakaolin based geopolymer (powder)	29.3	This work
Fly ash based geopolymer composite fiber	8.4	This work
Metakaolin based geopolymer composite fiber	3.7	This work

CHAPTER 5

CONCLUSIONS AND RECOMMENDATION

5.1 CONCLUSIONS

The fly ash and metakaolin based geopolymer were synthesized and the fly ash and metakaolin based geopolymer composite fiber were fabricated. All of geopolymer and geopolymer composite fiber were characterized and studied the factors affect adsorption ability. Moreover, the adsorption isotherm and adsorption kinetics were demonstrated.

The fly ash and metakaolin based geopolymer composed mainly of silica and alumina. Moreover, the geopolymer powder had a semi-crystalline structure. The metakaolin based geopolymer powder had higher volume of small particle size than fly ash based geopolymer powder. For the surface area, the fly ash based geopolymer powder had lower specific surface area compared to metakaolin based geopolymer powder with specific surface area of 85.01 and 20.36 m^2/g, respectively.

After that, the fly ash and metakaolin based geopolymer powder were mixed with PES polymer and fabricated to be the composite fiber. The fly ash and metakaolin based geopolymer composite fiber had porous structure with finger-like structure of pore (outer) and sponge structure of pore (core) and the geoplymer powder was uniformly dispersed in the fiber network. The maximum specific surface area of fly ash and metakaolin based geopolymer composite fiber were 71.67 and 53.11 m^2/g, respectively.

The geopolymer powder and geopolymer composite fiber were test to study the factors affect adsorption capacity and adsorption efficiency. The effect of contact time, geopolymer dosage, solution pH, temperature and initial concentration were studied. The removal of metal ions increased with an increasing of contact time geopolymer dosage, solution pH and temperature and with a decreasing of metal ions in solution. Moreover, the adsorption of metal ions from multi-metal cations solution

could be reduced adsorption capacity and adsorption efficiency in each cation owing to the competitive mechanism of each metal ions on active site. The geopolymer powder had higher adsorption efficiency than geopolymer composite fiber in the same contact time. From all parameter, the geopolymer powder adsorbed metal ions in order Pb^{2+}>Cu^{2+} >Cd^{2+} >Ni^{2+} and the geopolymer fiber adsorbed metal ions in order Pb^{2+}>Cd^{2+} >Cu^{2+} >Ni^{2+}.

The four model as Langmuir, Freundlich, Redlich-Peterson and Dubinin-Radushkevish isotherm models were adopted to fit for the experimental data. The Pb^{2+}, Cd^{2+}, Cu^{2+}, Ni^{2+} in mono- and multi-cations solution were fitted well with Langmuir, Freundlich and Redlich-Peterson model. However, only Cu^{2+} ions in mono-cation solution adsorbed by MKG composite fiber was fitted with Dubunin-Radushkevish model.

For kinetics study, the pseudo second order model was well explained the metal ions kinetics. In addition, the intrapraticle diffusion occurred in MKG powder adsorb.

The geopolymer powder and geopolymer composite fiber had good adsorption ability. It could be applied as a low cost and good alternative for wastewater treatment in the future.

5.2 RECOMMENDATION

- For adsorption of composite fiber, more amount of fiber and contact time should be consider and study.

- Desorption and leaching test should be study for the stability of geopolymer after adsorbed and different condition of water.

- More challenging for setting geopolymer powder and geopolymer composite fiber up on column bed pack test to study the continuous adsorption ability of geopolymer.

REFERENCES

[1] Komnitsas, K. and Zaharaki, D. 2007. Geopolymerisation: A review and prospects for the minerals industry. Minerals Engineering 20: 1261-1277.

[2] Davidovits, J. (2008). GEOPOLYMER Chemistry&Applications. France: Institut Géopolymère 16 rue Galilée F-02100 Saint-Quentin France.

[3] Davidovits, J., *Mineral polymers and methods of making them*, 1982, Google Patents.

[4] Davidovits, J., *Synthetic mineral polymer compound of the silicoaluminates family and preparation process*, 1984, Google Patents.

[5] Liew, Y.-M., Heah, C.-Y., Mohd Mustafa, A.B., and Kamarudin, H. 2016. Structure and properties of clay-based geopolymer cements: A review. Progress in Materials Science 83: 595-629.

[6] Rovnaník, P. 2010. Effect of curing temperature on the development of hard structure of metakaolin-based geopolymer. Construction and Building Materials 24: 1176-1183.

[7] Abdulkareem, O.A., Mustafa Al Bakri, A.M., Kamarudin, H., Khairul Nizar, I., and Saif, A.e.A. 2014. Effects of elevated temperatures on the thermal behavior and mechanical performance of fly ash geopolymer paste, mortar and lightweight concrete. Construction and Building Materials 50: 377-387.

[8] Medri, V., et al. 2010. Role of the morphology and the dehydroxylation of metakaolins on geopolymerization. Applied Clay Science 50: 538-545.

[9] Cui, X.-m., Liu, L.-p., Zheng, G.-j., Wang, R.-p., and Lu, J.-p. 2010. Characterization of chemosynthetic Al_2O_3–$2SiO_2$ geopolymers. Journal of Non-Crystalline Solids 356: 72-76.

[10] Barbosa, V. 2000. Synthesis and characterisation of materials based on inorganic polymers of alumina and silica: sodium polysialate polymers. International Journal of Inorganic Materials 2: 309-317.

[11] Tchadjié, L.N., et al. 2016. Potential of using granite waste as raw material for geopolymer synthesis. Ceramics International 42: 3046-3055.

[12] Li, C., Zhang, T., and Wang, L. 2014. Mechanical properties and microstructure of alkali activated Pisha sandstone geopolymer composites. Construction and Building Materials 68: 233-239.

[13] Wang, S.-D. 2000. The role of sodium during the hydration of alkali-activated slag. Advances in Cement Research 12: 65-69.

[14] Zhuang, X.Y., et al. 2016. Fly ash-based geopolymer: clean production, properties and applications. Journal of Cleaner Production 125: 253-267.

[15] Soutsos, M., Boyle, A.P., Vinai, R., Hadjierakleous, A., and Barnett, S.J. 2016. Factors influencing the compressive strength of fly ash based geopolymers. Construction and Building Materials 110: 355-368.

[16] Deb, P.S., Sarker, P.K., and Barbhuiya, S. 2015. Effects of nano-silica on the strength development of geopolymer cured at room temperature. Construction and Building Materials 101, Part 1: 675-683.

[17] Rattanasak, U., Chindaprasirt, P., and Suwanvitaya, P. 2010. Development of high volume rice husk ash alumino silicate composites. International Journal of Minerals, Metallurgy, and Materials 17: 654-659.

[18] Le-ping, L., Xue-min, C., Shu-heng, Q., Jun-li, Y., and Lin, Z. 2010. Preparation of phosphoric acid-based porous geopolymers. Applied Clay Science 50: 600-603.

[19] Douiri, H., Louati, S., Baklouti, S., Arous, M., and Fakhfakh, Z. 2014. Structural, thermal and dielectric properties of phosphoric acid-based geopolymers with different amounts of H_3PO_4. Materials Letters 116: 9-12.

[20] Davidovits, J. 1994. Properties of geopolymer cements. First international conference on alkaline cements and concretes 1: 131-149.

[21] Hanjitsuwan, S., et al. 2014. Effects of NaOH concentrations on physical and electrical properties of high calcium fly ash geopolymer paste. Cement and Concrete Composites 45: 9-14.

[22] Muñiz-Villarreal, M.S., et al. 2011. The effect of temperature on the geopolymerization process of a metakaolin-based geopolymer. Materials Letters 65: 995-998.

[23] Yao, X., Zhang, Z., Zhu, H., and Chen, Y. 2009. Geopolymerization process of alkali–metakaolinite characterized by isothermal calorimetry. Thermochimica Acta 493: 49-54.

[24] Blackstock, J.M., Neill, J., and Mcintosh, J.A., *Geopolymeric structural building units and methods of manufacture thereof*, 2012, Google Patents.

[25] Comrie, D.C. and Kriven, W.M. Composite Cold Ceramic Geopolymer in a Refractory Application. (ed.), Advances in Ceramic Matrix Composites IX, 211-225. John Wiley & Sons, Inc., 2006.

[26] Somna, K., Jaturapitakkul, C., Kajitvichyanukul, P., and Chindaprasirt, P. 2011. NaOH-activated ground fly ash geopolymer cured at ambient temperature. Fuel 90: 2118-2124.

[27] Lecomte, I., et al. 2006. (Micro)-structural comparison between geopolymers, alkali-activated slag cement and Portland cement. Journal of the European Ceramic Society 26: 3789-3797.

[28] Seco, A., et al. (2012). Types of Waste for the Production of Pozzolanic Materials-A Review. INTECH Open Access Publisher.

[29] Karakoç, M.B., et al. 2014. Mechanical properties and setting time of ferrochrome slag based geopolymer paste and mortar. Construction and Building Materials 72: 283-292.

[30] He, J., Jie, Y., Zhang, J., Yu, Y., and Zhang, G. 2013. Synthesis and characterization of red mud and rice husk ash-based geopolymer composites. Cement and Concrete Composites 37: 108-118.

[31] Tchakouté, H.K., Rüscher, C.H., Kong, S., Kamseu, E., and Leonelli, C. 2016. Geopolymer binders from metakaolin using sodium waterglass from waste glass and rice husk ash as alternative activators: A comparative study. Construction and Building Materials 114: 276-289.

[32] Ryu, G.S., Lee, Y.B., Koh, K.T., and Chung, Y.S. 2013. The mechanical properties of fly ash-based geopolymer concrete with alkaline activators. Construction and Building Materials 47: 409-418.

[33] Alshaaer, M. 2013. Two-phase geopolymerization of kaolinite-based geopolymers. Applied Clay Science 86: 162-168.

[34] Kumar, S. and Kumar, R. 2011. Mechanical activation of fly ash: Effect on reaction, structure and properties of resulting geopolymer. Ceramics International 37: 533-541.

[35] Abdullah, M.M.A.B., et al. 2012. Fly Ash Porous Material using Geopolymerization Process for High Temperature Exposure. International Journal of Molecular Sciences 13: 4388.

[36] Nazari, A., Bagheri, A., and Riahi, S. 2011. Properties of geopolymer with seeded fly ash and rice husk bark ash. Materials Science and Engineering: A 528: 7395-7401.

[37] Palomo, A., Grutzeck, M.W., and Blanco, M.T. 1999. Alkali-activated fly ashes: A cement for the future. Cement and Concrete Research 29: 1323-1329.

[38] Fernández-Jiménez, A., Palomo, J.G., and Puertas, F. 1999. Alkali-activated slag mortars: Mechanical strength behaviour. Cement and Concrete Research 29: 1313-1321.

[39] Swanepoel, J.C. and Strydom, C.A. 2002. Utilisation of fly ash in a geopolymeric material. Applied Geochemistry 17: 1143-1148.

[40] Xu, H. and Van Deventer, J.S.J. 2002. Geopolymerisation of multiple minerals. Minerals Engineering 15: 1131-1139.

[41] van Jaarsveld, J.G.S. and van Deventer, J.S.J. 1999. Effect of the Alkali Metal Activator on the Properties of Fly Ash-Based Geopolymers. Industrial & Engineering Chemistry Research 38: 3932-3941.

[42] Chindaprasirt, P., Jaturapitakkul, C., Chalee, W., and Rattanasak, U. 2009. Comparative study on the characteristics of fly ash and bottom ash geopolymers. Waste Management 29: 539-543.

[43] Görhan, G. and Kürklü, G. 2014. The influence of the NaOH solution on the properties of the fly ash-based geopolymer mortar cured at different temperatures. Composites Part B: Engineering 58: 371-377.

[44] Rattanasak, U. and Chindaprasirt, P. 2009. Influence of NaOH solution on the synthesis of fly ash geopolymer. Minerals Engineering 22: 1073-1078.

[45] Zuhua, Z., Xiao, Y., Huajun, Z., and Yue, C. 2009. Role of water in the synthesis of calcined kaolin-based geopolymer. Applied Clay Science 43: 218-223.

[46] Lee, W.K.W. and van Deventer, J.S.J. 2002. The effects of inorganic salt contamination on the strength and durability of geopolymers. Colloids and Surfaces A: Physicochemical and Engineering Aspects 211: 115-126.

[47] Djwantoro Hardjito, S.E.W.D.M.J.S. and Rangan, B.V. On the Development of Fly Ash-Based Geopolymer Concrete. Materials Journal 101:

[48] Chindaprasirt, P., Chareerat, T., and Sirivivatnanon, V. 2007. Workability and strength of coarse high calcium fly ash geopolymer. Cement and Concrete Composites 29: 224-229.

[49] Bakharev, T. 2005. Geopolymeric materials prepared using Class F fly ash and elevated temperature curing. Cement and Concrete Research 35: 1224-1232.

[50] Pavithra, P., et al. 2016. A mix design procedure for geopolymer concrete with fly ash. Journal of Cleaner Production 133: 117-125.

[51] Park, Y., Abolmaali, A., Kim, Y.H., and Ghahremannejad, M. 2016. Compressive strength of fly ash-based geopolymer concrete with crumb rubber partially replacing sand. Construction and Building Materials 118: 43-51.

[52] Al-Zboon, K., Al-Harahsheh, M.S., and Hani, F.B. 2011. Fly ash-based geopolymer for Pb removal from aqueous solution. Journal of Hazardous Materials 188: 414-421.

[53] Wang, S., Li, L., and Zhu, Z.H. 2007. Solid-state conversion of fly ash to effective adsorbents for Cu removal from wastewater. Journal of Hazardous Materials 139: 254-259.

[54] Li, L., Wang, S., and Zhu, Z. 2006. Geopolymeric adsorbents from fly ash for dye removal from aqueous solution. Journal of Colloid and Interface Science 300: 52-59.

[55] Van Jaarsveld, J.G.S., Van Deventer, J.S.J., and Lorenzen, L. 1997. The potential use of geopolymeric materials to immobilise toxic metals: Part I. Theory and applications. Minerals Engineering 10: 659-669.

[56] Lee, S., et al. 2016. Impact of activator type on the immobilisation of lead in fly ash-based geopolymer. Journal of Hazardous Materials 305: 59-66.

[57] Roviello, G., Ricciotti, L., Ferone, C., Colangelo, F., and Tarallo, O. 2015. Fire resistant melamine based organic-geopolymer hybrid composites. Cement and Concrete Composites 59: 89-99.

[58] Sakkas, K., Panias, D., Nomikos, P.P., and Sofianos, A.I. 2014. Potassium based geopolymer for passive fire protection of concrete tunnels linings. Tunnelling and Underground Space Technology 43: 148-156.

[59] Pouhet, R. and Cyr, M. 2016. Formulation and performance of flash metakaolin geopolymer concretes. Construction and Building Materials 120: 150-160.

[60] Nath, S.K., Maitra, S., Mukherjee, S., and Kumar, S. 2016. Microstructural and morphological evolution of fly ash based geopolymers. Construction and Building Materials 111: 758-765.

[61] Huang, X., et al. 2016. Immobilization of chromite ore processing residue with alkali-activated blast furnace slag-based geopolymer. Ceramics International 42: 9538-9549.

[62] Novais, R.M., Ascensão, G., Seabra, M.P., and Labrincha, J.A. 2016. Waste glass from end-of-life fluorescent lamps as raw material in geopolymers. Waste Management 52: 245-255.

[63] Sun, Z., et al. 2013. Synthesis and thermal behavior of geopolymer-type material from waste ceramic. Construction and Building Materials 49: 281-287.

[64] Ahmari, S. and Zhang, L. 2013. Durability and leaching behavior of mine tailings-based geopolymer bricks. Construction and Building Materials 44: 743-750.

[65] Duan, P., Yan, C., Zhou, W., and Ren, D. Development of fly ash and iron ore tailing based porous geopolymer for removal of Cu(II) from wastewater. Ceramics International

[66] Nazari, A. and Sanjayan, J.G. 2015. Synthesis of geopolymer from industrial wastes. Journal of Cleaner Production 99: 297-304.

[67] Abdulkareem, O.A., Mustafa Al Bakri, A.M., Kamarudin, H., Khairul Nizar, I., and Saif, A.e.A. 2014. Effects of elevated temperatures on the thermal behavior and mechanical performance of fly ash geopolymer paste, mortar and lightweight concrete. Construction and Building Materials 50: 377-387.

[68] Tiwari, M.K., Bajpai, S., and Dewangan, U.K. 2016. Fly ash utilization: A brief review in Indian context. International Research Journal of Engineering and Technology 3: 949-956.

[69] Ahmaruzzaman, M. 2010. A review on the utilization of fly ash. Progress in Energy and Combustion Science 36: 327-363.

[70] Vidat Choudhary, S.L. 2017. Fly Ash Utilization: A Review. International Journal of Civil Engineering and Technology 8: 301-312.

[71] Brigden, K., Santillo, D., and Stringer, R. 2002. Hazardous emissions from Thai coal-fired power plants. Toxic and potentially toxic elements in fly ashes collected from the Mae Moh and Thai Petrochemical industry coal-fired power plants in Thailand

[72] American society for testing and Materials, *Standard Specification for Coal Fly Ash and Raw or Calcined Natural Pozzolan for Use in Concrete*, 2002. p. 310-313.

[73] ปริญญา จินดาประเสริฐ และ อินทรชัย หอวิจิตร. (2528). ปูนซีเมนต์ปอร์ตแลนด์ผสมขี้เถ้าลอยแม่เมาะ. ขอนแก่น: สำนักงานเทคโนโลยีเพื่อพัฒนาชนบท คณะวิศวกรรมศาสตร์ มหาวิทยาลัยขอนแก่น.

[74] มูลนิธิส่งเสริมวิทยาศาสตร์และเทคโนโลยีในพระบรมราชูถัมภ์. การพัฒนาการใช้ประโยชน์เถ้าลอยลิกไนต์ในไทย. (ed.), หนังสือรางวัลนักเทคโนโลยีดีเด่นประจำปี พ.ศ.2545, 10-16. 2545.

[75] วราภรณ์ คุณาวนากิจ, คุณสมบัติพื้นฐานของเถ้าลอยลิกไนต์, 2536. p. 2-15.

[76] Rashad, A.M. 2013. Metakaolin as cementitious material: History, scours, production and composition –A comprehensive overview. Construction and Building Materials 41: 303-318.

[77] Siddique, R. and Iqbal Khan, M. Metakaolin. (ed.), Supplementary Cementing Materials, 175-230. Berlin, Heidelberg: Springer Berlin Heidelberg, 2011.

[78] Saikrasoon, A. 2014. SYNTHESIS OF POROUS GEOPOLYMER USING INORGANIC FOAMING AGENTS. วิทยานิพนธ์Degree of Master. Department of Materials Science Chulalongkorn University.

[79] Ladewig, B. and Al-Shaeli, M.N.Z. Fundamentals of Membrane Processes. (ed.), Fundamentals of Membrane Bioreactors: Materials, Systems and Membrane Fouling, 13-37. Singapore: Springer Singapore, 2017.

[80] Omidvar, M., Mousavi, S.M., Soltanieh, M., and Safekordi, A.A. 2014. Preparation and characterization of poly (ethersulfone) nanofiltration membranes for amoxicillin removal from contaminated water. Journal of Environmental Health Science and Engineering 12: 18.

[81] Madaeni, S.S., Farhadian, A., and Vatanpour, V. 2012. Effects of phase inversion and composition of casting solution on morphology and gas permeance of polyethersulfone/polyimide blend membranes. Advances in Polymer Technology 31: 298-309.

[82] Wang, F., Lu, X., and Li, X.-y. 2016. Selective removals of heavy metals (Pb2+, Cu2+, and Cd2+) from wastewater by gelation with alginate for effective metal recovery. Journal of Hazardous Materials 308: 75-83.

[83] Wan Ngah, W.S. and Hanafiah, M.A.K.M. 2008. Removal of heavy metal ions from wastewater by chemically modified plant wastes as adsorbents: A review. Bioresource Technology 99: 3935-3948.

[84] Papageorgiou, S.K., Katsaros, F.K., Kouvelos, E.P., and Kanellopoulos, N.K. 2009. Prediction of binary adsorption isotherms of Cu^{2+}, Cd^{2+} and Pb^{2+} on calcium alginate beads from single adsorption data. Journal of Hazardous Materials 162: 1347-1354.

[85] Ayawei, N., Ebelegi, A.N., and Wankasi, D. 2017. Modelling and Interpretation of Adsorption Isotherms. Journal of Chemistry 2017:

[86] Kara, İ., Yilmazer, D., and Akar, S.T. 2017. Metakaolin based geopolymer as an effective adsorbent for adsorption of zinc(II) and nickel(II) ions from aqueous solutions. Applied Clay Science 139: 54-63.

[87] Al-Harahsheh, M.S., Al Zboon, K., Al-Makhadmeh, L., Hararah, M., and Mahasneh, M. 2015. Fly ash based geopolymer for heavy metal removal: A case study on copper removal. Journal of Environmental Chemical Engineering 3: 1669-1677.

[88] Nakamoto, K., Ohshiro, M., and Kobayashi, T. 2017. Mordenite zeolite—Polyethersulfone composite fibers developed for decontamination of heavy metal ions. Journal of Environmental Chemical Engineering 5: 513-525.

[89] Onutai, S., Jiemsirilers, S., Thavorniti, P., and Kobayashi, T. 2015. Aluminium hydroxide waste based geopolymer composed of fly ash for sustainable cement materials. Construction and Building Materials 101, Part 1: 298-308.

[90] Visa, M. 2016. Synthesis and characterization of new zeolite materials obtained from fly ash for heavy metals removal in advanced wastewater treatment. Powder Technology 294: 338-347.

[91] Visa, M., Bogatu, C., and Duta, A. 2010. Simultaneous adsorption of dyes and heavy metals from multicomponent solutions using fly ash. Applied Surface Science 256: 5486-5491.

[92] Gueu, S., Yao, B., Adouby, K., and Ado, G. 2007. Kinetics and thermodynamics study of lead adsorption on to activated carbons from coconut and seed hull of the palm tree. International Journal of Environmental Science & Technology 4: 11-17.

[93] Gupta, V., Mohan, D., and Sharma, S. (1998). Removal of Lead from Wastewater Using Bagasse Fly Ash—A Sugar Industry Waste Material.

[94] Senthil Kumar, P. 2013. Adsorption of lead(II) ions from simulated wastewater using natural waste: A kinetic, thermodynamic and equilibrium study. Environmental Progress & Sustainable Energy 33: 55-64.

[95] Daud, Z.M.M., Latif, A.A., Hadi, N.N., and Sulaiman, S.N. 2006. Comparative studies of Oryza sativa L. husk and chitosan as lead adsorbent. Journal of Chemical Technology & Biotechnology 81: 1324-1327.

[96] Han, R., et al. 2006. Biosorption of copper(II) and lead(II) from aqueous solution by chaff in a fixed-bed column. Journal of Hazardous Materials 133: 262-268.

[97] Han, R., Zhang, J., Zou, W., Shi, J., and Liu, H. 2005. Equilibrium biosorption isotherm for lead ion on chaff. Journal of Hazardous Materials 125: 266-271.

[98] Gupta, V.K., Mohan, D., and Sharma, S. 1998. Removal of Lead from Wastewater Using Bagasse Fly Ash—A Sugar Industry Waste Material. Separation Science and Technology 33: 1331-1343.

[99] Novais, R.M., Buruberri, L.H., Seabra, M.P., and Labrincha, J.A. 2016. Novel porous fly-ash containing geopolymer monoliths for lead adsorption from wastewaters. Journal of Hazardous Materials 318: 631-640.

[100] Liu, Y., et al. 2016. A comparative study on fly ash, geopolymer and faujasite block for Pb removal from aqueous solution. Fuel 185: 181-189.

[101] López, F.J., Sugita, S., Tagaya, M., and Kobayashi, T. 2014. Metakaolin-based geopolymers for targeted adsorbents to heavy metal ion separation. Journal of Materials Science and Chemical Engineering 2: 16.

[102] Patnukao, P., Kongsuwan, A., and Pavasant, P. 2008. Batch studies of adsorption of copper and lead on activated carbon from Eucalyptus camaldulensis Dehn. bark. Journal of Environmental Sciences 20: 1028-1034.

[103] Monser, L. and Adhoum, N. 2002. Modified activated carbon for the removal of copper, zinc, chromium and cyanide from wastewater. Separation and Purification Technology 26: 137-146.

[104] BASSI, R., PRASHER, S.O., and Simpson, B. 2000. Removal of selected metal ions from aqueous solutions using chitosan flakes. Separation Science and Technology 35: 547-560.

[105] Kim, M.-S., Hong, K.-M., and Chung, J.G. 2003. Removal of Cu(II) from aqueous solutions by adsorption process with anatase-type titanium dioxide. Water Research 37: 3524-3529.

[106] Chu, K.H. 2002. Removal of copper from aqueous solution by chitosan in prawn shell: adsorption equilibrium and kinetics. Journal of Hazardous Materials 90: 77-95.

[107] Dimitrova, S.V. 1996. Metal sorption on blast-furnace slag. Water Research 30: 228-232.

[108] J., A.S. and A., B.P. 1995. Isotherm analyses for single component and multi-component metal sorption onto lignite. Journal of Chemical Technology & Biotechnology 62: 17-24.

[109] Sarioglu, M., Atay, Ü.A., and Cebeci, Y. 2005. Removal of copper from aqueous solutions by phosphate rock. Desalination 181: 303-311.

[110] Pan, S.-C., Lin, C.-C., and Tseng, D.-H. 2003. Reusing sewage sludge ash as adsorbent for copper removal from wastewater. Resources, Conservation and Recycling 39: 79-90.

[111] Yavuz, Ö., Altunkaynak, Y., and Güzel, F. 2003. Removal of copper, nickel, cobalt and manganese from aqueous solution by kaolinite. Water research 37: 948-952.

[112] Phuengprasop, T., Sittiwong, J., and Unob, F. 2011. Removal of heavy metal ions by iron oxide coated sewage sludge. Journal of Hazardous Materials 186: 502-507.

[113] Keochaiyom, B., et al. 2017. Synthesis and application of magnetic chlorapatite nanoparticles for zinc (II), cadmium (II) and lead (II) removal from water solutions. Journal of Colloid and Interface Science 505: 824-835.

[114] Bogusz, A., Nowak, K., Stefaniuk, M., Dobrowolski, R., and Oleszczuk, P. 2017. Synthesis of biochar from residues after biogas production with respect to cadmium and nickel removal from wastewater. Journal of Environmental Management 201: 268-276.

[115] Bulgariu, D. and Bulgariu, L. 2016. Potential use of alkaline treated algae waste biomass as sustainable biosorbent for clean recovery of cadmium(II) from aqueous media: Batch and column studies. Journal of Cleaner Production 112: 4525-4533.

[116] Mohapatra, M., Khatun, S., and Anand, S. 2009. Adsorption behaviour of Pb(II), Cd(II) and Zn(II) on NALCO plant sand. Indian Journal of Chemical Technology 16: 291-300.

[117] Yan, Y., et al. 2014. Conversion of waste FGD gypsum into hydroxyapatite for removal of Pb^{2+} and Cd^{2+} from wastewater. Journal of Colloid and Interface Science 429: 68-76.

[118] Qi, G., et al. 2016. Coal fly ash-derived mesoporous calcium-silicate material (MCSM) for the efficient removal of Cd(II), Cr(III), Ni(II) and Pb(II) from acidic solutions. P. Inviron. Sci. 31: 567-576.

[119] Visa, M. and Chelaru, A.M. 2014. Hydrothermally modified fly ash for heavy metals and dyes removal in advanced wastewater treatment. Applied Surface Science 303: 14-22.

[120] Unuabonah, E.I., Adebowale, K.O., Olu-Owolabi, B.I., Yang, L.Z., and Kong, L.X. 2008. Adsorption of Pb (II) and Cd (II) from aqueous solutions onto sodium tetraborate-modified Kaolinite clay: Equilibrium and thermodynamic studies. Hydrometallurgy 93: 1-9.

[121] Javadian, H., Ghorbani, F., Tayebi, H.A., and Asl, S.H. 2015. Study of the adsorption of Cd (II) from aqueous solution using zeolite-based geopolymer, synthesized from coal fly ash; kinetic, isotherm and thermodynamic studies. Arabian Journal of Chemistry 8: 837-849.

[122] Qiu, R., Cheng, F., and Huang, H. 2018. Removal of Cd^{2+} from aqueous solution using hydrothermally modified circulating fluidized bed fly ash resulting from coal gangue power plant. Journal of Cleaner Production 172: 1918-1927.

[123] Gönen, F. and Serin, D.S. 2012. Adsorption study on orange peel: removal of Ni (II) ions from aqueous solution. African Journal of Biotechnology 11: 1250-1258.

[124] Boddu, V.M., Abburi, K., Randolph, A.J., and Smith, E.D. 2008. Removal of Copper (II) and Nickel (II) Ions from Aqueous Solutions by a Composite Chitosan Biosorbent. Separation Science and Technology 43: 1365-1381.

[125] Güzel, F., Yakut, H., and Topal, G. 2008. Determination of kinetic and equilibrium parameters of the batch adsorption of Mn(II), Co(II), Ni(II) and Cu(II) from aqueous solution by black carrot (Daucus carota L.) residues. Journal of Hazardous Materials 153: 1275-1287.

[126] Semra, Ç. and Nuri, E.O. 2009. Ni^{2+} removal from aqueous solutions using conditioned clinoptilolites: Kinetic and isotherm studies. Environmental Progress & Sustainable Energy 28: 162-172.

[127] Alandis, N.M., Aldayel, O.A., Mekhemer, W.K., Hefne, J.A., and Jokhab, H.A. 2010. Thermodynamic and Kinetic Studies for the Adsorption of Fe(III) and Ni(II) Ions

From Aqueous Solution Using Natural Bentonite. Journal of Dispersion Science and Technology 31: 1526-1534.

[128] Bhattacharyya, K.G. and Sen Gupta, S. 2009. Calcined tetrabutylammonium kaolinite and montmorillonite and adsorption of Fe(II), Co(II) and Ni(II) from solution. Applied Clay Science 46: 216-221.

[129] Álvarez-Ayuso, E., García-Sánchez, A., and Querol, X. 2003. Purification of metal electroplating waste waters using zeolites. Water Research 37: 4855-4862.

[130] Bhattacharyya, K.G. and Gupta, S.S. 2008. Influence of acid activation on adsorption of Ni(II) and Cu(II) on kaolinite and montmorillonite: Kinetic and thermodynamic study. Chemical Engineering Journal 136: 1-13.

[131] Harja, M., Buema, G., Sutiman, D.M., and Cretescu, I. 2013. Removal of heavy metal ions from aqueous solutions using low-cost sorbents obtained from ash. Chemical Papers 67: 497-508.

APPENDIX

APPENDIX A

Table A-1 2θ, intensity and hkl values of quartz from 2003 JCPDS-International Center for Diffraction Data number: JCPDS 01-087-2096

Pattern : 01-087-2096 ***Radiation =*** 1.540598 ***Quality :*** Calculated

α-SiO_2

Silicon Oxide
Quartz low

Lattice : Hexagonal
S.G. : P3221 (154)

a = 4.91270
c = 5.40450

Z = 3

Mol. weight = 60.08
Volume [CD] = 112.96
Dx = 2.650
I/Icor = 2.88

ICSD collection code: 083849
ICSD space group comment: ICSD SG: P3221S IT is: 154 SG short form: P3221
Remarks from ICSD/CSD: REM RVP.
Temperature factor: ITF
Additional pattern: See PDF 78-2315.
Data collection flag: Ambient.

2th	i	h	k	l
20.862	216	1	0	0
26.644	999	0	1	1
36.552	60	1	1	0
39.473	59	1	0	2
40.298	26	1	1	1
42.459	43	2	0	0
45.803	24	2	0	1
50.149	96	1	1	2
50.629	3	0	0	3
54.884	26	0	2	2
55.335	11	0	1	3
57.243	2	2	1	0
59.971	58	1	2	1
64.046	10	1	1	3
65.799	3	3	0	0
67.756	32	1	2	2
68.155	41	2	0	3
68.327	42	0	3	1
73.479	11	1	0	4
75.674	14	3	0	2
77.686	7	2	2	0
79.898	14	2	1	3
80.059	8	2	2	1
81.185	12	1	1	4
81.506	14	3	1	0
83.854	8	1	3	1
84.969	1	2	0	4
87.091	1	2	2	2
87.462	1	3	0	3

Table A-2 2θ, intensity and hkl values of magnetite from 2003 JCPDS-International Center for Diffraction Data number: JCPDS 01-087-0245

Pattern : 01-087-0245 ***Radiation =*** 1.540598 ***Quality :*** Calculated

$Fe_{2.93}O_4$

Iron Oxide
Magnetite, syn

Lattice : Face-centered cubic
S.G. : Fd-3m (227)

Mol. weight = 227.63
Volume [CD] = 591.22

a = 8.39300

Z = 8

Dx = 5.115

I/Icor = 4.97

ICSD collection code: 050272
Temperature factor: ATF
Additional pattern: See PDF 86-1343, PDF 87-0246, PDF 86-1362 and PDF 86-1361.
Data collection flag: Ambient.

2th	*i*	*h*	*k*	*l*
18.294	96	1	1	1
30.091	299	2	2	0
35.444	999	3	1	1
37.076	72	2	2	2
43.076	206	4	0	0
47.163	5	3	3	1
53.439	87	4	2	2
56.966	278	5	1	1
62.554	367	4	4	0
65.772	7	5	3	1
70.966	28	6	2	0
74.003	68	5	3	3
75.004	27	6	2	2
78.967	22	4	4	4
81.904	4	7	1	1
86.756	29	6	4	2
89.653	99	7	3	1

Table A-3 2θ, intensity and hkl values of mullite from 2003 JCPDS-International Center for Diffraction Data number: JCPDS 01-082-0037

Pattern : 01-082-0037 **Radiation =** 1.540598 **Quality :** Calculated

$Al_2(Al_{2.5}Si_{1.5})O_{9.75}$

Aluminum Silicon Oxide
Mullite, syn

Lattice : Orthorhombic
S.G. : Pbam (55)

a = 7.54336
b = 7.69176
c = 2.88402
a/b = 0.98071
c/b = 0.37495

Z = 1

Mol. weight = 319.54
Volume [CD] = 167.34
Dx = 3.171
Dm = 3.000
I/Icor = 0.88

ICSD collection code: 074008
Remarks from ICSD/CSD: REM RVP.
Test from ICSD: At least one TF implausible.
Temperature factor: ITF
General comments: Hot pressed.
Additional pattern: See PDF 15-776.
Remarks from ICSD/CSD: R(Bragg)=0.077.
Test from ICSD: Calc. density unusual but tolerable.
Data collection flag: Ambient.

Balzar, D., Ledbetter, H., Am. Mineral., volume 78, page 1192 (1993)
Calculated from ICSD using POWD-12++

Radiation : CuKa1
Lambda : 1.54060
SS/FOM : F30=1000(0.0001,32)

Filter : Not specified
d-sp : Calculated spacings

2th	i	h	k	l	2th	i	h	k	l
16.446	534	1	1	0	89.119	44	4	2	2
23.108	1	0	2	0	*89.119	44	5	4	1
23.569	30	2	0	0					
25.985	650	1	2	0					
26.296	999	2	1	0					
30.983	177	0	0	1					
33.244	366	2	2	0					
35.273	480	1	1	1					
37.002	155	1	3	0					
37.604	20	3	1	0					
39.294	175	2	0	1					
40.867	549	1	2	1					
42.604	153	2	3	0					
42.940	32	3	2	0					
46.079	9	2	2	1					
47.229	8	0	4	0					
48.217	53	4	0	0					
48.837	4	1	4	0					
49.009	3	1	3	1					
49.491	74	3	1	1					
49.740	18	4	1	0					
50.819	17	3	3	0					
53.441	62	2	4	0					
53.603	35	2	3	1					
53.886	73	3	2	1					
54.121	110	4	2	0					
57.562	144	0	4	1					
58.423	67	4	0	1					
58.967	18	1	4	1					
59.763	14	4	1	1					
60.719	379	3	3	1					
60.936	200	4	3	0					
61.466	7	1	5	0					
62.706	5	5	1	0					
63.066	8	2	4	1					
63.679	63	4	2	1					
64.577	160	0	0	2					
65.473	40	2	5	0					
66.523	58	5	2	0					
67.146	11	1	1	2					
69.593	15	0	2	2					
*69.593	15	3	4	1					
69.795	49	2	0	2					
*69.795	49	4	4	0					
69.933	23	4	3	1					
70.427	99	1	5	1					
70.840	45	1	2	2					
70.985	70	2	1	2					
71.586	30	5	1	1					
71.890	22	3	5	0					
72.657	10	5	3	0					
73.865	18	0	6	0					
74.191	106	2	5	1					
74.595	46	2	2	2					
75.185	102	5	2	1					
75.569	33	6	0	0					
76.826	46	6	1	0					
*76.826	46	1	3	2					
77.201	20	3	1	2					
78.305	12	4	4	1					
78.786	4	2	6	0					
80.272	7	6	2	0					
*80.272	7	3	5	1					
80.482	19	2	3	2					
*80.482	19	4	5	0					
80.714	15	3	2	2					
81.060	26	5	3	1					
82.229	2	0	6	1					
83.433	1	1	6	1					
83.885	2	6	0	1					
84.514	7	4	0	2					
84.825	4	3	6	0					
85.039	1	1	4	2					
*85.039	1	6	1	1					
85.667	5	4	1	2					
86.062	4	6	3	0					
86.498	6	3	3	2					
87.031	16	2	6	1					
88.571	22	2	4	2					
88.729	17	4	5	1					

Table A-4 2θ, intensity and hkl values of hematite from 2003 JCPDS-International Center for Diffraction Data number: JCPDS 00-033-0664

Pattern : 00-033-0664 ***Radiation =*** 1.540598 ***Quality :*** High

Fe_2O_3

Iron Oxide
Hematite, syn
Also called: burnt ochre, colcothar, rouge

Lattice : Rhombohedral
S.G. : R-3c (167)

a = 5.03560
c = 13.74890

Z = 6

Mol. weight = 159.69
Volume [CD] = 301.93
Dx = 5.270
Dm = 5.260
I/Icor = 2.40

Optical data: A=2.94, B=3.22, Sign=-
Melting point: 1350-1360°
Color: Dark reddish brown
Sample source or locality: Sample from Pfizer, Inc., New York, USA, heated at 800 C for 3 days.
Additional pattern: To replace 13-534 and validated by calculated pattern 24-72.
General comments: Opaque mineral optical data on specimen from Elba, R_1R_0 =30.2, RR_2R_e=26.1, Disp.=16, VHN=1038 (mean at 100, 200, 300), Color values=1 .299, .309, 29.8, 2 .299, .309, 25.7.
Additional pattern: See ICSD 64599 (PDF 79-7).
General comments: Pattern reviewed by Syvinski, W., McCarthy, G., North Dakota State Univ., Fargo, North Dakota, USA, *ICDD Grant-in-Aid* (1990). Agress well with experimental and calculated patterns.
General comments: Additional weak reflection [indicated by brackets] was observed.
Common name: Also called: crocus mantis.
Common name: Also called: venetian red.
Common name: Also called: ferrite.
Common name: Also called: indian red.
Common name: Also called: crocus.
Temperature of data collection: Pattern taken at 25 C.
Data collection flag: Ambient.

2th	i	h	k	l
24.138	30	0	1	2
33.153	100	1	0	4
35.612	70	1	1	0
39.277	3	0	0	6
40.855	20	1	1	3
43.519	3	2	0	2
49.480	40	0	2	4
54.091	45	1	1	6
56.152	1	2	1	1
57.429	5	1	2	2
57.590	10	0	1	8
62.451	30	2	1	4
63.991	30	3	0	0
66.028	1	1	2	5
69.601	3	2	0	8
71.937	10	1	0	10
72.262	6	1	1	9
75.430	8	2	2	0
77.729	4	3	0	6
78.760	2	2	2	3
80.711	5	1	2	8
82.939	5	0	2	10
84.916	7	1	3	4
88.542	7	2	2	6
91.345	2	0	4	2
93.715	7	2	1	10
95.239	1	1	1	12
95.663	3	4	0	4
102.285	4	3	1	8
104.914	1	2	2	9
106.623	5	3	2	4
107.025	4	0	1	14
108.090	5	4	1	0
111.518	2	4	1	3
113.594	2	0	4	8
116.044	5	1	3	10
117.758	1	3	0	12
118.697	3	2	0	14
122.431	6	4	1	6
125.929	1	2	3	8
128.758	3	4	0	10
131.877	5	1	2	14
133.241	3	3	3	0
144.456	4	3	2	10
147.971	4	2	4	4

Table A-5 2θ, intensity and hkl values of muscovite from 2003 JCPDS-International Center for Diffraction Data number: JCPDS 00-007-0042

Pattern : 00-007-0042 **Radiation =** 1.540598 **Quality :** Indexed

$(K,Na)(Al,Mg,Fe)_2(Si_{3.1}Al_{0.9})O_{10}(OH)_2$

Potassium Aluminum Silicate Hydroxide
Muscovite-3T

Lattice : Hexagonal
S.G. : P3121 (152)

a = 5.20300
c = 29.98800
Z = 3

Mol. weight = 398.42
Volume [CD] = 703.05
Dx = 2.823
Dm = 2.820

Optical data: A=1.555, B=1.589, Q=1.590, Sign=-, 2V=15(3)°
Color: White
Sample source or locality: Specimen from Sultan Basin, Snohomish County, Washington, USA.
General comments: See Axelrod, Grimaldi, *Am. Mineral.*, **34** 559 (1949) for optical, chemical, thermal and X-ray data.
Additional pattern: See ICSD 26818 (PDF 74-1107); See ICSD 27170 (PDF 74-1392); See ICSD 75952 (PDF 82-1852); See ICSD 75953 (PDF 85-1855).
Data collection flag: Ambient.

2th	i	h	k	l
8.862	100	0	0	3
17.760	55	0	0	6
19.757	20	1	0	0
19.891	20	1	0	1
22.944	10	1	0	4
24.738	8	1	0	5
26.742	100	0	0	9
28.681	10	1	0	7
30.983	16	1	0	8
34.618	16	1	1	1
34.967	25	1	1	2
35.907	12	0	0	12
36.542	8	1	1	4
37.702	8	1	1	5
39.967	6	2	0	0
40.567	4	1	1	7
41.050	4	2	0	3
42.277	12	1	1	8
44.006	4	2	0	6
45.330	45	0	0	15
46.134	8	1	1	10
48.240	2	1	1	11
55.514	10	1	1	14
56.103	4	2	1	5
57.013	4	2	1	6
59.557	2	2	1	8
60.854	6	1	1	
61.708	12	3	0	0

Table A-6 2θ, intensity and hkl values of kaolinite from 2003 JCPDS-International Center for Diffraction Data number: JCPDS 01-089-6538

Pattern : 01-089-6538 **Radiation =** 1.540598 **Quality :** Calculated

$Al_2(Si_2O_5)(OH)_4$

Aluminum Silicate Hydroxide
Kaolinite

Lattice : Anorthic (triclinic)
S.G. : C1 (0)

a = 5.15400 **alpha =** 91.69
b = 8.94200 **beta =** 104.61
c = 7.40100 **gamma =** 89.82
a/b = 0.57638 **Z =** 2
c/b = 0.82767

Mol. weight = 258.16
Volume [CD] = 164.96
Dx = 2.599
I/Icor = 1.00

ICSD collection code: 087771
ICSD space group comment: ICSD SG: C1 IT is: 1 SG short form: C1
Temperature factor: ATF
Temperature factor: ITF
Sample source or locality: Specimen from Keokuk, Iowa, USA.
Data collection flag: Ambient.

Neder, R.B., Burghammer, M., Grasl, Th., Schulz, H., Bram, A., Fiedler, S., Clays Clay Miner., volume 47, page 487 (1999)
Calculated from ICSD using POWD-12++

Radiation : CuKa1
Lambda : 1.54060
SS/FOM : F30=180(0.0048,35)

Filter : Not specified
d-sp : Calculated spacings

2th	i	h	k	l
12.355	999	0	0	1
19.851	177	0	2	0
20.336	510	-1	1	0
*20.336	510	1	1	0
21.265	481	-1	-1	1
21.537	220	-1	1	1
23.129	329	0	-2	1
23.763	154	0	2	1
24.856	564	0	0	2
25.994	19	1	-1	1
26.341	184	1	1	1
28.321	39	-1	-1	2
28.791	49	-1	1	2
31.532	6	0	-2	2
32.483	65	0	2	2
34.985	115	-2	0	1
*34.985	115	-1	3	0
35.126	77	1	3	0
35.433	91	-1	-3	1
35.541	87	1	-1	2
35.986	155	2	0	0
*35.986	155	1	1	2
37.667	55	0	0	3
38.408	215	-2	0	2
38.493	301	1	-3	1
*38.493	301	-1	-1	3
39.081	33	-1	1	3
39.226	226	1	3	1
40.058	25	-1	-3	2
40.330	4	0	4	0
40.415	3	-2	-2	1
40.636	8	-2	2	1
41.096	24	-1	3	2
41.196	33	2	0	1
41.350	15	-2	2	0
41.514	7	2	2	0
41.964	3	0	-4	1
42.374	17	0	-2	3
42.713	7	0	4	1
43.311	3	-2	-2	2
43.485	4	0	2	3
43.885	10	-2	2	2
45.464	66	-2	0	3
45.594	93	1	-3	2
45.878	7	2	-2	1
46.378	25	2	2	1
46.755	44	1	3	2
47.274	25	0	-4	2
47.533	7	1	1	3
47.958	22	-1	-3	3
48.632	21	0	4	2
49.361	21	-1	3	3
49.500	30	2	0	2
49.640	41	-2	-2	3
50.346	8	-1	-1	4
50.485	12	-2	2	3
50.989	27	-1	1	4
*50.989	27	0	0	4
53.461	26	2	-2	2
54.242	16	2	2	2
*54.242	16	-2	-4	1
54.373	18	-3	1	1
*54.373	18	-1	5	0
54.568	26	1	5	0
*54.568	26	-1	-5	1
55.055	85	-2	4	0
*55.055	85	-2	0	4
55.217	112	1	-3	3
*55.217	112	2	4	0
55.452	46	0	-4	3
55.582	24	-3	-1	2
55.789	32	-3	1	2
*55.789	32	0	2	4
56.189	12	-3	1	0
56.287	10	3	1	0
56.438	12	-2	-4	2
56.684	66	1	3	3
56.792	48	1	-5	1
57.269	8	0	4	3
57.383	11	-2	4	2
57.703	3	1	5	1
57.883	7	-1	-5	2
58.154	34	-1	-3	4
58.596	6	-2	-2	4
*58.596	6	2	-4	1
59.202	3	-1	5	2
59.437	9	2	4	1
59.635	30	-2	2	4
*59.635	30	1	-1	4
59.824	36	-1	3	4
59.992	43	-3	-1	3
*59.992	43	2	0	3
60.318	7	-3	1	3
*60.318	7	1	1	4
61.047	6	3	-1	1
61.284	4	3	1	1
61.642	5	-2	-4	3
62.275	114	-3	-3	1
*62.275	114	0	6	0
62.426	109	-3	3	1
63.104	6	-2	4	3
63.369	18	0	-6	1
*63.369	18	2	-2	3
63.733	13	1	5	2
63.869	18	-3	3	2
*63.869	18	-3	3	0
64.016	14	-1	-5	3
*64.016	14	-1	1	5
64.185	24	0	6	1
*64.185	24	3	3	0
64.333	32	2	2	3
65.099	11	0	0	5
65.833	12	0	-4	4
65.953	7	-1	5	3
66.355	8	2	4	2
66.553	11	-2	0	5
66.740	10	1	-3	4
67.036	3	-3	-1	4
67.220	14	-3	-3	3
67.307	13	0	-6	2
67.495	12	-3	1	4
68.025	19	0	4	4
68.183	16	0	-2	5
*68.183	16	-3	3	3
68.354	13	3	-3	1
68.465	10	1	3	4
68.567	8	3	-1	2
68.937	9	3	1	2
*68.937	9	0	6	2
69.022	7	3	3	1
69.462	4	-2	-4	4
*69.462	4	0	2	5
69.602	15	-2	-2	5
70.166	49	1	-5	3
*70.166	49	-1	-3	5
70.826	1	-2	2	5
71.373	2	-2	4	4
72.079	44	-1	3	5
72.274	63	1	5	3
*72.274	63	2	0	4
73.230	17	-2	-6	1
73.707	32	-4	0	1
*73.707	32	1	-1	5
73.906	30	-4	0	2
*73.906	30	-2	6	0
74.244	8	2	6	0
74.401	4	1	1	5
74.977	17	-2	-6	2
75.135	14	-3	3	4
*75.135	14	2	-2	4
75.381	9	3	-3	2
75.680	3	2	4	3
76.204	24	-2	6	2
76.313	27	0	6	3
*76.313	27	4	0	0
76.413	20	2	2	4
*76.413	20	3	3	2
76.518	16	-3	-1	5
76.736	13	-4	0	3
*76.736	13	-3	-5	1
76.872	17	2	-6	1
*76.872	17	-1	7	0
77.052	23	-1	-7	1
*77.052	23	1	7	0
77.207	21	-4	-2	1
*77.207	21	-4	-2	2
77.513	11	-4	2	2
77.603	13	-3	-5	2
77.762	11	-1	7	1
77.835	11	-1	-1	6
77.980	12	2	6	1
78.149	8	0	-4	5
78.301	6	-3	5	0
78.477	13	3	-1	3
*78.477	13	-3	5	2
78.715	9	3	5	0
78.824	6	1	-7	1
*78.824	6	3	1	3
79.423	5	-2	-6	3
79.683	14	-4	2	0
*79.683	14	-1	-7	2
79.822	11	-2	0	6
79.937	14	1	7	1
*79.937	14	-4	-2	3
80.037	11	1	-3	5
80.426	10	0	0	6
*80.426	10	-4	2	3
80.713	6	0	4	5
81.101	1	-3	-5	3
81.282	3	-1	7	2
81.395	3	-2	6	3
81.583	4	4	0	1
81.945	7	-2	4	5
82.034	8	1	3	5
82.252	7	3	-5	1
*82.252	7	-4	0	4
82.601	6	-3	5	3
*82.601	6	-2	-2	6

Table A-7 2θ, intensity and hkl values of quartz from 2003 JCPDS-International Center for Diffraction Data number: JCPDS 01-089-8934

Pattern : 01-089-8934 **Radiation =** 1.540598 **Quality :** Calculated

SiO_2

Silicon Oxide
Quartz α

Lattice : Hexagonal
S.G. : P3221 (154)

a = 4.91370
c = 5.40470

Z = 3

Mol. weight = 60.08
Volume [CD] = 113.01
Dx = 2.649
I/Icor = 3.03

ICSD collection code: 089276
Remarks from ICSD/CSD: REM TEM 298.
Data collection flag: Ambient.

2th	i	h	k	l
20.858	212	1	0	0
26.640	999	0	1	1
36.544	66	1	1	0
39.470	67	1	0	2
40.291	31	1	1	1
42.450	49	2	0	0
45.794	26	2	0	1
50.142	111	1	1	2
50.627	4	0	0	3
54.875	32	0	2	2
55.331	15	0	1	3
57.230	2	2	1	0
59.958	79	1	2	1
64.039	14	1	1	3
65.783	3	3	0	0
67.743	47	1	2	2
68.147	59	2	0	3
68.311	59	0	3	1
73.474	18	1	0	4
75.659	23	3	0	2
77.667	12	2	2	0
79.885	23	2	1	3
80.040	13	2	2	1
81.177	20	1	1	4
81.486	25	3	1	0
83.833	14	1	3	1
84.960	2	2	0	4
87.072	1	2	2	2
87.446	2	3	0	3

Table A-8 2θ, intensity and hkl values of alunite from 2003 JCPDS-International Center for Diffraction Data number: JCPDS 00-003-0616

Pattern : 00-003-0616 ***Radiation =*** 1.540598 ***Quality :*** Deleted

$K_2O \cdot 3Al_2O_3 \cdot 4SO_3 \cdot 6H_2O$

Potassium Aluminum Sulfate Hydrate
Alunite

Lattice : Not assigned
S.G. : (255)

Mol. weight = 828.40

Dm = 2.600

Deleted and rejected by: Delete: see A. Pabst letter July 4, 1953.
Sample source or locality: Specimen from Normanville, Hindmarsh Co., South Australia.
Color: Colorless
Optical data: B=1.580, Q=1.592, Sign=+
Data collection flag: Ambient.

2th	i	h	k	l
15.398	50			
18.052	75			
22.962	25			
25.064	75			
26.750	75			
28.127	25			
29.757	100			
35.744	25			
39.312	50			
40.606	25			
43.254	25			
47.835	85			
52.553	75			
55.660	25			
59.179	25			
61.799	75			
65.186	25			
67.307	25			
73.329	50			
79.079	50			
82.352	25			
85.017	25			
89.934	25			

APPENDIX B

Table B-1 Adsorption values of FAG powder on effect of contact time

Solution system	Time (min)	Metal							
		Pb^{2+}		Cd^{2+}		Cu^{2+}		Ni^{2+}	
		Efficiency (%)	Capacity (mg/g)	Efficiency (%)	Capacity (mg/g)	Efficiency (%)	Capacity (mg/g)	Efficiency (%)	Capacity (mg/g)
Multi-cations	5	87.173	6.974	87.173	1.592	40.832	3.267	9.429	0.754
	10	91.031	7.282	91.031	1.899	40.412	3.232	10.671	0.853
	15	88.379	7.0703	88.379	1.910	41.501	3.320	12.201	0.976
	30	90.322	7.225	90.322	2.035	43.554	3.484	12.686	1.014
	60	95.774	7.662	95.774	2.429	46.250	3.670	16.071	1.285
	120	95.074	7.6059	95.073	2.554	46.657	3.732	24.012	1.920
	180	98.085	7.847	98.085	2.701	56.217	4.497	27.188	2.175
Mono-cations	5	97.550	7.804	67.970	5.438	67.452	5.396	54.381	4.350
	10	98.597	7.888	68.997	5.519	67.077	5.366	55.646	4.452
	15	98.882	7.910	70.533	5.642	70.244	5.619	55.204	4.416
	30	98.618	7.88943	69.637	5.571	71.201	5.696	56.965	4.557
	60	98.821	7.907	71.887	5.751	75.387	6.031	57.392	4.591
	120	99.919	7.993	76.329	6.106	85.907	6.872	56.554	4.524
	180	98.242	7.859	72.564	5.805	89.979	7.198	59.953	4.796

Table B-2 Adsorption values of FAG powder on effect of geopolymer dose

solution system	Dose (g)	Metal							
		Pb^{2+}		Cd^{2+}		Cu^{2+}		Ni^{2+}	
		Efficiency (%)	Capacity (mg/g)	Efficiency (%)	Capacity (mg/g)	Efficiency (%)	Capacity (mg/g)	Efficiency (%)	Capacity (mg/g)
Multi-cations	0.02	46.687	3.735	6.513	0.521	23.402	1.8721	6.201	0.496
	0.04	73.634	5.890	13.611	1.089	32.866	2.629	16.812	1.345
	0.06	88.263	7.061	22.209	1.777	37.370	2.990	19.268	1.541
	0.08	89.033	7.122	23.634	1.890	43.610	3.489	23.679	1.894
	0.1	95.074	7.606	31.929	2.554	46.657	3.732	24.011	1.920
	0.12	94.540	7.563	31.252	2.500	46.701	3.736	24.889	1.991
	0.14	96.606	7.728	39.279	3.142	56.367	4.509	28.672	2.294
Mono-cations	0.02	84.939	6.795	33.508	2.680	54.142	4.331	0.248	0.020
	0.04	97.500	7.800	49.250	3.940	69.995	5.599	37.982	3.039
	0.06	99.085	7.927	60.645	4.851	78.913	6.313	42.483	3.399
	0.08	99.624	7.970	68.225	5.458	85.122	6.810	50.330	4.026
	0.1	99.919	7.993	76.329	6.106	85.907	6.872	56.554	4.524
	0.12	99.034	7.922	80.727	6.458	92.876	7.430	61.769	4.941
	0.14	99.116	7.929	84.396	6.751	96.552	7.724	61.622	4.930

Table B-3 Adsorption values of FAG powder on effect of solution pH

solution system	pH	Metal							
		Pb^{2+}		Cd^{2+}		Cu^{2+}		Ni^{2+}	
		Efficiency (%)	Capacity (mg/g)	Efficiency (%)	Capacity (mg/g)	Efficiency (%)	Capacity (mg/g)	Efficiency (%)	Capacity (mg/g)
Multi-cations	1	1.054	0.084	0	0	0	0	0	0
	2	10.010	0.801	0	0	0	0	0	0
	3	60.050	4.804	6.577	0.526	21.094	1.687	9.238	0.739
	5	95.073	7.606	31.929	2.554	46.657	3.732	24.011	1.921
Mono-cations	1	0	0	0	0	0	0	15.064	1.205
	2	8.811	0.705	0	0	2.132	0.170	17.641	1.411
	3	77.398	6.192	26.190	2.095	34.561	2.765	37.416	2.993
	5	99.919	7.993	76.329	6.106	85.907	6.873	56.554	4.524

Table B-4 Adsorption values of FAG powder on effect of temperature

solution system	Temperature (°C)	Metal							
		Pb^{2+}		Cd^{2+}		Cu^{2+}		Ni^{2+}	
		Efficiency (%)	Capacity (mg/g)	Efficiency (%)	Capacity (mg/g)	Efficiency (%)	Capacity (mg/g)	Efficiency (%)	Capacity (mg/g)
Multi-cations	25	95.074	7.606	31.929	2.554	46.657	3.732	24.012	1.921
	35	96.181	7.694	36.390	2.911	54.620	4.370	31.905	2.552
	45	96.632	7.730	35.893	2.871	62.191	4.975	38.676	3.094
Mono-cations	25	99.919	7.993	76.329	6.106	85.907	6.873	56.554	4.524
	35	98.895	7.912	80.690	6.455	92.532	7.402	62.390	4.991
	45	99.685	7.975	82.852	6.628	96.225	7.698	65.184	5.215

Table B-5 Adsorption values of FAG powder on initial concentration

solution system	Initial concentration (mg/L)	Metal							
		Pb^{2+}		Cd^{2+}		Cu^{2+}		Ni^{2+}	
		Efficiency (%)	Capacity (mg/g)	Efficiency (%)	Capacity (mg/g)	Efficiency (%)	Capacity (mg/g)	Efficiency (%)	Capacity (mg/g)
Multi-cations	10	96.177	3.847	55.255	2.210	81.204	3.248	31.808	1.272
	20	95.073	7.606	31.929	2.554	46.657	3.732	24.011	1.920
	40	95.784	15.325	18.766	3.002	47.121	7.539	21.785	3.486
	60	96.336	23.121	18.617	4.468	31.834	7.640	13.423	3.221
	80	96.989	31.036	16.851	5.392	24.407	7.810	12.781	4.090
	100	97.345	38.938	16.191	6.477	19.569	7.827	0	0
	120	98.430	47.246	17.390	8.347	19.594	9.405	0	0
Mono-cations	10	97.012	3.880	82.874	3.315	92.080	3.683	57.330	2.293
	20	99.919	7.993	76.328	6.106	85.907	6.873	56.554	4.524
	40	97.627	15.620	61.713	9.874	48.089	7.694	41.841	6.695
	60	94.377	22.650	43.161	10.359	38.756	9.301	42.326	10.158
	80	87.609	28.035	32.253	10.3209	29.232	9.354	36.340	11.629
	100	87.553	35.021	30.881	12.352	23.745	9.498	33.052	13.221
	120	89.490	42.955	26.649	12.791	16.422	7.883	29.458	14.140

APPENDIX C

Table C-1 Adsorption values of MKG powder on effect of contact time

solution system	Time (min)	Metal							
		Pb^{2+}		Cd^{2+}		Cu^{2+}		Ni^{2+}	
		Efficiency (%)	Capacity (mg/g)	Efficiency (%)	Capacity (mg/g)	Efficiency (%)	Capacity (mg/g)	Efficiency (%)	Capacity (mg/g)
Multi-cations	5	98.0534	7.844	45.680	3.654	62.646	5.011	12.627	1.010
	10	99.441	7.955	55.878	4.470	69.690	5.575	29.436	2.354
	15	99.643	7.971	64.126	5.130	77.613	6.209	32.592	2.607
	30	99.200	7.936	72.269	5.781	85.818	6.865	35.238	2.819
	60	100	8.061	67.168	5.373	81.1533	6.492	32.522	2.601
	120	100	8.149	79.279	6.342	88.678	7.094	39.083	3.126
	180	100	8.058	81.229	6.498	89.850	7.188	43.721	3.497
Mono-cations	5	88.054	7.044	55.680	4.454	72.646	5.812	52.628	4.210
	10	89.441	7.1553	65.878	5.270	79.691	6.375	59.435	4.755
	15	90.917	7.273	75.089	6.007	80.941	6.475	61.089	4.887
	30	95.321	7.626	79.504	6.360	81.737	6.539	69.209	5.536
	60	96.788	7.743	81.530	6.522	82.701	6.616	70.053	5.604
	120	97.175	7.774	80.216	6.417	85.120	6.810	72.215	5.777
	180	97.106	7.768	82.297	6.583	85.377	6.830	72.811	5.825

Table C-2 Adsorption values of MKG powder on effect of geopolymer dose

solution system	Dose (g)	Metal							
		Pb^{2+}		Cd^{2+}		Cu^{2+}		Ni^{2+}	
		Efficiency (%)	Capacity (mg/g)	Efficiency (%)	Capacity (mg/g)	Efficiency (%)	Capacity (mg/g)	Efficiency (%)	Capacity (mg/g)
Multi-cations	0.02	75.231	6.018	18.194	1.455	23.417	1.873	1.552	0.124
	0.04	94.393	7.551	30.435	2.435	39.393	3.151	6.067	0.485
	0.06	99.952	7.996	49.243	3.939	54.606	4.369	12.063	0.961
	0.08	100	8	53.106	4.249	69.292	5.543	14.973	1.198
	0.1	100	8	79.279	6.342	88.678	7.094	39.083	3.127
	0.12	100	8	81.597	5.728	89.146	6.652	40.508	2.121
	0.14	100	8	84.827	6.786	95.722	7.658	45.661	2.853
Mono-cations	0.02	77.610	6.209	68.112	5.449	73.915	5.913	52.477	4.198
	0.04	79.277	6.342	74.7590	5.981	76.511	6.121	53.709	4.297
	0.06	83.3232	6.666	79.272	6.342	80.837	6.470	57.160	4.573
	0.08	89.297	7.144	79.582	6.367	83.213	6.657	62.542	5.003
	0.1	97.175	7.774	80.216	6.417	85.120	6.810	72.215	5.777
	0.12	100	8	80.761	6.461	88.936	7.115	74.474	5.958
	0.14	100	8	81.207	6.496	88.667	7.093	74.890	5.991

Table C-3 Adsorption values of MKG powder on effect of solution pH

solution system	pH	Metal							
		Pb^{2+}		Cd^{2+}		Cu^{2+}		Ni^{2+}	
		Efficiency (%)	Capacity (mg/g)	Efficiency (%)	Capacity (mg/g)	Efficiency (%)	Capacity (mg/g)	Efficiency (%)	Capacity (mg/g)
Multi-cations	1	7.505	0.600	2.615	0.209	0	0	0	0
	2	14.094	1.128	5.094	0.407	3.176	0.254	0.247	0.020
	3	100	8	43.088	3.447	56.364	4.509	15.309	1.225
	5	100	8	79.279	6.342	88.678	7.094	39.083	3.127
Mono-cations	1	0	0	0	0	0	0	0	0
	2	53.183	4.254	45.064	3.605	52.132	4.171	37.640	3.011
	3	77.510	6.201	66.648	5.331	66.737	5.339	52.470	4.198
	5	97.175	7.774	80.216	6.417	85.120	6.810	72.215	5.777

Table C-4 Adsorption values of MKG powder on effect of temperature

solution system	Temperature (°C)	Metal							
		Pb^{2+}		Cd^{2+}		Cu^{2+}		Ni^{2+}	
		Efficiency (%)	Capacity (mg/g)	Efficiency (%)	Capacity (mg/g)	Efficiency (%)	Capacity (mg/g)	Efficiency (%)	Capacity (mg/g)
Multi-cations	25	100	8	79.280	6.342	88.678	7.094	39.083	3.127
	35	98.950	7.916	80.094	6.168	90.138	6.811	40.108	2.969
	45	99.547	7.964	83.299	6.663	93.386	7.471	46.085	3.687
Mono-cations	25	97.175	7.774	80.216	6.417	85.120	6.810	72.215	5.777
	35	98.556	7.884	82.390	6.591	87.300	6.984	76.054	6.084
	45	100	8	85.173	6.814	89.530	7.162	79.426	6.354

Table C-5 Adsorption values of MKG powder on initial concentration

solution system	Initial concentration (mg/L)	Metal							
		Pb^{2+}		Cd^{2+}		Cu^{2+}		Ni^{2+}	
		Efficiency (%)	Capacity (mg/g)	Efficiency (%)	Capacity (mg/g)	Efficiency (%)	Capacity (mg/g)	Efficiency (%)	Capacity (mg/g)
Multi-cations	10	100	4.045	95.922	3.837	94.116	3.764	79.400	3.176
	20	100	8.149	79.280	6.342	88.678	7.094	39.082	3.127
	40	99.133	15.861	43.944	7.031	48.874	7.820	16.860	2.698
	60	97.640	23.433	24.516	5.884	39.100	9.384	9.735	2.336
	80	96.821	30.983	18.276	5.848	27.849	8.911	8.254	2.641
	100	84.875	29.950	7.699	3.080	15.659	6.263	2.187	0.875
	120	82.278	39.494	3.601	1.728	11.041	5.300	2.011	0.965
Mono-cations	10	100	4	88.920	3.557	97.562	3.902	87.561	3.502
	20	97.175	7.774	80.216	6.417	85.120	6.810	72.215	5.777
	40	94.167	15.067	79.557	12.730	83.281	13.325	67.446	10.791
	60	92.450	22.188	77.723	18.653	77.834	18.680	67.176	16.122
	80	92.884	29.723	73.751	23.600	74.890	23.964	66.190	21.180
	100	90.293	36.117	70.192	28.077	72.264	28.906	64.859	25.943
	120	88.907	42.675	62.160	29.837	65.888	31.626	61.097	29.326

APPENDIX D

Table D-1 Adsorption values of FAG composite fiber on effect of contact time

solution system	Time (h)	Metal							
		Pb^{2+}		Cd^{2+}		Cu^{2+}		Ni^{2+}	
		Efficiency (%)	Capacity (mg/g)	Efficiency (%)	Capacity (mg/g)	Efficiency (%)	Capacity (mg/g)	Efficiency (%)	Capacity (mg/g)
Multi-cations	0.25	15.713	1.257	3.953	0.316	6.008	0.481	1.998	0.160
	0.5	14.197	1.136	9.447	0.756	6.047	0.484	4.334	0.347
	1	18.444	1.476	13.988	1.119	8.760	0.701	8.643	0.691
	3	18.624	1.490	18.817	1.505	13.796	1.104	13.319	1.066
	6	23.544	1.883	26.360	2.109	12.386	0.991	15.292	1.223
	12	33.293	2.663	29.639	2.371	17.959	1.437	17.219	1.378
	24	47.751	3.820	31.728	2.538	21.047	1.684	19.016	1.521
	48	75.726	6.058	34.617	2.769	27.308	2.185	25.125	2.010
	72	82.143	6.571	33.651	2.692	27.878	2.230	26.476	2.118

solution system	Time (h)	Metal							
		Pb^{2+}		Cd^{2+}		Cu^{2+}		Ni^{2+}	
		Efficiency (%)	Capacity (mg/g)	Efficiency (%)	Capacity (mg/g)	Efficiency (%)	Capacity (mg/g)	Efficiency (%)	Capacity (mg/g)
Mono-cations	0.25	9.616	0.769	11.866	0.949	4.609	0.369	8.014	0.641
	0.5	14.126	1.130	15.670	1.254	5.059	0.405	8.989	0.720
	1	16.171	1.294	27.561	2.205	7.231	0.578	15.541	1.243
	3	30.272	2.422	27.561	2.205	13.441	1.075	18.481	1.478
	6	55.361	4.429	33.264	2.661	13.674	1.094	22.816	1.825
	12	77.960	6.237	35.441	2.835	24.992	1.999	23.552	1.884
	24	96.570	7.726	55.814	4.465	37.830	3.026	31.888	2.551
	48	100	8	67.515	5.401	48.584	3.887	46.405	3.712
	72	100	8	77.404	6.192	69.385	5.550	60.501	4.840

Table D-2 Adsorption values of FAG composite fiber on effect of geopolymer dose

solution system	Dose (g)	Metal							
		Pb^{2+}		Cd^{2+}		Cu^{2+}		Ni^{2+}	
		Efficiency (%)	Capacity (mg/g)	Efficiency (%)	Capacity (mg/g)	Efficiency (%)	Capacity (mg/g)	Efficiency (%)	Capacity (mg/g)
Multi-cations	0.05	29.990	2.399	25.771	2.0617	14.212	1.137	13.975	1.118
	0.1	47.751	3.820	31.728	2.539	21.047	1.684	19.016	1.521
	0.25	55.768	4.461	41.882	3.351	39.238	3.139	14.222	1.138
	0.5	74.092	5.927	54.816	4.385	45.946	3.676	32.395	2.592
Mono-cations	0.05	65.417	5.233	42.180	3.374	37.492	2.999	21.052	1.684
	0.1	96.570	7.726	55.814	4.465	37.830	3.0263	31.888	2.551
	0.25	98.699	7.896	56.975	4.558	48.584	3.887	46.405	3.712
	0.5	100	8	63.225	5.058	56.885	4.551	52.751	4.220

Table D-3 Adsorption values of FAG composite fiber on effect of solution pH

solution system	pH	Metal							
		Efficiency (%)		Capacity (mg/g)		Efficiency (%)		Capacity (mg/g)	
		Efficiency (%)	Capacity (mg/g)	Efficiency (%)	Capacity (mg/g)	Efficiency (%)	Capacity (mg/g)	Efficiency (%)	Capacity (mg/g)
Multi-cations	1	5.619	0.449	4.289	0.343	3.240	0.259	1.383	0.110
	2	9.451	0.756	9.337	0.747	3.769	0.302	11.264	0.901
	3	22.824	1.826	13.049	1.044	7.400	0.592	12.761	1.020
	5	47.751	3.820	31.728	2.538	21.047	1.684	19.016	1.521
Mono-cations	1	56.936	4.555	5.904	0.472	0	0	2.285	0.183
	2	62.652	5.012	5.954	0.476	1.142	0.091	2.587	0.207
	3	68.470	5.478	9.412	0.753	6.966	0.557	14.768	1.181
	5	96.570	7.726	55.814	4.465	37.830	3.026	31.888	2.551

Table D-4 Adsorption values of FAG composite fiber on effect of temperature

solution system	Temperature (°C)	Metal							
		Pb^{2+}		Cd^{2+}		Cu^{2+}		Ni^{2+}	
		Efficiency (%)	Capacity (mg/g)	Efficiency (%)	Capacity (mg/g)	Efficiency (%)	Capacity (mg/g)	Efficiency (%)	Capacity (mg/g)
Multi-cations	25	47.751	3.820	31.728	2.538	21.047	1.684	19.016	1.521
	35	57.076	4.566	32.426	2.594	21.993	1.759	20.191	1.615
	45	60.439	4.835	36.109	2.889	23.897	1.912	22.197	1.776
Mono-cations	25	96.570	7.726	55.814	4.465	37.830	3.026	31.888	2.551
	35	100	8	75.066	6.005	70.447	5.636	39.718	3.177
	45	100	8	80.039	6.403	69.136	5.531	42.792	3.423

Table D-5 Adsorption values of FAG composite fiber on initial concentration

solution system	Initial concentration (mg/L)	Metal							
		Pb^{2+}		Cd^{2+}		Cu^{2+}		Ni^{2+}	
		Efficiency (%)	Capacity (mg/g)	Efficiency (%)	Capacity (mg/g)	Efficiency (%)	Capacity (mg/g)	Efficiency (%)	Capacity (mg/g)
Multi-cations	10	57.904	2.316	52.741	2.110	38.267	1.530	35.407	1.416
	20	47.751	3.820	31.728	2.538	21.047	1.683	19.016	1.521
	40	36.412	5.826	26.790	4.286	17.816	2.850	13.509	2.161
	60	30.126	5.910	21.849	5.243	15.718	3.772	10.808	2.593
	80	18.363	5.876	17.189	5.500	13.043	4.174	6.342	2.029
	100	17.430	6.972	13.829	5.531	10.330	4.132	6.185	2.474
	120	16.054	7.706	12.367	5.936	9.156	4.395	6.069	2.913
Mono-cations	10	100	4.196	63.125	2.525	51.447	2.057	48.252	1.930
	20	96.570	7.726	55.813	4.465	37.829	3.026	31.888	2.551
	40	50.154	8.025	31.3676	5.018	23.704	3.792	21.763	3.482
	60	40.044	9.611	27.852	6.684	20.178	4.842	18.523	4.445
	80	26.369	8.438	29.811	9.540	21.701	6.944	16.094	5.150
	100	29.460	11.784	25.270	10.108	21.193	8.477	18.610	7.444
	120	23.830	11.438	21.871	10.498	20.084	9.640	17.551	8.424

APPENDIX E

Table E-1 Adsorption values of MKG composite fiber on effect of contact time

solution system	Time (h)	Metal							
		Pb^{2+}		Cd^{2+}		Cu^{2+}		Ni^{2+}	
		Efficiency (%)	Capacity (mg/g)	Efficiency (%)	Capacity (mg/g)	Efficiency (%)	Capacity (mg/g)	Efficiency (%)	Capacity (mg/g)
Multi-cations	0.25	7.208	0.576	4.948	0.395	1.693	0.135	2.174	0.173
	0.5	8.825	0.706	6.175	0.494	4.518	0.361	5.319	0.425
	1	8.945	0.715	7.948	0.635	8.592	0.687	8.007	0.640
	3	9.959	0.796	8.970	0.717	9.071	0.725	7.542	0.603
	6	11.656	0.932	13.650	1.092	10.615	0.849	8.796	0.703
	12	15.251	1.220	15.053	1.204	13.341	1.067	9.231	0.738
	24	17.128	1.370	16.044	1.283	15.333	1.226	9.611	0.768
	48	41.676	3.334	18.495	1.479	16.999	1.359	10.045	0.803
	72	48.952	3.916	19.642	1.571	18.198	1.455	12.004	0.960

solution system	Time (h)	Metal							
		Pb^{2+}		Cd^{2+}		Cu^{2+}		Ni^{2+}	
		Efficiency (%)	Capacity (mg/g)	Efficiency (%)	Capacity (mg/g)	Efficiency (%)	Capacity (mg/g)	Efficiency (%)	Capacity (mg/g)
Mono-cations	0.25	14.062	1.125	5.434	0.434	2.855	0.228	2.755	0.220
	0.5	13.808	1.104	9.230	0.738	2.673	0.213	3.881	0.310
	1	14.062	1.125	19.952	1.596	3.523	0.281	6.569	0.525
	3	22.192	1.775	23.954	1.916	8.523	0.681	6.569	0.525
	6	34.502	2.760	23.188	1.855	13.182	1.054	12.836	1.026
	12	35.276	2.822	35.861	2.868	21.219	1.697	15.927	1.274
	24	49.822	3.985	41.049	3.283	35.183	2.814	24.529	1.962
	48	67.606	5.408	60.746	4.859	41.706	3.336	36.004	2.880
	72	81.580	6.526	63.405	5.072	57.569	4.605	37.869	3.029

Table E-2 Adsorption values of MKG composite fiber on effect of geopolymer dose

solution system	Dose (g)	Metal							
		Pb^{2+}		Cd^{2+}		Cu^{2+}		Ni^{2+}	
		Efficiency (%)	Capacity (mg/g)	Efficiency (%)	Capacity (mg/g)	Efficiency (%)	Capacity (mg/g)	Efficiency (%)	Capacity (mg/g)
Multi-cations	0.05	17.025	1.362	12.809	1.024	15.118	1.209	8.814	0.705
	0.1	17.128	1.370	16.044	1.283	15.333	1.226	9.611	0.768
	0.25	26.287	2.102	22.736	1.818	17.567	1.405	16.291	1.303
	0.5	46.846	3.747	33.600	2.688	25.893	2.071	19.725	1.578
Mono-cations	0.05	30.254	2.420	28.353	2.268	21.219	1.697	11.592	0.927
	0.1	49.822	3.985	41.049	3.283	35.183	2.814	24.529	1.962
	0.25	55.101	4.408	54.011	4.320	41.706	3.336	32.795	2.623
	0.5	66.280	5.302	61.923	4.953	57.569	4.605	48.504	3.880

Table E-3 Adsorption values of MKG composite fiber on effect of solution pH

solution system	pH	Metal							
		Pb^{2+}		Cd^{2+}		Cu^{2+}		Ni^{2+}	
		Efficiency (%)	Capacity (mg/g)	Efficiency (%)	Capacity (mg/g)	Efficiency (%)	Capacity (mg/g)	Efficiency (%)	Capacity (mg/g)
Multi-cations	1	4.121	0.329	0	0	0	0	0	0
	2	7.534	0.602	7.038	0.563	6.680	0.534	1.441	0.115
	3	15.04	1.203	9.707	0.776	9.133	0.730	4.407	0.352
	5	17.128	1.370	16.044	1.283	15.333	1.226	9.611	0.768
Mono-cations	1	54.738	4.379	4.026	0.322	2.314	0.185	2.217	0.177
	2	55.919	4.473	5.377	0.430	3.104	0.248	2.772	0.221
	3	58.168	4.653	7.831	0.626	5.037	0.402	8.098	0.647
	5	62.322	4.985	41.049	3.283	35.183	2.814	24.529	1.962

Table E-4 Adsorption values of MKG composite fiber on effect of temperature

solution system	Temperature (°C)	Metal							
		Pb^{2+}		Cd^{2+}		Cu^{2+}		Ni^{2+}	
		Efficiency (%)	Capacity (mg/g)	Efficiency (%)	Capacity (mg/g)	Efficiency (%)	Capacity (mg/g)	Efficiency (%)	Capacity (mg/g)
Multi-cations	25	17.128	1.370	16.044	1.283	15.333	1.226	9.611	0.768
	35	24.790	1.983	16.286	1.302	15.703	1.256	10.296	0.823
	45	28.952	2.316	19.683	1.574	16.973	1.357	12.925	1.034
Mono-cations	25	49.822	3.985	41.049	3.283	35.183	2.814	24.529	1.962
	35	96.493	7.719	66.485	5.318	59.782	4.782	32.022	2.561
	45	99.524	7.961	70.067	5.605	61.975	4.958	46.656	3.732

Table E-5 Adsorption values of MKG composite fiber on initial concentration

solution system	Initial concentration (mg/L)	Metal							
		Pb^{2+}		Cd^{2+}		Cu^{2+}		Ni^{2+}	
		Efficiency (%)	Capacity (mg/g)	Efficiency (%)	Capacity (mg/g)	Efficiency (%)	Capacity (mg/g)	Efficiency (%)	Capacity (mg/g)
Multi-cations	10	37.634	1.505	28.316	1.132	28.760	1.150	22.962	0.918
	20	17.128	1.370	16.044	1.283	15.333	1.226	9.6118	0.768
	40	16.460	2.633	13.339	2.134	12.486	1.997	13.506	2.160
	60	15.469	3.712	11.500	2.760	11.813	2.835	10.625	2.550
	80	13.492	4.317	10.899	3.487	10.762	3.443	9.826	3.144
	100	12.283	4.913	10.821	4.328	10.391	4.156	8.908	3.563
	120	12.011	5.765	8.983	4.312	8.382	4.023	5.481	2.631
Mono-cations	10	73.272	2.930	59.370	2.374	34.395	1.375	34.274	1.370
	20	49.822	3.985	41.049	3.283	35.183	2.814	24.529	1.962
	40	21.368	3.418	23.659	3.785	20.211	3.233	14.283	2.285
	60	18.182	4.363	15.991	3.838	14.951	3.588	11.546	2.771
	80	11.181	3.577	11.335	3.627	10.435	3.339	10.445	3.342
	100	9.260	3.704	10.193	4.077	9.212	3.684	8.677	3.471
	120	8.697	4.174	8.4745	4.067	8.279	3.974	7.687	3.689

VITA

Miss Sujitra Onutai was born in Bangkok on 22nd March 1988. She received her Bachelor's Degree in Materials Science, Faculty of Science from Chiangmai University in 2009. After graduation, she continued with her Master Degree in the field of Ceramic in Materials Science, Faculty of Science, Chulalongkorn University. In 2010-2012, she had received a scholarship from Thailand Institute of Science and Technology (TGIST). In 2013, she was doctoral students under Double Doctoral Degree Program from collaboration with Chulalongkorn University and Nagaoka University of Technology. She graduated the first doctoral degree at Nagaoka University of Technology in 2016. She studied about geopolymer materials holds master and doctoral degrees.

Publication papers

- Onutai, S., Kobayashi, T., Thavorniti, P., & Jiemsirilers, S. (2018). The Adsorption of Cadmium Ions on Fly Ash Based Geopolymer Particles. Key Engineering Materials, 766, 65-70.

- Onutai, S., Kobayashi, T., Thavorniti, P., & Jiemsirilers, S. (2018). Metakaolin based geopolymer from Thailand as an adsorbent for adsorption of multi- and mono- cations from aqueous solution. Accepted in Key Engineering Materials.

Academic Conference presentations

- Onutai, S., Kobayashi, T., Thavorniti, P., & Jiemsirilers, S. Development of fly ash based geopolymer materials apply for many applications, Meiji University-Chulalongkorn University Advanced Material Chemistry Workshop, Bangkok, Thailand on February 23, 2017. (Oral presentation)

- Onutai, S., Kobayashi, T. & Jiemsirilers, S. Fly ash based geopolymer as an adsorbent for heavy metal ions from aqueous solution. Asia Conference on Mechanical and Materials Engineering (ACMME 2017), Tokyo, Japan on June 9-11, 2017. (Oral presentation and excellent oral presentation awards)

- Onutai, S., Kobayashi, T., Thavorniti, P., & Jiemsirilers, S. The Adsorption of Cadmium Ions on Fly Ash Based Geopolymer Particles. International Conference on Traditional and Advanced Ceramics 2017 (ICTA 2017), Bangkok, Thailand on August 31-September 1, 2017. (Poster presentation)

- Onutai, S., Kobayashi, T., Thavorniti, P., & Jiemsirilers, S. Removals of Multi Heavy Metals in Aqueous Solution from Fly Ash Based Geopolymer Powder. The First Materials Research Society of Thailand International Conference (1st MRS Thailand International Conference), Chiang mai, Thailand on October 31 – November 3, 2017. (Poster presentation)